DOCTORAL THESIS

ANION-EXCHANGE MEMBRANES FROM END-OF-LIFE REVERSE OSMOSIS MEMBRANES

Indirect recycling approach for a circular water sector

Hydrology and Water Resource Management Doctoral Program.
Analytical Chemistry, Physical Chemistry and Chemical Engineering department.

Amaia Ortiz de Lejarazu Larrañaga
2022

Universidad de Alcalá

Programa de Doctorado en Hidrología y Gestión de los Recursos Hídricos

Anion-Exchange Membranes from end-of-life Reverse Osmosis membranes: indirect recycling approach for a circular water sector

TESIS DOCTORAL

Amaia Ortiz de Lejarazu Larrañaga

2022

Universidad de Alcalá

Programa de Doctorado en Hidrología y Gestión de los Recursos Hídricos

Anion-Exchange Membranes from end-of-life Reverse Osmosis membranes: indirect recycling approach for a circular water sector.

Tesis Doctoral presentada por:

Amaia Ortiz de Lejarazu Larrañaga

Dirigida por:

Dra. Serena Molina Martínez

Dr. Juan Manuel Ortiz Díaz-Guerra

Departamento de Química Analítica, Química Física e Ingeniería Química

Alcalá de Henares, 2022

Acknowledgements

The research work presented in this doctoral thesis is part of the national projects INREMEM (Innovation in Membrane Recycling, Ref. CTM2015-65348-C2-1-R) and INREMEM 2.0 (Hybrid wastewater treatments based on recycled membranes with the objective of zero liquid discharge (ZLD), Ref. RTI2018-096042-B-C21), which are supported by Spanish Ministry of Science and Innovation (MCI), and State Research Agency (AEI), and are co-financed by the European Regional Development Fund (ERDF). These entities have also supported the program "*Retos investigación*" CTM2015-74695-JIN (AEI/ERDF, UE). I would like to express my gratitude to the program of predoctoral contracts for training doctors (FPI). This program is financed by MCI, AEI, ERDF, and European Social Fund, (ESF) by the grant number BES-2016-076244. I would like to acknowledge to the European project TRANSFOMEM (Transformation of disposed reverse osmosis membranes into recycled ultra-and nanofiltration membranes, Ref. LIFE+ ENV/ES/000751), for providing a broad knowledge on direct membrane recycling. My sincere gratitude to Mikrolin Hungary Ltd., company for completing the polypropylene recycling process and supply. The support received from the E3TECH Excellence Network under project CTQ2017- 90659-REDT (MCIUN, Spain) is recognized. This work was also supported by the Associate Laboratory for Green Chemistry – LAQV which is financed by national Portuguese funds from FCT/MCTES (UIDB/50006/2020).

I would like to express my sincere gratitude to the Institute of Polymer Science and Technology of the Spanish National Research Council (ICTP-CSIC), for the close collaboration maintained during these years. As well as, to the section Process Engineering for Sustainable Systems (PROCESS) at KU Leuven, and to the LAQV-REQUIMTE, Department of Chemistry at NOVA School of Science and Technology (FCT, Universidade NOVA de Lisboa), for hosting me as a visiting scholar in their institutions, where a substantial part of the presented investigation was carried out. Lastly, the

support from the University of Alcalá and IMDEA Water are particularly acknowledged.

Como todo trabajo de investigación, esta tesis es el fruto de la colaboración entre muchas personas e instituciones, a las cuales quiero expresar mi agradecimiento en estas últimas líneas.

En primer lugar, al instituto IMDEA Agua por haberme dado la oportunidad de realizar este trabajo y por todo el apoyo recibido durante estos años. En especial a nuestro director y jefe de línea, Prof. Eloy García-Calvo.

Muy en especial a mis directores de tesis, Dra. Serena Molina y Dr. Juan Manuel Ortiz, porque sin ellos esta tesis no habría sido posible. A Serena, por confiar en mi para realizar este trabajo, por su indispensable ayuda para el desarrollo de la metodología de elaboración de las membranas y por su gran apoyo durante todos estos años. A Juanma, por hacer que la electroquímica parezca sencilla, por explicarme sus ideas y por ilustrarme con su gran devoción por la ciencia. Quiero agradecer a ambos toda su dedicación durante estos años y todas sus revisiones y correcciones, las cuales han mejorado sustancialmente este trabajo. He tenido la suerte de contar con su cercanía y disponibilidad, sin olvidarme del *coaching*, tan necesario durante estos años de formación como investigadora.

Quisiera agradecer al Dr. Rodrigo Navarro, por toda su ayuda y dedicación, durante el desarrollo de la metodología de elaboración de las membranas. Por su colaboración durante todos estos años y por realizar los análisis sobre las propiedades mecánicas de las membranas (Capítulo 3) y los análisis de ATR-FTIR (Capítulo 7).

I would like to acknowledge Prof. Bart Van der Bruggen for giving me the opportunity to work in his research group at KU Leuven. To Dr. Yan Zhao, for teaching so many things (including how to write my first paper), for our fruitful collaboration, as well as, for introducing me into the group.

I am grateful to Prof. João G. Crespo and Prof. Svetlozar Velizarov, for all their support during my stay at FCT-UNL and afterwards, and for their important contribution to bring the last work of this thesis to a successful

outcome. I am very grateful that I was accepted to work in their research group even under the complicated pandemic situation that we lived in 2020. I would like to acknowledge Dr Sylwin Pawlowski and Dr Claudia F. Galinha, for conducting all the statistical analysis related to 2D fluorescence spectroscopy, for our scientific discussions, for their interest in this work and for their great contribution to improve the manuscript. I would like to express my gratitude to Dr Vanessa Otero for accepting the challenging work that was proposed to her regarding the confocal micro-Raman analysis and for her contribution to this last work.

A todo el grupo de Tecnología de Membranas de IMDEA, en especial a la Dra. Junkal Landaburu-Aguirre, por aceptarme en su grupo de investigación y a la Dra. Raquel García-Pacheco, por ser una fuente de inspiración en el mundo del reciclaje de membranas. A Jorge por ayudarme a mejorar mis presentaciones y gráficos, pero, sobre todo, por todo el tiempo compartido tanto dentro como fuera de IMDEA. A Laura y Helena, por todo el tiempo compartido entre oficina y laboratorios y a Anamary, por dar continuidad a este trabajo.

A todos los compañeros y excompañeros de IMDEA Agua, con los que he compartido grandes momentos tanto dentro como fuera del instituto, por hacer del instituto un lugar más agradable en el que trabajar. En especial a todo el grupo de Bioe, por permitirme intrusiones constantes en su laboratorio, resolver un millón de mis dudas y proporcionarme muchos de los materiales que he necesitado para llevar a cabo este trabajo. Muy en especial a Marina, por su increíble disponibilidad para ayudarme durante todos estos años, demostrando una paciencia infinita y una gran dedicación a la investigación. También a los compañeros de Ecotoxicología, con los que he tenido la suerte de compartir grandes momentos, sobre todo fuera del trabajo. Muy en especial a Alba por compartir conmigo todos estos años y por todas las aventuras que hemos vivido juntas.

A los amigos que me han brindado su apoyo durante estos años. A la familia, en especial a mi aita, Fiden, y a mi ama, Marta, por facilitarme el

camino. A Arantza por visitarme allá donde esta tesis me ha llevado. A Ania, por todo su cariño y a David por diseñar la portada de esta tesis. A Eric, por acompañarme en este viaje. Por todo, gracias.

"'We never know the worth of water till the well is dry."

– Thomas Fuller'

"Nothing in life is to be feared, it is only to be understood. Now is the time to understand more, so that we may fear less."

– Marie Skłodowska-Curie

A mi familia

Contents

List of Figures

List of Supplementary Figures

List of Tables

List of Supplementary Tables

Nomenclature

Abbreviations

800-60	Membrane prepared using Amberlite® IRA-402 ion-exchange resin, 800 μm casting thickness and 60 min solvent evaporation, without mechanical support
ABS	Acrylonitrile butadiene styrene
AC	Alternating Current
Act-Amb-RE	Amb-RE after the activation treatment
AEM	Anion-Exchange Membrane
AFM	Atomic Force Microscopy
Amb	Membrane prepared using Amberlite® IRA-402 ion-exchange resin, without mechanical support
Amb-RE	Membrane prepared using Amberlite® IRA-402 resin, using EoL RO membrane as support
ATR-FTIR	Attenuated Total Reflectance Fourier Transform Infrared Spectroscopy
BWRO	Brackish Water Reverse Osmosis desalination
CC	Constant Current
CEM	Cation-Exchange Membrane
DCMD	Direct Contact Membrane Distillation
DD	Donnan Dialysis
ED	Electrodialysis
EDX	Energy Dispersive X-ray spectroscopy

EEM	Excitation Emission Matrix
EoL	End-of-life
Eq.	Equation
FC	Fuel Cell
Fig.	Figure
FO	Forward Osmosis
IEC	Ion-Exchange Capacity
IEM	Ion-Exchange Membrane
IEMB	Ion-Exchange Membrane Bioreactor
LCD	Limiting Current Density
Lew	Membrane prepared with Lewatit ® Sybron Ionac® SR-7 ion-exchange resin, without mechanical support
Lew-RE	Membrane prepared with Lewatit ® Sybron Ionac® SR-7 ion-exchange resin, using EoL RO membrane as support
MC	Microcistyn
NF	Nanofiltration
PA	Polyamide
PCA	Principal Component Analysis
PET	Polyester
PP	Polypropylene
PSF	Polysulfone
Pur	Membrane prepared using Purolite ® A600/9413 ion-exchange resin, without mechanical support

Pur-RE	Membrane prepared using Purolite ® A600/9413 ion-exchange resin, using EoL RO membrane as support
PVC	Polyvinylchloride
r-800-60	Membrane prepared using Amberlite® IRA-402 ion-exchange resin, 800 μm casting thickness and 60 min solvent evaporation, using EoL RO membrane as support
RED	Reverse Electrodialysis
RE-UF	Recycled ultrafiltration-like membrane
RO	Reverse Osmosis
SEM	Scanning Electron Microscopy
SWRO	Sea Water Reverse Osmosis desalination
TFC	Thin Film Composite
THF	Tetrahydrofuran
UF	Ultrafiltration
WC	Water content
WCA	Water Contact Angle

Symbols

P_A^B	Permselectivity towards B in respect to A
$\Delta n_{dil,}$	Variation of the mol number in the dilute compartment
ΔV_m	Measured potential difference (V)
ΔV_t	Theoretical potential difference (V)
A	Area
a_i	Activity coefficient of the ion i

C_i	Concentration of component i
D	Diffusion coefficient
E	Energy consumption ($kWh \cdot m^{-3}$)
E_m	Potential difference (V)
I	Current (A)
I_d	Current density ($mA \cdot cm^2$)
J_w	Flux of fresh water, freshwater production or nominal desalination rate ($L \cdot m^{-2} \cdot h^{-1}$)
J_i	Flux of the component i ($mol \cdot m^{-2} \cdot h^{-1}$)
l	Thickness
q	Circulated charge ($Cul \cdot m^{-3}$)
R	Electrical resistance (Ω)
R_m	Membrane electrical resistance ($\Omega \cdot cm^2$)
S	Separation Efficiency (%)
t_i^m	Ion transport number in the membrane phase
W_{dry}	Weight of dry membrane (g)
W_{wet}	Weight of wet membrane (g)
z_i	Ion charge
α	Permselectivity (%)
η	Current efficiency (%)

I. Resumen

El continuo aumento del número de membranas de Osmosis Inversa (OI) desechadas anualmente genera un gran problema medioambiental. En este contexto, el desarrollo de alternativas que permitan su reutilización y reciclaje contribuye a la reducción de los residuos generados en los procesos de desalación y promueve la transición hacia la economía circular en el sector del agua. Estudios previos han abordado la reutilización y el reciclaje directo de las membranas. Sin embargo, el reciclaje indirecto, mediante la apertura del módulo y la extracción y gestión individualizada de sus componentes puede suponer una alternativa más adecuada cuando las membranas presentan un gran deterioro. El objetivo de esta tesis doctoral es el reciclaje indirecto de membranas de OI desechadas como membranas de intercambio aniónico, y su validación en diferentes procesos para el tratamiento de aguas.

En primer lugar, se desarrolló la metodología de preparación de las membranas de intercambio aniónico. La metodología consistió en extender una disolución polimérica que incorporaba una resina de intercambio iónico sobre el soporte de membrana desechada (previamente acondicionada). Se estudió la influencia del grosor de la mezcla extendida y el tiempo de evaporación del disolvente en las propiedades de las membranas y se realizó una caracterización completa de las membranas, con el objetivo de identificar las condiciones de preparación más adecuadas. Mediante esta técnica, se obtuvieron membranas con una alta permselectividad (87 %). Sin embargo, su resistencia eléctrica era relativamente alta (77 $\Omega \cdot cm^2$), lo que se tradujo en consumo energético relativamente elevado derivado de su uso en electrodiálisis. A pesar de ello, se verificó la viabilidad técnica de las membranas en desalación de agua salobre mediante electrodiálisis (ED), obteniendo un 84.5 % de eliminación de sales. Además, se abordó el reciclaje de los espaciadores del influente (hechos de polipropileno) y se diseñó una celda de ED a escala de

laboratorio con un 84 % de plástico reciclado (el 54 % del peso total de la celda, considerando también los materiales metálicos).

En segundo lugar, con el objetivo de disminuir la resistencia eléctrica de las membranas preparadas, se desarrolló un postratamiento de activación de bajo coste. El tratamiento consistió en la inmersión consecutiva de las membranas en disoluciones ácidas (HCl) y alcalinas (NaOH). Este tratamiento podría fomentar la disociación en los grupos funcionales de las membranas, haciéndolas más reactivas a los contra-iones. Se estudió el efecto combinado de la concentración y el tiempo de exposición de las disoluciones de ácido y base empleadas, en las propiedades electroquímicas de las membranas. El tratamiento seleccionado alcanzó una reducción del 37 % de la resistencia eléctrica de la membrana respecto al valor original, sin dañar la permselectividad. Además, se estudió el rendimiento de las membranas (antes y después del tratamiento de activación) en ED para la desalación de agua salobre. El tratamiento de activación incrementó la producción de agua potable (de 1.2 a 4.9 $L \cdot h^{-1} \cdot m^{-2}$), y redujo el consumo energético del proceso (de 5.2 a 3.0 $kWh \cdot m^{-3}$), demostrando una mayor eficiencia en la utilización de la corriente (un aumento del 38 % al 71 %).

Posteriormente, se trabajó en el desarrollo de membranas de intercambio aniónico con propiedades monoselectivas, con el objetivo de ampliar las posibles aplicaciones de las membranas desarrolladas. Para ello, se estudió la modificación superficial de membranas de intercambio aniónico comerciales. Esta modificación se basó en la bioquímica de adhesión de los moluscos bivalvos al sustrato y en reacciones de amino condensación. Se analizó la química superficial de la membrana mediante diferentes técnicas de caracterización y se llevaron a cabo experimentos de desalación para evaluar la selectividad de la membrana modificada hacia aniones monovalentes. La membrana modificada demostró mayor selectividad que la membrana original, alcanzando una eficiencia de separación entre iones multivalentes (SO_4^{2-}) y monovalentes (Cl^-) (S_{60} (%))

del 17 %, frente al 5 % en la membrana original. El recubrimiento, que se demostró estable frente a la aplicación de un potencial eléctrico inverso, otorgó a las membranas mayor resistencia frente al ensuciamiento orgánico.

Dada la creciente contaminación por altas concentraciones de nitrato en las masas de agua naturales, es necesario desarrollar nuevas tecnologías que permitan su separación selectiva. Bajo este contexto, se prepararon membranas de intercambio aniónico con afinidad hacia el ion nitrato, a partir de membranas de OI desechadas, utilizando diferentes resinas de intercambio iónico. Se estudió la influencia en la separación selectiva de los contra-iones del i) tipo de resina de intercambio iónico utilizada, ii) la utilización de la membrana desechada de OI como soporte, y iii) la densidad de corriente aplicada durante los experimentos de electro-separación. Los resultados demostraron que el tipo de resina de intercambio iónico utilizada puede modificar los números de transporte de los aniones en la membrana, aumentando el número de transporte del nitrato (t_i^m, 0.48), en detrimento del número de transporte del sulfato (t_i^m, 0.23), lo que podría facilitar su separación selectiva de mezclas multicomponentes.

Finalmente, se estudió la aplicación de las membranas de intercambio iónico previamente desarrolladas, en los sistemas de diálisis de Donnan (DD) y biorreactor de membranas de intercambio iónico (IEMB), para la eliminación de nitrato de un agua contaminada, con el objetivo de alcanzar calidades de agua aptas para su consumo. Se estudió la distribución de los grupos de intercambio iónico en la sección de la membrana mediante microscopía Raman confocal. Se evaluó la estabilidad de las membranas frente a un tratamiento de limpieza químico y frente al ensuciamiento orgánico mediante espectroscopia de fluorescencia 2D y el análisis estadístico de los resultados (análisis de componentes principales). La membrana preparada con la resina Purolite® A600/9149 (Pur-RE) demostró la mayor estabilidad y el mejor rendimiento en el transporte de nitrato,

alcanzando una media del 56 % de eliminación en 24 h. La implementación de un biorreactor en el sistema de IEMB, permitió además la eliminación del nitrato mediante desnitrificación biológica. Debido a la naturaleza difusiva del transporte iónico en estos procesos, se minimiza la energía requerida para llevarlos a cabo., lo que podría contribuir a la implementación de estas membranas. Además, el coste relativamente bajo de los materiales utilizados en la preparación de las membranas podría suponer un beneficio económico en la implementación del concepto de reciclaje de membranas presentado en esta tesis.

De forma complementaria, se estudió la adecuación de otros materiales reciclados (provenientes del módulo de OI desechado) para la preparación de membranas En este estudio se concluyó que, bajo las condiciones estudiadas, la membrana desechada después de una alta dosis de NaClO, era el soporte más adecuado para la preparación membranas de intercambio iónico.

En conclusión, esta tesis doctoral presenta una innovadora metodología que permite el reciclaje indirecto de las membranas de OI al final de su vida útil para la preparación de membranas de intercambio aniónico, y demuestra la viabilidad técnica de las membranas preparadas en diferentes procesos de tratamiento de aguas. Esta investigación pretende, por lo tanto, contribuir a la transición hacia una economía circular, como parte de los objetivos establecidos por la Comisión Europea a través del el Pacto Verde Europeo.

II. Abstract

The increasing number of end-of-life (EoL) Reverse Osmosis (RO) membrane modules yearly dumped in landfills comprises an important environmental concern. In this context, the development of innovative membrane reuse and recycling alternatives can help reducing the waste generation and fostering the transition towards a circular economy in the water sector. Previous studies have been devoted to the development of membrane reuse and direct recycling alternatives. Whilst, in the case of excessively damaged membranes, an indirect recycling approach could be a more suitable alternative. Indirect recycling entails the deconstruction of the RO module, allowing for the individual management of membranes and plastic components. This thesis aims to develop a new methodology to enable the indirect recycling of EoL RO membranes as Anion-Exchange Membranes (AEMs), and to validate the technical feasibility of the prepared membranes for different water treatment processes.

Firstly, membrane preparation methodology was developed. The AEMs were prepared by casting and phase inversion methods, using the preconditioned EoL RO membranes as supporting material. The influence of the casting thickness and the solvent evaporation time in membrane properties was studied. Besides, a complete membrane characterization was carried out, to select the optimum membrane preparation conditions. The selected combination resulted in AEMs with a high permselectivity (87 %), although the electrical resistance was relatively high (77 $\Omega \cdot cm^2$), which increased the energy consumption associated to their use in electrodialysis (ED). Despite, the technical viability of the membranes in brackish water desalination by electrodialysis (ED) was successfully validated, achieving an 84.5 % of salt removal. Furthermore, the management of the polypropylene (PP) feed spacers from the EoL RO module was undertaken, as a result, a laboratory ED stack with an 84 % of

recycled plastic (54 % of the total weight of the stack, also considering the metallic components) was designed.

Secondly, with the aim to reduce the electrical resistance of the prepared membranes a low-cost activation treatment was developed. The activation treatment consisted of the subsequent immersion of the membranes in diluted acid (HCl) and alkali (NaOH) solutions. This treatment could promote the complete dissociation of the functional groups in the membrane, making them more reactive to the counter-ions. The effect of acid and alkali concentrations and exposition times on the electrochemical properties were studied, in order to select the most suitable combination. In such a way, 37 % reduction of the membrane electrical resistance was achieved, in respect to the original value. The performance of activated and non-activated membranes in brackish water desalination by ED was compared. Results showed that the proposed activation treatment increased freshwater production in more than four-fold (from 1.2 to 4.9 L $h^{-1}m^{-2}$), with a considerable reduction of energy consumption (from 5.2 to 3.0 $kWh \cdot m^{-3}$) and a great improvement in the current utilization efficiency (from 38 % to 71 %).

Thirdly, with the objective to broaden the applications of the developed membranes, monovalent selective AEMs were prepared by surface modification of commercial ones. For that purpose, a two-step modification process, based on mussel inspired surface biochemistry and amide condensation reactions, was conducted. The membrane surface chemistry was investigated by different characterization techniques. Desalination experiments were conducted to evaluate the selectivity of the membrane towards monovalent anions. The resulting membrane showed an enhanced separation efficiency between multivalent (SO_4^{2-}) and monovalent (Cl^-) counter-ions in comparison with the original membrane (S_{60} 17 %, in respect to a 5 %, in the original membrane). The stability of the coating was successfully evaluated by the application of a reverse electric

field in ED. In addition, the resulting membrane acquired an increased resistance to organic fouling.

The increasing pollution of nitrate in natural waters, reinforces the demand of alternative technologies to enable its selective separation. In this context, AEMs with a high affinity for nitrates were prepared, using the EoL RO membranes as support. Different ion-exchange resins were tested for the preparation of the membranes and the influence in ion fractionation of i) the type of ion-exchange resin, ii) the use of the EoL RO membrane as support, and iii) the operating current density during the separation process were studied. Results revealed that the employed anion-exchange resin could tune up the transport numbers of the anions in the membrane and enhance the transport of nitrates (t_i^m, 0.48) over sulphates (t_i^m, 0.23), thus facilitating the fractionation of the counter-ions.

Subsequently, the developed AEMs were tested under Donnan dialysis (DD) and related processes, such as the Ion-Exchange Membrane Bioreactor (IEMB). In an effort to gain a better understanding of such AEMs, confocal μ-Raman spectroscopy was employed to assess the distribution of the ion-exchange sites through the thickness of the membrane. In addition, 2D fluorescence spectroscopy was used to evaluate alterations in the membranes caused by fouling and chemical cleaning. Among the prepared AEMs, the one with Purolite ion-exchange resin (Pur-RE) demonstrated the best stability and the highest performance for nitrate removal, reaching a 56 % average of removal within 24 h in DD and the IEMB systems, with the latter furthermore allowing for the simultaneous complete elimination of the pollutant by biological denitrification, avoiding therefore its discharge into the environment. Due to the diffusive nature of the ionic transport, such processes are operated at a minimum energy requirement. In addition, the use of the RO upcycled AEMs could bring about a more affordable alternative than the use of commercial membranes.

Complementarity, the use of different components of the EoL RO module (i.e., membranes after different pretreatments and permeate

spacers) for the preparation of AEMs was attempted. In that respect, the membrane prepared using the EoL RO, after a high exposure dose to sodium hypochlorite (NaClO) (i.e., with UF-like properties) achieved the best electrochemical properties.

Overall, the present doctoral thesis presents an innovative methodology to enable the indirect recycling EoL RO membranes as AEMs and demonstrates the technical feasibility of using the developed membranes for different water treatment processes. Therefore, it attempts to contribute to the transition to a circular economy, as part of the objectives of the European Commission in sustainable growth set trough the European Green Deal.

III. List of publications

This thesis is based on the publications listed below.

Scientific paper 1 (published), as Chapter 3

A. Lejarazu-Larrañaga, S. Molina, J. M. Ortiz, R. Navarro, E. García-Calvo, Circular economy in membrane technology: Using end-of-life reverse osmosis modules for preparation of recycled anion-exchange membranes and validation in electrodialysis, J. Memb. Sci. 593 (2020) 117423. http://doi:10.1016/j.memsci.2019.117423.

Scientific paper 2 (published), as Chapter 4

A. Lejarazu-Larrañaga, S. Molina, J. M. Ortiz, G. Riccardelli, E. García-Calvo, Influence of acid/base activation treatment in the performance of recycled electromembrane for freshwater production by electrodialysis, Chemosphere. 248 (2020). http://doi:10.1016/j.chemosphere.2020.126027.

Scientific paper 3 (published), as Chapter 5

A. Lejarazu-Larrañaga, Y. Zhao, S. Molina, E. García-Calvo, B. Van der Bruggen, Alternating current enhanced deposition of a monovalent selective coating for anion-exchange membranes with antifouling properties, Sep. Purif. Technol. 229 (2019) 115807. http://doi:10.1016/j.seppur.2019.115807.

Scientific paper 4 (published), as Chapter 6

A. Lejarazu-Larrañaga, J. M. Ortiz, S. Molina, Y. Zhao and E. García-Calvo, Nitrate-Selective Anion-Exchange Membranes Prepared using Discarded Reverse Osmosis Membranes as Support, Membranes 10 (2020) 377. https://doi.org/10.3390/membranes10120377.

Scientific paper 5 (published), as Chapter 7

A. Lejarazu-Larrañaga, J. M. Ortiz, S. Molina, S. Pawlowski, C. F. Galinha, V. Otero, E. García-Calvo, S. Velizarov, J. G. Crespo, Nitrate removal by Donnan Dialysis and Ion-Exchange Membrane Bioreactor using upcycled end-of-life Reverse Osmosis membranes as Anion-Exchange Membranes, Membranes 12 (2022) 101. https://doi.org/10.3390/membranes12020101

Book chapter 1 (published), as Appendix A

A. Lejarazu-Larrañaga, S. Molina, J. M. Ortiz, E. García-Calvo, Preparación de membranas de intercambio iónico sobre soportes reciclados de membranas desechadas, VIII Jornadas de Jóvenes Investigadores de la UAH (pp. 207-215), Universidad de Alcalá, Ed.: Alcalá de Henares, Spain, 2021; ISBN 978-84-18254-50-5.

1

Chapter 1. General introduction

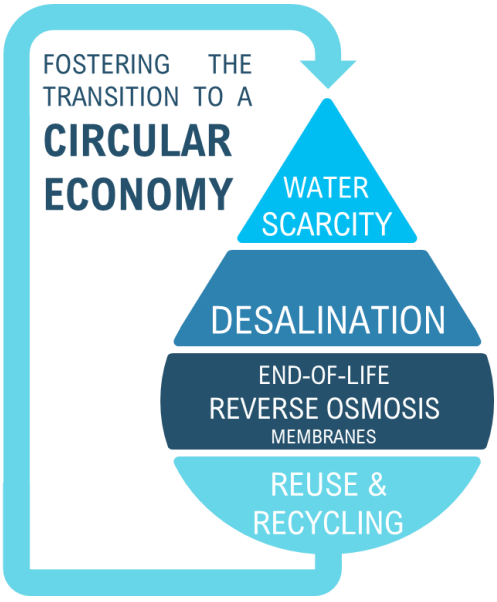

1.1. Water scarcity and pollution

Freshwater is one of the most vital natural resources in the world. However, it accounts only for the 3 % of the total water in the planet. Moreover, only the 0.7 % of the freshwater is easily available as surface water, while the rest is frozen in poles, in the atmosphere, or filling deep aquifers (Fig. 1) [1].

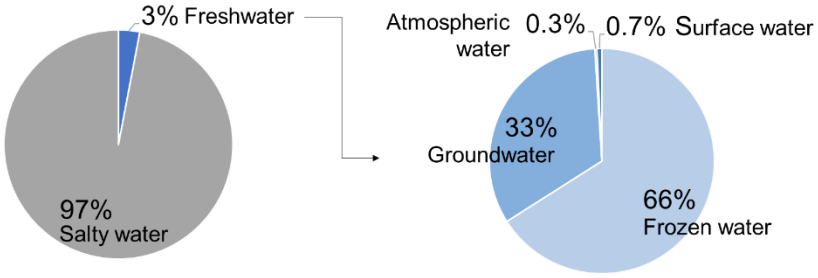

Figure 1. Distribution of the global water sources [1].

The search for an adequate freshwater supply has define historically demographic distribution, as freshwater is essential for all human activities [2]. On the one hand, climate change and consequent variations in precipitations and temperatures, have accelerated and intensified droughts and desertification processes. On the other hand, population and economic growth have raised water consumption, pushing an increased number of people to face water scarcity [3]. Water demand has grown 6 folds in the last century and it is expected to keep growing in the future, as the current water management patters remain unchanged [2]. In addition, the increasing anthropogenic pollution of the water sources exacerbates water scarcity. Under this scenario, it is estimated that currently 4.0 billion of people (two thirds of the global population) live under severe water scarcity conditions for at least one month a year, and 0.5 billion of people face severe water scarcity all year round. [4]. As a result, water scarcity (in terms of quantity and quality) has become one of the most challenging issues facing humanity in the 21st century [1,5].

There are many interconnected factors influencing freshwater availability, roughly represented in Fig. 2.

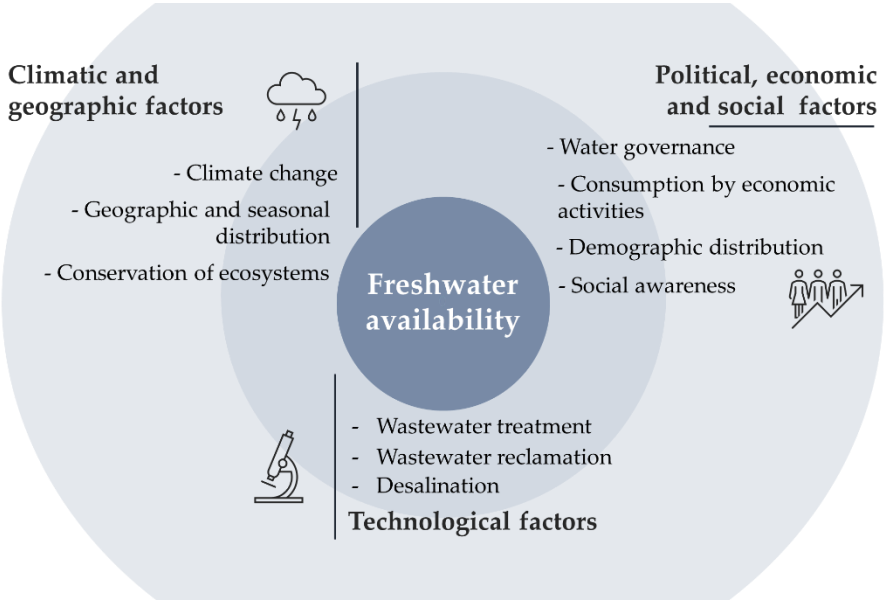

Figure 2. Conceptual scheme of the main factors influencing freshwater availability.

Nowadays, desalination is frequently employed to increase freshwater availability in water scarce areas. To illustrate, it is estimated that more than the 1 % of the total consumed fresh water in the world is produced by desalination to date [6]. The following section presents a global outlook of desalination with a special focus on RO technology.

1.2. Desalination

Desalination is the process by which salts are removed from the sea or the brackish water (SW and BW, respectively), producing a high-quality water for irrigation, domestic or industrial usage.

Before the 1990s, thermal desalination processes such as Multi-Stage Flash (MSF) and Multi-Effect Distillation (MED) dominated the desalination market. However, thermal desalination is highly energy intensive process and thus, its practical application has been mainly limited

to oil-rich but water scarce countries located in the Middle East [7]. Even to date, almost half of the installed desalination capacity (47.5 %) belongs to Middle East and North Africa regions [7]. The development of more efficient membrane-based desalination technologies has dropped the energy consumption of desalination, making it a more affordable alternative for freshwater supply [8]. Since 1990s, the cost of RO desalination became lower than MSF desalination. Currently, RO is the most energy efficient desalination technology, [9] and consequently, it is nowadays the most widely used, accounting in 2018 for the 84 % share of the total number of operational desalination plants, and entailing the 69 % of the total desalinated water produced in the world (Fig. 3) [7].

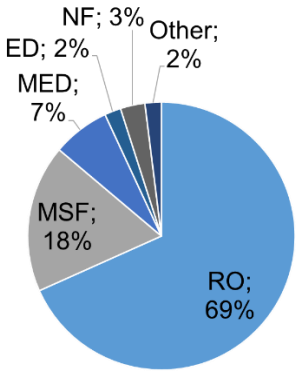

Figure 3. Installed desalination capacity by technology in 2018 [7]. MSF, Multi-stage flash distillation; MED, Multi-effect distillation; ED, Electrodialysis; NF, Nanofiltration.

The increasing freshwater scarcity to meet the water demand keeps the desalination market rising constantly [10,11]. To illustrate, in 2018, more than 15,906 desalination plants were operating in over 150 countries, producing approximately 95.37 million $m^3 \cdot day^{-1}$ of freshwater [7]. Only one year after, in 2019, the total number of installed desalination plants was reported as 21,123, with a freshwater production capacity of approximately 126.57 million $m^3 \cdot day^{-1}$ [11], entailing therefore an increase of almost 30 % of the installed capacity. Furthermore, RO desalination is forecasted to

grow at a constant Compound Annual Growth Rate (CAGR) of around 10.6 % over the period 2018-2025 [12].

In spite of increasing freshwater availability, the use of RO desalination still involves several impacts that should be addressed, such as i) the energy costs associated to desalination (1.5 – 5 $kWh \cdot m^{-3}$), correlated to large greenhouse emissions [13]; ii) the production of brines with a high salt concentration (~ 55 million $m^3 \cdot day^{-1}$) [7]; iii) the costs associated to membrane replacement (~ 13 % of the total cost in SW RO desalination) [14]; and iv) the management of end-of-life (EoL) RO membranes (> 840,000 EoL $modules \cdot year^{-1}$ in 2015) [15].

1.3. Reverse Osmosis membranes

RO membranes are polymeric semipermeable membranes that, under a high working pressure (40–50 bar for SW and 20 bar for BW), are permeable to water while retain salts, dissolved organic matter, viruses and other compounds present in a solution [9]. RO attains a high rejection of monovalent salts (99 - 99.7 % rejection of NaCl [15]), being sea and brackish water desalination are its main applications [16].

The first RO membranes (developed in 1960s), were made of cellulose acetate, while the current market is rather dominated by Thin Film Composite Polyamide (TFC-PA) membranes [17]. TFC membranes are those assembled with several layers of diverse polymeric materials [18]. In the case of TFC-PA RO membranes, a ultrathin dense polyamide layer (PA, ~ 0.2 μm thick, pore size < 1 nm,) acts as the selective layer, supported by a thicker a porous layer such as polysulfone (PSF, ~ 40 μm thick) and a considerably thicker layer as mechanical support, such as non-woven polyester (PET, ~ 100 μm thick) (Fig. 4) [19].

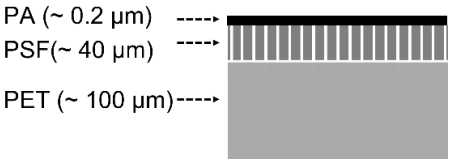

Figure 4. Schematic representation of a TFC-PA RO membrane composition. PA, polyamide; PSF, polysulfone; PET, polyester.

The separation mechanism in RO is different from other pressure driven membranes, where the main separation mechanism is sieving through tiny pores in the membrane. In the case of RO membranes, due to the presence of a dense surface layer, the solutes permeate in the membrane by dissolving in the membrane material and diffusing trough the membrane against the concentration gradient. This transport mechanism is known as solution-diffusion model [20].

At industrial scale, RO membranes are commonly fabricated in a spiral wound module configuration with the objective to increase the membrane area in a reduced space and to confer to the module of a high pressure resistance, as illustrated in Fig. 5 [21]. Apart from the RO membranes, the RO module incorporates other kind of polymeric materials such as, acrylonitrile butadiene styrene (ABS) end caps and permeate tube, polypropylene (PP) feed spacers, polyester (PET) permeate spacers, the fiberglass outer casing, rubber, o rings and some glued parts containing epoxy-like components [22].

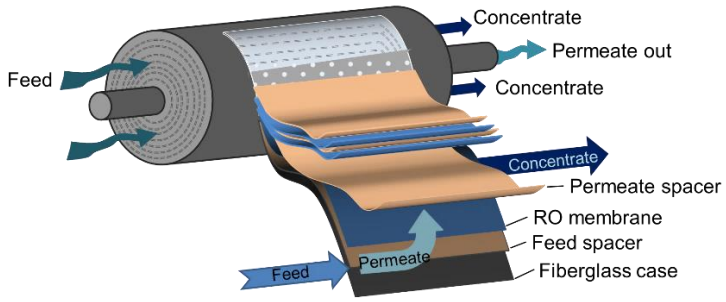

Figure 5. Illustration of a spiral wound RO module. From [21].

1.3.1. Membrane fouling and replacement

Fouling is the deposition of undesired compounds on the membrane surface or inside membrane pores. Based on its nature, fouling can be divided on i) scaling or inorganic fouling, caused by the precipitation of inorganic salts (i.e., calcium sulphate, calcium carbonate); ii) organic fouling, caused by the deposition of organic substances (i.e., humic acids, proteins, lipids); iii) colloidal fouling, which corresponds to the deposition of suspended particles, including inorganic (i.e., aluminium silicates, iron hydroxides), and organic particles (i.e., polysaccharides, proteins); lastly iii) biofouling, caused by the adhesion and growth of microorganisms in the membrane surface, which results in the formation of a biofilm [23].

In RO membranes, fouling leads to a permeability decline, requiring higher working pressures and more frequent cleanings. Thus, it increases the energy costs, accelerates membrane deterioration and subsequently, reduces membrane lifespan [15,23]. In RO desalination, it is estimated an annual membrane replacement rate ranged from 5 %, in the case of Brackish Water RO desalination (BWRO), to 20 % in Sea Water RO desalination (SWRO) [24]. Combined with the installed desalination capacity, J. Landaburu-Aguirre et al. [15], based on the desalination data from 2015, estimated a worldwide annual dischargement of more than 840,000 end-of-life (EoL) RO modules (>14,000 tonnes of plastic waste generation). Considering the forecasted growth rate of the desalination market, J. Senán-Salinas et al. [25], estimated that by 2025 more than 2,000,000 EoL RO

modules might be discarded in the world. Hereby, plastic waste generation and management represent a critical challenge for the sustainable growth of RO desalination industry.

1.4. Membrane technology towards the transition to a circular economy

The European Commission (EC) aims to become the first climate neutral continent in 2050, and advocates for the transition to a sustainable economic model. To achieve such goals, the directive 2008/98/EC on waste [26], stablished a waste management hierarchy, following the principles of a circular economy (Fig. 6a). Later on 2019, the European Green Deal [27], launched a number of transformative policies to foster the transition to a sustainable economic growth. In this regards, the Circular Economy Action Plan [28], provided more specific strategies for the implementation of circular economy principles. Circular economy aims to close the loops of materials and energy, to reduce the pressure on raw materials and waste generation, bringing more sustainability into the economic model.

On contrary to the green policies set by the EC on waste management, the most common fate of EoL RO modules is currently landfill disposal, or less regularly, energy recovery [29]. This situation increases the economic costs and the environmental concerns associated to RO desalination. In this regards, research and innovation are needed to support the transition of membrane technology and related market, towards a circular economy (Fig. 6b).

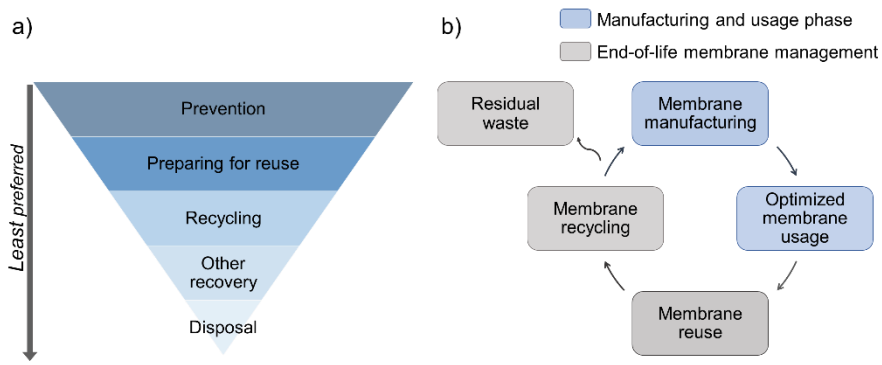

Figure 6. a) Waste prevention and management hierarchy encouraged by the EC trough the directive 2008/98/EC [26], and b) schematic representation of a the application of circular economy principles to membrane technology, adapted from [15].

As depicted in Fig 6b, the transition of membrane technology towards a circular economy requires the involvement of all the membrane lifespan, including: i) revision and upgrading of manufacturing techniques, ii) optimization of the maintenance during their service time, and iii) implementation of reuse and recycling alternatives for the EoL membranes. Hereof, Section 1.4.2 is dedicated to review recent advances in membrane manufacturing, feed pretreatment and membrane cleaning methods, and Section 1.4.3. reviews leading edge membrane reuse and recycling methodologies., giving also brief insights of currently employed membrane management routes (landfill disposal and energy recovery).

1.4.1. Main limitations and expected impacts of the implementation of EoL RO reuse and recycling alternatives

In spite of the proven technical feasibility of membrane reuse and recycling alternatives (further detailed in Section 1.4.3.), these management options are rarely applied at industrial scale to date [30]. The main limitations for their implementation might be related to the actual policies and social context, while solutions to tackle them in the near future are summarized in Fig.7

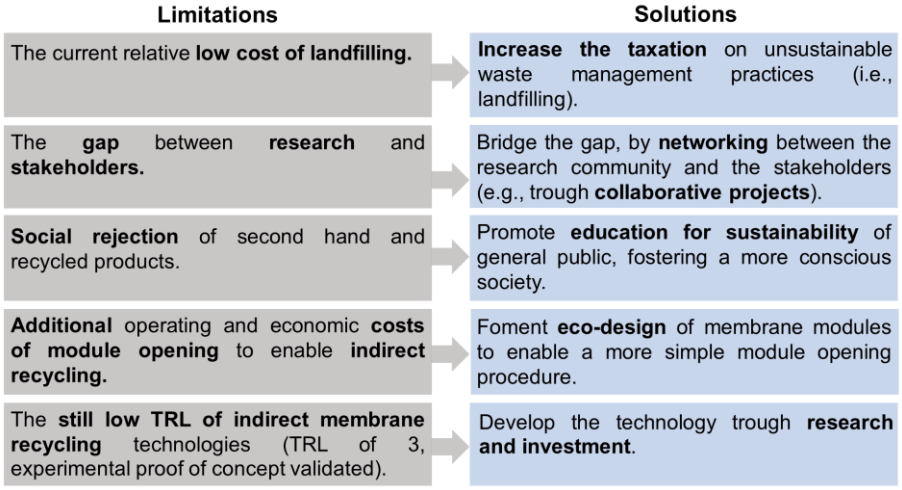

Figure 7. Main limitations and potential solutions to bring membrane recycling technologies to the market. TRL, Technology Readiness Level.

The implementation of membrane reuse and recycling alternatives might result in a number of positive impacts, briefly analysed in Fig. 8. For instance, it might contribute to a greener economic growth, while increasing the social awareness on sustainability trough the dissemination of the research findings, as well as, reducing waste generation and environmental impact associated to RO desalination.

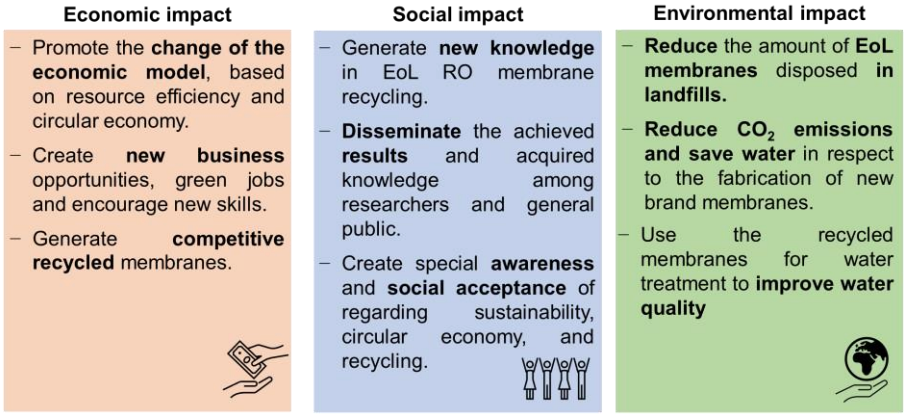

Figure 8. Expected economic, social, and environmental impacts of implementing membrane reuse and recycling alternatives.

In conclusion, membrane-based processes should be revised to better approach the objectives of the EC on sustainable economic growth. In spite of the proven technical feasibility of reuse and recycling alternatives, social and economic limitations have been encountered for the implementation of such technologies. Hence, indicating the urgency to bridge the gap between science, social and industrial stakeholders. The implementation of leading-edge membrane reuse and recycling technologies could help increasing the service time of the membranes and hence, reducing pressure on raw materials and waste generation of membrane-based processes, and promoting the transition towards a circular economy.

1.4.2. RO membrane manufacturing and usage for a circular economy transition

Ecodesign in RO membrane manufacturing

It is estimated that the 80 % of the environmental impacts associated to a product could be reduced at the design stage [31]. Ecodesign involves the consideration of all the environmental impacts related to its lifespan (i.e., manufacturing, usage and EoL management), along with other conventional considerations (i.e., performance, cost, technical feasibility). To apply ecodesign principles to RO membrane design, the following aspects should be considered (Fig. 9).

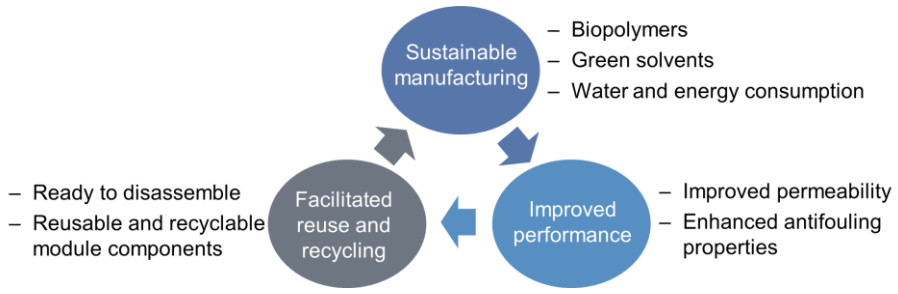

Figure 9. Main aspects to be considered in RO membrane ecodesign.

The integration of ecodesign in RO membrane manufacturing involves a rational replacement of commonly used petroleum-based polymers (i.e.,

PET, PSF, PA) and organic solvents (i.e., hexane, m-phenyldiamine) by other biobased greener chemicals [32]. Such substitution requires of significant research and technological development. A considerable number of publications have been devoted to the preparation of biobased membranes, however, industrial applications of such membranes have not been addressed yet [33]. In addition, ecodesign of RO membrane modules should facilitate the implementation of membrane reuse and recycling strategies once their service time has been expired. For instance, in order to facilitate indirect membrane recycling approach, the modification of the fiberglass casing should be undertaken, in order to simplify the deconstruction process of the RO module. On contrast, most of the research is focused on the prevention of fouling, with the aim to extent the durability of the membranes.

Fouling prevention strategies for an enlarged durability

The prevention and mitigation of fouling ensures an enlarged durability of RO membranes. Commonly applied strategies are the development of antifouling membranes and the implementation of advanced feed pretreatment methods and membrane cleaning protocols, as summarized in Fig. 10.

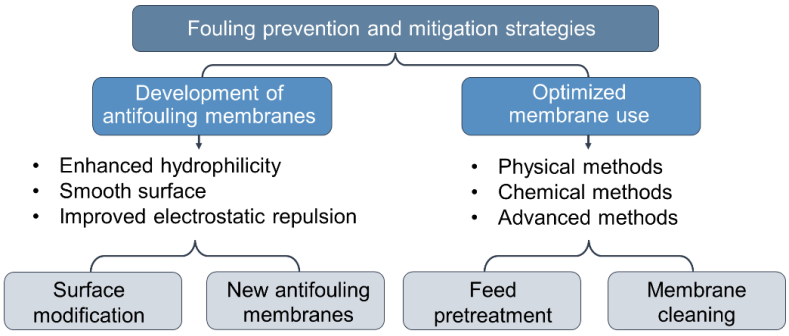

Figure 10. Summary of optimized membrane manufacturing and usage.

Membrane surface characteristics have a great influence on fouling deposition. In such a way, a high hydrophilicity, a smooth surface and enhanced electrostatic repulsion to common foulants results in enhanced

antifouling properties [23,34]. To achieve such properties different strategies can be followed, including surface modification of commercially available RO membranes [35–37], and synthesis of new membranes, which incorporates advanced materials [38], a highly hydrophilic substrate [39], or a highly hydrophilic PA layer [40,41], among others.

Another strategy to reduce fouling at the RO stage is the elimination of the main foulants from the feed during a pretreatment stage. Conventional pretreatment methods require a larger amount of chemicals and a larger space than advanced pretreatment methods, resulting in higher economic costs [42]. Whereas, advanced methods are those based on membrane filtration processes using microfiltration (MF), ultrafiltration (UF) or nanofiltration membranes (NF) [14,15,43]. Membrane-based pretreatment has been demonstrated to be more effective and reduce, in a higher extent, membrane replacement rate at RO stage [14]. It is worth mentioning that feed pretreatment is a potential application for the recycled UF and NF-like membranes [44].

Despite of the improvement on antifouling properties of the membranes, and the implementation of adequate feed pretreatment methods, at last membrane fouling remains inevitable. Cleaning methods are then industrially applied for the reduction of fouling, achieving a partial recovery of the initial hydraulic permeability. Cleaning agents are applied based on the type of fouling to be removed, and include physical (i.e., flushing and backwashing with pressurized water [45]), and chemical cleaning agents (acids, chelating agents, surfactants and biocides [46]). Other advanced physical cleaning methods are based on ultrasonic [47] and electromagnetic fields [48]. Although, frequent cleanings reduce the production of the RO plant, as it has to be stopped for the application of the cleaning protocols.

1.4.3. EoL RO membrane management alternatives

As mentioned, even if fouling mitigation strategies have been developed and are currently applied at industrial scale, at last membrane performance is depleted and membranes are replaced, generating an increasing amount of waste. According to the Life Cycle Assessment performed in [49], EoL RO membrane management should follow the following hierarchy represented in Fig. 11.

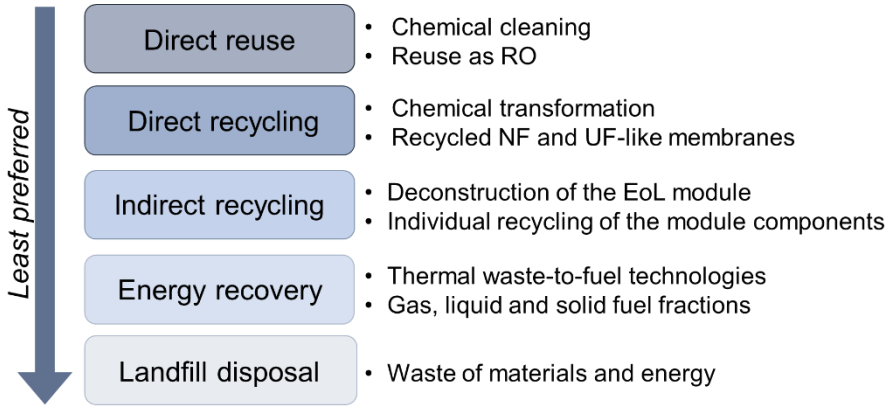

Figure 11. Summary of EoL membrane management alternatives in order of priority, according to [49].

As depicted in Fig. 11, reuse and recycling alternatives should be preferentially attempted. In the last years, such alternatives have been intensively researched [44,50–66]. Nevertheless, landfilling and energy recovery are still the most frequently used practices for EoL RO membrane management.

1.4.3.1. Direct reuse

Direct reuse aims to recover the RO performance (in terms of permeability and salt rejection capacity) by a chemical cleaning, without the intended degradation of the selective PA layer. Previous studies [50], proposed a chemical cleaning based on the use of an alkaline cleaner (i.e., a mix of NaOH, phosphate surfactants and sequesters) followed by an acid cleaner (i.e., a mix of HCl and H_3PO_4). In some cases, a third step might be applied using either oxidizing agents (i.e., H_2O_2), or a second round of the

alkaline treatment (Fig. 12). Those treatments resulted in some alteration of RO salt rejection capacity (i.e., a % rejection change ranged between -29 % to 8 %), along with the enhancement of the membrane permeability (i.e., from ~3 $L \cdot m^{-2} h^{-1}$ in new brand RO elements, up to 261 $L \cdot m^{-2} h^{-1}$ after the cleaning treatment), enabling their reuse in several applications of a lower water quality requirement. The tested applications include, desalination as "sacrifice" membranes (in the first positions of a pressure tube where the effect of fouling is more pronounced) [50], reclaimed water production in tertiary wastewater treatment [50,59], and landfill leachate treatment [60].

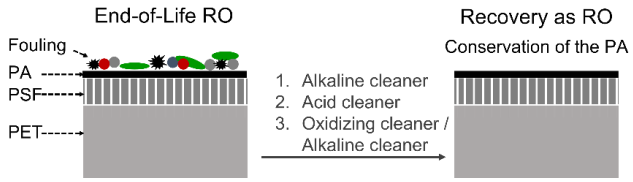

Figure 12. Schematic illustration of EoL RO membrane recovery for direct reuse as RO. PA, polyamide; PSF, polysulfone; PET, polyester.

Nevertheless, EoL membranes frequently present an excessive deterioration for direct reusing purposes (i.e., an excessive reduction of the salt rejection capacity, an excessive amount of fouling or other physical damages). In these cases, membrane recycling is a potential management alternative for EoL RO membranes [29].

1.4.3.2. Direct recycling

Direct recycling aims to modify the filtration properties of EoL RO membranes, to obtain membranes with nanofiltration (NF) or ultrafiltration (UF) properties in terms of salt rejection capacity and hydraulic permeability. PA-TFC RO membrane recycling methodologies have been developed based on the low tolerance of the PA to the exposure to oxidizing agents. In such a way, fouling can be eliminated while the dense PA layer is intentionally degraded either partially, attaining NF properties, or totally, attaining UF properties (see Fig. 13 and Table 1). Since the first studies were conducted in early 2000s, different oxidizing agents have been tested, including H_2O_2, NaOH, K_7MnO_4 and NaClO [61–63]. Among them,

NaClO achieved the greatest permeability increase in the recycled membranes, therefore, it was used in further studies [44,63–65].

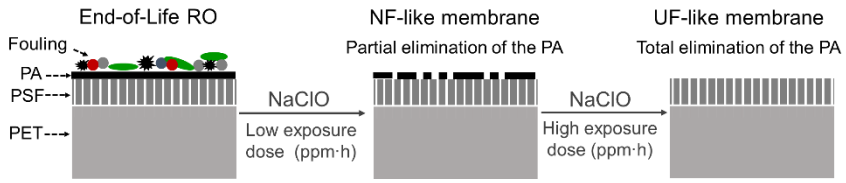

Figure 13. Schematic illustration of EoL RO membrane direct recycling by transformation to NF and UF-like membranes. PA, polyamide; PSF, polysulfone; PET, polyester. Adapted from [44].

Table 1. Main characteristics of RO, NF and UF membranes. From [9,18].

	Reverse Osmosis (RO)	**Nanofiltration (NF)**	**Ultrafiltration (UF)**
Pore size (μm)	<0.001	0.01 - 0.001	0.1 - 0.01
Hydraulic permeability ($L \cdot m^{-2} \cdot h^{-1} \cdot bar^{-1}$)	0.05-1.5	1.5-30	10-1,000
Working pressure (bar)	20 - 50	3 - 20	0.1 - 5
Separation mechanism	Solution-diffusion model	Sieving and charge effect	Sieving effect
Rejection capacity	Monovalent salts.	Multivalent salts, small organic compounds	Macromolecules, bacteria, viruses

The exposure dose needed to reach NF-like properties was ranged between 1,000-150,000 ppm·h, and that to achieve UF-like properties was ranged between 10,000-400,000 ppm·h [67]. There are several factors contributing to those broad exposure dose ranges, including i) the initial conditions of the RO membrane (i.e., the % salt rejection and hydraulic permeability of the EoL membrane); ii) the type of RO membrane (designed for SWRO or BWRO); and iii) storage conditions (i.e., dry-stored membranes need to be pretreatment with an aqueous ethanol solution for the rewetting of the pores [65]). In general terms, highly damaged

membranes and SWRO membranes require a higher exposure dose to the oxidizing agent for the elimination of the PA layer [67].

The surface of recycled NF and UF-like membranes has been extensively characterized and the performance has been evaluated at laboratory and pilot scale [44,63,68,69]. The recycled membranes have been validated for various applications including, i) natural brackish water desalination to produce water of a lower quality requirement (i.e., for irrigation) [44]; ii) as pretreatment of the feed before the RO stage [44]; iii) as fusible or sacrifice membranes in desalination (covering the positions of the RO pressure vessel where fouling is more frequent) [44], iv) as tertiary treatment in wastewater reclamation [61,62], and v) for the production of safe drinking water in a household gravity driven water treatment system [70].

The implementation of membrane reuse and direct recycling alternatives could result in several life services of the RO membranes by a stepwise downcycling process. Afterwards, indirect recycling could be an alternative for spent recycled membranes and for highly damaged EoL RO membranes (chemical or mechanical damage) [29].

1.4.3.3. Indirect recycling

Indirect recycling aims to separate the components of the RO module (plastics and membranes) for an individual management. For that purpose, the spiral wound configuration of module is deconstructed, and membranes and other plastic materials are taken out, as illustrated in Fig. 14. The composition of a conventional 8'' RO module is detailed in Fig. 15. In such a way, plastic components of the EoL RO module could be included in existing recycling routes. For instance, introduction of permeate and feed spacers into the manufacturing of textile material, or conventional recycling of polypropylene (PP) components (i.e., feed spacers) [15,22,29]. In addition, the recovery of flat sheet membranes increases the versatility of membrane recycling and modification alternatives in respect to a close, spiral wound module configuration.

Figure 14. Deconstruction of the EoL RO membrane for its indirect recycling. a) membrane autopsy (taking out membrane coupons) (From [71]), b) end cap, c) fiberglass casing, d) disposition of the feed spacer, RO membrane and permeate spacer in the spiral wound module, e) permeate tube.

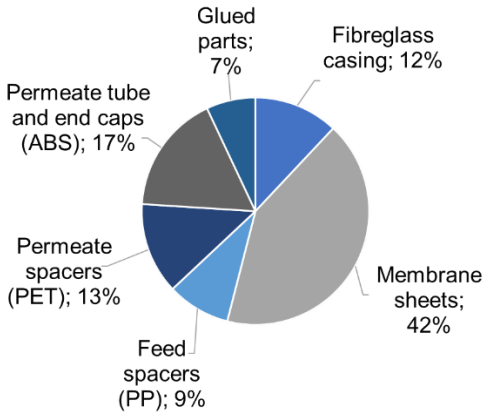

Figure 15. Composition (in percentage by weight) of a conventional 8´´ RO module. ABS, acrylonitrile butadiene styrene; PET, polyester; PP, polypropylene. From [22].

Once the flat sheet EoL membranes have been taken out from the module, a preconditioning step is applied (i.e., a dose exposure to NaClO), in order to eliminate the fouling and to obtain a relatively uniform surface. Afterwards, different membrane modification techniques have been recently investigated, as summarized in Fig. 16. J. Morón-López et al. [51,52,66], developed microcystin (MC) degrading biofilms on the surface of recycled membranes, testing different NaClO exposure doses (Fig. 16a). In this case, a low exposure dose to the oxidizing agent resulted in a greater adhesion of the biofilm to the membrane. The bioactive membranes were used in a Membrane Biofilm Reactor (MBfR), being able to remove 2 ppm MC within 24 h. In addition, this concept was demonstrated to be economically competitive in respect to conventional treatments for MC removal [66]. L. Rodríguez-Sáez et al. [53], modified the surface of preconditioned membranes (after a high exposure dose to NaClO), using biobased compounds (catechol and polyethyleneimine), with the aim to increase the hydrophilicity (and thus, antifouling properties) of the membrane surface. The use of the recycled membranes (the surface modified and the unmodified ones, with UF-like properties), for wastewater treatment in a Membrane Bioreactor (MBR) system was envisaged (Fig. 16b) [53]. J. Contreras et al. [57], modified preconditioned EoL RO membranes (after a high NaClO exposure dose) and permeate spacers, trough electrospinning of a polyvinylidene fluoride nanofibrous layer. The performance of the resulting membranes was tested under direct contact membrane distillation (DCMD) for desalination of brines (Fig. 16c). The modified recycled membranes achieved high salt rejection factors (99.99 %), although, in the case of recycled permeate spacers, a lower performance was found (i.e., low rejection factor). In addition, J. Contreras et al. [58], tested the recycled membranes, after different preconditioning treatments, in Forward Osmosis (FO) application for wastewater treatment. The preconditioned membrane showing the best performance (i.e., after a high exposure dose to NaClO), was further modified by interfacial polymerization adding a thin polyamide (PA) or a polyester (PET) layer

(Fig. 16d). They reported similar morphological and structural characteristics of the recycled membranes in respect to commercial FO membranes. Besides, the rejection of Humic Acids (HA) and salts (NaCl) was higher than in the case of one of the tested commercial FO membranes.

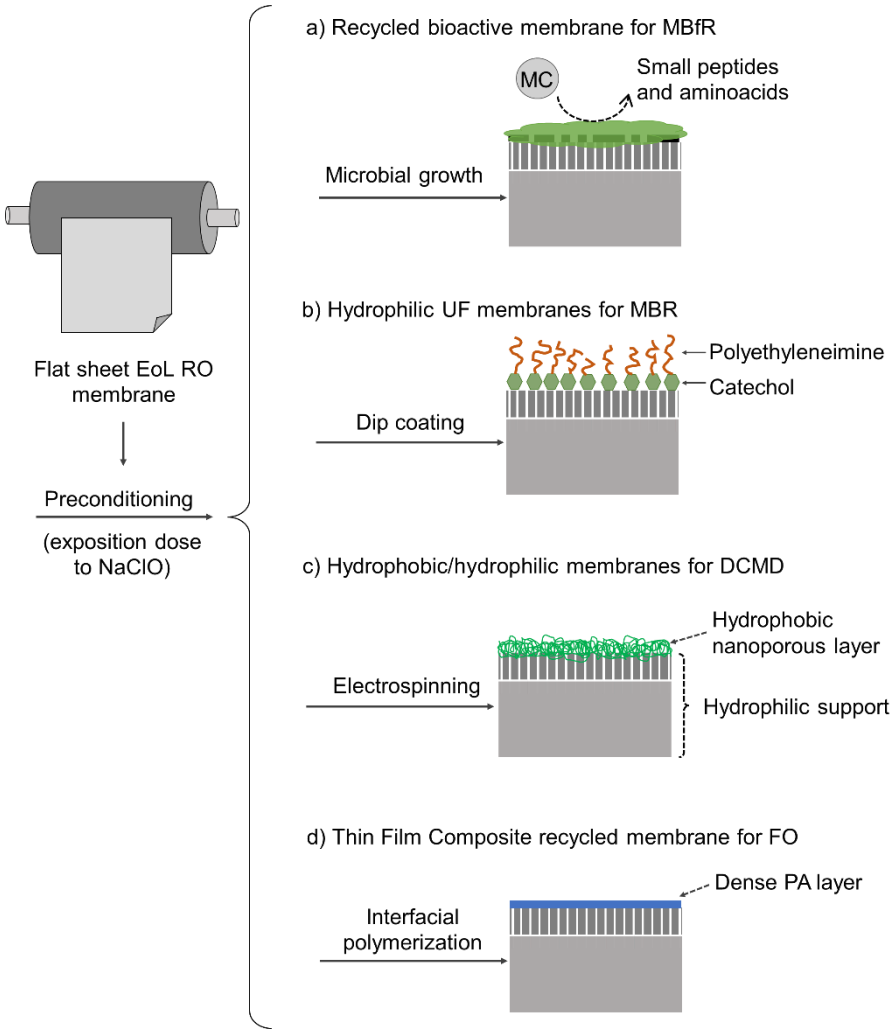

Figure 16. Indirect EoL RO membrane recycling. Schematic representations of membrane modification methodologies for the preparation of a) bioactive membranes for microcystin (MC) removal in MBfR [52], b) hydrophilic membranes for MBR systems [53], c) hydrophobic/hydrophilic membrane for DCMD [57], d) Thin Film Composite membranes for FO application [58].

Another innovative alternative for the indirect recycling of EoL membranes is the development of Ion-Exchange Membranes. Such

alternative has been explored in the present thesis, and therefore it is further detailed in an individual section (Section 1.5.).

1.4.3.4. Energy recovery

When reuse and recycling alternatives are no longer suitable practices, and in the case of spent recycled membranes, energy recovery can help reducing the volume of the waste and recovering the energy contained in plastic materials for an industrial or domestic use [72]. As mentioned above, plastics have an inherent high hydrocarbon content, in particular in EoL RO membrane materials it is ranged between 30 and 88 % [22]. Currently most employed techniques for energy recovery from solid plastic waste are incineration, gasification and pyrolysis [73]. Another alternative is the use of the plastic waste as a partial coke substitute in electric arc furnace steel making processes [22]. Nevertheless, process conditions have to be optimized in order to avoid emissions to air, soil, surface water and groundwater, as well as risks to human health [74]. In addition, the produced gas and liquid fuels commonly require of further upgrading [75]. Nevertheless, several LCA studies have concluded that thermal waste-to-fuel technologies, and specially pyrolysis, involve a lower environmental impact than landfill disposal [73,76].

1.4.3.5. Landfill disposal

Currently, landfill disposal is the most frequent fate of EoL RO membranes [15,49,63]. However, landfilling results in concerning environmental impacts such as, land occupation, generation of greenhouse emissions, the production of toxic leachates (which can contaminate groundwaters), odours and visual impact [77,78], the loss of valuable raw materials and energy [79], and emissions associated to the transport of EoL RO membranes to landfill facilities [25].

1.5. Preparation of Anion-Exchange Membranes from end-of-life Reverse Osmosis membranes

1.5.1. Overview of Ion-Exchange Membranes

Ion-Exchange Membranes (IEMs) are semipermeable membranes containing fixed charged functional groups in the polymer matrix. Such electromembranes have a wide range of applications in different type of processes, including:

– *Electro-membrane separation processes* [80]*:*

Electrodialysis (ED): brackish water desalination, separation of heavy metals from wastewater, concentration of brines and table salt production, among others.

Diffusion dialysis: recovery of acids and bases from a mixture of ions.

Donnan dialysis (DD) and related processes: water softening, elimination of ionic micropollutants from water, and acid recovery in industrial spent streams.

ED with bipolar membranes: production of acid and bases from the corresponding salts.

– *Processes involving an electrochemical reaction for the synthesis of certain chemical products* [81,82]*:*

Electrosynthesis and electrolysis: in chlor-alkali industry to produce chlorine, sodium hydroxide and hypochlorite, among others or in water electrolysis to produce hydrogen and oxygen.

– *Processes for energy production by the conversion of chemical reactions into electrical energy* [83–85]*:*

Fuel cells (FC): to produce energy from the chemical reaction between a fuel (e.g., hydrogen, methanol) with an oxidant (e.g., oxygen).

Redox Flow Batteries: to produce energy from reversible oxidation and reduction reactions of working fluids (e.g., vanadium salts dissolved in concentrated acid solutions).

Reverse Electrodialysis (RED): to produce energy from salinity gradients.

– *Microbial Electrochemical Technologies (METs)* [86,87]:

Microbial Fuel Cells (MFCs): to produce energy from the bioelectrochemical oxidation of chemical compounds (i.e., organic matter).

Microbial Desalination Cells (MDCs): Is the integration of a MFC with ED, and enables to couple wastewater treatment with desalination, avoiding the use of external energy inputs.

Depending on the charge of the fixed functional groups, IEMs can be divided on two main categories:

– Anion-Exchange Membranes (AEMs), containing positively charged functional groups, such as strong basic quaternary amines ($-N^+R_3$) or weak basic tertiary amines ($-NH^+-R_2$).

– Cation-Exchange Membranes (CEMs), containing negatively charged fixed functional groups, such as strong acid sulfonic groups ($-SO_3^-$) or weak acid carboxylic groups ($-COO^-$).

The selectivity of IEMs results from Donnan exclusion effect, which involves the exclusion of the co-ions (ions with the same charge as the membrane), due to the presence of fixed charged functional groups in the membrane. To illustrate, in an AEMs, the anions (counter-ions) can permeate trough the membrane while cations (co-ions) are rejected (Fig. 17). Complementary, in a CEM, cations are transported (counter-ions) while anions (co-ions) are retained by the membrane.

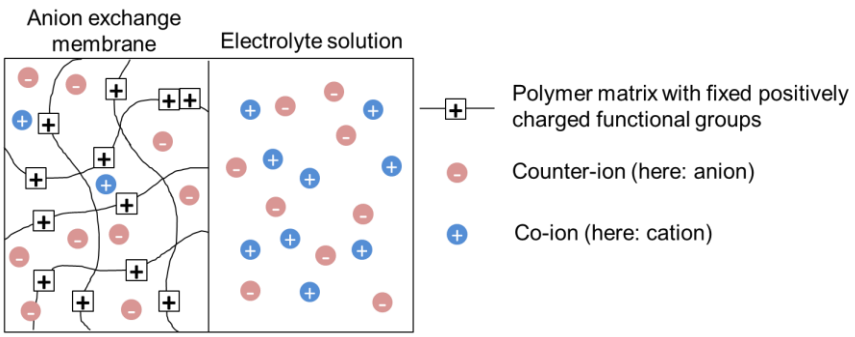

Figure 17. Principle of ionic separation by IEMs. Adapted from [80].

In theory, the concentration of mobile counter-ions in the membrane is approached to the fixed charged density of the membrane. Nevertheless, in practical applications other effects such as the hydration radii of the ions, steric effects, and distribution of the fixed functional groups in the membrane, should be also considered. In general terms, multivalent ions have a lower mobility than monovalent ions in the membrane, and ions with lower hydrated radii have a higher mobility than highly hydrated ions [80]. Membrane permselectivity is also affected by the characteristics of the solutions surrounding the membrane and concentration polarization effects [88].

1.5.2. Homogeneous and Heterogeneous Ion-Exchange Membranes

Regarding the distribution of the functional groups in the membrane homogeneous and heterogenous membranes can be distinguished. Homogeneous IEMs are prepared by introducing an ionic moiety directly on the polymer matrix. This results in a relatively homogenous and uniform distribution of the ion-exchange sites over the entire membrane and facilitates the transport of the counter-ions trough the membrane. On contrast, heterogeneous IEMs are prepared by mixing a finely grounded ion-exchange resin with an uncharged polymer binder, which results in an uneven distribution of the ion-exchange sites in the membrane matrix and could generate a tortuous path of the counter-ions trough the membrane (Fig. 18) [85]. Due to the presence of non-conducting regions, heterogeneous membranes usually have a higher electrical resistance in comparison to homogenous ones. Despite, they exhibit generally better mechanical properties and a lower cost of production than homogenous membranes [89].

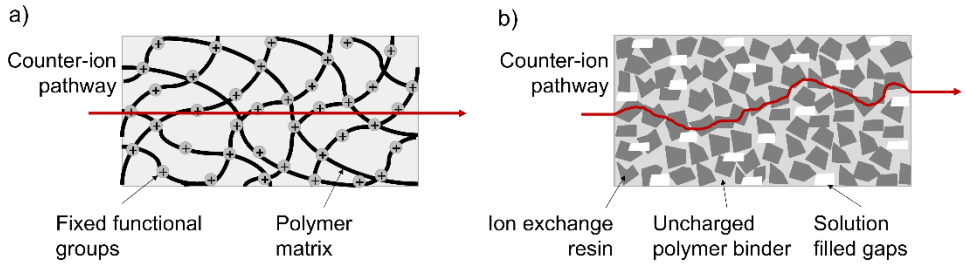

Figure 18. Schematic representation of the counter-ion pathways in a) homogeneous IEM, b) heterogeneous IEM. Adapted from [85].

Membrane properties play an essential role in the process performance. In this relation, ideal properties of an IEM are a high permselectivity, a low electrical resistance, good mechanical, chemical and thermal resistance, and a low production cost. Nevertheless, it is challenging to optimize these properties as they have, in general, a counter acting effect to each other, and thus a compromise needs to be arranged. For instance, membrane permselectivity can be upgraded by increasing the crosslinking of the polymer matrix, however, a highly crosslinked membrane will lead to a high electrical resistance, resulting in an increased energy consumption of the separation process [90].

1.5.3. Selective Ion-Exchange Membranes.

Conventional IEMs are used to separate anions and cations, but monovalent and multivalent ions are exchanged indiscriminately [91]. Whereas for certain applications target ions need to be removed from a solution and therefore, a speciation between differently charged ions is required. For instance, the extraction of lithium (Li^+) from brines [92,93]; the separation of specific ions from industrial wastewater [94,95]; the recovery of nutrients from RO brines in the food industry, or from urban wastewater [96,97] are examples where monovalent selective membranes facilitate the extraction of valuable compounds from waste streams. Monovalent selectivity is also required for the production of safe drinking water from surface water and groundwater when it is polluted with toxic anions, such as fluoride (F^-) [98] or nitrate (NO_3^-) [99].

The preparation of IEMs with selectivity to specific counter-ions has been intensively researched since the 1950s [80,100]. Despite this, the achievement of membranes with high permselectivity to specific ions together with other desired membrane properties (low cost of production, chemically and mechanically stable, low electrical resistance) is still challenging to date [101,102].

There are several mechanisms for achieving selectivity to specific counter-ions in IEMs, roughly based on i) sieving effect, ii) enhanced Donnan-exclusion effect, and iii) specific interactions between the ions in the solution and the ionic sites in the membrane [103]. First, the sieving effect can be enhanced by narrowing the ion channel paths and obtaining dense membrane structures, for instance, by increasing the cross-linking of the polymers in the membrane matrix [104,105] or by the deposition of a highly cross-linked layer on the membrane surface [106]. Second, the Donnan-exclusion effect against multivalent ions can be increased by the deposition of an oppositely charged layer on the membrane surface. There are several techniques for surface modification, including adsorption [107,108], coating [89] and layer-by-layer deposition of charged materials [109,110]. Third, specific interactions between the membrane and the ions in the solution can promote a selective separation, such as host–guest molecular interactions [111] or hydrophobic interactions [112–114].

1.5.4. Preparation of heterogeneous AEM

As mentioned, heterogenous IEMs are prepared by dispersing a finely grounded ion-exchange resin into a polymeric mixture containing a film forming polymer binder. Several techniques have been reported, including press moulding [115,116], casting [117,118], and 3D printing [119,120]. To date, press moulding is the most employed technique for the fabrication of commercial heterogeneous IEM (e.g., Ralex® membranes from MEGA a.s., Czech Republic [115]).

In this thesis, a new methodology for the indirect recycling of RO membranes as support in the preparation of Ion-Exchange Membranes (IEMs), more concretely Anion-Exchange Membranes (AEMs) has been developed. The employed methodology has been based on casting a polymeric mixture on the surface of a flat sheet EoL RO membrane (previously transformed to UF-like properties) (Fig. 19). The polymeric mixture has been prepared by dissolving a polymer binder in an organic solvent and adding a finely grounder anion-exchange resin to the mixture.

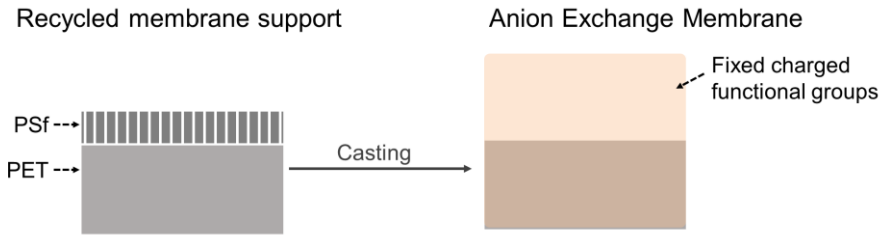

Figure 19. Schematic illustration of EoL RO membrane indirect recycling by transformation to AEM.

Such recycling methodology involves a challenging modification of the properties of the EoL RO membrane, that will be transformed from a pressure filtration membrane to an electric potential driven membrane. Thus, a high number of charged fixed functional groups have to be introduced in the recycled membrane support to provide of a significant co-ion exclusion capacity. The resulting membranes have been validated in different applications such as: electrodialysis (ED) [54,55], selective electro-separation of nitrate [56], and nitrate removal from drinking water by Donnan Dialysis (DD) and Ion-Exchange Membrane Bioreactor (IEMB) systems [71]. The scope and outline of the thesis is further detailed in Chapter 2.

2

Chapter 2. Scope and outline of the thesis

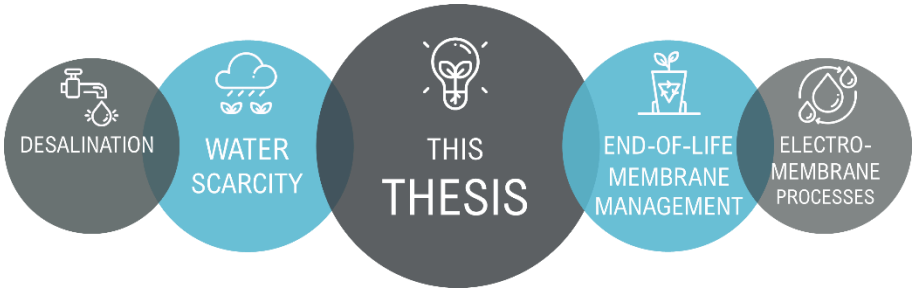

1.1. Justification of the thesis

In previous studies carried out by our research group at IMDEA Water, an innovative methodology for the direct recycling of EoL by transformation into NF and UF membranes was developed [121]. Furthermore, the performance of the recycled membranes was validated at real-site pilot scale for several applications (i.e., in RO pretreatment, desalination and wastewater treatment) [44]. Despite, due to membrane deterioration, direct recycling is not always a suitable recycling alternative. In these cases, and for discarded recycled membranes, indirect recycling has been proposed for the valorisation of the EoL membrane modules. Indirect recycling involves the deconstruction of the RO module for an individual management of the plastic components and the membranes, and therefore, it is an innovative approach to promote the transition towards a circular economy.

1.2. Research objectives and thesis outline

According to the aforementioned, the main objective of the present thesis is to explore a new methodology to enable the indirect recycling of EoL RO membranes by their transformation into AEMs. In addition, different strategies are investigated with the objective to enhance the selectivity of AEMs. Further, the validation of the technical feasibility of the membranes under different water treatment processes is pursued, including desalination, selective ion separation, selective nitrate separation, and nitrate removal from drinking water. The next chapters have been structured according to the follow sub-objectives addressed during the present work:

Chapter 3: Preparation of Anion-Exchange Membranes from end-of-life Reverse Osmosis membranes for Electrodialysis.

- To define the optimum preparation methodology of the AEMs using EoL RO membranes as support.

- To test the feasibility of using these membranes in brackish water desalination by ED.
- To propose the recycling of PP components of the EoL module, as different plastic components to set up an ED stack.

Chapter 4: Activation of Anion-Exchange Membranes prepared from end-of-life Reverse Osmosis membranes for an enhanced performance in Electrodialysis.

- To reduce the electrical resistance of the prepared AEMs by a low-cost acid/base activation treatment.
- To improve the membrane performance in brackish water desalination by ED.

Chapter 5: Preparation of monoselective Anion-Exchange Membranes with antifouling properties by surface modification.

- To increase the monoselective and the antifouling properties of a commercial AEM by surface modification.
- To evaluate i) the selectivity of the membrane for monovalent anions, ii) the stability of the coated layer, and iii) the enhancement of the antifouling properties of the modified membranes.

Chapter 6: Nitrate-Selective Anion-Exchange Membranes prepared from end-of-life Reverse Osmosis membranes.

- To develop nitrate selective AEMs from EoL RO membranes, based on the preparation methodology described in Chapter 2, using different types of anion-exchange resins.
- To test the influence of i) the type of ion-exchange resin, ii) the use of the recycled membrane as support, and iii) the operational current density in the separation process.

Chapter 7: Nitrate removal by Donnan Dialysis and Ion-Exchange Membrane Bioreactor systems using upcycled end-of-life Reverse Osmosis membranes.

– To test the performance of the membranes developed in Chapter 6, for the removal of nitrate from a polluted water under Donnan Dialysis (DD) and the Ion-Exchange Membrane Bioreactor (IEMB) systems to meet drinking water standards.

The research framework is represented in Fig. 20.

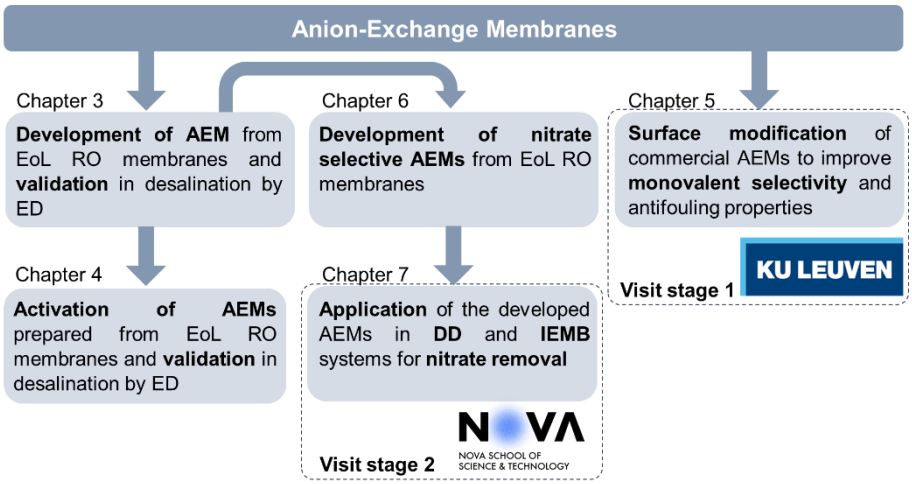

Figure 20. Research framework of the present thesis.

3

Chapter 3. Preparation of Anion-Exchange Membranes from end-of-life Reverse Osmosis membranes for Electrodialysis

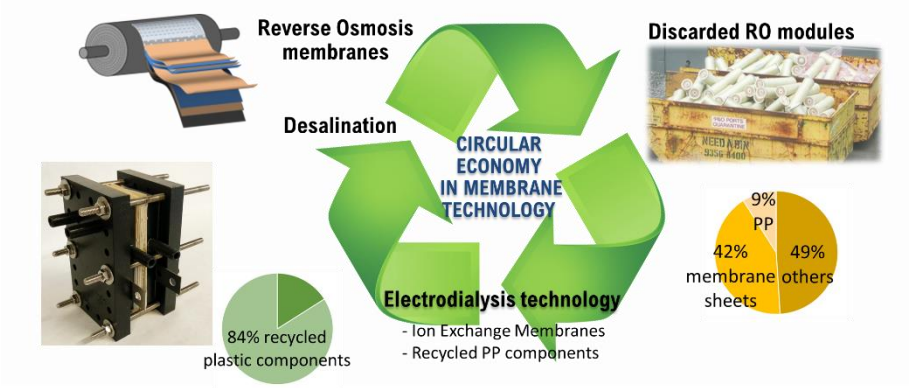

This Chapter has been published as:

A. Lejarazu-Larrañaga, S. Molina, J.M. Ortiz, R. Navarro, E. García-Calvo, Circular economy in membrane technology: Using end-of-life reverse osmosis modules for preparation of recycled anion-exchange membranes and validation in electrodialysis, J. Memb. Sci. 593 (2020) 117423. https://doi.org/10.1016/j.memsci.2019.117423 .

3.1. Introduction

In the current chapter, for the first time, the preparation of heterogeneous AEM by using discarded reverse osmosis membranes, pre-conditioned as support is proposed. The influence of factors, such as casting thickness and solvent evaporation time in membrane properties have been addressed in order to determine the optimal preparation conditions. The morphology of the membranes has been deeply studied and physicochemical and electrochemical properties have been analysed. Membrane performance in brackish water desalination has been evaluated by experiments in a lab scale ED system. All the results have been compared with commercial heterogeneous membranes. In addition, PP feed spacers from discarded RO modules have been also recycled for their use in the ED stack in two ways: i) directly reused as turbulence promoters (spacers) between the membranes, ii) reprocessed by melting and extruded to form the end caps and anolyte/catholyte compartments. Complementarily, different recycled support from the EoL RO module have been tested for the preparation of the AEMs (see Appendix A). Therefore, this study pretends to be an innovative approach that could open an alternative within the indirect recycling of discarded reverse osmosis membranes, avoiding their disposal in landfills, and moving membrane technology into a circular economy.

3.2. Materials and methods

3.2.1. Chemical reagents.

Sodium hypochlorite (NaClO, 14 %), tetrahydrofuran (THF) sodium chloride (NaCl), potassium nitrate (KNO_3) and sodium sulphate (Na_2SO_4) were purchased from Scharlab S.L., Spain. Commercial bulk polymerized polyvinylchloride (PVC, Mw 112,000 $g \cdot mol^{-1}$) was supplied by ATOCHEM S.A., Spain. Amberlite® IRA-402, strongly basic anion-exchanger (Cl^- form, total exchange capacity ≥ 1.0 mol/L) was supplied by Merck KGaA, Germany. MilliQ water was employed throughout the experiments.

3.2.2. Membranes

An EoL Polyamide thin film composite (PA-TFC) RO membrane module (TM 720-400 (Toray Industries, Inc., Japan)), used for more than three years in brackish water desalination (real site), was recycled in this study.

The performance of the prepared membranes was compared with commercial Ralex ® heterogeneous anion-exchange AMH-PES®. This membrane was selected as a referential membrane due to its heterogenous structure, high durability, high mechanical stability, and relatively low commercial cost. Commercial Ralex ® CMH-PES cation-exchange membrane was also used in the ED system. These membranes were supplied by Mega a.s., Czech Republic.

3.2.3. Recycling an end-of-life Reverse Osmosis module

The EoL RO module was first immersed into NaClO solution in a passive pilot recycling system described in [67]. The recycling protocol was described in [44], i.e. 800,000 ppm·h of free chlorine solution (NaClO, ~ 9000 ppm). During this treatment, the polyamide (PA) layer of the RO membranes was completely eliminated. The module was then opened by membrane autopsy and membrane coupons and polypropylene feed spacers were taken out.

The extracted membranes were stored wet to be used as mechanical support in the preparation of the recycled anion-exchange membranes. The PP feed spacers were stored to be used in the ED cell assembly in two ways i) directly reused as turbulence promoters (spacers), ii) reprocessed by melting, and extruded as end plates and anolyte/catholyte compartments. The process of PP recycling is described in the Supplementary Material (Section 3.5). The material was processed and supplied free of charge by the company Mikrolin Ltd., Hungary.

3.2.4. Anion-Exchange Membrane preparation

The membranes extracted from the RO module, were used as support in the preparation of the heterogeneous AEM. The membranes were prepared by casting and phase inversion methods as it is represented in Fig. 21.

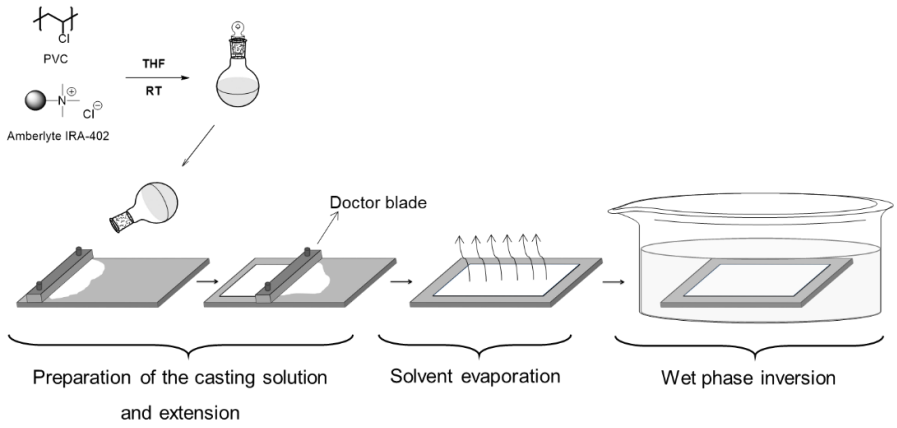

Figure 21 Preparation of heterogeneous AEM by casting technique and phase inversion method.

Firstly, the anion-exchange resin (Amberlite® IRA-402) was dried at 40ºC for 48 hours, pulverized into fine particles in a ball mill (MM400, from Retsch ® GmbH, Germany) and sieved to desired mesh size (-300 + 400 mesh). The polymer binder (PVC) was dissolved into the solvent (THF) in a glass flask by stirring for more than 8 hours (THF: PVC, 20:1 (v/w)). A specific quantity of grinded resin was dispersed in the solution and vigorously mixed for 30 minutes (resin: PVC, 1:1 (w/w)). Then, the polymeric solution was sonicated for 1.5 hours and stirred for other 30 minutes to obtain a uniform particle distribution. Finally, the mixture was casted by a doctor blade onto the recycled membrane support fixed in a glass plate, using different casting thickness (600, 700 and 800 μm). Membranes were dried for different times (7.5, 15, 30, 60 and 90 minutes) at room temperature (25ºC) before their immersion into a MilliQ water bath (20 ± 1 ºC). Finally, the AEM were equilibrated in 0.5 M NaCl solution for at least 24 hours before testing. Table 2 shows membrane codification in

relation to the preparation conditions (i.e., casting thickness and solvent evaporation time before the wet phase inversion).

Table 2. Membrane codification in relation to the preparation conditions.

Membrane [a]	Casting thickness (μm)	Solvent evaporation time (min)
r-600-7.5	600	7.5
r-600-30		30
r-600-60		60
r-600-90		90
r-700-7.5	700	7.5
r-700-30		30
r-700-60		60
r-700-90		90
r-800-15	800	15
r-800-30		30
r-800-60		60
r-800_90		90

[a] Composition of polymeric solution: Solvent to polymer binder (THF: PVC) (w/v), (20:1); anionic resin to polymer binder (Amb402: PVC) (w/w), (1:1).

3.2.5. Membrane characterization

3.2.5.1. Scanning Electron Microscopy

The morphological properties in the surface and in the cross-section of the membranes were examined by scanning electron spectroscopy (SEM) (XL30 ESEM model, from Phillips N.V., Netherlands). For analysing the cross-section, the membranes were broken properly after being frozen into liquid nitrogen. All the samples (surface and cross-section) were gold-sputtered with a sputter coater Polaron SC7640 model (from Quorum Technologies Ltd, United Kingdom), to achieve 13–15 nm thickness prior to the SEM analysis. All the analysed membranes were previously dried at 50 ºC for 48 hours.

3.2.5.2. Thickness, Water Content, Ion-Exchange Capacity

Membrane thickness was measured in swollen state by a digital micrometre IP65 model (from Mitutoyo Corp., Japan) (0- 25mm ± 0.001mm). Before the measurement, the membrane was wiped off with a filter paper. At least, six measurements were carried out for each membrane and the average value was reported.

The water content (*WC*) was obtained by gravimetric method, as the weight difference between the dried and swollen membranes. For this purpose, samples were kept in MilliQ water for at least 72 hours. The membranes were weighted in wet state (W_{wet}) and then dried in an oven at 50°C until a constant weight (W_{dry}). The *WC* was calculated following the Equation (Eq.) (1) [122]:

$$WC = \left(\frac{W_{wet} - W_{dry}}{W_{dry}}\right) \cdot 100\ \% \quad (1)$$

For each membrane three different samples were measured, and the average value was reported.

The evaluation of Ion-Exchange Capacity (IEC) was performed by spectrophotometric method [123]. For this purpose, membranes were initially submerged in 0.1 L KNO_3 1 M for 24 hours. Then the samples were carefully washed with MilliQ water and placed in 0.1 L NaCl 0.5 M for 24 hours. The concentration of nitrates in NaCl solution was measured by UV-Vis spectrophotometer (UV-1800, from Shimadzu Corp., Japan) following the Standard Method of the APHA for nitrate measurement in water [124]. Finally, membranes were dried in an oven at 50ºC until constant weight was attained. IEC (mmol·g^{-1}) was calculated by Eq. (2):

$$IEC = \left(\frac{n_{NO_3^-}}{W_{m\ dry}}\right) \quad (2)$$

where $n_{NO_3^-}$ (mmol) is the NO_3^- mol number present in the NaCl solution, and $W_{m\ dry}$ (g) is the dry weight of the membrane. From each

membrane, three different samples were measured, and the average value was reported.

3.2.5.3. *Electrochemical properties*

Test cell

The electrochemical properties of the recycled AEMs were evaluated by using the test cell schematized in Fig. 22. The test cell was comprised of two Pyrex glass bottles of 0.25 L capacity each. Between the bottles the membrane under investigation was placed (effective area 4.52 cm^2). In order to minimize the concentration polarization in the boundary layer of the membrane, both solutions were mixed vigorously by magnetic stirrers. The potential drop in the cell was measured by two Ag/AgCl 3.5 M KCl reference electrodes. For measuring the electrical resistance, two carbon felt sheet were used as anode and cathode.

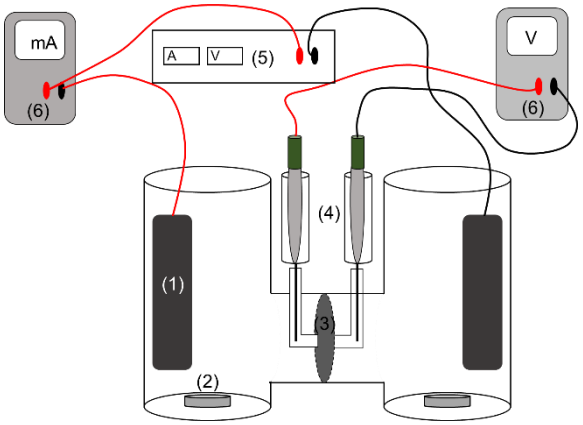

Figure 22. Schematic diagram of the test cell. (1) Carbon felt sheet, (2) magnetic stirrer, (3) membrane under investigation, (4) Ag/AgCl reference electrodes, (5) direct current (DC) power supply and (6) multimetre.

Permselectivity

The permselectivity measures the ability of the membrane to discriminate between anions and cations. The permselectivity of the recycled AEMs was analysed by placing the membranes in the test cell (Fig. 22). Each compartment was filled with 0.1 M NaCl and 0.5 M NaCl solutions. The system was equilibrated under stirring and the stabilized potential difference across the membrane was measured (ΔV_m). Following the Eq. (3), the permselectivity was calculated from the ratio of measured potential difference and the theoretical potential for an ideal 100 % permselective membrane [90].

$$\alpha = \frac{\Delta V_{exp}}{\Delta V_t} \cdot 100\ \% \tag{3}$$

where, α (%) is the permselectivity, ΔV_m is the measured potential difference and ΔV_t is the theoretical potential difference for a 100 % permselective membrane, under the previously described experimental conditions. ΔV_t was calculated by using Nernst equation (Eq. (4)).

$$E_m = \frac{R \cdot T}{z \cdot F} \cdot \ (2t_i - 1) \cdot ln\frac{a_1}{a_2} \tag{4}$$

where, E_m (V) is the potential difference; R ($J \cdot mol^{-1} \cdot K^{-1}$) the gas constant; T (K) temperature under standard conditions; z is the electrovalence of the employed electrolyte; F ($C \cdot mol^{-1}$) is Faraday constant; t_i is the transport number for 100 % permselective membrane ($t_i = 1$); a_1 and a_2 are the activity coefficients of NaCl 0.5 M and 0.1 M solutions, respectively [125]. For each membrane, three different samples were measured, and the average value was reported.

Electrical resistance

The electrical resistance of the prepared membranes was assessed by placing the membranes in the test cell described above (Fig. 22). Both compartments were filled with NaCl 0.5 M solution. The voltage drop in the cell was recorded at different currents, with and without the membrane.

The electrical resistance was calculated from the graphical representation of Ohm´s law (Eq. (5)), where *R (Ω)* is the slope of the line.

$$R = \frac{U}{I} \tag{5}$$

Membrane electrical resistance (R_m (Ω·cm²)) was calculated as follows [90].

$$R_m = (R_2 - R_1) \cdot A \tag{6}$$

where R_2(Ω) is the resistance of the cell with the membrane; R_1(Ω) is the resistance of the cell without the membrane and A (cm²) is the effective surface. For each membrane, three different samples were measured, and the average value was reported.

3.2.5.4. Diffusion coefficients

Diffusion coefficients were evaluated by placing the membrane under investigation in the test cell schematized in Fig. 22 (in this case, no external potential is applied in the system). MilliQ water and 0.6 M NaCl solution were poured in each bottle. Solutions were stirred for several days, and the conductivity change in each bottle was measured by conductimetry using an EC-Metro BASIC 30+ from Crison S.L.U., Spain. Diffusion coefficients were calculated by the graphical representation of Fick´s first law (Eq. (7)) [122],

$$J_D = -D \cdot \frac{dC}{dl} \tag{7}$$

where, J_D (mol·m⁻²·s⁻¹) is the flux of ions through the membrane, D (m²·s⁻¹) is the diffusion coefficient, dC (mol·m⁻³) is the concentration gradient (the driving force), and dl (m) is membrane thickness. In order to estimate the diffusion coefficient D, the linear region of the experiments was considered, where the slope of the curve C vs *time* has constant value, and assuming $dC \approx \Delta C$ and $dl \approx l$.

3.2.5.5. Mechanical properties

Tensile strength and Young's modulus were measured in an Synergie 200 testing machine (from MTS ® Systems Corp., USA) equipped with a 100 Newton load cell. All samples were cut according to ISO 37:2017 and were equilibrated in MilliQ water for 48 hours. A crosshead speed of 2 $mm \cdot min^{-1}$ was used. Strain was measured from cross-head separation and referred to 10 mm initial length [118,126]. At least five samples from each membrane were tested to obtain the average values.

3.2.6. Desalination experiments

A lab scale electrodialysis stack designed by the authors was used to carry out the brackish water desalination experiments. The stack was assembled by 4 unit cells (Fig. 23). The schematic diagram of the experimental system is represented in Fig. 24. In this way, two desalination experiments were performed. The first one was conducted using a stack composed by 4 recycled AEMs and 5 commercial CEMs; and the second one was carried out using only Ralex ® commercial membranes (4 AEMs and 5 CEMs) purchased from Mega a.s., Czech Republic.

The active area for each membrane was 16 cm^2, and the overall effective AEM surface was 64 cm^2. Feed spacers from the EoL RO module were recycled as turbulence promoters. These PP woven spacers are 0.8 mm thickness and 3 mm mesh size. Moreover, end plates and compartments of the ED stack were machined using recycled PP (see Supplementary Material Section 3.5.). Finally, the employed electrodes were dimensionally stable electrodes for anode (DSE, Titanium coated with iridium oxide, provided by Inagasa S.A., Spain), and stainless steel for cathode (from Tamesanz S.A., Spain). The power supply was an EA-PS 5080-10A (0-80V) (from EA Elektro-Automatik GmbH & Co. KG, Germany).

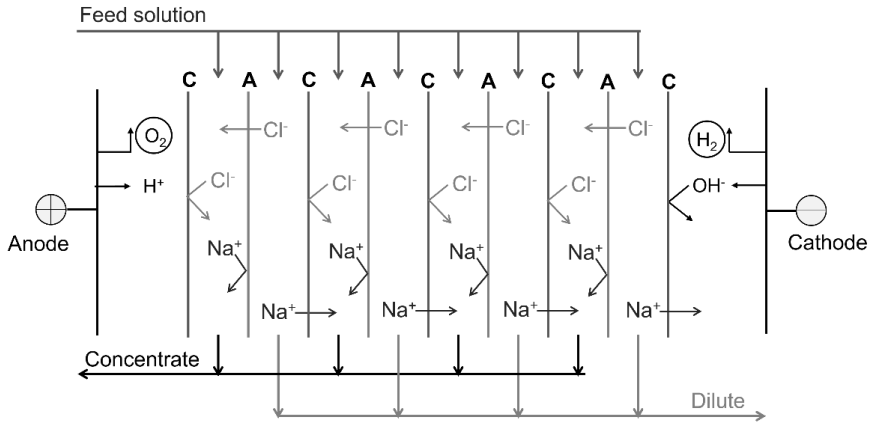

Figure 23. Configuration of the ED stack. C, Cation-Exchange Membrane; A, Anion-Exchange Membrane.

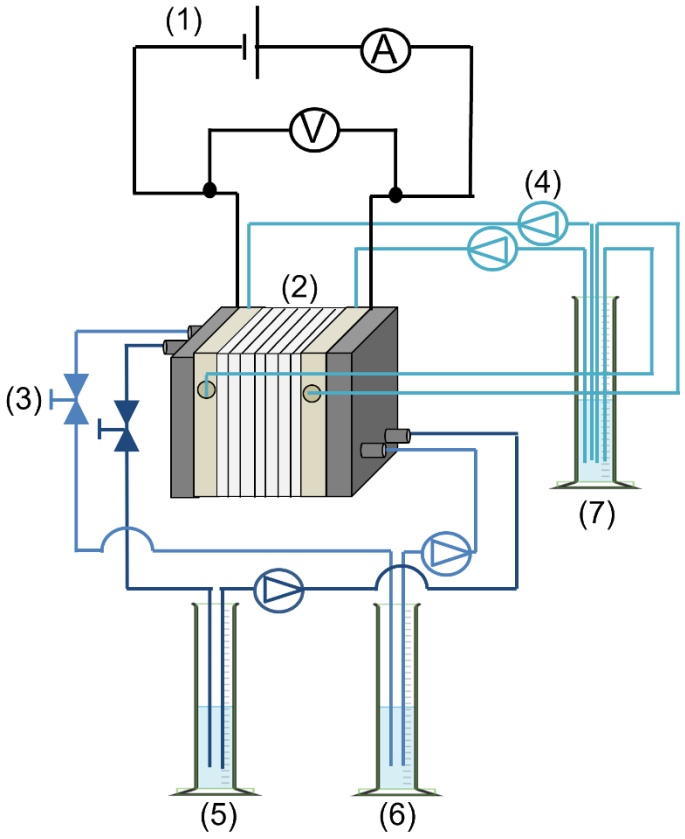

Figure 24. Diagram of the experimental ED setup (1) Power supply, (2) ED stack, (3) sampling valves, (4) peristaltic pumps, (5) concentrate, (6) dilute, (7) electrode rinse.

The experiments were carried out at constant voltage; the initial current density was 5 mA·cm^{-2}. 51.3 mM NaCl solutions (0.5 L) were used as feed (i.e., 3 g·L^{-1}, simulating the concentration of brackish water) in dilute and concentrate compartments. The anolyte/catholyte compartment was filled with 0.5 L Na_2SO_4 0.05 M solution. The flow rate of the three different streams was set to 1.2 L·h^{-1}. All the experiments were carried out in batch mode and at room temperature. The conductivity change in each compartment was measured by an EC-Metro BASIC 30+ conductivity meter from Crison instruments S.A., and the concentration of NaCl was calculated by a calibration curve. Ionic chromatography was used to measure Cl^- concentration in the dilute samples as well, and the results using both methods were in good agreement.

Membrane performance was analysed in terms of desalination time, salt removal, circulated charge per m^3, flux of salt and freshwater production. These terms were calculated following the Eq. (8), (9) and (10).

$$q = \frac{N \int I \cdot dt}{V} \tag{8}$$

where q (Cul·m^{-3}) is the circulated charge to obtain 1 m^3 of freshwater (i.e., NaCl concentration below 0.5 g·L^{-1} [127]); N, the number of unit cells; I (A) the intensity average during the experiment; t (s), experimental time and $V\ (m^3)$ the volume of the dilute compartment.

$$J_{NaCl} = \frac{\Delta n_{NaCl}}{N \cdot A \cdot \Delta t} \tag{9}$$

where J_{NaCl} (mol·m^{-2}·h^{-1}) is the flux of salt, Δn is mol variation of NaCl in the dilute compartment during the experiment, N the number of cells, A (m^2) membrane active surface and t (h) experimental time.

$$J_w = \frac{V_{dil}}{N \cdot A \cdot \Delta t} \tag{10}$$

where J_w (L·m^{-2}·h^{-1}) is freshwater production or nominal desalination rate (NDR) (NaCl concentration less than 0.5 g·L^{-1} [127]), V_{dil} (L) is the

volume of the dilute compartment (volume of produced freshwater), A (m^2) is the membrane effective surface and t_d (h) the experimental time.

3.3. Results and discussion

3.3.1. Scanning Electron Microscopy (SEM)

Surface SEM micrographs were obtained to observe the morphology of the recycled support, an anion-exchange membrane prepared by this methodology (r-800-60) and a commercial membrane (AMH-PES). The images are shown in Fig. 25.

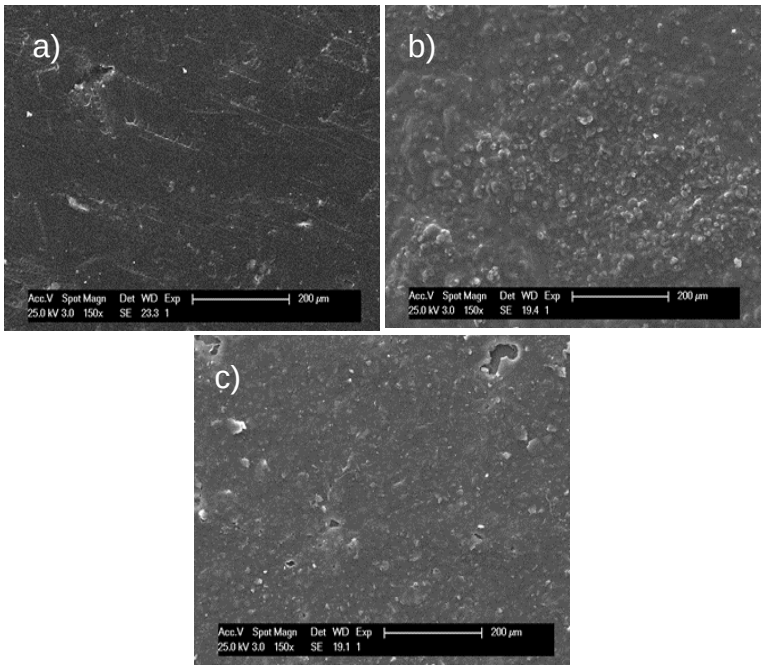

Figure 25. Surface SEM micrographs: a) recycled support, b) r-800-60 and c) AMH-PES.

As it can be observed, the surface of the recycled support (Fig. 25a) has less roughness than the prepared anion-exchange membrane (Fig. 25b) and the commercial one (Fig. 25c). In addition, a uniform distribution of the resin particles into the polymer matrix can be noticed in r-800-60 (Fig. 25b). This homogeneous distribution can be achieved due to the sonication of the polymeric solution. Sonication increases the viscosity of the mixture by

decreasing the aggregation and sedimentation of particles and thus, improves the homogeneity in ionic site distribution in the resultant membrane [128–130]. Resultant membrane surface is dense and rough, the amount of polymer binder is enough to cover the ionic resin particles and to create a continuous phase free of crack and voids in the surface [131].

Fig. 26 shows the cross-section micrographs of the recycled support, r-800-60 and AMH-PES.

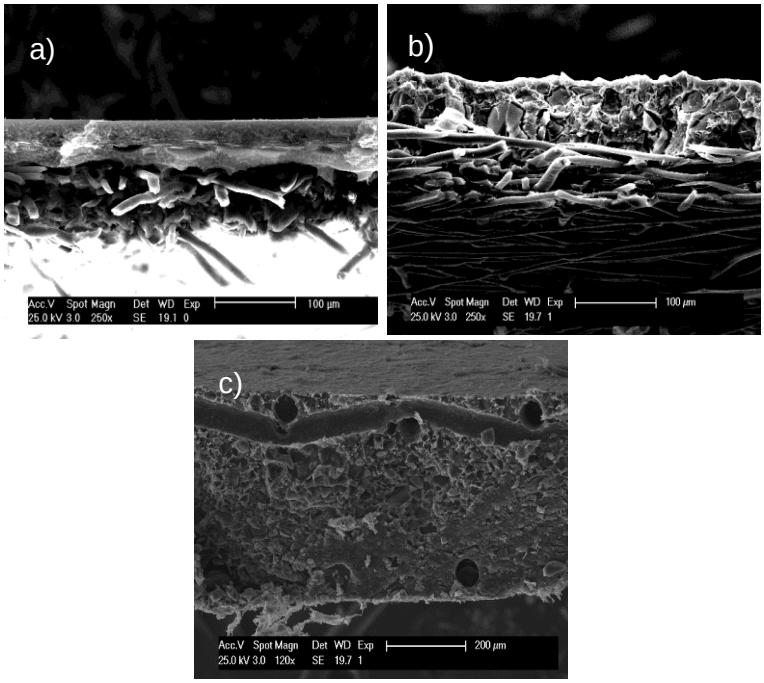

Figure 26. Cross-section SEM micrographs, a) recycled support, b) r-800-60 and c) AMH-PES.

The SEM images of the cross-section reveal significant differences between the aforementioned membranes. On the one hand, the cross-section of the recycled membrane support (Fig. 26a) is composed by two layers (a polyester layer and a polysulfone layer). However, in the prepared AEM (Fig. 26b), the polymeric matrix is almost totally embedded in the mechanical support. This fact could influence the mechanical properties of the AEM by maintaining the mechanical stability inherited from the discarded reverse osmosis membranes (recycled membrane support) (see

Section 3.3.4). On the other hand, AMH-PES (Fig. 26c) shows a conglomerated structure traversed by few fibres. In these heterogeneous membranes (Fig. 26b and 26c), the binder and the resin particles across the membrane does not follow any pattern.

3.3.2. Thickness, water content and Ion-Exchange Capacity

Fig. 27 shows a) final membrane thickness, b) water content (WC) and c) Ion-Exchange Capacity (IEC) of the recycled AEMs for different solvent evaporation times using different casting thicknesses.

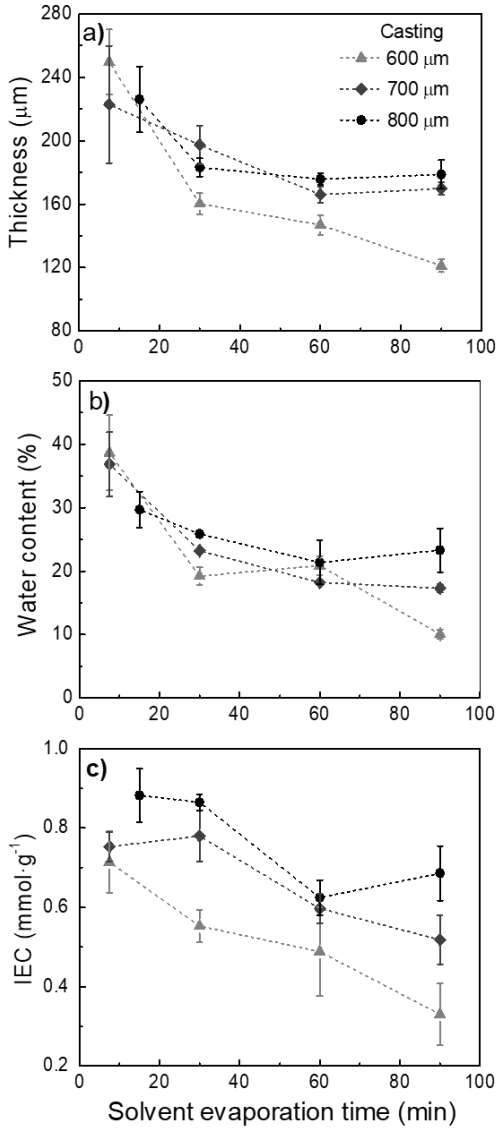

Figure 27. a) Thickness, b) water content and c) IEC of recycled AEMs prepared by using 600, 700, 800 μm casting thickness and 7.5, 15, 30, 90 min solvent evaporation time.

Fig. 27a, 27b and 27c show a reduction in membrane thickness, WC and IEC while the solvent evaporation time increases or when thinner castings are employed (i.e., 600º μm), in general terms. The employment of longer evaporation times reduces the membrane thickness, probably due to

a larger penetration of the extended polymer solution into the mechanical support [132] and also associated to the compaction of the membrane structure before the phase inversion [118]. Likely, thinner membranes with a more compact structure have fewer cavities for swelling the water and thus, lower water content [133]. Related to this effect, fewer cavities could affect the availability of ion-exchange groups exposed to the water phase, and consequently the IEC is negatively affected (as reported in the literature [90]). In addition, membranes produced by thicker coatings, are more likely to have greater IEC as they contain a larger amount of functional groups ready for the ion-exchange in the membrane matrix [133].

It is worth mentioning that the solvent evaporation time must be enough (depending on the casting thickness) to form a continuous phase in order to avoid the deconstruction of the structure during the wet phase inversion. For example, 800 microns casting and a solvent evaporation time of 7.5 minutes, causes the membrane deconstruction during the wet phase inversion.

On the other hand, commercial AMH-PES membranes have an average thickness of 645 μm and thus, they are significantly thicker than all the prepared membranes in this study (approx. 120 - 250 μm). Additionally, the WC and the IEC in the commercial membrane (WC, 49.8 %; IEC, 2.19 $mmol \cdot g^{-1}$) are also considerably higher than in the prepared AEMs (WC, 10 - 39 %; IEC, 0.33-0.88 $mmol \cdot g^{-1}$) (see Table 3). These properties (thickness, WC, and IEC) are related to the electrochemical properties of the membranes. In general terms, thinner membranes have lower electrical resistance; high IEC is related to high permselectivity; and high WC has a negative effect on the permselectivity, but can reduce the electrical resistance [90].

3.3.3. Electrochemical properties

To select the optimum membrane preparation conditions, the evaluation of the electrochemical properties (permselectivity and electrical

resistance) was carried out. Fig. 28 shows the permselectivity and the electrical resistance of the recycled AEMs for different solvent evaporation times using different casting thicknesses.

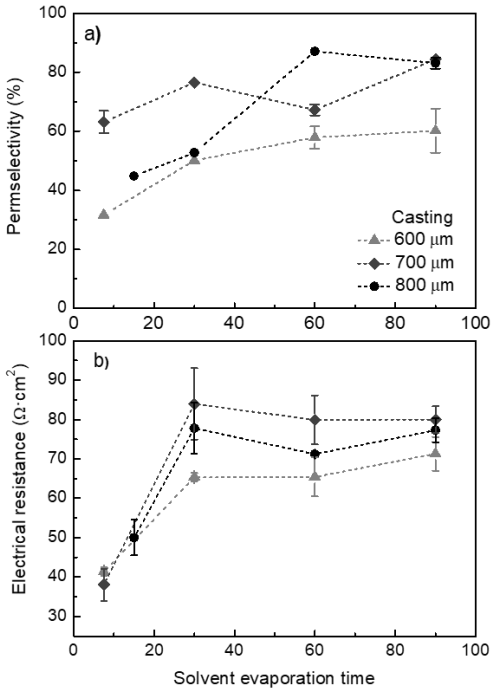

Figure 28. a) Permselectivity (α) and b) surface electrical resistance (R) of recycled AEMs prepared by using 600, 700, 800 μm casting thickness and 7.5, 15, 30, 90 min solvent evaporation time.

Fig. 28a shows that, in general, longer evaporation times produce membranes with higher permselectivity. This could be attributed to the formation of a dense membrane surface and the compaction of the membrane structure (as it has been explained above in Section 3.3.2.) [118]. It is worth mentioning that the permselectivity of r-700-90, r-800-60, and r-800-90 (84 %, 87 % and 83 %, respectively) is comparable with commercial membranes (84 % in the case of AMH-PES measured under the same conditions (see Table 3). As can be noticed in Fig. 28b, there is an increase of the electrical resistance within the solvent evaporation time. This could be attributed to the formation of a denser membrane surface, the

compaction of the membrane structure and the consequent reduction of water channels [118].

The electrochemical properties have a counteracting effect, thus when permselectivity is enhanced, membrane electrical resistance also increases [90]. Thus, it is necessary to arrange a compromise in order to select the optimum membrane preparation conditions. In this sense, membranes prepared with a casting thickness of 600 microns seem not to be enough to achieve good permselectivity (less than 60 %) although their electrical resistance is the lowest. Accordingly, the membranes prepared using 700 and 800 μm castings show higher resistance values but the permselectivity is also higher (when the solvent evaporation time is correctly chosen), being in some cases comparable with commercial membranes. Within the three optimal membranes with high permselectivity values (r-700-90, r-800-60 and r-800-90, r-800-60 was selected as the optimum membrane (i.e., 800 microns casting and 60 min solvent evaporation time). This membrane shows the highest permselectivity value (87 %) and the lowest resistance (77 Ω cm^2).

The electrochemical properties of the selected membrane (r-800-60) have been compared with the recycled support and with the commercial AMH-PES in Table 3.

Table 3. Electrochemical properties, thickness, water content and IEC of r-800-60, recycled support, and AMH-PES (commercial membrane).

Membrane	α (%)	R (Ω·cm^2)	Thickness (μm)	WC (%)	IEC (mmol g^{-1})
r-800-60	87 ± 0	77 ± 3	176 ± 4	21 ± 4	0.62 ± 0.04
Recycled support	0.± 0	17 ± 2	126 ± 1	49 ± 1	0.12 ± 0.02
AMH-PES	84 ± 3	19 ± 3	645 ± 5	49.8 ± 0.4	2.19 ± 0.09

Firstly, it can be observed that the recycled support has an electrical resistance similar to the commercial AEM, and it does not present permselectivity, as expected. Once the surface of recycled support is modified (i.e., r-800-60), the electrical resistance is significantly increased, as well as the permselectivity, that is slightly higher compared to the commercial membrane. So, it could be considered that the proposed strategy for membrane recycling into ion-exchange membrane is successful and adequate to provide electrochemical properties to the recycled support. On the other hand, the high electric resistance would increase the energy consumption in the ED process when these membranes are used. Thus, this property should be addressed in forthcoming research in order to decrease the energy consumption for the prepared AEMs. Thus, the high electrical resistance of the recycled membrane should be addressed in forthcoming research in order to decrease the energy consumption. A suitable strategy would be the activation of the membranes [134] or the employment of smaller resin particles in the polymeric solution [131]. Both approaches could help to modify the structure (i.e., increase the ion-exchange capacity) of the membrane and affect positively the conductivity of the membrane.

3.3.4. Mechanical properties

To analyse the mechanical properties of the selected membrane (r-800-60), tensile strength and Young's modulus have been measured. There are several works in which ion-exchange membranes are prepared by a similar methodology but without using any mechanical support [129,135]. To test how the use of the support can improve the mechanical properties, a membrane without mechanical support has been prepared by the same conditions (i.e., 800 microns casting and 60 min solvent evaporation time, 800-60). For this comparison, Table 4 shows the tensile strength and Young's modulus for the membranes: r-800-60, 800-60, recycled membrane support and commercial AMH-PES.

Table 4. Mechanical properties of r_800-60, 800-60, recycled membrane support and commercial AMH-PES.

Membrane	Tensile strength *(MPa)*	Young's modulus *(MPa)*
r-800-60	17 ± 4	399 ± 81
800-60	9 ± 1	100 ± 19
Recycled support	71 ± 5	1344 ± 46
AMH-PES	14 ± 1	124 ± 7

The value of the tensile strength of the recycled support is the highest of the whole series (71 MPa). Comparatively, the tensile strength value of the selected membrane r-800-60 is considerably lower, (17 MPa), this could be due to the introduction of the loading resin particles into the polymeric matrix, even so this value is still higher than the commercial membrane (14 MPa) and the membrane 800-60 (9 MPa). This demonstrates that the recycled support could provide an improvement to the rupture resistance of the membranes, since they somehow inherit the mechanical stability of the discarded reverse osmosis membranes (recycled support). On the other hand, other factors that could also affect the improvement of the mechanical properties of the recycled membranes are the membrane thickness and the polymer binder used. The relationship between membrane thickness and mechanical properties has been extensively devoted. A decrease in the thickness leads to an improvement in the mechanical properties of the membrane [136]. Additionally, regarding the polymer used, PVC is a very versatile polymer that combines its excellent film-forming properties with its high binder ability [137,138]. Therefore, the combination of overall factors described above lead to a more robust ion-exchange recycled membrane than commercial one.

3.3.5. Diffusion coefficients

The passive transport of ions across the membrane due to the concentration gradient is defined by the diffusion coefficients. The use of the recycled support could greatly decrease the diffusion phenomena in the

resulting AEMs. This hypothesis was corroborated by comparing the diffusion coefficients of r-800-60 and 800-60 (without EoL RO membrane as mechanical support), $4 \cdot 10^{-12}$ $m^2 \cdot s^{-1}$and $8 \cdot 10^{-12}$ $m^2 \cdot s^{-1}$, respectively. The value for the commercial membrane was found to be $5 \cdot 10^{-12}$ $m^2 \cdot s^{-1}$. In this sense, the AEM prepared from EoL RO membrane has the lowest diffusion coefficient. This can be due to the formation of a dense, low conductive membrane with a relatively low swelling degree, which hinder the flux of ions through the membrane due to diffusion [139]. Thickness can be also related with the diffusion coefficient and generally, thicker membranes have lower diffusion coefficients. Additionally, in the case of the AEMs prepared from EoL RO, the EoL membrane could have a significant contribution to both the diffusion coefficient and the electric resistance. This could increase the efficiency of the process when high concentration gradients need to be achieved [140]. Interestingly, 800-60 membrane (prepared without any mechanical support), has the highest diffusion rate. This increase of the diffusion permeability entails the migration of co-ions through the membrane, thus can decrease membrane selectivity [139,141].

3.3.6. Desalination experiments

The potential application of the prepared AEMs in electrodialysis was validated by conducting desalination experiments in a lab scale ED system designed by the authors and described before (see Section 3.2.6). Two different experiments were performed: a) using a stack composed by the prepared AEMs and commercial CEMs (r-800-60 // CMH-PES), and b) using a stack composed by commercial AEMs and CEMs (AMH-PES // CMH-PES). It is important to note that spacers in ED process are relevant elements. In our case, PP feed spacers from discarded RO modules have been directly reused as turbulence promoters (spacers) in the ED stack for the desalination experiments, thus maintaining the recycling approach. In order to perform a suitable comparison of ED experiments, the same plastic spacers have been used for both experiments (commercial and prepared AEM). The experimental results are depicted in Fig. 29 and Table 5.

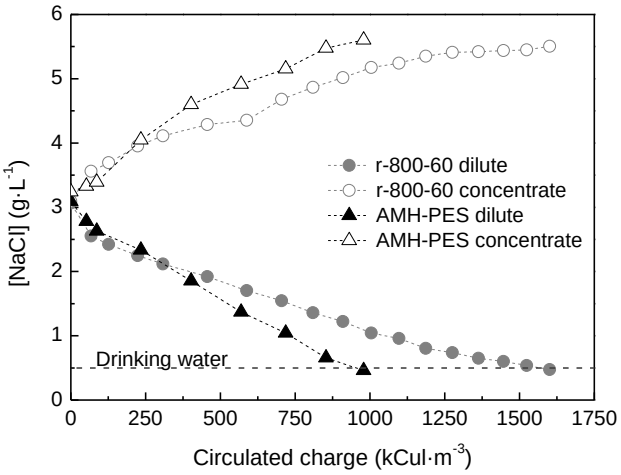

Figure 29. Desalination experiments by ED using recycled membranes (r-800-60) and commercial membranes (AMH-PES). The line represents the maximum NaCl concentration in drinkable water according to [127].

Fig. 29 exhibits the concentration change in the dilute and concentrate compartments. Three different regions can be slightly distinguished. The first one is related to relatively high salt concentration in the dilute compartment (from 3.1 to 2.2º$g \cdot L^{-1}$), in this case, the flux of salt by using the prepared AEMs is higher than that with the commercial membranes (0.91 and 0.72 $mol \cdot m^{-2} \cdot h^{-1}$, respectively), for the same circulated charge. A second region can be distinguished at dilute concentrations ranged between 2.2 and 1 $g \cdot L^{-1}$ NaCl, here the flux of ions by using recycled membranes is drastically decreased (0.24 $mol \cdot m^{-2} \cdot h^{-1}$ by using the system with recycled membranes and 0.54 $mol \cdot m^{-2} \cdot h^{-1}$ with commercial membranes). The third region is established at concentrations below 1 $g \cdot L^{-1}$ in the diluted compartment. In this case, the electrical resistance of the system rises due to the low concentrations of ions to carry the electric charge in the dilute compartment. Here, the flux of ions of both systems is relatively low (0.10 $mol \cdot m^{-2} \cdot h^{-1}$ with the prepared AEMs and 0.24º$mol \cdot m^{-2} \cdot h^{-1}$ with commercial membranes). The experimental results of salt removal, desalination time, circulated charge and nominal desalination rate are shown in Table 5.

Table 5. Experimentally calculated values for energy consumption and water production using a) prepared AEMs (r-800-60), or b) commercial membranes (AMH-PES).

	a)	**r-800-60**	**b)**	**AMH-PES**
Salt removal (%)		84.5		85.1
Desalination time (h) [a]		14.5		6.5
Circulated charge ($kC \cdot m^{-3}$) [a]		12,808		7,884
Freshwater production ($L \cdot m^{-2} \cdot h^{-1}$) [a]		4.67		10.34

[a] The results were calculated for a final NaCl concentration of 0.5 $g \cdot L^{-1}$, according to [127].

As it can be observed, the percentage of salt removal for both experiments (i.e., commercial, and prepared AEMs) is around 85 %, indicating the technical feasibility of using these novel membranes for the desalination process. The time to produce a certain volume of freshwater is higher by using the system with the prepared AEMs, and as consequence, the freshwater production is lower (4.67 and 10.34 $L \cdot m^{-2} \cdot h^{-1}$, for recycled and commercial respectively). In the same line, the circulated charge to produce a cubic meter of freshwater is higher for the prepared AEMs, as consequence of their higher electrical resistance. However, it could be considered that the prepared AEMs operate with a good level of permselectivity when concentration is above 2.2 $g \cdot L^{-1}$ of NaCl.

Finally, this study proposes for first time an innovative methodology for the indirect recycling of EoL RO modules and shows the technical viability of using the AEMs prepared from EoL RO membranes for electrodialysis in brackish water desalination. Further research should be conducted on reducing the electrical resistance of the prepared AEMs and on broadening their potential applications. Moreover, long term experiments should be carried out in order to validate the proposed methodology and determine the useful life of recycled membranes for scaling up applications.

3.4. Conclusions

In this work, the indirect recycling of EoL RO module (membranes and PP components) into an ED stack has been attempted for the first time. On the one hand, AEMs have been prepared by casting a polymeric solution onto a discarded RO membrane, preconditioned as a support. The performances and morphologies of these AEMs have been deeply studied, and the technical feasibility of using such membranes in ED has been validated by conducting brackish water desalination experiments. On the other hand, PP parts of the discarded modules have been recycled into end plates, compartments, and turbulence promoters of the ED stack. A stack with 84 % of recycled plastic has been assembled (54 % of the total weight of the stack, considering the metallic parts). The primary findings drawn from this study are summarized as follows:

- The surface morphology of the prepared membrane shows a homogeneous distribution of the ion-exchange resin into the polymer matrix, similar to the commercial one.

- Among the tested combinations, 800 microns of casting thickness with a solvent evaporation time of 60 min (r-800-60 membrane) were selected as the optimum membrane preparation conditions. These conditions resulted in membranes with a high permselectivity (87 %, similar to the commercial membrane measured under the same conditions).

- The technical feasibility of using such AEMs in brackish water desalination by ED was successfully validated. The achieved desalination rate was comparable with that of commercial membranes, although the nominal desalination rate was lower, and the energy consumption was higher due to the electrical resistance of the prepared AEMs.

- Further research should be conducted on the reduction of the electrical resistance of the prepared AEMs. This improvement would help to implement the concept of recycled membranes in real applications, enabling new approaches related to circular economy in the water sector and increasing the sustainability of water separation processes.

3.5. Supplementary Material

ED stack construction using recycled plastic (PP).

In this section, the steps for ED stack construction using recycled plastic (PP) are described:

Step 1. Shredding and grinding: During the shredding, the waste is chopped into smaller parts (7-10 cm). The shredded material is fed into grinder where the grinding blades cut the material into smaller parts. The size of the pellets depends on the sleeve one uses but usually ranges between 1 and 3 cm (Fig. S 1).

Figure S 1. Grinded plastic waste.

Step 2. Separation and cleaning: the grinded material is fed into a tank filled with water. Fans forward the material in the tank meanwhile the dirt/ contamination separates from the grinded material. The material coming out from the tank goes into a centrifuge cascade. Then, the material is forwarded into big bags with high output blowers. At the end of the process the grinded, cleaned material has maximum 5 % of moisture what can be taken out during regranulation.

Step 3. Dry mixing: grinded material is mixed according to the specific application requirements and ready to be fed into the extruder line.

Step 4. Regranulation: the material is fed into the cascade extruder line. The plastic melts in the extruder due to external heating and internal friction heat. Moisture is removed with vacuum pump. The melt is filtered to separate the potential contamination from the hot melt. Since a cascade system is used, the melt is filtered twice causing a high-quality pellet as a result of the process. From the filtered melt, the fibres are cooled back and grinded into pellets. Pellets are used as a raw material for MDC plates (Fig. S 2).

Figure S 2. Recycled plastic pellets as raw material for ED parts.

Step 5. Extrusion/ compression moulding: the grinded pellets are mixed (dry mixture) and fed to the extruder. The dry mixture melts in the extruder and a homogeneous melt comes out from the extruder. The hot melt (230ºC) melt is put to the mould installed in the hydraulic press (Fig. S 3). After this step, a flat sheet of recycled PP is obtained (Fig. S 4).

Figure S 3. Hot melt taking out from the extruder and putting into the mould.

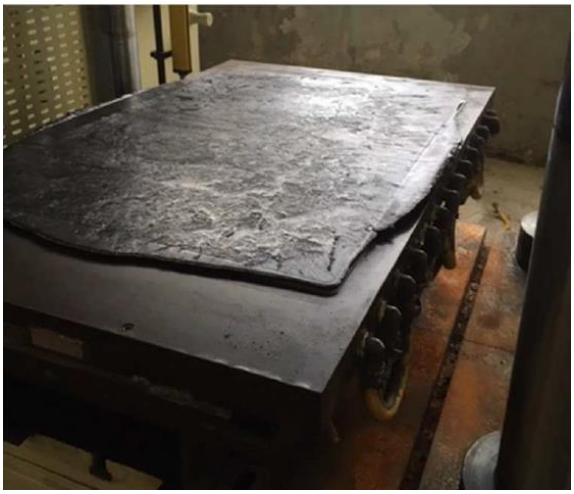

Figure S 4. Flat sheet after moulding and cooling down.

Step 6. Machining of ED end plates and compartments and selection of PP feed spacers parts for turbulence promoters (Fig. S 5).

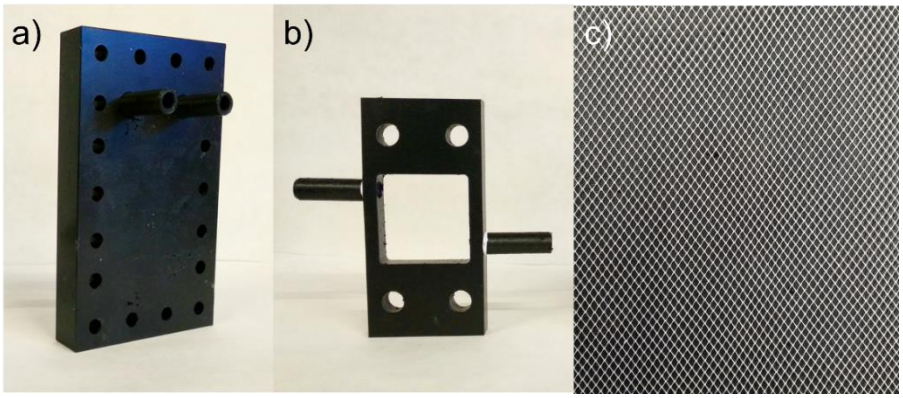

Figure S 5. a) End cap and b) anolyte and catholyte compartment c) turbulence promoter.

Step 7. Assembling of the ED stack (Fig. S 6).

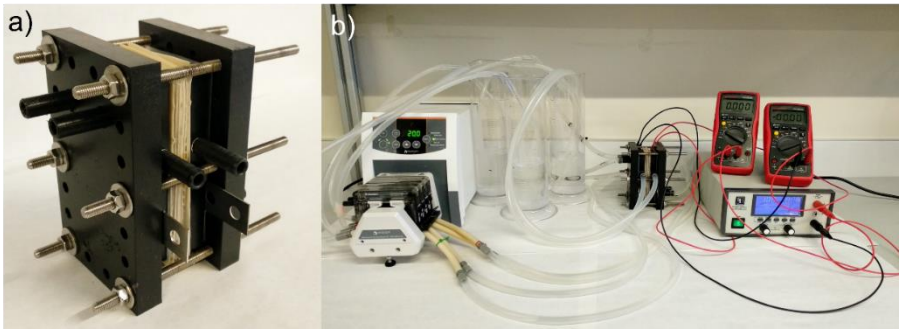

Figure S 6. a) ED stack, b) ED system

Table S 1 shows the composition of the ED stack used in this study and the percentage in weight of recycled plastic components in the stack (excluding the metallic parts such as nuts and electrodes).

Table S 1. Composition (by weight) of the ED cell used in this study.

		Weight (g)
Brand new components	Silicone compartments	54
	Cationic membranes (CMH-PES)	19
	Electrodes (anode and cathode)	73
	Nuts, washers, and screws	195
Recycled components	PP turbulence promoters	4
	Ends caps	316
	Anolyte/catholyte compartments	73
	Recycled membranes	3
ED cell	Recycled components [a]	54 % (w/w)
	Recycled plastic [b]s	84 % (w/w)

[a] Calculated considering the total mass of the cell (i.e., plastic and metallic components).
[b] Calculated considering the mass of the plastic components of the cell (i.e., excluding electrodes, nuts, washers, and screws).

4

Chapter 4. Activation of Anion-Exchange Membranes prepared from end-of-life Reverse Osmosis membranes for an enhanced performance in Electrodialysis

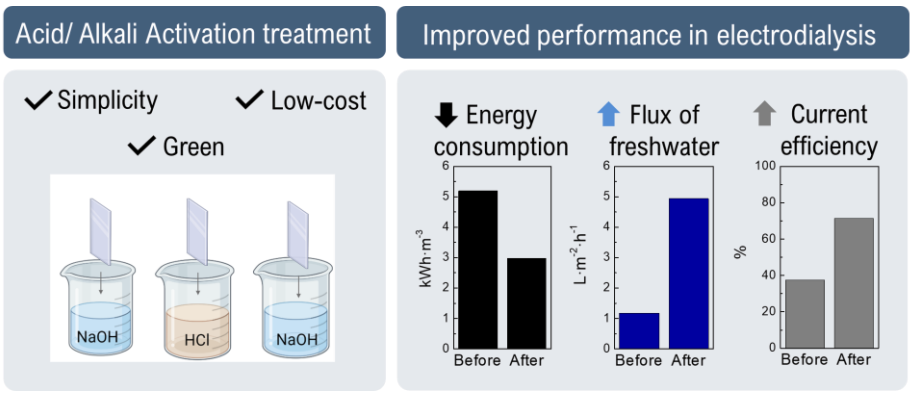

This Chapter has been published as:

A. Lejarazu-Larrañaga, S. Molina, J.M. Ortiz, G. Riccardelli, E. García-Calvo, Influence of acid/base activation treatment in the performance of recycled electromembrane for freshwater production by electrodialysis, Chemosphere. 248 (2020) 126027. https://doi.org/10.1016/j.chemosphere.2020.126027

4.1. Introduction

The AEMs developed from upcycled RO membranes demonstrated a high permselectivity, however, their high electrical resistance could compromise their implementation in ED (Chapter 3). With the aim to improve the electrochemical properties of heterogeneous IEMs, previous studies have reported the use of chemical acid/alkali activation posttreatments [123,134,142]. Those treatments could promote the alternating conversion of AEMs to OH^- and Cl^- forms, reaching a complete dissociation of the functional groups in the membrane, and making them more reactive to counter-ions. In such a way, L. Brožová et al. [134], reported an effective reduction of the electrical resistance of Ralex ® membranes. Nevertheless, in their study the effect of the activation treatment on membrane permselectivity was not reported. In spite of the simplicity and the low cost associated to acid/alkali activation treatments, very scarce research has been devoted to their study. On contrast, most of the research in this area is focused on additive blending using advanced materials (e.g., conductive nanoparticles), which could result in both high costs and adverse environmental impacts [143].

In the current chapter, a simple and low-cost activation treatment for the developed AEMs is proposed. The activation treatment consisted of the consecutive immersion of membranes in diluted acid and alkali aqueous solutions (i.e., HCl and NaOH). Furthermore, due to the low concentrations of acid and alkali solutions that were used, this treatment is presumably more environmentally friendly than other modification techniques employing nanomaterials. Firstly, the influence of acid and alkali concentrations in combination with the exposure times on the electrochemical properties of the membranes was studied. Secondly, the performance of activated, non-activated and commercial membranes in brackish water desalination by ED was compared.

4.2. Materials and methods

4.2.1. Chemical reagents

NaClO (14 % (v/v) as free chlorine), THF, NaOH, HCl (35 % (w/w)), NaCl and Na_2SO_4 were purchased from Scharlab S.L., Spain. PVC (Mw 112,000 $g \cdot mol^{-1}$) was supplied by ATOCHEM S.A., Spain. Amberlite® IRA-402, strongly basic anion-exchanger (Cl^- form, total exchange capacity ≥ 1.0 $mol \cdot L^{-1}$) was supplied by Merck KGaA, Germany. MilliQ water was used throughout the experiments.

4.2.2. Membranes

An EoL PA-TFC RO membrane (TM 720-400 (Toray)) was used as mechanical support for the preparation of the membranes (details are given in Section 3.2.3).

Commercial Ralex® membranes, AMH-PES and CMH-PES (from Mega a.s., Czech Republic) were used in the ED system.

4.2.3. Membrane preparation

The pre-treatment of the EoL RO membrane and the preparation of the recycled AEMs by casting and phase inversion were described in Sections 3.2.3 and 3.2.4 (Chapter 3), respectively. In this study, the membranes were prepared by extending an 800 μm casting solution and evaporating the solvent at room temperature during 60 min before the phase inversion. (i.e., on the same basis as r-800-60 in Chapter 3). In the present chapter and henceforth, these membranes are named as Amb-RE, referring to the employed ion-exchange resin (Amberlite® IRA-402, abbreviated as Amb) and the use of the recycled support (abbreviated as RE).

4.2.4. Activation treatment

The activation treatments performed in this study are summarized in Table 6. Two different concentrations of NaOH (0.1 and 0.01 M) and HCl (0.1 M and 0.01 M) were tested. The pH of the solutions was not adjusted.

During each cycle, the membranes were immersed (static immersion, room temperature) in the solution for different times (0.5, 2, 4 or 8 h). After each step, the membranes were rinsed with MilliQ water and immersed in MilliQ water for at least 16 h. Finally, the membranes were equilibrated in NaCl solution (0.5 M) for at least 24 h prior to the analysis. After the activation treatment, the membrane showing the greatest improvement of its electrochemical properties was selected, referred to as Act-Amb-RE henceforth.

Table 6. Steps of the activation treatments.

Step	Reagent	Immersion time (h)			
1.	NaOH (0.01 M)	0.5	2	4	8
2.	Milli Q water	16	16	16	16
3.	HCl (0.01 M)	0.5	2	4	8
4.	Milli Q water	16	16	16	16
5.	NaOH (0.01 M)	0.5	2	4	8
6.	Milli Q water	16	16	16	16
7.	NaCl (0.5 M)	24	24	24	24
Activated membrane		**A1**	**B1**	**C1**	**D1**

Step	Reagent	Immersion time (h)			
1.	NaOH (0.1 M)	0.5	2	4	8
2.	Milli Q water	16	16	16	16
3.	HCl (0.1 M)	0.5	2	4	8
4.	Milli Q water	16	16	16	16
5.	NaOH (0.1 M)	0.5	2	4	8
6.	Milli Q water	16	16	16	16
7.	NaCl (0.5 M)	24	24	24	24
Activated membrane		**A2**	**B2**	**C2**	**D2**

4.2.5. Membrane characterization

4.2.5.1. Electrochemical properties

The procedures for measuring calculating the electrical resistance and the permselectivity are described in Section 3.2.5.3 (Chapter 3).

Additionally, in this chapter, the relative change of the electrochemical properties due to the activation treatment is reported (Eq. (11)).

$$Relative\ change\ (x_f, x_0) = \left(\frac{x_f - x_0}{x_0}\right) \cdot 100\ \% \quad (11)$$

Three membrane samples were subjected to each activation treatment and the average of the relative change (in terms of electrical resistance and permselectivity) was reported. By using the Eq. (11) the influence of the standard deviation of the initial values was minimized.

4.2.5.2. Thickness, Water Content, and Ion-Exchange Capacity measurements

The procedure for measurement membrane thickness, WC and IEC was described in Section 3.2.5.2 (Chapter 3). Each property was analysed before and after the activation treatment in three different membrane samples.

4.2.5.3. Surface characterization

The surface and cross-sectional morphology of the prepared membranes was analysed by SEM (XL30 ESEM model, Phillips N.V., Netherlands). The methodology was described in Section 3.2.5.1 (Chapter 3).

The water contact angle (WCA) was determined using a CAM200 instrument (KSV Instruments, USA) by the sessile drop technique. First, the membrane under study was fixed on a glass support. After that, a drop of 4.5 μL Milli Q water was placed on the membrane surface using a Hamilton syringe. For each membrane, 10 water drops were measured, and the

average was calculated. The measurements were carried out at room temperature.

4.2.6. Electrodialysis experiments

The experimental system for conducting ED experiments was described in Section 3.2.6 (Chapter 3). The ED stack was assembled by 4 unit-cells (4 AEMs and 5 CEMs alternately disposed). Three different stack configurations were investigated: a) Commercial AEMs, and commercial CEMs (AMH-PES/ CMH-PES); b) the developed AEMs, and commercial CEMs (Amb-RE/ CMH-PES); c) the developed AEMs after the activation treatment, and commercial CEMs (Act-Amb-RE/ CMH-PES).

4.2.6.1. Determination of the Limiting current density

The LCD can be defined as the maximum current that is effectively used for the transport of the ions through the membranes [103]. For an effective use of the applied current, it is recommended not to exceed the 80 % of the LCD of the system [153]. In the present work, the LCD of different ED systems was analysed to define the optimum current range for each one.

The LCD was determined by the *R* vs. *1/j* curves as it was described before by [144]. Three different stack configurations described above were tested. A solution of NaCl (3 $g \cdot L^{-1}$, average brackish water salt concentration) was used as feed in the dilute and concentrate tanks and Na_2SO_4 (0.05 M) solution was used for electrode rinse. Both solutions were recirculated over the ED stack at a constant flow of 20 $mL \cdot min^{-1}$ and at room temperature. The applied potential was increased stepwise, and the electric current was recorded at each step after 30 s. The LCD was determined by identifying the value of *1/j* in which the electrical resistance shows the minimum value. The LCD value of each system was considered to design the brackish water ED experiments.

4.2.6.2. Brackish water desalination experiments

The desalination experiments were carried out using three different stack configurations described above. The dilute and concentrate compartments were both filled with 0.5 L NaCl solution (3 g·L^{-1}). The electrode rinse compartment was filled with 0.5 L of Na_2SO_4 (0.05 M). The flow rate was set to 20 mL·min^{-1}. The experiments were performed in batch mode, at constant voltage and at room temperature. The applied potential was set at the 80 % of the LCD, as suggested in the literature [145], to prevent any undesirable consequences of operating above the LCD. The conductivity change in each compartment was measured by a conductivity meter (EC-Metro BASIC 30+, from Crison S.L.U.) and the concentration of NaCl was calculated by a calibration curve.

The desalination performance of each system was analysed in terms freshwater production (Eq. (10) of the Chapter 3), energy consumption (Eq. (12)) and current efficiency (Eq. (13)) [146]:

$$E = \frac{\int_0^t U \cdot I \cdot dt}{V_{dil}} \tag{12}$$

where E (kWh·m^{-3}) is the energy consumption, U_t (V) is the applied electric potential, I (A) is the electric current, V_{dil} (m^3) is the volume of produced freshwater, and t (s) is the experimental time.

$$\eta = \frac{z \cdot F \cdot \Delta n_{dil}}{N \cdot \int_0^t I \cdot dt} \cdot 100 \tag{13}$$

where η (%) is the current efficiency, z is the valence of the transported ion, F is Faraday´s constant (F=96,485 C·mol^{-1}), $\Delta n_{dil,}$ is the mol number of

NaCl transported during the experimental time, N is the number of unit cells, I (A) is the electrical current and t (s) is the experimental time.

4.3. Results and discussion

4.3.1. Selection of the most suitable treatment based on the electrochemical properties.

The initial values of electrical resistance and permselectivity were measured for each membrane sample. On the one hand, the initial value of the electrical resistance (R_0) was 76 ± 18 Ω·cm^2 (number of samples (n)= 24), relatively high in comparison with the commercial AMH-PES (19 ± 3 Ω·cm^2), measured under the same conditions. The high electrical resistance of the recycled membranes could be attributed to the use of the discarded membrane as mechanical support [54]. On the other hand, the initial permselectivity of the recycled membranes was 80 ± 5 % (n=24), which can be considered similar to the commercial AMH-PES, measured under the same conditions (84 ± 3 %). In this sense, the main objective of the activation treatment is to decrease the electrical resistance while maintaining the permselectivity.

Fig. 30 shows the relative change in the electrochemical properties of the Amb-RE subjected to the different activation treatments described in Section 4.2.4 of the current chapter.

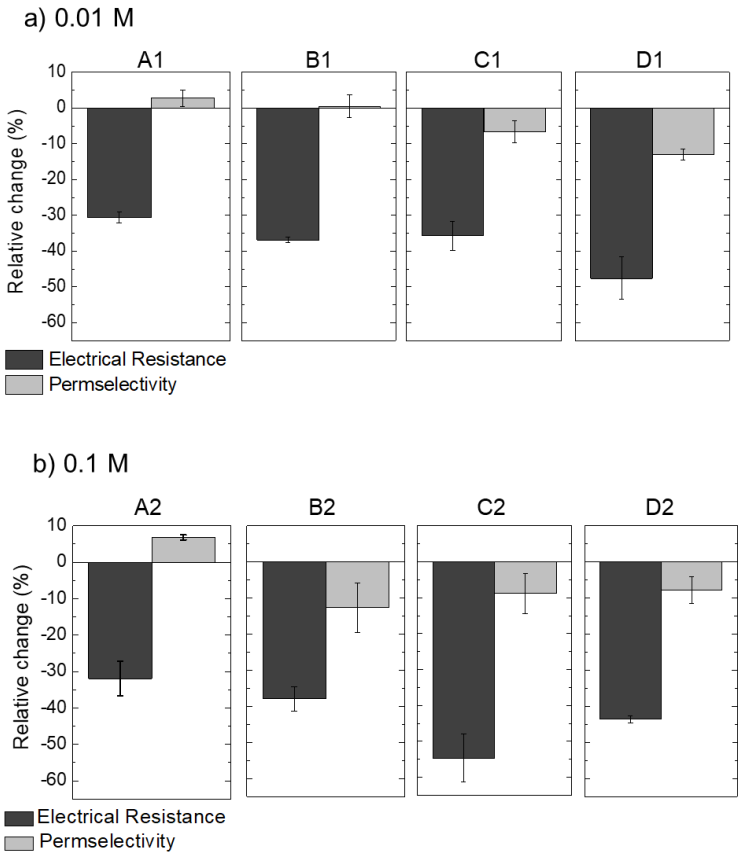

Figure 30. Relative change of electrical resistance and permselectivity of the membranes under study after the activation treatments using a) 0.01 M acid and alkali solutions (A1, B1, C1, D1) and b) 0.1 M acid and alkali solutions (A2, B2, C2, D2).

As it can be observed, the exposition to acid/alkali treatment significantly decreased the electrical resistance of the membranes in all the cases. The electrical resistance was decreased a minimum of 31 % with the less aggressive treatment (A1) and it reached a decrease of 55 % with one of the most aggressive treatment (C2). Considering the initial average values of the electrical resistance (R_0, 76 Ω·cm²), the final values after subjecting the membrane to the less and the most effective treatment would be 53 Ω·cm² and 34 Ω·cm² respectively. The decrease in the electrical resistance of the recycled membranes was found higher than the values reported before by [134], where the areal resistance of AMH-PES

membrane was decreased 25 % after being subjected to 5 step activation treatment with HCl and NaOH solutions (1 M). Regarding the permselectivity, on the one hand, it was damaged after being subjected to 0.01 M solutions during 4 h or longer exposure cycles (i.e., -7 % in C1 and -13 % in D1) and to 0.1 M solutions during 2 h or longer exposure cycles (i.e., -13 % in B2, -9 % in C2 and -8 % in D2 treatments). This effect could be attributed to the damage of the polymer matrix and the formation of additional porosity in the membrane or to the loss of functional groups in the resin particles of the membrane [147,148]. On the other hand, it was appreciated an increase in membrane permselectivity at short exposition cycles (i.e., 3 % in A1, 0.5 % in B1 and 7 % in A2). This effect could be related to the effective dissociation of the functional groups in the membrane, which could strengthen the in Donnan exclusion [149].

In conclusion, a compromise needs to be arranged between decreasing the electrical resistance without losing permselectivity. Therefore, B1 treatment (0.01 M solutions and 2 h cycles) was selected as the optimum activation conditions. In this case, membranes with an initial electrical resistance of 90 ± 1 $\Omega \cdot cm^2$ achieved 57 ± 1 $\Omega \cdot cm^2$ after the B1 treatment, thus a reduction of 37 % was accomplished. At the same time, the permselectivity was maintained unchanged (from 77 ± 9 % at the initial measurements to 77 ± 10 % after B1 treatment). The electrical resistance of the recycled membranes after the activation treatment is still higher than the commercial AMH-PES. However, the difference with the initial value is significant and thus, the treatment is considered as an effective way to effectively decrease the electrical resistance without compromising the permselectivity. Finally, for further experimentation in the electrodialysis system the activated recycled membranes (Act-Amb-RE) were subjected to the B1 treatment.

4.3.2. Thickness, Water Content, and Ion-Exchange Capacity

Table 7 shows the average values of thickness, Water Content (WC) and Ion-Exchange Capacity (IEC) of the Amb-RE and the Act-Amb-RE (activated following the B1 treatment).

Table 7. Thickness, Ion-Exchange Capacity (IEC) and Water Content (WC) of the Amb-RE and Act-Amb-RE (subjected to B1 activation treatment).

Membrane	Thickness (μm)	IEC (mmol·g^{-1})	WC (%)
Amb-RE	176 ± 10	0.60 ± 0.07	21 ± 4
Act-Amb-RE	198 ± 14	0.63 ± 0.06	21 ± 3

The membrane thickness was slightly increased after B1 activation treatment. Besides, the WC and the IEC of the membranes were also raised due to the B1 treatment. The increase in membrane thickness can be associated to the higher water content [147]. Moreover, the increase in IEC is probably related to the better accessibility of the counter-ions in the solution to the membrane functional groups. This ameliorated accessibility (and thus, IEC) is related to the greater dissociation of the functional groups and the higher swelling of the activated membrane which also contribute to the increase in membrane conductivity [123].

4.3.3. Surface characterization

Fig. 31 shows SEM micrographs and water contact angles (WCA) of the recycled and activated membranes.

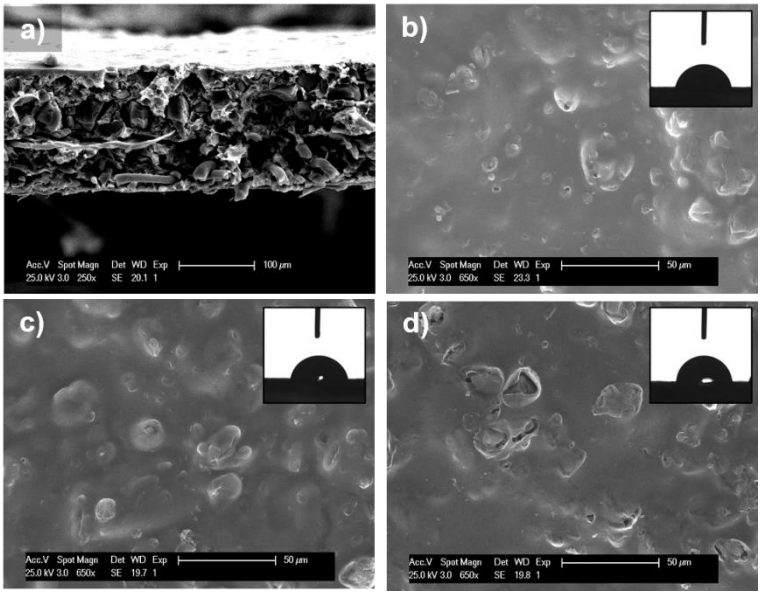

Figure 31. SEM images and water contact angles (WCAs) of the membranes. a) Amb-RE membrane cross-section, b) Amb-RE membrane surface, c) Surface of Act-Amb-RE membrane after B1 activation treatment, d) Surface of Act-Amb-RE membrane after B2 activation treatment

Fig. 31a presents the cross-sectional analysis of the Amb-RE. As it can be seen, the polymeric matrix is entirely embedded in the discarded membrane support [54]. Fig. 31b shows the surface of the Amb-RE. Here, the resin particles can be distinguished protruding on the surface. Fig. 31c and 31d correspond to activated membranes after B1 and B2 activation treatments. The surface of Fig. 31d presents more fissures probably as consequence of the exposure to more aggressive acid and alkali concentrations.

On the other hand, the wettability of membranes was studied by contact angle measurement [150]. The obtained values were quite similar: 81 ± 1 º, 82 ± 1 º and 83 ± 1 for the recycled membrane, and for the B1 and B2 activated membranes, respectively. Thus, the hydrophilicity of the membranes was not affected by the activation treatment.

4.3.4. Electrodialysis experiments

4.3.4.1. Limiting current density measurements.

When an external potential is applied to an ED system, the current is used for ion migration from the dilute side to the concentrate compartment. This movement of ions generates a boundary layer close to the membrane surface in the dilute compartment, where the concentration of the ion is lower than in the bulk solution. This phenomenon is known as concentration polarization. Then, the limiting current density (LCD) is achieved when the concentration of the ions in the boundary layer reaches zero. If the external potential keeps increasing, the current is not used for ion migration but for water splitting and for the subsequent electric charge transport due to migration of H^+ and OH^- ions. As result, the current efficiency decreases (from the desalination point of view) and the energy consumption increases. Additionally, in the over limiting current region, the membranes can be damaged by the pH changes and salts can be precipitated in the concentrate compartment due to the alkalization of the solution [122].

Fig. 32 shows a common method for experimental LDC measurements, as suggested in the literature [144]. By representing *R* vs *1/j* curves, LCD could be determined identifying the value of *1/j* in which the resistance shows the minimum value. It is important to indicate that only AEMs were replaced, maintaining the same experimental conditions, as it was explained in the Section 4.2.6. By doing this, it is possible to consider that changes in the ED system behaviour could be attributed to the characteristics of the AEMs.

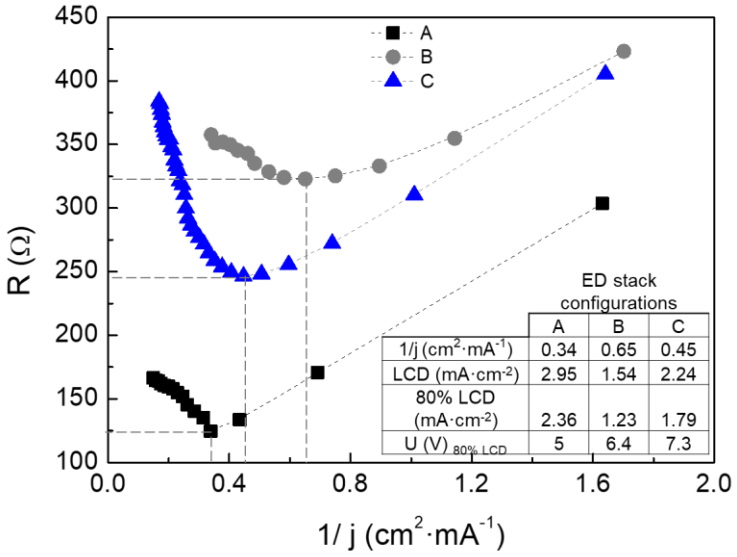

Figure 32. *R* vs. *1/j* curves used for the calculation of the LCD [144]. The studied stack configurations are: (A) AMH-PES / CMH-PES, (B) Amb-RE / CMH-PES, (C) Act-Amb-RE / CMH-PES.

The system composed by commercial membranes (A) shows the higher value of LCD (2.95 mA·cm^{-2}), which may be associated with the greater area of the conductive surface of AMH-PES membranes (caused by the use of a larger proportion of ionic resin in respect to the polymer binder) [151]. Besides, the system composed by Act-Amb-REs (C) shows an LCD of 2.24 mA·cm^{-2}, while the system with Amb-REs (B) shows the lowest value of LCD (1.54 mA·cm^{-2}). The difference between (B) and (C) could be attributed to the activation of the charged groups in the membrane surface, which could help to promote the accessibility of the counter-ions to the conductive zones, decreasing the concentration polarization.

For an efficient current utilization, the ED should be operated at 80 % of the LCD [145]. So, the obtained results were used to define the optimum voltage for each experiment. In this way, the brackish water desalination experiments were carried out at 5 V in A stack configuration (commercial membranes), 6.4 V in B stack configuration (recycled membranes) and 7.3

V in C stack configuration (activated membranes), ensuring that over limiting current is not reached during the desalination process.

4.3.4.2. Brackish water desalination experiments

The three different ED stack configurations described in Section 4.2.6. were tested to compare the performance of commercial (A), recycled (B) and activated membranes (C) for brackish water desalination in electrodialysis. Fig. 33 shows the salt concentration in the dilute compartment during the desalination experiments.

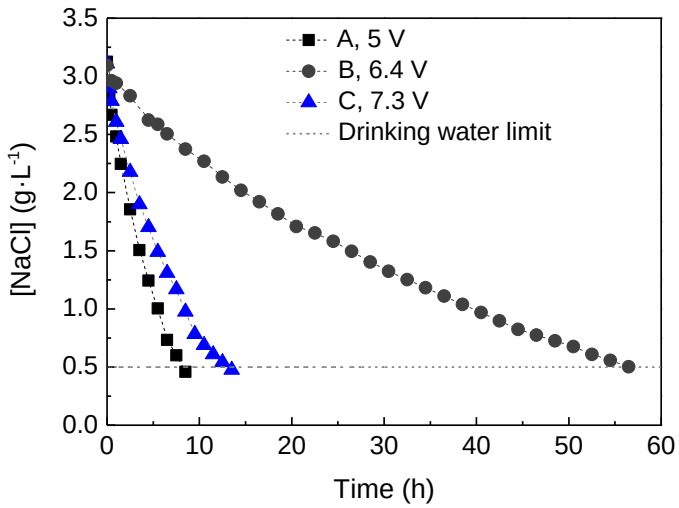

Figure 33. Brackish water desalination experiments by using three different ED stack configurations: (A) AMH-PES/ CMH-PES, (B) Amb-RE / CMH-PES, (C) Act-Amb-RE / CMH-PES.

As it can be observed, the system assembled by commercial membranes (A) is the fastest in producing 0.5 L of freshwater (i.e., NaCl concentration in dilute tank below 0.5 $g \cdot L^{-1}$, equivalent to an electric conductivity of 1 $mS \cdot cm^{-1}$), due to the lower electrical resistance of the commercial membranes. Additionally, the low LCD and the high electrical resistance of B stack configuration makes ion transport very slow,

increasing the experimental time to 56.5 h. Differently, the activation treatment reduces the desalination time to 13.5 h in C.

Fig. 34 shows the freshwater production, energy consumption and current efficiency of each stack configuration during brackish water desalination experiments.

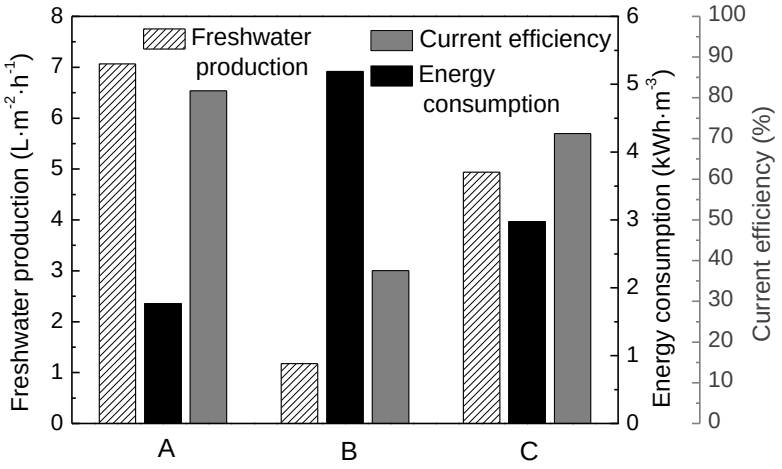

Figure 34. Freshwater production, energy consumption and current efficiency of the three ED stack configurations during brackish water desalination experiments: (A) COM-AEM / COM-AEM; (B) Amb-RE / COM-CEM; (C) Act-Amb-RE / COM-CEM.

As it can be observed, the system, experiment A shows the highest water production rate (7.1 $L \cdot m^{-2} \cdot h^{-1}$), with the lowest energy consumption (1.8 $kWh \cdot m^{-3}$) and the highest current efficiency (82 %). Secondly, the system B (with recycled membranes) shows the lowest water production (1.2 $L \cdot m^{-2} \cdot h^{-1}$), and the highest energy consumption (5.2 $kWh \cdot m^{-3}$), due to the high electrical resistance of the membranes and the low current efficiency (38 %). Differently, the system C (with activated membranes) increased the water production rate more than four-fold in respect to the non-activated membranes (4.9 $L \cdot m^{-2} \cdot h^{-1}$), moreover, it required much lower amount of energy for the desalination process (3.0 $kWh \cdot m^{-3}$), due to the

lower electrical resistance of the activated membranes and the greatly improved current efficiency (71 %).

In this line, the employed activation treatment effectively increased the performance of the Amb-REs for brackish water desalination by electrodialysis. The increase of freshwater production can be attributed to the decrease of the electric resistance and the increase in desalination efficiency (current utilization) in C (with activated membranes) in respect to B (with non-activated membranes). These experiments indicate that activated Amb-RE (C system) could perform efficiently for desalination of brackish water, demonstrating the technical feasibility of recycling EoL RO modules for ion-exchange membrane processes. Even the lower production and slightly higher energy consumption compared to commercials, the expected lower cost of the recycled ion-exchange membranes, as well as the lower negative environmental impact associated to the use of recycled elements, could enable the implementation of such recycled membranes in sustainable processes based on ion membrane separation in the next future.

4.4. Conclusions

The current work demonstrated the effectivity of an acid/alkali activation treatment in decreasing the electric resistance of AEMs prepared from upcycled RO membranes, leading to a better performance of the use of such membranes in ED. The main conclusions of this study are:

- The adequate combination of concentration and exposition time to the acid and alkali solutions (i.e., 0.01 M solutions and 2 h each exposition cycle), resulted in a considerable decrease of the electric resistance (i.e., 37 % reduction in respect to the initial values), without compromising membrane permselectivity.
- The selected activation treatment did not affect to the membrane surface morphology and hydrophilicity.
- The performance of the activated membranes in brackish water desalination by ED was considerably improved in respect to the initial

values. Results showed a considerable increase of freshwater production (from 1.2 $L \cdot h^{-1} \cdot m^{-2} \cdot$ to 4.9 $L \cdot h^{-1} \cdot m^{-2}$), an enhanced current efficiency (from 38 % to 71 %) and a remarkable reduction of energy consumption (from 5.2 $kWh \cdot m^{-3}$ to 3.0 $kWh \cdot m^{-3}$), in respect to the use of non-activated membranes.

- Overall. the proposed activation treatment is a simple and low-cost strategy that could help to the implementation of such RO upcycled membranes in sustainable electro-separation processes in the next future.

5

Chapter 5. Preparation of monoselective Anion-Exchange Membranes with antifouling properties by surface modification

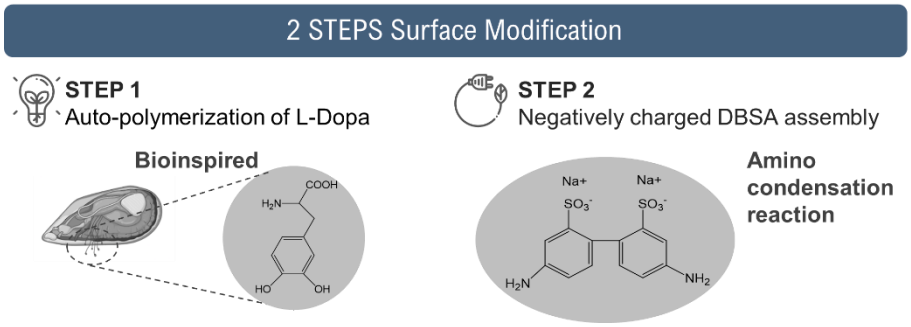

.

This Chapter has been published as:

A. Lejarazu-Larrañaga, Y. Zhao, S. Molina, E. García-Calvo, B. Van der Bruggen, Alternating current enhanced deposition of a monovalent selective coating for anion-exchange membranes with antifouling properties, Sep. Purif. Technol. 229 (2019) 115807. https://doi.org/10.1016/j.seppur.2019.115807

5.1. Introduction

Catecholamines represent the proteins responsible of the adhesive capacity of the blue mussel (*Mytilus edulis*) [152,153]. In recent years, they have gain attention due to their ability to auto polymerize in aqueous solutions and to attach to a wide range of surfaces, including polymeric membranes [154–156]. This has been a great advance in surface science due to the difficulty of modifying inert surfaces composed by low reactive bonds and for the possibility to create an adhesive layer in wet conditions [153,157]. The oxidation and polymerization reactions of catecholamines can be efficiently accelerated by using oxidant triggers such as cupric sulphate ($CuSO_4$) and hydrogen peroxide (H_2O_2), which have been found to also enhance the homogeneity and stability of the coating [158–160]. Additionally, catecholamine coatings provide a highly hydrophilic membrane surface, which effectively reduces membrane fouling [35,158,161,162]. Moreover, these coatings show a great reactivity to amino and thiol groups and thus, they can act as an adhesive interface layer for an easy post-functionalization [153,163]. Even if dopamine is the most widely used catecholamine, L-3,4-dihydroxyphenylalanine (L-Dopa) has been found of special interest due to the incorporation of a carboxylic acid group in its chemical structure. Therefore, L-Dopa coated membranes can create a highly stable covalent bonding between the carboxylic acid group and amine containing compounds by amino condensation reaction [158]. In this sense, a charged compound can be strongly bond to the polymerized L-polyDopa (L-PDA) surface to achieve monovalent selective properties. In addition, the application of an alternating current (AC) during the coating process has been found to accelerate the reaction kinetics and to greatly enhance the stability and homogeneity of the resultant coating [91,164,165].

This chapter shows a convenient modification route to obtain a monovalent selective AEMs by a two-step deposition process. A complete membrane characterization has been performed in order to understand the obtained membrane properties. The presence of the monoselective coating

has been confirmed by surface characterization and the selective separation capacity was confirmed by desalination experiments. Furthermore, the addition of a negatively charged layer greatly enhances the resistance to organic fouling. The feasibility of the presented methodology for obtaining monovalent selective separation was corroborated.

5.2. Materials and methods

5.2.1. Chemical reagents

Tris (hydroxymethyl) aminomethane (Tris-HCl, 99.8 %), HCl (36.5 % (v/v)), NaOH, copper sulphate ($CuSO_4$), Na_2SO_4, NaCl, and L-3,4-dihydroxyphenylalanine (L-Dopa) were purchased from Sigma Aldrich KGaA (Germany). Hydrogen peroxide (H_2O_2, 35 %) was obtained from Chem-Lab N.V., Belgium. 4,4'-Diamino-2,2'-biphenyldisulfonic Acid (DBSA, up to 30 % hydrate) was purchased from Cymit Quimica S.L., Spain. N-(3-Dimethylaminopropyl)-N′-ethylcarbodiimide hydrochloride (EDC·HCl), N-Hydroxysuccinimide (NHS), Sodium dodecylbenzenesulfonate (SDBS) and bovine serum albumin (BSA) were acquired from Aladdin Industrial Co. Ltd., China. All the chemicals were used without further purification, MilliQ water was used throughout the experiments.

5.2.2. Membranes

Neosepta AMX anion-exchange and CMX cation-exchange membranes used in the experiments were purchased from Astom Corp., Japan.

5.2.3. Construction of the monoselective layer

The monoselective layer was constructed by two modification steps. The modified membrane area was 28.27 cm^2. In the first step (Fig. 35), L-Dopa was coated on the surface of an AMX membrane by oxidation and autopolymerisation reaction. The buffer solution was a mixture of 50 mM

Tris-HCl and 5 mM $CuSO_4$. The pH of the buffer solution was adjusted to 8.8 by adding an adequate amount of HCl. 0.3 g L-Dopa were dissolved in 150 ml buffer solution, the mixture was then poured into the modification cell. Subsequently, 0.2 mL H_2O_2 was added to favour the oxidation and polymerization of L-Dopa into L-PDA. The solution was stirred at 200 rpm for 4 h at room temperature. After the modification, AMX-LPDA membranes were rinsed with MilliQ water and stored wet.

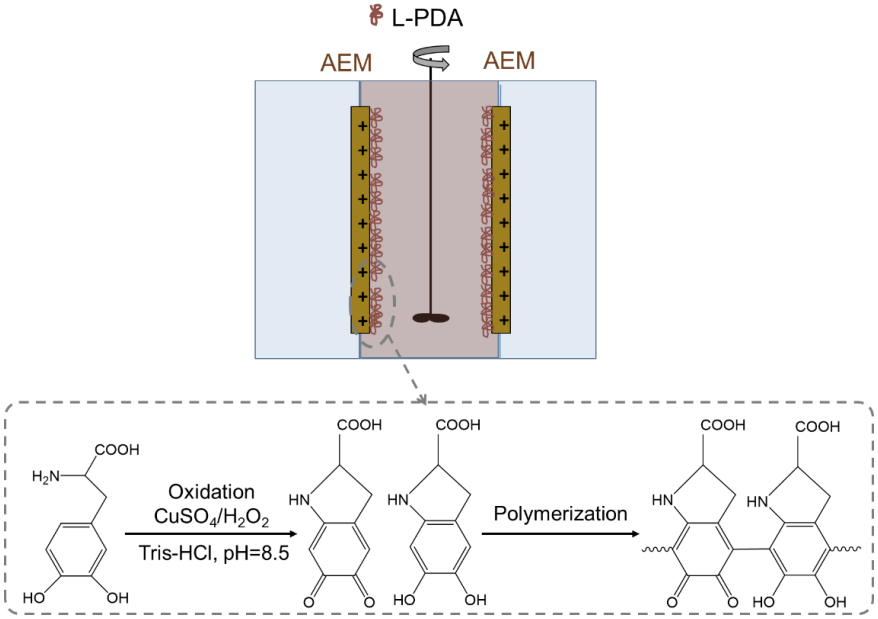

Figure 35. First modification step, experimental setup, and chemical reaction.

The second modification step is represented in Fig. 36. In this step, 4,4'-diamino-2,2'-biphenyldisulfonic acid (DBSA) was chemically bonded to AMX-LPDA by amide condensation reaction. The reaction was favoured by the application of an alternating current (AC) (PPS series programmable AC Power source, from Everfine Corp., China). Firstly, 1 g DBSA was dissolved in 1000 mL of 0.5 M NaCl aqueous solution. An adequate amount of NaOH was added to the mixture in order to dissolve the DBSA. The pH of the solution was kept in the range between 5 and 9 by the addition of the necessary amount of HCl. 150 mL of the mixture were poured into the modification cell, in the compartment facing the active side of the

membrane. Then, 0.1 g EDC·HCl and 0.06 g NHS were added as reaction catalysts, the solution was stirred for 10 min to totally dissolve the catalysts. A solution of Na_2SO_4 0.2 M was continuously circulated for electrode rinse. An electrical potential of 15 V at a frequency of 50 Hz AC was applied to speed up the reaction and to enhance the homogeneity and stability of the coating [91,166,167]. The solutions were stirred at 200 rpm for 12 h at room temperature. Finally, the resulting membranes were rinsed with MilliQ water and stored wet.

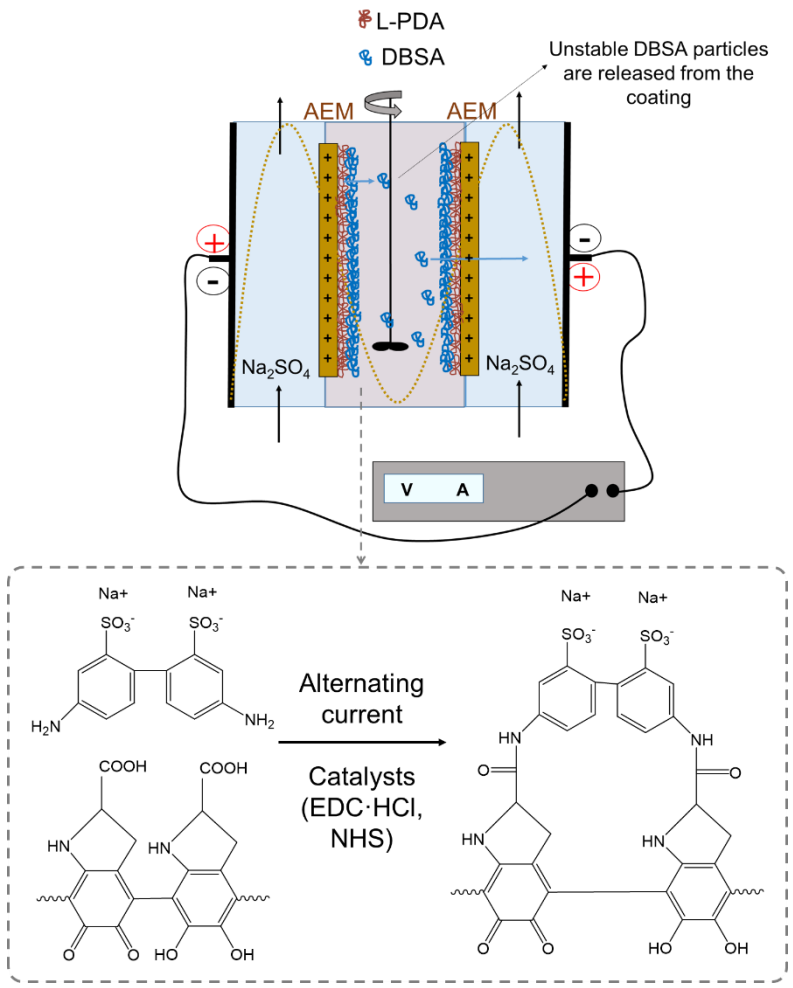

Figure 36. Second modification step, experimental setup, and chemical reaction.

5.2.4. Surface characterization

Fourier attenuated atomic force microscopy (ATR-FTIR) (Nicolet 6700 from Thermo Fisher Scientific S.A., USA) was employed to investigate the functional groups in the membrane surface. Prior to the analysis, membranes were dried at 60º for 48 hours in a vacuum oven.

An atomic force microscope (AFM) (Bruker Corp., USA) was used to evaluate surface roughness. The membranes were previously dried in a vacuum oven at 60º for 48 hours. The analysis was performed in tapping mode. The area of the captions was 1 μm^2. The root average roughness (R_a, the average deviation of the peaks and valleys from a mean height) and the root square roughness (R_q, standard deviation of the peaks and valleys) were calculated by the average of three values from each sample.

A contact angle meter (OCA20, Dataphysics Instruments GmbH, Germany) was used to evaluate the surface hydrophilicity. A droplet of deionized water (2.0 μL) was provided by a micropipette. A circle fitting analysis software was utilized to record the contact angle. Prior to the analysis, membranes were dried at 60º in a vacuum oven.

5.2.5. Evaluation of electrochemical properties

A four compartments cell shown in Fig. 37 was used to measure surface electro resistance and current-voltage curves (C-V curves) of the membranes. A potentiostat/galvanostat (WY605, Everfine Photo-e-info Co. Ltd., China) was utilized to apply a constant direct current (DC) to the system. Two Ag/AgCl reference electrodes were used to measure the voltage drop in the system. Before taking each measurement, the system was stabilized for 30 seconds, in order to reach a steady state in each membrane. The effective membrane area was 7.06 cm^2.

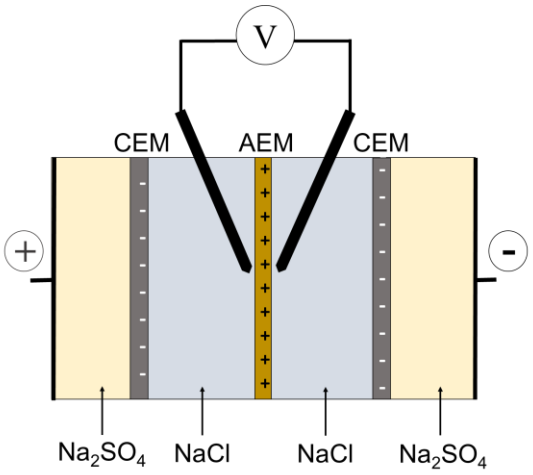

Figure 37. Four compartments cell used for membrane electrochemical characterization. AEM is the membrane, CEM are auxiliary membranes

5.2.5.1. *Electrical resistance*

A solution of 0.5 M NaCl was used as feed and a 0.2 M Na_2SO_4 solution was used as the electrode rinse. The solutions were continuously pumped in order to avoid concentration polarization in the feed and to equilibrate the electrode rinse solution. A current of 0.04 A was applied and the voltage drop was measured by a digital Multimetre. The surface electric resistance was calculated as:

$$R_m = \frac{U - U_0}{I} \cdot S \tag{14}$$

where R_m (Ω cm^2), is membrane electro resistance; U (V), measured voltage drop; U_0 (V), is the voltage drop of the system (without membrane); I (A), the applied current and S (cm^2) the effective membrane area. For each membrane, three measurements of the voltage drop were taken, and the average and standard deviation is reported.

5.2.5.2. *Current-voltage curves*

A solution of 0.05 M NaCl was employed as feed and a 0.2 M Na_2SO_4 solution was circulated as the electrode rinse solution. Both solutions were continuously circulated, in order to avoid concentration polarization in the

feed, and to equilibrate the electrode rinse solution. The current was increased stepwise from 0.01 to 0.2 A and voltage drop was recorded in each step. To obtain the C-V curves, the current density, I_d *(mA·cm^{-2})* and the voltage drop, *U (V)*, were graphically represented. The obtained C-V curves were analysed and the Limiting Current Density (LCD) of each membrane was determined.

5.2.6. Selective separation of monovalent anions

The selective separation capacity of the membranes was tested by ED experiments. The employed setup is represented in Fig. 38.

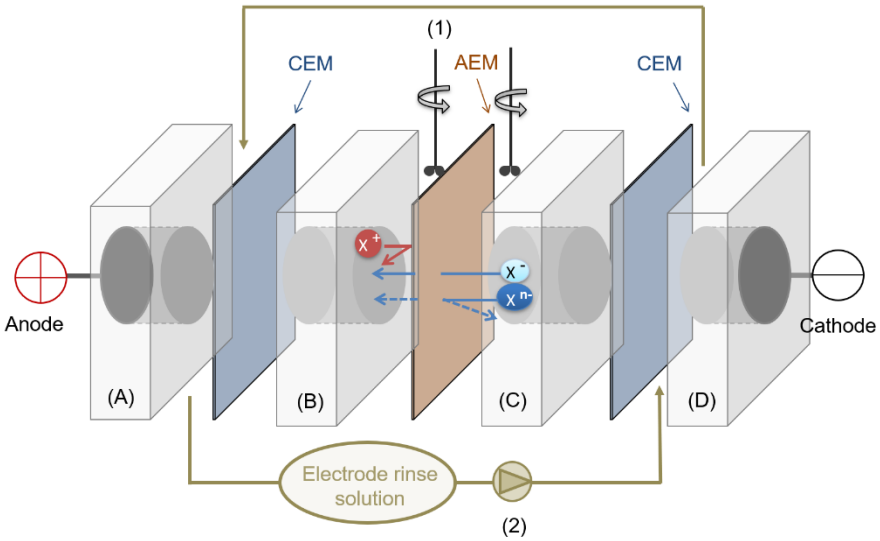

Figure 38. Experimental set up employed for the evaluation of membrane transport properties. CEM: cation-exchange membrane (Neosepta CMX). AEM: anion-exchange membrane (under analysis). Electrodes: dimensional stable electrodes (Ti/mixed metal oxides). Electrode compartments (a, d): 5 cm thickness, 28.27 cm^2 cross-sectional area, recirculation of the solutions. Concentrate (b) and dilute (c) compartments: 5 cm thickness, 19.64 cm^2 cross-sectional area, under stirring. (1) Mechanical rod stirrer, (2) peristaltic pump.

The active area for the membrane under investigation in this setup was 19.63 cm^2. A mixture of monovalent and divalent salts (0.05 M NaCl and Na_2SO_4) was used as feed and stirred at 150 rpm, 0.2 M Na_2SO_4 was circulated for electrode rinse. The active surface of the modified

membranes was placed facing the dilute compartment. The experiments were carried out at 8 mA·cm^{-2} constant current. The decrease of Cl^- and SO_4^{-2} concentrations in the dilute compartment was analysed by Ionic Chromatography (Dionex ICS-1600 from Thermo Fisher Scientific S.A., USA).

The separation efficiency, S_t (%), was used to evaluate the efficiency in the selective separation of components A and B (multivalent and monovalent anions, respectively). $S(t) > 0$ suggests that a selective separation was achieved. $S(t)$ was calculated as [168,169]:

$$S(t) = \frac{(c_A(t)/c_A(0)) - (c_B(t)/c_B(0))}{(1 - c_A(t)/c_A(0)) + (1 - c_B(t))/c_B(0))} \cdot 100 \quad (15)$$

where $c_A(0)$ and $c_B(0)$ are the initial concentrations of components A and B; $c_A(t)$ and $c_B(t)$ are the concentrations of A and B at time t.

The permselectivity (P_A^B) refers to the transport properties of the anions through the membrane. $P_A^B > 1$ indicates a favourable transport of component B (monovalent ion) in respect to component A (multivalent ion). It was calculated as follows [158]:

$$P_A^B = \frac{t_B/t_A}{c_B/c_A} = \frac{J_B \cdot c_A}{J_A \cdot c_B} \quad (16)$$

where t_A and t_B are the transport number of component A and B (dimensionless); c_A and c_B (mol·L^{-1}) are concentrations; J_A and J_B (mol·m^{-2}·s^{-1}) are the flux of the components A and B.

$$J_i = \frac{V \cdot \frac{dc_i}{dt}}{A} \quad (17)$$

where V (L) is the volume of solution; dc_i (mol·L^{-1}), is the concentration change of the component i at time t; dt (s), the time and A (m^2) is the membrane active area.

5.2.7. Stability of the monoselective layer

The prepared membranes were subjected to an accelerated stability test, the procedure was described before in [170]. For that purpose, the membrane under investigation was placed in the setup shown in Fig. 38; however, the active area of the membrane was faced to the concentrate compartment at this time. A 0.5 M NaCl solution was used as feed and stirred at 150 rpm, 0.2 M Na_2SO_4 was circulated as the electrode rinse solution. A direct current (DC) of 0.2 A was applied for 3 hours. Under the electric field, the unstable negatively charged DBSA would be detached from the membrane surface and move towards the anode. After this procedure, the selective separation of monovalent anions was tested again and compared with the pristine AMX-LPDA#DBSA membrane in terms of selective separation capacity (ED experiments, separation efficiency and permselectivity).

5.2.8. Evaluation of antifouling properties

Sodium dodecylbenzenesulfonate (SDBS) and bovine serum albumin (BSA) were used as organic foulants to evaluate membrane antifouling properties. For that purpose, 100 ppm of the foulant was dissolved in a 0.5 M NaCl solution and poured into the dilute compartment of the ED cell (Fig. 38). A 0.5 M NaCl solution was pumped through the concentrate compartment. The experiments were carried out for 3 hours under 0.2 A DC current. After this procedure, the electrical resistance surface was measured again and was compared with the pristine membranes.

5.3. Results and discussion

5.3.1. Surface characterization

The functional groups on the membrane surface were determined by ATR-FTIR; the resultant spectra are shown in Fig. 39.

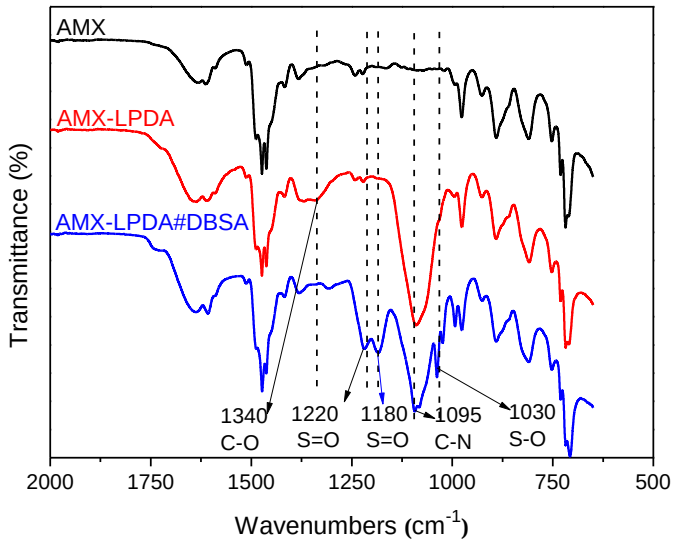

Figure 39. ATR-FTIR spectra of AMX, AMX-LPDA and AMX-LPDA#DBSA membranes.

It can be observed the presence of new bands after the modification with L-Dopa and after DBSA assembly. After the first modification step, AMX-LPDA membrane presents a characteristic peak at 1340 cm^{-1}, which belongs to the asymmetric stretching vibration of C-O in the carboxylic group of L-Dopa [171]. This membrane shows also a peak at 1095 cm^{-1}, which corresponds to the of C-N bonds of L-PDA [172]. The final membrane (AMX-LPDA#DBSA) shows the same peak (1095 cm^{-1}) that could be associated to the amide group formed by the condensation reaction between L-PDA and DBSA, and to the uncoated L-PDA. Moreover, AMX-LPDA#DBSA membrane shows other two new peaks at 1220 and 1180 cm^{-1}, which indicate the presence of the asymmetric stretching vibrations of the S=O, and a peak at 1030 cm^{-1} which belongs to the symmetric and asymmetric stretching vibrations of S-O. These peaks evidence the presence of DBSA in the final membrane [92,158,166].

Fig. 40 shows the water contact angles (WCAs) and surface 3D AFM images of the membranes.

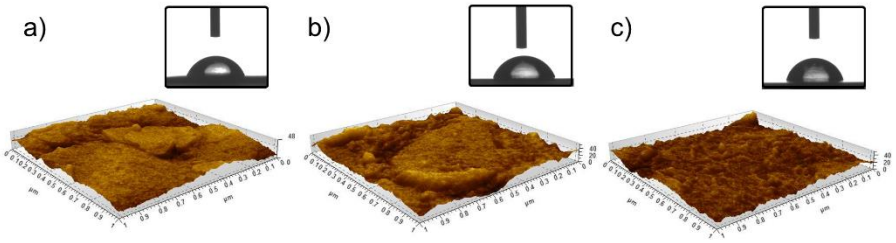

Figure 40. Surface water contact angle (WCA) and 3D AFM images of a) original AMX, b) AMX-LPDA and c) AMX-LPDA#DBSA.

The surface hydrophilicity and roughness are directly related with membrane antifouling properties. Low water contact angles indicate a high hydrophilicity and hence, better antifouling properties [173]. At the same time, rough membranes are more prone to fouling than membranes with a smooth surface, especially to colloidal fouling [174,175]. The original AMX membrane had a WCA of 69.9º± 0.1º and a relatively smooth surface (R_q 6.0 ± 0.4 nm and R_a 4.6 ± 0.3 nm). The AMX-LPDA membrane shows a small increase in WCA (72.4º ± 0.6º) and in roughness (R_q 11 ± 2 nm and R_a 9 ± 2 nm), which was attributed to the non-uniform self-aggregation of L-PDA [176]. The AMX-LPDA#DBSA shows the highest WCA (79º± 2º); however, the stepwise increase in WCA is relatively small and the resultant membrane is still considered hydrophilic. The roughness of the resultant membrane is also higher (R_q 17 ± 1 nm and R_a 12.8 ± 0.7 nm); this is postulated to be due to the assembly of oodles molecules (DBSA), which cause the formation of a high number of small peaks [158], as can be observed in Fig. 40c.

5.3.2. Electrochemical properties

Table 8 shows the electrical resistance of the membranes.

Table 8. Surface electro resistance (R (Ω·cm²)) of the membranes

Membrane	R (Ω·cm²)
AMX	1.5 ± 0.03
AMX-LPDA	3.5 ± 0.02
AMX-LPDA#DBSA	3.6 ± 0.1

As can be noticed, the electrical resistance increases stepwise with the coating process. This could be attributed to the formation of additional layers on the membrane surface that compromise the electric conductivity [177]. However, the electrical resistance of the resultant membrane is still relatively low (3.6 Ω·cm²).

Polarization curves (C-V curves) were measured in order to analyse the transport properties through the membrane and the Limiting Current Density (LCD) (Fig. 41).

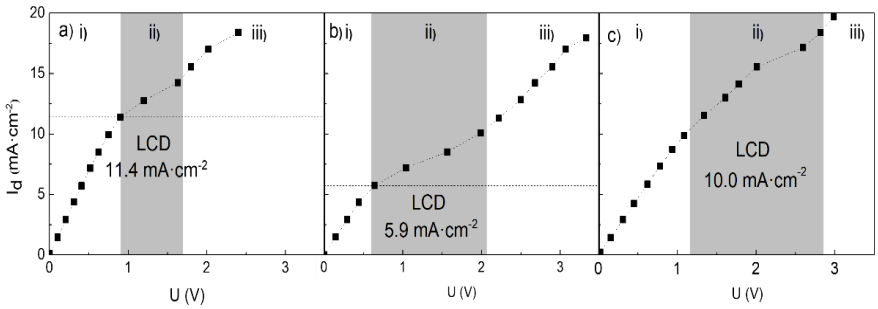

Figure 41. Current-Voltage curves of a) AMX, b) AMX-LPDA and c) AMX-LPDA#DBSA membranes. i) Ohmic region, ii) LCD and plateau region iii) Over limiting current region.

Three regions were distinguished in the C-V curves. Firstly, the Ohmic region (i) at low current densities is represented by a linear increase of the voltage drop within the current density. At higher current densities, the LCD is achieved, and the plateau region starts when the concentration of

ions close to the membrane surface facing the dilute compartment reaches zero (ii). The LCDs of the membranes were graphically determined: 11.4 $mA \cdot cm^{-2}$ for AMX (Fig. 41a), 5.9 $mA \cdot cm^{-2}$ for AMX-LPDA (Fig. 41b) and 10.0 $mA \cdot cm^{-2}$ for AMX-LPDA#DBSA (Fig. 41c). The LCD of the membranes is often affected by the conductivity of the membranes and the concentrations of the solutions. As it is shown in Fig. 41, in the 0.1 M NaCl solution, with increasing of the membrane surface electric resistance, the LCD is decreased. In addition, the charged groups on the membrane surface also affect to the LCD of the membrane. Thus, the LCD value of resulting membrane was lower than original AMX, but higher than AMX-LPDA. For an efficient use of the energy, membranes should be operated under the LCD. At higher current densities, the over limiting current region (iii) can be distinguished. In these regions, the current is carried by the OH^- and H^+ ions formed as a consequence of water splitting [178,179].

5.3.4. Selective separation of monovalent ions and stability of the coating

The concentration changes of monovalent (Cl^-) and multivalent (SO_4^{2-}) in the dilute compartment during ED experiments are represented in Fig. 42.

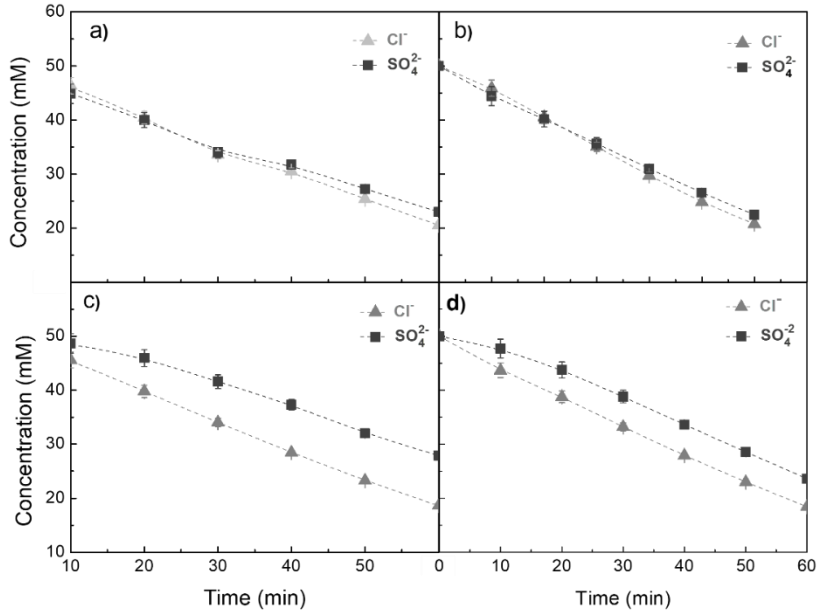

Figure 42. Concentration changes in the dilute compartment of monovalent (Cl^-) and divalent (SO_4^{2-}) ions during 60 minutes of ED experiments at 8 $mA \cdot cm^{-2}$ CC. a) Original AMX, b) AMX-LPDA, c) AMX-LPDA#DBSA, d) after stability test AMX-LPDA#DBSA.

As can be observed, both types of anions are slightly separated after 60 min ED by the original AMX membrane or the AMX-LPDA coated membrane (Fig. 42a and 42b, respectively). However, the AMX-LPDA#DBSA membrane shows a clear separation capacity between monovalent and multivalent ions (Fig. 42c). Moreover, it has been proved that AMX-LPDA#DBSA keeps the selective separation capacity after being subjected to the accelerated stability test described in Section 5.2.7 (Fig. 42d). In respect to the ionic fluxes, the original AMX membrane shows a flux of 2.34 $mol \cdot m^{-2} \cdot h^{-1}$ for chloride ions and 2.15 $mol \cdot m^{-2} \cdot h^{-1}$ for sulphate ions. In the other hand, the coated membrane (AMX-LPDA#DBSA) has an ionic flux of 2.47 $mol \cdot m^{-2} \cdot h^{-1}$ for chloride and 1.84 $mol \cdot m^{-2} \cdot h^{-1}$ for sulphate, indeed, the ionic flux of multivalent anions is decreased due to the presence of the monoselective coating.

The separation eficiency (S) and permselectivity (P) were calculated for each membrane after 60 minutes of ED experiment. The results are shown in table 9.

Table 9. Separation efficiency (S_{60} (%)) and permselectivity (P_{60}) of the membranes after 60 minutes ED experiment.

Membrane	S_{60} (%)	$P_A^B{}_{60}$
AMX	4.9	1.25
AMX-LPDA	2.9	1.14
AMX-LPDA#DBSA	17.3	2.13
Stability-AMX-LPDA#DBSA	9.0	1.53

The original membrane (AMX) already shows a mild separation capacity of 4.9 % between monovalent and multivalent ions and a permselectivity for monovalents of 1.25 (P_A^B > 1, indicates selective separation). After L-PDA coating, the membrane (AMX-LPDA) does not improve in selectivity for monovalents anions. However, after DBSA assembly (AMX-LPDA#DBSA membrane), the separation capacity is increased to 17.3 % and the permselectivity is doubled (P_A^B up to 2.13). After the accelerated stability test, the separation eficiency and the permselectivity were slightly decreased (9.0 % and 1.53, respectively), although these values are still higher than the original AMX membrane and the AMX-LPDA membrane.

5.3.5. Antifouling properties

Organic colloids, surfactants and proteins are present in natural and waste waters. These compounds are typically negatively charged, and thus electrostatically attracted by the positive charges of AEMs. For this reason organic fouling is the principal type of fouling affecting AEMs [158,180,181]. In this study, the surfactant sodium dodecylbenzenesulfonate (SDBS) and the protein bovine serum albumin (BSA) were used as organic foulants. Fig. 43 shows the electrical resistance

of the membranes before and after being subjected to three hours accelerated fouling tests.

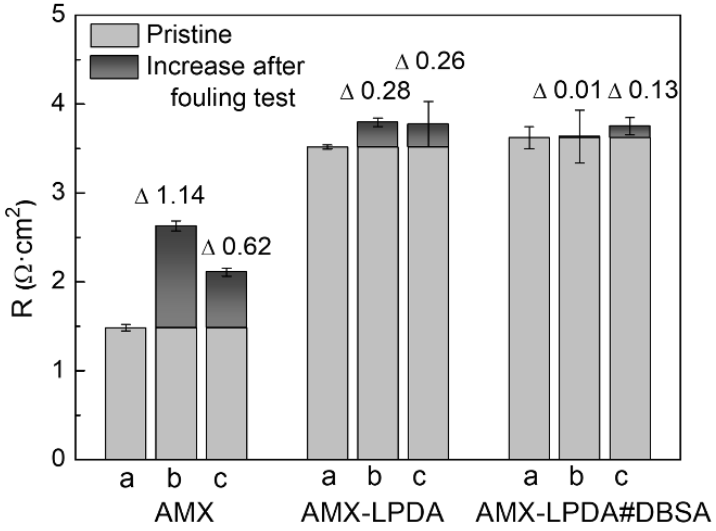

Figure 43. Electrical resistance of the membranes: a) before the fouling test, b) after SDBS fouling test and c) after BSA fouling test.

As can be observed, the unmodified AMX membrane shows a significant increase of electrical resistance after both fouling tests (an increase of 1.14 Ω·cm² after SDBS and 0.62 Ω·cm² after BSA). Both surface modified membranes (AMX-LPDA and AMX-LPDA#DBSA) show an enhanced antifouling effect. Nevertheless, the resistance to fouling of the resulting membrane (AMX-LPDA#DBSA) is the largest (only 0.01 Ω·cm² increase after SDBS and 0.13 Ω·cm² increase after BSA), probably due to the negatively charged DBSA assembly, which increases the repulsion of negatively charged organic foulants [166,181,182].

5.4. Conclusions

In the current Chapter, the monovalent selectivity and antifouling properties of a commercial AEM were improved by surface modification, in a two steps process. The first step was based on the adhesion capacity of

catecholamines under aqueous media by oxidative autopolymerisation. The second step consisted of bonding a negatively charged chemical compound to the coating, by amino condensation reaction, boosted by the application of an alternating current electric field. The main findings of this work are:

- Surface characterization of the membranes confirmed the presence of L-PDA and DBSA on the membrane surface.
- The electric resistance of the membrane was slightly augmented by the coating.
- The selective separation of monovalent anions was increased from 4.9 % in the original membrane up to 17.3 % in the resulting membrane (after 60 min desalination process). Further, the stability of the coating was successfully evaluated after the application of a reverse electric field.
- The resulting membrane showed an improved resistance to organic fouling, probably related to an enhanced electrostatic repulsion of negatively charged organic foulants.
- Overall, this work shows the feasibility of the suggested surface modification strategy, to enhance monoselective and antifouling properties of AEMs. Further research should be conducted on the implementation of the prepared membranes in specific applications such as nitrate or fluoride removal from drinking water or nutrient recovery from RO brines in the food industry or from urban wastewater.

6

Chapter 6. Nitrate-Selective Anion-Exchange Membranes prepared from end-of-life Reverse Osmosis membranes

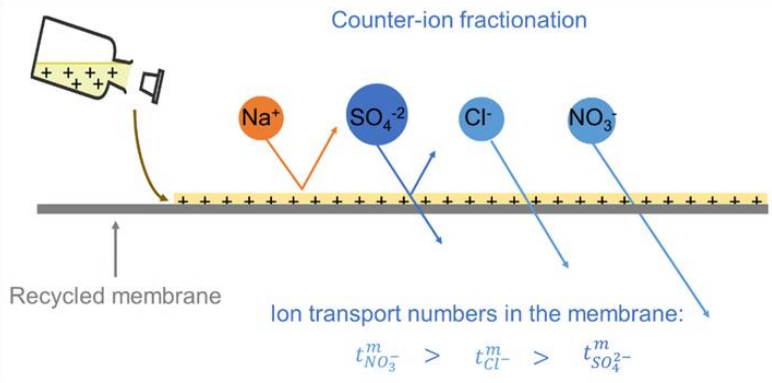

.

This Chapter has been published as:

A. Lejarazu-Larrañaga, J.M. Ortiz, S. Molina, Y. Zhao, E. García-Calvo, Nitrate-selective anion-exchange membranes prepared using discarded reverse osmosis membranes as support, Membranes. 10 (2020) 377. https://doi.org/10.3390/membranes10120377

6.1. Introduction

Nitrate pollution in natural waters has become a worldwide issue, mainly caused by the abusive use of nitrogen-rich fertilizers, uncontrolled sludge and slurry dumping, and a poor wastewater treatment (i.e., an uncompleted biological denitrification process) [183]. The excessive concentration of nitrates in surface and groundwater causes the eutrophication of rivers and lakes and the pollution of drinking water. In addition, nitrate is toxic to human health, causing methemoglobinemia and it is associated with cancer and adverse reproductive outcomes [184]. Thus, the European Commission limits nitrate concentration in drinking water to a maximum level of 50 ppm, along with the recommendation to keep it below 25 ppm [127,185]. This situation has motivated an increasing research on the development of effective technologies for nitrate removal [186].

In the current chapter, different strategies for increasing the selectivity to nitrates were combined. First, different types of anion-exchange resins were employed for membrane preparation. These resins differed in the length of the alkyl chains bonded as substituents to the quaternary amine, which promoted differences in the hydrophobic interactions of the resulting membranes. These hydrophobic interactions could enhance the repulsion of highly hydrated ions (i.e., sulphates) while promoting the permeation of ions accompanied by less water solvation molecules (i.e., nitrates). Second, the use of a recycled pressure filtration membrane with ultrafiltration properties as mechanical support could to help boosting the sieving effect. Finally, the influence of the operational current density during in ion fractionation was tested. Ternary mixtures of sodium salts containing an equimolar concentration of anions (NO_3^-, Cl^- and SO_4^{2-}) were used to compare the flux of each anion through the membranes. Results showed that the type of anion-exchanger could constitute the main parameter affecting the selective separation of anions.

6.2. Materials and methods

6.2.1. Chemical reagents

NaClO (14 % (v/v) as free chlorine, THF, NaCl, Na_2SO_4 and sodium nitrate ($NaNO_3$) were purchased from Scharlab S.L., Spain. PVC (Mw = 112,000 g·mol^{-1}) was supplied by ATOCHEM S.A., Spain. Amberlite® IRA-402 and Lewatit® Sybron Ionac® SR-7 anion-exchange resins were supplied by Merck KGaA, Germany. Purolite® A600/9413 anion-exchange resin was supplied by MemBrain® s.r.o., Czech Republic. The characteristics of the anion-exchange resins are reported in Table 10. MilliQ water was used throughout the experiments.

Table 10. Properties of the anion-exchange resins used in this study.

Anion-Exchange Resin	Amberlite® IRA-402	Purolite® A600/9413	Lewatit® Sybron Ionac® SR-7
Matrix	Styrene–divinyl benzene cross-linked copolymer	Styrene–divinyl benzene cross-linked copolymer	Styrene–divinyl benzene cross-linked copolymer
IEC (equiv.·L^{-1}) *	1.2	1.6	0.8
Ion-exchange group	R–$(CH_3)_3N^+$	R–$(CH_3)_3N^+$	R–$(C_3H_7)_3N^+$
Ionic form	Cl^-	Cl^-	Cl^-

* IEC: ion-exchange capacity.

6.2.2. Membranes

An EoL polyamide thin film composite (PA-TFC) RO membrane (TM 720–400, Toray Industries, Inc., Japan), used and discarded by a brackish water desalination plant located in Spain, was used in this study as a mechanical support in membrane preparation [54], for more details see Section 3.2.3.

Ralex® AMH-PES membrane from Mega a.s. (Czech Republic) was used to compare the performance of the prepared membranes with a commercial one. Neosepta CMX membranes from Astom Corp. (Japan)

were used as auxiliary CEMs, for the separation of anolyte/catholyte compartments, in electro-separation experiments.

6.2.3. Anion-Exchange Membrane preparation

The pre-treatment of the EoL RO membrane and the preparation of the recycled AEMs by casting and phase inversion were described in Sections 3.2.3 and 3.2.4 (Chapter 3), respectively. The membranes were prepared by extending an 800 μm casting solution and evaporating the solvent at room temperature during 60 min before the phase inversion.

In this study, different membranes were prepared using the ion-exchange resins listed in Table 10. In addition, a batch of membranes were prepared using the recycled membrane as mechanical support (i.e., casting the polymeric mixture on the PSF side of the membrane), these membranes were named henceforth as Amb-RE, Pur-RE and Lew-RE, (membranes prepared with Amberlite® IRA-402, Purolite® A600/9413 and Lewatit® Sybron Ionac® SR-7 ion-exchange resins, respectively). To elucidate the effect of the recycled membrane support in the fractionation of the counter-ions, another batch of membranes were prepared without using any mechanical support (i.e., casting the polymeric mixture directly on the glass plate), these membranes were named henceforth as Amb, Pur and Lew (membranes prepared with Amberlite® IRA-402, Purolite® A600/9413 and Lewatit® Sybron Ionac® SR-7 ion-exchange resins, respectively). Table 11 summarizes the membranes under study.

Table 11. Summary of the analysed membranes.

Membrane	Anion-Exchange Resin	Mechanical Support
Commercial AMH-PES	Unspecified (ion-exchange group, R–$(CH_3)_3N^+$)	Polyester
Recycled ultrafiltration-like membrane (RE-UF)	None	Polyester
Amb-RE	Amberlite® IRA-402	RE-UF
Amb		Without support
Pur-RE	Purolite® A600E/9149	RE-UF
Pur		Without support
Lew-RE	Lewatit® Sybron Ionac® SR-7	RE-UF
Lew		Without support

6.2.4. Membrane Characterization

6.2.4.1. Scanning Electron Microscopy (SEM) and Energy-Dispersive X-ray Spectroscopy (EDX)

The surface morphology of the prepared membranes was analyzed by SEM using an XL30 ESEM Model (Phillips N.V., Amsterdam, the Netherlands). The membrane elemental composition was analyzed using a Bruker Nano X-ray detector by dispersive energy (EDX) and equipped with an XFlash detector 5030 coupled to a FESEM S-8000 Model (Hitachi, Ltd., Tokyo, Japan). Prior to the analysis, the samples were dried at 50°C for 48 h. Then, all the samples were chrome sputtered with a Sputter Coater Quorum Q150T ES model (Quorum Technologies Ltd., Laughton, United Kingdom) to achieve 13–15 nm-thickness.

6.2.4.2. Thickness, Ion-Exchange Capacity, Water Content

The procedure for measurement membrane thickness, WC and IEC was described in Section 3.2.5.2 (Chapter 3).

6.2.4.3. Electrochemical Properties

The procedures for measuring calculating the electrical resistance and the permselectivity are described in Section 3.2.5.3 (Chapter 3).

6.2.5. Evaluation of the selective ion transport properties

The evaluation of the separation capacity was performed in a four compartments test cell (see Fig. 38, Chapter 5), under active conditions (i.e., by the application of an external potential). The effective membrane area was 19.64 cm^2. Dimensionally stable electrodes (DSE, titanium coated with iridium oxide, provided by Inagasa S.A., Barcelona, Spain) were employed as anode and cathode. The membrane under analysis was placed between the dilute and the concentrate compartments. Neosepta CMX CEMs were used to separate the anolyte and catholyte compartments. A solution of Na_2SO_4 0.2 M was circulated for electrode rinse by a peristaltic pump (3.6 $L \cdot h^{-1}$). An equimolar mixture of monovalent and divalent anions (Cl^-, NO_3^- and SO_4^{2-}, 50 mM) added as their sodium salts was used as feed. The volume of the dilute and concentrate compartments was 0.1 L, mechanical rod stirred were used for proper mixing. The experiments were performed at constant current (CC), at two different current densities (3.5 $mA \cdot cm^{-2}$ and 10 $mA \cdot cm^{-2}$). In this way, the effect of the current density on the selective separation was evaluated for each studied membrane. All the experiments were performed at room temperature (25 °C). The overall performance of the process was controlled by conductivity measurements using a conductivimeter (PC 52+ DHS XS, from XS instruments). The concentration of each anion in the diluted compartment during the experiments was measured using an 861 advanced compact IC Metrohm ionic chromatograph. Membrane transport properties were evaluated in terms of ionic molar flux (J_i^m), transport numbers (t_i^m), permselectivity between ions or relative transport number (P_B^A). These terms were calculated following the Eq. (18) to (21).

The total flux of ions through the membrane from the dilute to the concentrate compartment is directly related to the current density,

$$j = F \sum |z_i| J_i^m \quad (18)$$

where j (mA·cm^{-2}) is the current density, F is Faraday's constant, z_i is the electric charge of the ion and J_i^m is the flux of the ion.

In this sense, the flux of each ion (J_i^m) could be expressed with the next equation [187]:

$$J_i^m = t_i^m \frac{j}{|z_i| \cdot F} \quad (19)$$

where t_i^m is the transport number of the ion in the membrane phase.

The transport number of an ion in the membrane phase (t_i^m), quantifies the fraction of the charge that is carried through the membrane by a specific ion during the electro separation process can be calculated as:

$$t_i^m = \frac{|z_i| \cdot J_i^m}{\sum |z_i| \cdot J_i^m}, \quad (20)$$

The permselectivity between two anions or relative transport number of A to B (P_B^A) (Eq. (21)) indicates the ratio of charge that is transported by component A compared to component B (usually the ion with lower transport number in the membrane) divided by the ratio of concentrations (in equivalents) of both ions [188]:

$$P_B^A = \frac{t_A / t_B}{C_A / C_B} \quad (21)$$

where t_A and t_B are the transport numbers of A and B ions in the membrane phase, and CA and C_B (eq.·L^{-1}) are the concentrations, both for components A and B. The interest of this parameter is because it is useful to predict the behavior of the studied membrane in electrodialysis separations under different experimental conditions.

If we measure in an experiment the transport numbers for A and B, t_A = 0.6 and t_B = 0.4, in a solution with CA = C_B = 1 eq·L^{-1} and having the same

electric charge $z_A = z_B = 1$, the value of the relative transport number of A to B will be $P_B^A = 1.5$. In this simple example, it is possible to deduce that 1.5 equivalents of component A are transported through the membrane by migration for each equivalent of B that is transported.

Even if the transport number of each ion depends on its concentration in the solution, the parameter P_B^A could be considered reasonably constant during the experiment (when $j < j_{lim}$ and using diluted concentrations). Hence, if the experiment is repeated with CA = 2 eq·L^{-1} and C_B = 1 eq·L^{-1}, as the value of P_B^A = 1.5, it is possible to conclude that the rate $\frac{t_A}{t_B}$ = 3, indicating that 3 equivalents of component A would be transported for each equivalent of B. From a general point of view, $P_B^A > 1$ indicates a preferential transport of component A in respect to component B. It should be avoided to mix up the concepts of permselectivity between the counter-ions A and B (P_B^A) with the permselectivity between counter-ions and co-ions (α), reported in Eq. (3) of the Chapter 3.

Hence, P_B^A is measured under active conditions (i.e., by the application of an external potential), and it is related to the separation efficiency between the counter-ions in a multi-component mixture (i.e., NO_3^-, Cl^-, SO_4^{2-}). Though α refers to the affinity of the membrane for a reference counter-ion (i.e., Cl^- in EMs) in respect to a reference co-ion (i.e., Na^+ or K^+ in EMs), it is measured under passive conditions (i.e., without applying any external potential) and it is related to the current efficiency during the electro separation process.

Additionally, the separation efficiency (*S*) of the membranes was calculated and reported as Supplementary Material. The separation efficiency was introduced by [168] as an alternative for more common parameters such as the separation factor in other membrane technologies (i.e., nanofiltration). It reflects the relative difference in transport rate (see Supplementary Material, Eq. (S1)–(S9)) and ranges from 0 (no separation) to 1 (complete separation, i.e., $C_B(t) = 0$; component B completely removed from the dilute fraction).

6.3. Results and discussion

6.3.1. Membrane characterization

6.3.1.1. Main characteristics of the recycled membrane support

The recycled membrane support has been thoroughly characterized in previous works [63,69]. In the present work, the EoL RO membranes were subjected to 800,000 ppm·h NaClO. This exposition dose ensures the complete elimination of the fouling and the active polyamide layer and thus, the achievement of UF-like properties in terms of rejection (colloidal and macro compounds) and water permeability (10 – 50 $L \cdot m^2 \cdot h^{-1} \cdot bar^{-1}$) [63].

With respect to the morphology, the recycled membrane support is composed of two different polymeric layers: the polyester (PET) layer, as a mechanical reinforcement and the polysulfone (PSF) layer, with a microporous structure [69]. This membrane support is relatively tight in comparison with other mechanical supports employed in IEM preparation (i.e., nonwoven polyester fabric [134]). On the one hand, the lower porosity of the recycled membrane support could promote a better permselectivity to the resulting IEMs. On the other hand, it could also limit the electrical conductivity of the membranes. Further, the recycled membrane support is characterized to have a very high mechanical stability, inherited from the EoL RO membrane.

6.3.1.2. Anion-Exchange Membrane Morphology and Elemental Composition

Fig. 44 shows the SEM surface micrographs of RE-UF, Amb-RE, Pur-RE and Lew-RE.

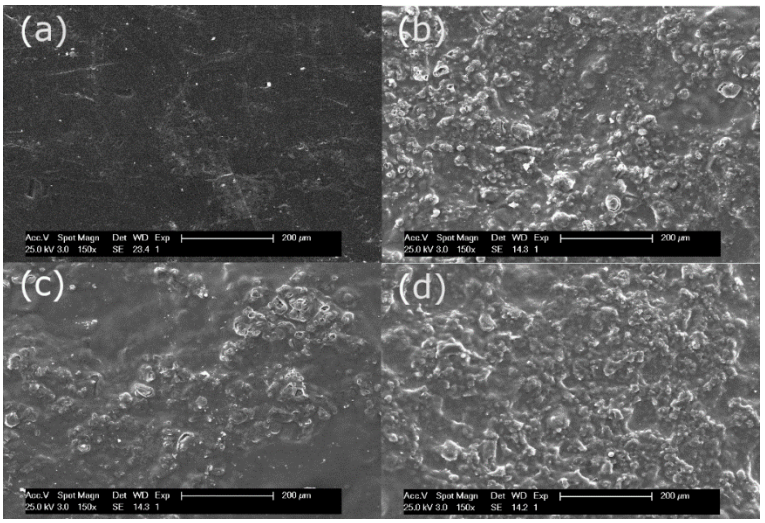

Figure 44. SEM surface micrographs of (**a**) Recycled ultrafiltration-like membrane (RE-UF), (**b**) Amb-RE, (**c**) Pur-RE and (**d**) Lew-RE.

Fig. 44a shows the polysulfone surface of the RE-UF membrane. It can be observed that this surface is smooth and free of foulants, confirming the success of the oxidative chemical cleaning. In Fig. 44b–44d, it can be observed the distribution of the ion-exchange resin particles on the membrane surface, bonded by the film-forming PVC. Amb-RE and Lew-RE membranes (Fig. 44b-44d) show a homogeneous distribution of the resin particles. Sonication and stirring of the polymeric mixture (before the casting) enhances the dispersion of the resin particles, reducing their agglomeration and precipitation and thus, achieving a homogeneous distribution on the membrane surface [131,189]. Differently, Pur-RE (Fig. 44c) shows a less uniform distribution, presenting areas with fewer ionic particles, which could be caused by a poor dispersion of the resin particles in the polymeric solution. Interactions between the Purolite ® A600/9413 anion-exchanger and the polymeric mixture could cause agglomeration and precipitation of particles and the consequent nonhomogeneous distribution of the resin particles in the membrane surface. The unequal distribution of the ion-exchange resin particles could cause anomalies and defects in the physicochemical and electrochemical properties of the resulting membranes [131]. Further, the Pur-RE membrane presents some

cracks in its surface that could promote an indiscriminate exchange of ions, reducing the permselectivity.

Additionally, EDX analysis was performed to study the chemical composition in both sides of prepared EMs (coated layer and support layer). The content of elemental measurements is shown in Table 12. The EDX images are presented in the Supplementary Materials, Fig. S 7. Complementarily, the EDX analysis of the RE-UF surface was performed; the elemental chemical composition is detailed in Supplementary Table S2.

Table 12. Chemical composition analysis by EDX: coated layer and support layer of the membranes with RE-UF.

Coated Layer						
	Amb-RE		**Pur-RE**		**Lew-RE**	
Element	% Weight	% Atomic	% Weight	% Atomic	% Weight	% Atomic
C	57.63	77.53	51.84	74.00	52.48	72.96
N	0.04	0.05	0.05	0.06	0.23	0.27
O	5.69	5.74	4.58	4.90	7.89	8.23
S	0.60	0.30	0.64	0.34	0.51	0.27
Cl	36.04	16.39	42.90	20.70	38.89	18.27
Support Layer						
	Amb-RE		**Pur-RE**		**Lew-RE**	
Element	% Weight	% Atomic	% Weight	% Atomic	% Weight	% Atomic
C	74.78	82.34	64.80	71.62	62.52	69.13
N	0.00	0.00	0.00	0.00	0.01	0.01
O	17.81	14.71	33.38	27.67	36.98	30.67
S	4.64	1.92	0.85	0.35	0.24	0.10
Cl	2.77	1.03	0.96	0.36	0.24	0.09

The elements C, N, O, S and Cl were observed by EDX analysis on both sides of each membrane. The Cl indicated the presence of PVC, added as a

binder in the casting mixture. Subsequently, Cl was not detected on the surface of the RE-UF (see Supplementary Material, Table S 2). The presence of Cl in the support layer indicates that the PVC solution has penetrated the membrane support. This could be caused by the fact that the employed organic solvent (THF) has dissolved the polysulfone layer. The penetration of the PVC into the recycled support provides high adherence to the coated layer and the consequent enhancement of the mechanical properties in AEMs [54]. Still, the % atomic of Cl is higher on the coated side than on the support side. This could be owing to the fact that the PVC solution was not fully embedded in recycled support. The low % of atomic of N found in the coated layer could mean that the resin particles are almost totally covered by the PVC film. A. Awasthi et al. [190] have reported 4.24 atomic % of N in EDX analysis of this type of pure resins (without being embedded into a polymer matrix). Further, N was not detected in the support layer. It would seem reasonable to consider that the resin contained in the PVC layer is not homogeneously distributed in the entire cross-section of the polyester support. This would increase the heterogeneity in the distribution of the ionic sites across the membrane section, which could result in tortuous and noncontinuous channels for the exchange of ions. This finding is in accordance with the high resistance results found in these membranes (see Section 6.3.1.4).

6.3.1.3. Thickness, Water Content, and Ion-Exchange Capacity

Fig. 45 reports the average thickness, water content (WC) and ion-exchange capacity (IEC) of the studied membranes.

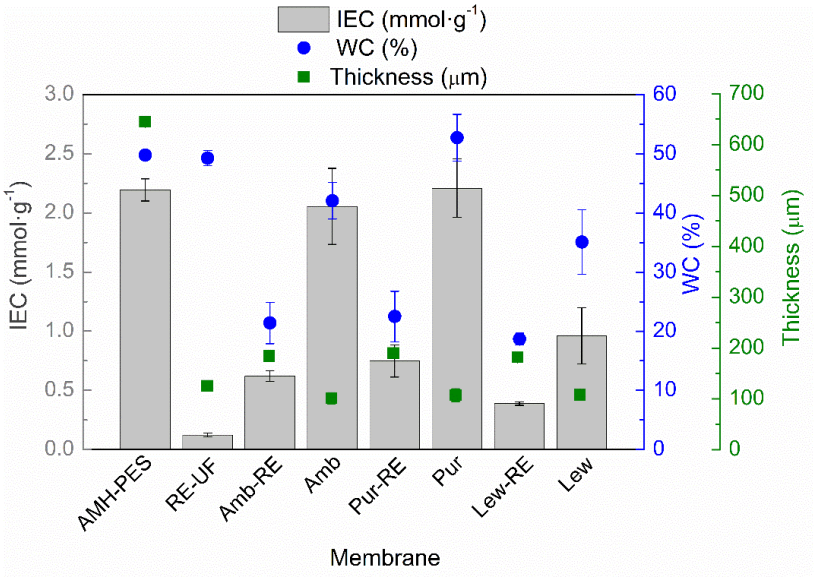

Figure 45 Ion-exchange capacity (IEC, mmol·g^{-1}); water content (WC, %) and thickness (μm) of the studied membranes.

As it can be observed, the highest thickness corresponds to AMH-PES, as two layers of polyester as a support are added during production to ensure mechanical stability. The recycled membrane support (RE-UF) has an average thickness of 126 μm. After the casting, the solvent evaporation and the phase inversion, the average thickness of the prepared membranes is around 185 μm. Interestingly, membranes without mechanical support have an average thickness of 106 μm. These measurements indicate that the polymeric solution has penetrated the mechanical support, lowering the thickness of EMs in respect to the sum of RE-UF support and membranes without support. As mentioned before, this could promote the high adherence of the coated layer to the recycled support, providing mechanical stability to the whole membrane.

The IEC of a membrane is directly related to its swelling capacity (WC) [90]. In this way, higher IEC is reflected in a greater WC, as can be observed in Fig. 45. The only exception is the case of RE-UF support, which having near-zero IEC (as it is vacant of fixed functional groups), shows a high wettability. This can be attributed to the porous structure of the polysulfone in the RE-UF membrane, which increases the volume of the cavities where

water can be contained [69]. On the contrary, the use of the RE-UF membrane in IEM preparation reduces the WC, probably due to the formation of a compact membrane structure, where the coating is embedded on the support, reducing the cavities for containing water. Further, the IEMs without mechanical support have a higher water content that could be caused by greater penetration of water in the membrane structure during the phase inversion, conforming cavities where water can be contained. Thus, the reduced IEC of the membranes with RE-UF support can be attributed to both the lower WC of these membranes and to the lowered number of functional groups per membrane mass in respect to the membranes without RE-UF. The IEC and the WC of the membranes prepared with Lewatit ® Sybron Ionac® SR-7 anion-exchangers are particularly low. This could be related to the presence of propyl chains bonded to the quaternary amine ($R–(C_3H_7)_3N^+$), instead of the methyl groups ($R–(CH_3)_3N^+$), that are present in Amberlite® IRA-402 and Purolite ® A600/9413 resins (Table 11). The increase in the length of the alkyl chain bonded to the N^+ group is related to an increased hydrophobicity of the ionic sites, which could reduce the WC and IEC of the resulting membranes [112,188]. The low WC and IEC of the EMs prepared using the recycled support could compromise the electrical conductivity of the membranes (see Section 6.3.1.4).

6.3.1.4. Electrochemical properties

Fig. 46 shows the electrical resistance (R) and the permselectivity (α) of the membranes.

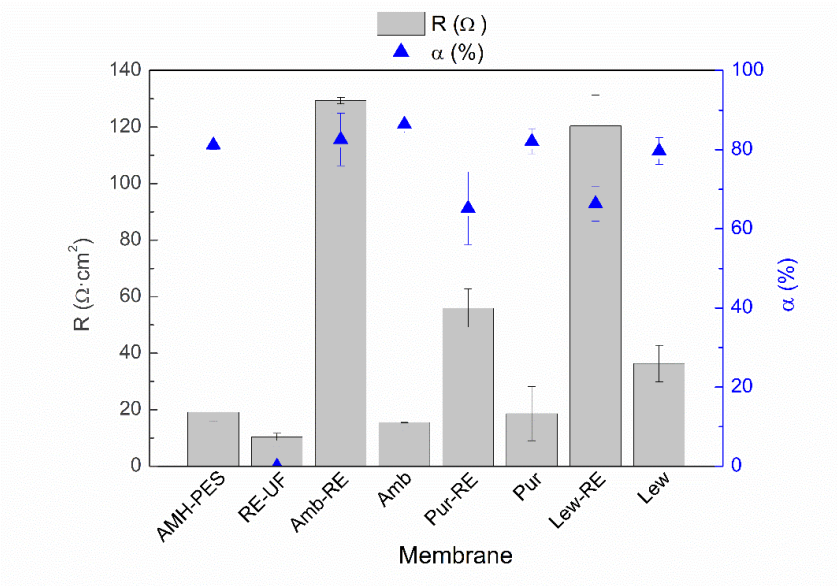

Figure 46. Electrical resistance (R, Ω·cm²) and permselectivity (α, %) of the studied membranes.

As mentioned before, membrane properties are closely related to each other. In such a way that, high IEC and water content promote connected ion channel paths through the membrane, increasing the electrical conductivity. Moreover, excessive swelling can result in a loose structure, with too expanded ion channel paths, which can generate an indiscriminate exchange of ions and reduce the permselectivity [90,188]. In Fig. 46, it can be noticed that the electrical resistance of the prepared EM is considerably higher than the simple sum of the resistances of the coating and the RE-UF support. This effect could be attributed to the differences in the distribution of the ion-exchange resin between the coated layer and the support layer, as it was demonstrated by EDX analysis (Table 12). Moreover, the formation of a compact membrane structure with a low WC and IEC could also contribute to the reduction of membrane conductivity [80,90,135]. Differently, the Pur-RE membrane shows lower electric resistance than other membranes with mechanical support, which could be caused due to an accumulation of anion-exchange resin particles or to the presence of cracks in the surface of the tested membranes (see Fig. 46b). Membranes

without the mechanical support show a relatively low electrical resistance, more similar to the commercial membrane (AMH-PES). However, without mechanical support, the membranes are fragile and break easily, which could limit their practical use in an electrodialysis stack [54].

Regarding the permselectivity to counter-ions, membranes prepared with Amberlite® IRA-402 anion-exchanger (with or without RE-UF) show the best results in the range of the commercial AMH-PES. Pur-RE and Lew-RE show lower values in comparison with the rest of the membranes. As mentioned before, the inhomogeneity and the presence of cracks in the surface of Pur-RE could cause a reduced permselectivity to counter-ions (see Fig. 46b). In the case of Lew-RE, the lower permselectivity could be related to the reduced IEC of this membrane (see Fig. 45).

6.3.2. Evaluation of the selective ion transport properties

Fig. 47 shows the decreasing concentration of anions in the diluted compartment and their molar fluxes during electro-separation experiments (j = 3.5 mA·cm^{-2}). The membranes under analysis were AMH-PES and membranes with RE-UF support. Additionally, results corresponding to the experiments performed at j = 10 mA·cm^{-2} are reported as Supplementary Materials in Fig. S8.

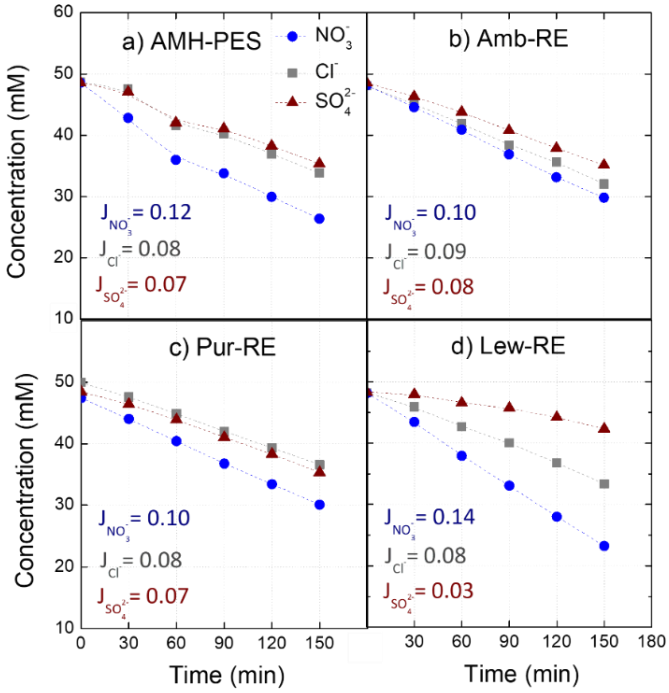

Figure 47. Evolution of anion concentration in the diluted compartment and molar fluxes (J_i, mmol·m^{-2}·s^{-1}) during electro-separation experiments. The membranes under study were: (a) AMH-PES, (b) Amb-RE, (c) Pur-RE, (d) Lew-RE. Feed: NO_3^-, Cl^- and SO_4^{2-} (50 mM) added as their sodium salts. j = 3.5 mA·cm^{-2}.

First, it can be noticed that nitrates permeate faster with respect to other anions through all the membranes. This effect has been attributed in previous studies to the higher hydration energy of nitrates (see Table 13). Higher hydration energy reduces the amount of water solvation molecules, favoring the interaction between the ion and the functional groups in the membrane and increasing the permeation rate [112,114,188].

Table 13. Ionic radii, hydrated ionic radii and hydration energy of the studied anions [191,192].

Ion	Ionic Radii (Å)	Hydrated Radii (Å)	Hydration Energy (kJ·mol^{-1})
Cl^-	1.81	3.32	−381
NO_3^-	2.64	3.35	−314
SO_4^{2-}	2.9	3.79	−1059

Further, the use of different anion-exchange resins in membrane preparation strongly affects to molar fluxes of each anion through the membrane. In this sense, Lew-RE membrane could be suitable for ion fractioning, as it achieved a minimized flux of divalent ions ($J_{SO_4^{2-}}$ = 0.03 mmol·m^{-2}·s^{-1}), and a differentiation between the fluxes of monovalent ions (J_{Cl^-} = 0.08 mmol·m^{-2}·s^{-1} and $J_{NO_3^-}$ = 0.14 mmol·m^{-2}·s^{-1}). The differences in the ionic molar fluxes will be reflected in their transport numbers and, consequently, in the permselectivity between the counter-ions (relative transport number) and in the separation efficiency. The performance in ion fractioning of Lew-RE could be related to the hydrophobic propyl chains in the quaternary amine in Lewatit ® Sybron Ionac® SR-7 anion-exchanger. The presence of hydrophobic alkyl chains in the ion-exchange group increases the repulsion of highly hydrated ions (i.e., sulfates) and enhances the transport of less solvated ions (i.e., nitrates) [112–114,188,193]

The ion transport number measures the amount of charge that is carried by each counter-ion through the membrane phase. Thus, a faster permeation of nitrate will be reflected in a higher transport number. In this study, the effect of the operating current density in the transport numbers was investigated. Fig. 48 shows the differences in ion transport numbers in the experiments conducted at 3.5 and 10 mA·cm^{-2}, using AMH-PES and the membranes with RE-UF support. Complementarily, the results for the membranes without mechanical support are shown in Fig. S 9 (see Supplementary Materials).

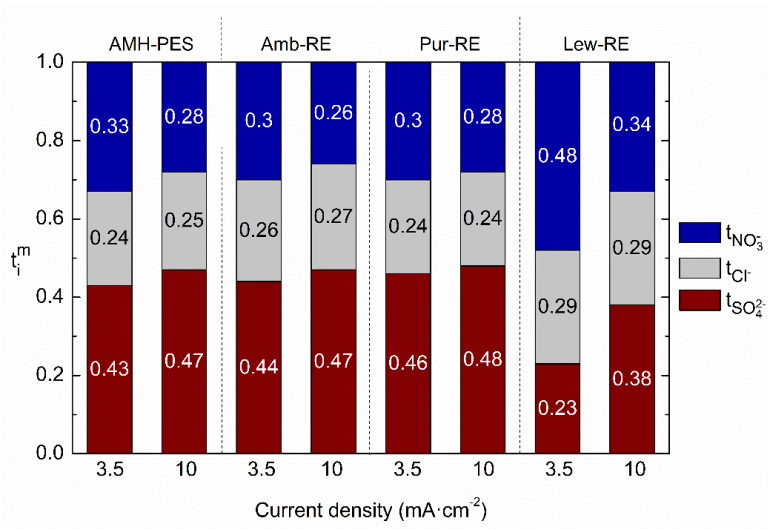

Figure 48. Ion transport numbers (t_i) of the counter-ions in the membrane in relation to the operating current (j = 3.5 and 10 mA·cm^{-2}). Membranes: AMH-PES, Amb-RE, Pur-RE, Lew-RE.

It can be observed that operating at relatively low current density (3.5 mA·cm^{-2} instead of 10 mA·cm^{-2}) facilitates the transport of monovalent ions (nitrates and chlorides) in detriment of divalent ones (sulphates) in all the tested membranes. The effect is greater in Lew-RE, where the transport number of sulphates is decreased from 0.38 to 0.23 and the transport number of nitrates enhanced from 0.34 to 0.48 when lowering the operational current density. In addition, the differentiation between the transport numbers of chloride and nitrate in Lew-RE (j = 3.5 mA·cm^{-2}) could result in an efficient separation between the monovalent anions. Interestingly, the employed current density did not significantly affect the transport numbers of chloride in any membrane. The decreased capacity for ion fractioning when operating at high current density could be associated with a decreased Donnan exclusion effect as a result of the saturation of the fixed charged groups in the membrane by the presence of a high concentration of counter-ions in the membrane phase [194]. Further, the higher apparent activation energy of multivalent ions could require a larger amount of electric charge to overcome the energetic barrier and to be transported, avoiding, to some extent, their transport when relatively low

current densities are used. [94,195,196]. By the comparison of Fig. 48 and Fig. S 9 (in Supplementary Material), it can be noticed that the use of the RE-UF support enhanced the transport numbers of nitrate from 0.42 to 0.48 while reduced the transport number of sulphates from 0.29 to 0.23 (data from Lew and Lew-RE, respectively, when j = 3.5 mA·cm^{-2}). Thus, indicating a positive effect in ion fractionation of the use of the RE-UF membrane. In this line, Fig. 49 further analyses the effect of the RE-UF support in permselectivity between counter-ions (or relative transport number). In Fig. 49, the results corresponding to the experiments conducted at j = 3.5 mA cm^{-2} are presented, while the results of the experiment conducted at 10 mA cm^{-2} are reported as Supplementary Material in Fig. S 10.

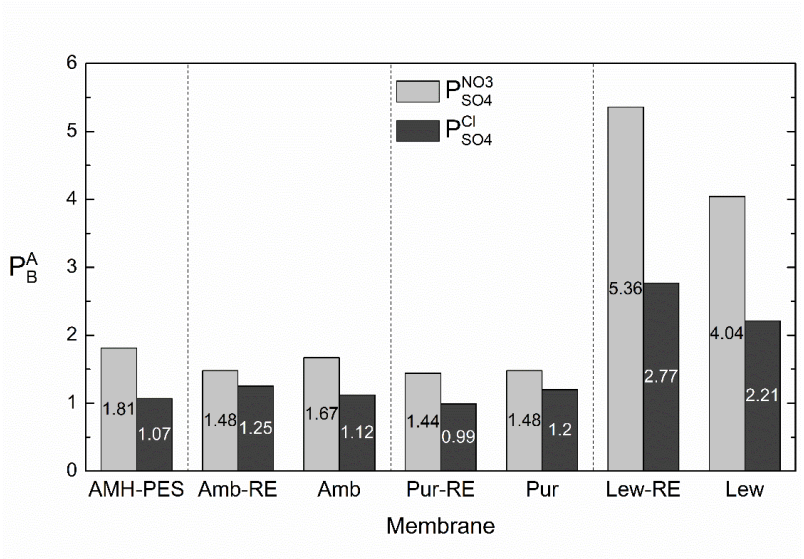

Figure 49. Differences in the permselectivity between the counter-ions (P) with and without the recycled membrane support (j = 3.5 mA·cm^{-2}).

It can be observed that, in concordance with the transport numbers (Fig. 48 and Fig. S 9), the use of the recycled membrane as support increased the permselectivity between monovalent and multivalent ions in the case of membranes containing Lewatit ® Sybron Ionac® SR-7 anion-exchanger. In numbers, $P_{SO_4^{2-}}^{NO_3^-}$ was increased from 4.04 to 5.36 and $P_{SO_4^{2-}}^{Cl^-}$ from 2.21 to

2.77 due to the use of RE-UF support. We first attributed this result to an apparent sieving effect achieved by the use of the RE-UF combined with the coating layer. However, it should be noticed that the positive effect in permselectivity associated with the use of RE-UF membrane was only achieved in membranes containing Lewatit ® Sybron Ionac® SR-7 resin. Hence, to obtain selective heterogeneous membranes, the selection of the anion-exchange resin is of primary importance.

Overall, the use of Lewatit ® Sybron Ionac® SR-7 anion-exchanger produces membranes with an enhanced transport of nitrates over sulphates. These membranes could be used for the fractionation of monovalent and divalent anions (i.e., nitrate and sulphate, chloride, and sulphate) and for the separation between monovalent anions (i.e., nitrate and chloride), which could facilitate the purification of water for drinking purposes. The efficiency in ion fractionation is increased when the separation is performed at low current density, and the membrane is prepared using a recycled pressure filtration membrane as support. Further, the separation efficiency should be considered in order to define the optimum duration of the separation process.

This work shows an upcycling alternative for end-of-life reverse osmosis membranes by using them as support in an ion-exchange membrane preparation. By means of this, the separation efficiency of the resulting membranes can be upgraded. The use of selective ion-exchange resins could be an interesting alternative when target compounds need to be removed from a multi-component mixture. For elucidating the potential application of these membranes, further research on the determination of their economic competitiveness should be conducted. As part of the circular economy approach, these membranes could be tested for nitrate recovery from wastewaters, closing the loops of waste recovery in water purification systems [197], even though the high electrical resistance of the membranes could make them more suitable for passive transport processes such as Donnan dialysis. In parallel, the adequation of using another type

of discarded membranes as support could be studied (for instance, discarded ultrafiltration or nanofiltration membranes). Overall, this work is a first attempt at producing nitrate selective membranes by upcycling discarded reverse osmosis membranes.

6.4. Conclusions

This work shows a simple method for the preparation of AEMs with nitrate selective transport properties. The primary remarks of the present study are:

- AEMs were prepared by casting method using a recycled pressure filtration membrane (RE-UF) as support. A homogeneous distribution of the ionic resin on the membrane surface was obtained. Despite differences in anion-exchange resin distribution across the membrane section were found.

- The use of an anion-exchanger with strengthen hydrophobicity in the functional groups increased the transport of less solvated ions (i.e., nitrates), while highly hydrated ions were repulsed by hydrophobic forces (i.e., sulphates).

- The use of a relatively low current density during the experiment further enhanced the transport of ions with lower charge (monovalent).

- The use of a recycled pressure filtration membrane (RE-UF) as support increased the transport number of nitrates while decreased the transport number of sulphates in the case of membranes containing nitrate selective anion-exchange resin. Moreover, the use of such recycled membranes provided mechanical stability, and it is an attempt to face the waste management challenge of reverse osmosis desalination. In this line, another type of discarded membranes could be tested as mechanical support.

- It can be concluded that the type of anion-exchange resin used in membrane preparation is of primary importance in the preparation of selective heterogeneous AEMs

6.5. Supplementary material

6.5.1. Supplementary material and methods:

The separation efficiency S of component A and B was evaluated as [168]:

$$S\,(t) = \frac{\left(\frac{C_B(t)}{C_B(0)}\right) - \left(\frac{C_A(t)}{C_A(0)}\right)}{\left(1 - \frac{C_B(t)}{C_B(0)}\right) + \left(1 - \frac{C_A(t)}{C_A(0)}\right)} 100\ \% \qquad \text{(S1)}$$

where C_A and C_B are the concentrations of A and B in the dilute solution. It is assumed that B is the slowest permeating component, so that in the dilute compartment, the relative concentration of B is always larger than the relative concentration of A.

The separation efficiency reflects the relative difference in the transport rate between the components in the solution and it is ranged from 0 (no separation) to 1 (complete separation, i.e., $C_B(t)$=0; component B completely removed from the dilute fraction). As indicated in the literature [168], the separation efficiency is relatively constant as a function of time, after some initial fluctuations, and it is independent of the geometry of the equipment (e.g. size of the membranes), but may be influenced by the applied voltage.

The separation efficiency can be calculated on the base of the change in molar concentration of each ion with time as it was shown in Eq. (S 1). Following Eq. (S 2) to (S 8), it can be considered the separation efficiency as function of the ion transport numbers.

If it is considered that $C_B(t)$ and $C_A(t)$ could be theoretically calculated as indicated below,

$$C_B\,(t) = C_B\,(0) - \frac{t_B^m\, j\, A}{|z_B|\, F\, V}\,. \qquad \text{(S 2)}$$

being t_B^m the transport number of the component B in the membrane phase, j (mA·cm^{-2}) the current density, A (cm^2) membrane effective area, z_i the valence of the ion i, F (C·mol^{-1}) Faraday's constant and V (cm^3) the

volume of the dilute compartment. Similarly, the next equation could be used for component A,

$$C_A\,(t) = C_A\,(0) - \frac{t_A^m\; j\; A}{|z_A\,|F\; V}\cdot \tag{S 3}$$

In order to simplify Eq. (S 1), it is possible to define k as indicated below,

$$k = \frac{j\; A}{F\; V}\cdot \tag{S 4}$$

and then, Eq. (S 2) could be expressed as,

$$C_B\,(t) = C_B\,(0) - \frac{t_B^m}{|z_B|}k\cdot \tag{S 5}$$

Then Eq. (S 1) could be written as:

$$S\,(t) = \frac{\left(\frac{C_B(0) - \frac{t_B^m}{|z_B|}k}{C_B(0)}\right) - \left(\frac{C_A(0) - \frac{t_A^m}{|z_A|}k}{C_A(0)}\right)}{\frac{-\frac{t_B^m}{|z_B|}k}{C_B(0)} - \frac{\frac{t_A^m}{|z_A|}k}{C_A(0)}}\cdot 100\ \% \tag{S 6}$$

When the experiment is carried out with equal initial concentrations for both components, i.e., $C_A\,(0) = C_B\,(0)$, A and B have the same charge (for example, $|z_B| = |z_A| = 1$), Eq. (S 6) is simplified as indicated below,

$$S\,(t) = \frac{t_A^m - t_B^m}{-\,(t_A^m + t_B^m)}\,100\ \%\cdot \tag{S 7}$$

And thus,

$$S\,(t) = \frac{t_A^m - t_B^m}{t_A^m + t_B^m}\cdot 100\ \% \tag{S 8}$$

In this particular case, ($C_A(0) = C_B(0)$, $|z_B| = |z_A| = 1$), the separation efficiency (S) could be considered as an indirect measurement of the difference between transport numbers for A and B, as reported in [168]. In this way, $S = 0$ % indicates that $t_A^m = t_B^m$, thus both ions are transported with the same velocity through the membrane (i.e., the ions transport the same amount of electric charge during migration). If the value of S = 50 % it is

easy to determine using S6 that $t_A = 3\,t_B$, indicating a higher migration/transport of A compared to B through the membrane. Finally, the value of *S* = 100 % would indicate that all the charge is transported by A (i.e. $t_A^m + t_B^m \approx t_A^m$), and the transport of charge due to B is negligible. Finally, for mixtures of monovalent and multivalent ions, the valence of each ion should be considered and thus,

$$S\,(t) = \frac{\frac{t_A^m}{|z_A|} - \frac{t_B^m}{|z_B|}}{\frac{t_A^m}{|z_A|} + \frac{t_B^m}{|z_B|}} \cdot 100\,\% \qquad \text{(S 9)}$$

In this case, *S* = 0 % indicates that $\frac{t_A^m}{|z_A|} = \frac{t_B^m}{|z_B|}$. If it is considered the case in which $|z_A| = 1$ (monovalent ion) and $|z_B| = 2$ (divalent ion), then $2t_A = t_B$ and thus, the divalent ion is transporting twice the charge of the monovalent ion, being the molar flux of both ions the same. When the value of S = 50 %, it could be calculated using the Eq. (S 9) the value of $t_A = \frac{3}{2}t_B$. Again, if *S* = 100 %, then $t_B^m \approx 0$, and all the charge is transported by component A.

It is important to note that the previous analysis would be accurate as long as i) initial concentrations are equal (i.e., $C_A(0) = C_B(0)$) and ii) and the transport number for each ion could be considered constant (i.e., no significant change of concentration for $C_A(t)$ and $C_B(t)$ during the experiments).

6.5.2. Supplementary results and discussion

6.5.2.1. Membrane characterization

Fig. S 7 shows the Energy-dispersive X-ray (EDX) images of the RE-UF membrane (used as support) and the prepared AEMs. In this figure, the elemental composition of the coated layer and the support layer of the AEMs can be observed.

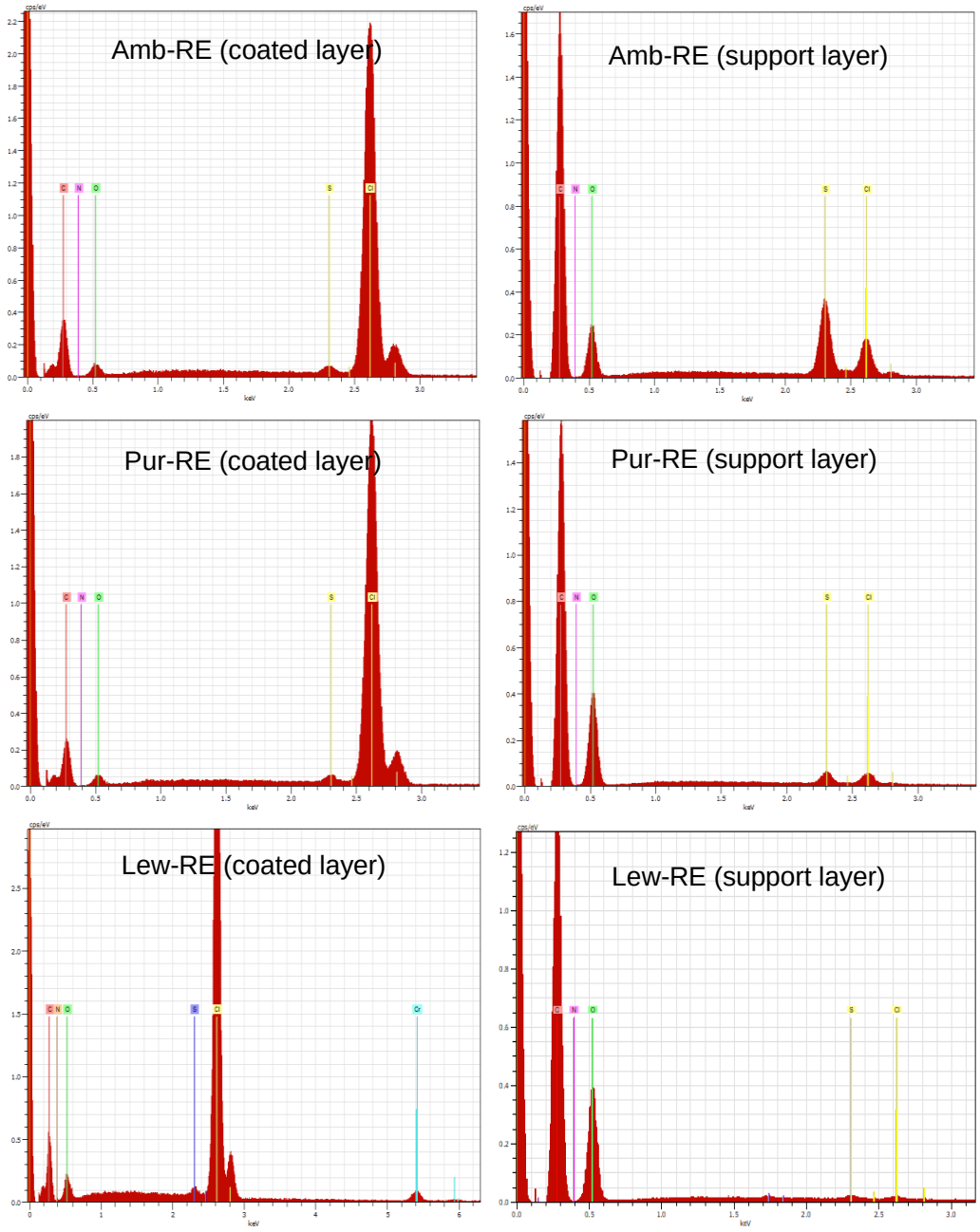

Figure S 7. Energy dispersive X-ray (EDX) images of (a) polysulfone surface in the RE-UF support, (b) coated layer and (c) support layer in Amb-RE membrane; (d) coated layer and (e) support layer in Pur-RE membrane, (f) coated layer and (g) support layer in Lew-RE membrane

Table S 2. Chemical composition analysis by EDX of the polysulfone surface of the RE-UF membrane.

Element	% Weight	% Atomic
C	73.74	78.56
N	4.97	4.54
O	20.95	16.75
Al	0.27	0.13
S	0.07	0.03
Cl	0	0

All the prepared membranes show Cl in their elemental composition, due to the casting of the polymeric solution containing PVC as binder. The presence of Cl was not detected in the surface of the RE-UF membrane, indicating that all the Cl in the prepared membranes corresponds to the PVC in the polymeric solution. As explained in the manuscript, a peak of Cl was observed in both sides of the prepared membranes (in the coated and the support layers). The peak of Cl in the coated layer is large, due to the dense film of PVC formed in the membrane surface. However, the amount of PVC that totally crossed the RE-UF support was very low as it is reflected in the low signal of Cl in the support layer.

In the prepared AEMs, the peak of N corresponds to the amine group in the anion-exchange resin. The low intensity of N peaks confirms that the resin particles are covered by a dense film of PVC. *N* was not found in the support layer which could reflect an unequal distribution of the ion-exchange particles across the membrane section (lower concentration of ion-exchange particles embedded in the RE-UF support in comparison with the coated layer).

6.5.2.2. Evaluation of the selective ion transport properties

Fig. S 8, shows the decreasing concentration of anions in the dilute compartment and molar fluxes during the electro-separation experiments

performed at 10 mA·cm^{-2}. The tested membranes were AMH-PES and membranes with recycled support.

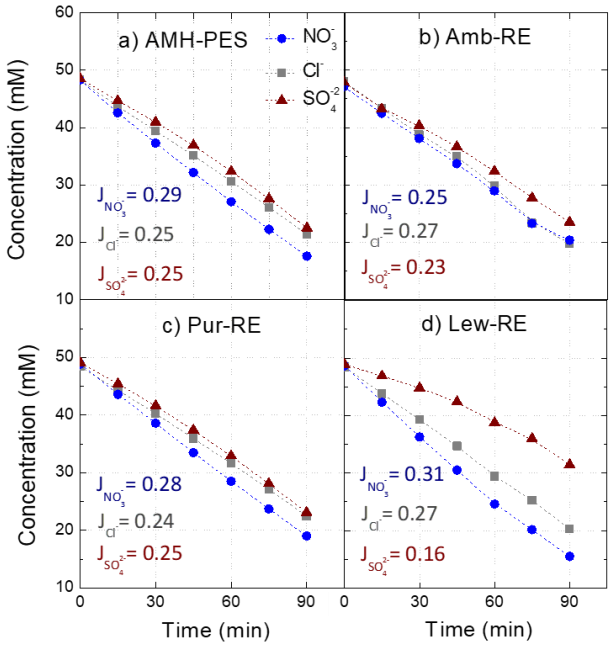

Figure S 8. Evolution of anion concentration in the diluted compartment and molar fluxes (J_i, mmol·m^{-2}·s^{-1}) during electro-separation experiments. The membranes under study were: (a) AMH-PES, (b) Amb-RE, (c) Pur-RE, (d) Lew-RE. Feed: NO_3^-, Cl^- and SO_4^{2-} (50 mM) added as sodium salts. j= 10 mA·cm^{-2}.

It can be observed that the molar fluxes are increased in respect to Fig. 47, due to the increase of the current density. As explained in the manuscript, in all the tested membranes, the permeation of nitrate is faster than the fluxes of chlorides and sulphates which can be related to the higher hydration energy of nitrates. In addition, the capacity for achieving an effective ion fractionation relies upon the anion-exchanger used in membrane preparation. In this manner, the use of Lewatit ® Sybron Ionac® SR-7 anion-exchanger declines the flux of sulphates while increases the flux of nitrates. This effect could be attributed to the hydrophobic propyl chains in the functional group of the Lewatit ® Sybron Ionac® SR-7 anion-exchanger.

Fig. S 9 shows the differences in transport properties of the membranes without mechanical support when conducting the experiment at 3.5 and 10 mA·cm^{-2}.

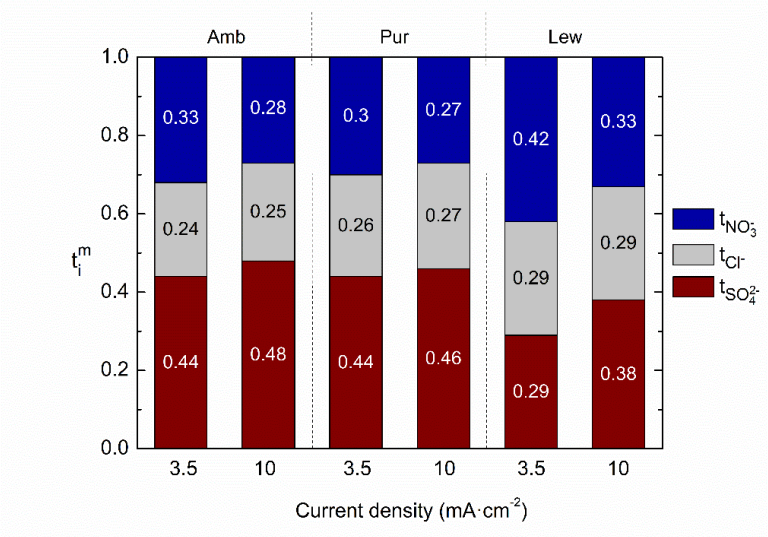

Figure S 9. Transport numbers (t_i) of the counter-ions in the membrane in relation with the operating current (j= 3.5 and 10 mA·cm^{-2}). Membranes: Amb, Pur and Lew (membranes without mechanical support).

It can be observed that, in concordance with the manuscript, conducting the experiments at 3.5 mA·cm^{-2} results in a larger transport of nitrates in detriment of sulphates. The effect is greater in the case of Lew membrane where the transport number of sulphate is reduced from 0.38 to 0.29 while the transport number of nitrate is enhanced from 0.33 to 0.42 when lowering the operating current density (from 10 to 3.5 mA·cm^{-2}). As mentioned in the manuscript, the decrease in the rejection of sulphate at 10 mA·cm^{-2} can be attributed to a decreased Donnan exclusion effect. While at 3.5 mA·cm^{-2} the higher apparent activation energy of sulphates could reduce its transportation through the membrane. In addition, it can be observed a great differentiation between the transport numbers of nitrate and chloride in Lew membrane, further increased when the experiment is operated at low current density ($t_{NO_3^-}$ 0.42 and t_{Cl^-} 0.29).

Fig. S 10 shows the permselectivity between counter-ions (relative transport number) in respect to sulphates, achieved by the membranes when operating at 10 mA·cm^{-2}. In this figure, the effect of the mechanical support in the permselectivity between counter-ions can be appreciated.

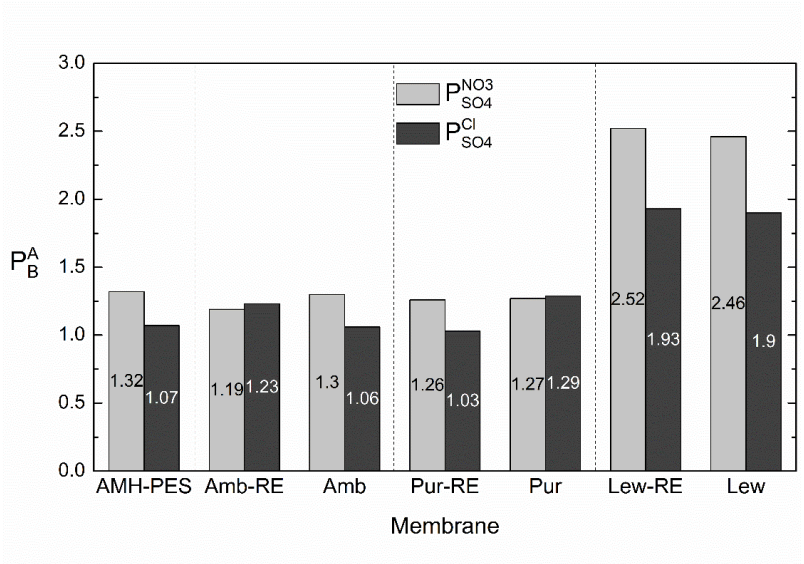

Figure S 10. Differences in the permselectivity between the counter-ions (*P*) with and without the recycled membrane support (*j*= 10 mA·cm^{-2}).

It can be observed that, in comparison with Fig. 49, the permselectivity was decreased in all the cases due to operating at 10 mA·cm^{-2}. In the case of membranes containing Lewatit ® Sybron Ionac® SR-7 anion-exchanger, the use of the RE-UF membrane as mechanical support slightly enhanced the permselectivity to monovalent ions. However, the main differences in permselectivity between counter-ions rely on the type of anion-exchanger used in membrane preparation and in the use of an adequate operating current during the separation experiments.

Another parameter for analysing the differences in the transport properties between the ions is the separation efficiency (*S*). Fig. S 11 and S 12 show the evolution of the separation efficiency during the experiments performed at 3.5 and 10 mA·cm^{-2}, respectively.

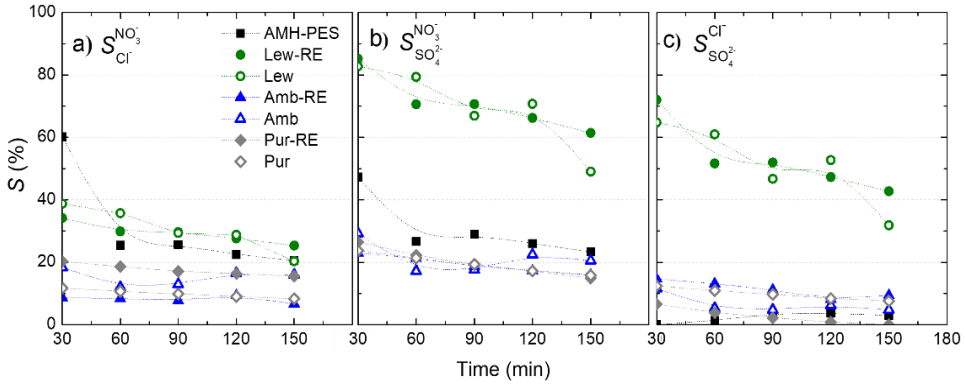

Figure S 11. Evolution of the separation efficiency (S) during the experiments at j = 3.5 mA·cm^{-2} in all the tested membranes. a) Separation efficiency between chloride and nitrate ions, b) separation efficiency between nitrate and sulphate ions, c) separation efficiency between chloride and sulphate ions.

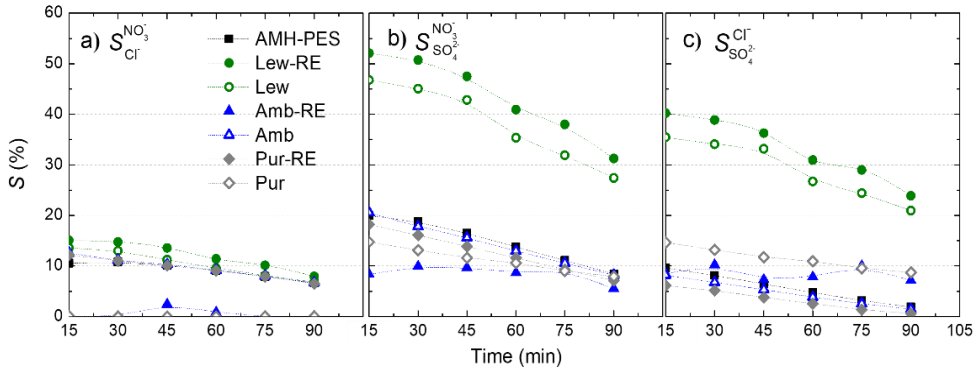

Figure S 12. Evolution of the separation efficiency (S) during the experiments at j = 10 mA·cm^{-2} in all the tested membranes. a) Separation efficiency between chloride and nitrate ions, b) separation efficiency between nitrate and sulphate ions, c) separation efficiency between chloride and sulphate ions.

As mentioned before, S reflects differences in the transport between the components A and B. In a general sense, a large difference between the transport numbers of A and B is reflected in higher separation efficiency (see Eq. (S 2) and (S 9)). As a consequence, S is in concordance with previously explained results ($S_{SO_4^{2-}}^{NO_3^-} > S_{SO_4^{2-}}^{Cl^-} > S_{Cl^-}^{NO_3^-}$). Again, Lew-RE membrane show the highest separation efficiency, achieving $S_{SO_4^{2-}}^{NO_3^-}$ = 85 %,

$S_{SO_4^{2-}}^{Cl^-}$= 72 % and $S_{Cl^-}^{NO_3^-}$ = 34 % in the beginning of the experiment (30 min) when it is conducted at low current density (j = 3.5 mA·cm^{-2}) (Fig. S 11). The separation efficiency was considerably decreased in the experiments conducted at 10 mA·cm^{-2}, and in this case, Lew-RE achieved $S_{SO_4^{2-}}^{NO_3^-}$= 52 %, $S_{SO_4^{2-}}^{Cl^-}$= 40 % and $S_{Cl^-}^{NO_3^-}$ =15 % in the beginning of the experiment (15 min) (Fig. S 12).

This parameter further demonstrated the feasibility of using Lew-.RE-UF membrane for ion fractioning. In the case of Amb-RE and Pur-RE, the separation efficiency is almost constant during the experiment as long as the concentrations of the counter-ions are maintained in an equimolar relation. However, in the case of the membranes prepared with Lewatit ® Sybron Ionac® SR-7 anion-exchanger, (Lew-RE and Lew), the separation efficiency shows a decreasing tendency during the experiment. These results can be attributed to differences in the permeation rates of nitrate, chloride, nitrate, and sulphate, which results in a faster depletion of nitrates, followed by chlorides, in the dilute compartment. When the concentration of nitrate and chloride in the dilute compartment is too low to transport the electric charge that is being applied to the system, then sulphates will be transported through the membrane, decreasing the separation efficiency as it is observed in Fig. S 11 and S 12. Overall, S is a parameter that can be useful to define the optimum duration of the separation process for maintaining of high separation efficiency.

7

Chapter 7. Nitrate removal by Donnan Dialysis and Ion-Exchange Membrane Bioreactor systems using upcycled end-of-life Reverse Osmosis membranes

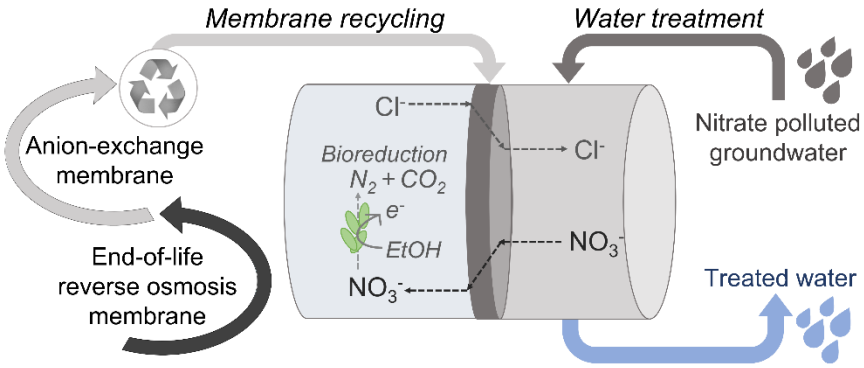

This Chapter has been published as:

A. Lejarazu-Larrañaga, J. M. Ortiz, S. Molina, S. Pawlowski, C. F. Galinha, V. Otero, E. García-Calvo, S. Velizarov, J. G. Crespo, Nitrate removal by Donnan Dialysis and Ion-Exchange Membrane Bioreactor using upcycled end-of-life Reverse Osmosis membranes as Anion-Exchange Membranes. Membranes, 12 (2022) 101. https://doi.org/10.3390/membranes12020101

7.1. Introduction

As mentioned in previous Chapters (Chapters 3, 4 and 6), the RO upcycled AEMs have a good permselectivity but a relatively high electrical resistance, which increases the energy consumption associated with their use in electrodialysis (ED) [54]. In that respect, an electrochemical potential gradient driven process, such as Donnan Dialysis (DD) and its integration with biotransformation, referred to as the Ion-Exchange Membrane Bioreactor (IEMB), could entail a more suitable application for such RO upcycled AEMs.

DD utilizes counter-diffusion of two or more ions through an ion-exchange membrane to achieve their separation. The diffusive flux of a counter ion trough an IEM, caused by a concentration gradient, leads to the establishment of an electrochemical potential across the membrane, generating the uphill transport of the counter-ions in the opposite direction. As a consequence of the diffusive nature of the ionic transport, the energy requirements of DD are minimized, in comparison to that of ED [122]. Indeed, owing to its simplicity of installation and low operating costs (under batch operation conditions DD can be operated even without pumping), DD has been presented as an appropriated technology for household water treatment in remote rural areas of developing countries (not connected to centralized water supply facilities) [198–200].

Likewise, the IEMB combines DD principle with a biological conversion process in the receiver compartment, providing the simultaneous transport and bioreduction of the target counter-ion in a single device and in a single step [201]. In previous studies, IEMB process achieved a high efficiency in drinking water denitrification when using Neosepta ACS membrane [202]. However, the high cost of such membrane could compromise the practical implementation of the IEMB concept, and thus, the use of more affordable membranes is highly desirable [203]. In this

context, the AEMs prepared from upcycled RO membranes could entail a more economic approach.

In the present work, the use of AEMs upcycled from end-of-life RO membranes in DD and IEMB processes for the removal of nitrate from a synthetic polluted water was studied and compared with the performance of a Ralex ® AMH-PES commercial AEM from Mega a.s. Further, membrane structure was analysed by confocal μ-Raman spectroscopy and alterations in the membranes due to fouling and the chemical cleaning were evaluated by 2D fluorescence spectroscopy. Finally, a preliminary estimation of the material cost to manufacture the upcycled membranes was performed.

7.2. Materials and methods

7.2.1. Chemical reagents

NaClO (14 % (v/v) free chlorine), THF, Na_2SO_4 and ammonium chloride (NH_4Cl) were purchased from Scharlab, S.L., Spain. NaCl, $NaNO_3$, di-potassium hydrogen phosphate anhydrous (**K_2HPO_4**), humic acids (HA), Amberlite® IRA-402 and Lewatit ® Sybron Ionac ® SR-7 anion-exchange resins were supplied by Merck KGaA, Germany. Purolite® A600/9413 anion-exchange resin was supplied by MemBrain ® s.r.o., Czech Republic. Potassium dihydrogen phosphate (KH_2PO_4) was purchased from Chem-lab NV, Belgium; sodium hydrogen phosphate (NaH_2PO_4) from Panreac Química S.L.U., Spain; magnesium sulphate heptahydrate ($MgSO_4 \cdot 7H_2O$) from LabChem Inc., USA; NaOH from Fisher Scientific Co. LLC., USA, and citric acid from VWR chemicals, USA. PVC (Mw =112,000 $g \cdot mol^{-1}$) was supplied by ATOCHEM, Spain. MilliQ water was used throughout the experiments.

7.2.2. Membranes

The methodology to obtain the preconditioned recycled membrane support and the AEMs is described in detail in Sections 3.2.3 and 3.2.4

(Chapter 3) [54]. In the present chapter, Purolite® A600/9149, Amberlite® IRA-402 and Lewatit® Sybron Ionac® SR-7 anion-exchange resins were used for the preparation of Pur-RE, Amb-RE and Lew-RE membranes. respectively. The main properties of Pur-RE, Amb-RE and Lew-RE membranes were measured in Chapter 6 and are summarized in Table 14. The microstructure of such membranes was characterized before (Chapters 3, 4 and 6), and it is further analysed by confocal μ-Raman spectroscopy in the present work (Section 7.3.1.). As described in previous Chapters, the prepared membranes show a considerably uniform distribution of the ion-exchange resin at the membrane surface, having a heterogeneous microstructure due to the presence of conductive (ion-exchange resin particles) and non-conductive regions (PVC, PET and PSf). Therefore, a commercial membrane with an heterogenous structure was used as referential membrane, in this case, Ralex ® AMH-PES from Mega a.s., which was selected due to its durability, high mechanical stability and relatively low commercial cost.

Table 14. Main characteristics of the membranes under study. Thickness, water content, Ion-Exchange Capacity (IEC), electrical resistance and permselectivity were experimentally measured under the same conditions, and previously reported (data from [56]). AMH-PES membrane composition is detailed by the provider (data from [204]).

Anion-Exchange Membrane	AMH-PES	Pur-RE	Amb-RE	Lew-RE
Mechanical support	Polyester (PET)	End-of-life RO	End-of-life RO	End-of-life RO
Polymer binder	Polyethylene (PE)	PVC	PVC	PVC
Ion-exchange resin	Unspecified	Purolite® A600/9149	Amberlite® IRA-402	Lewatit® Sybron Ionac® SR-7
Ion-exchange group	$R-(CH_3)_3N^+$	$R-(CH_3)_3N^+$	$R-(CH_3)_3N^+$	$R-(C_3H_7)_3N^+$
Membrane thickness (μm)	645 ± 5	190 ± 4	184 ± 7	182 ± 7
Water content (%) [a]	50 ± 0	23 ± 4	21 ± 4	19 ± 1
IEC ($mmol \cdot g^{-1}$) [b]	2.19 ± 0.09	0.75 ± 0.14	0.62 ± 0.04	0.39 ± 0.01
Permselectivity (%) [c]	81 ± 1	65 ± 9	83 ± 7	66 ± 4
Electrical resistance ($\Omega \cdot cm^2$) [d]	19 ± 3	56 ± 7	129 ± 1	120 ± 11

[a] Gravimetric method

[b] Immersed in KNO_3 1 M for 24h under stirring (100 rpm); immersed in NaCl 0.5 M for 24h under stirring (100 rpm); UV-VIS spectrophotometric determination of the nitrate released in NaCl solution.

[c] Measured in 0.1 and 0.5 M NaCl solutions.

[d] Measured in 0.5 M NaCl solution.

7.2.3. Confocal micro-Raman spectroscopy

In this work, confocal μ-Raman spectroscopy was used to analyse the asymmetric distribution of the polymeric composition and the ion-exchange sites, along the thickness of the PU-RE membrane. Since the same membrane preparation methodology was employed to prepare all the membranes (Pure-RE, Amb-RE and Lew-RE) and only the type of the ion exchange resin was different, analogous structures are expected in all the prepared membranes. To assess that structure, Pur-RE membrane was selected for confocal micro-Raman spectroscopy characterisation since that membrane showed the best performance under DD and IEMB operating conditions (results shown in section 7.3.2). A Labram 300 Jobin Yvon spectrometer from Horiba Ltd., Japan was used, equipped with a solid-state laser operating at 532 nm. The laser beam was focused with a 50× Olympus objective lens. The analysis was performed with a neutral density filter of 0.6 optical density, with 15-s exposure time and 20 scans. Spectra were recorded as an extended scan and presented with a break between 1025 and 1085 cm^{-1} to remove the contribution of bands attributed to nitrate compounds. For obtaining the cross-section, the membrane was frozen into liquid nitrogen and broken properly. The analyses were performed in 10 consecutive points in a row across the membrane section, from the coated side to the PET side of the membrane. The distance between the analysed points was about 20 μm.

7.2.4. Donnan Dialysis (DD) and Ion-Exchange Membrane Bioreactor (IEMB) experiments

7.2.4.1. Model solutions, test cell and analytical methods

The model polluted water, referred as feed henceforth, consisted of deionized water supplemented with 80 $mg \cdot L^{-1}$ of nitrate (added as $NaNO_3$). This concentration was selected as a model high nitrate concentration (> 50 $mg \cdot L^{-1}$), as it was used before in [205]. The receiver aqueous solution contained chloride as a major counter-ion (3545 $mg \cdot L^{-1}$ of Cl^-, added as

NaCl) and a mixture of inorganic nutrients (1000 mg·L^{-1} K_2HPO_4, 592 mg·L^{-1} KH_2PO_4, 500 mg·L^{-1} NaH_2PO_4, 233 mg·L^{-1} NH_4Cl and 1000 mg·L^{-1} $MgSO_4 \cdot 7H_2O$ [206]) to support the microbial growth in the bioreactor (when operating as IEMB). In order to maintain the same ionic strength in DD and IEMB operation conditions, the nutrient enriched water media was used as a receiver solution also for DD experiments. The receiver compartment in the IEMB (referred to as biocompartment, hereafter) was additionally supplemented with microbial culture (as described in Section 7.2.4.3.) and ethanol (at a rate of 400 mg·L^{-1} day^{-1} EtOH) to ensure the presence of the carbon source in the IEMB experiments.

The same test cell (Fig. 50) was used in DD and IEMB experiments. The membrane effective area was 11.3 cm^2 and the volume of each of the two compartments was 175 mL. The coated side of the membrane was faced to the feed compartment (polluted water). During the experiments, the solutions were continuously stirred to minimize possible concentration polarization effects. Before the experiments, all tested membranes (listed in Table 14) were equilibrated by immersion in the receiver solution (i.e., the salt mixture, without the microbial culture and ethanol) for 2 days.

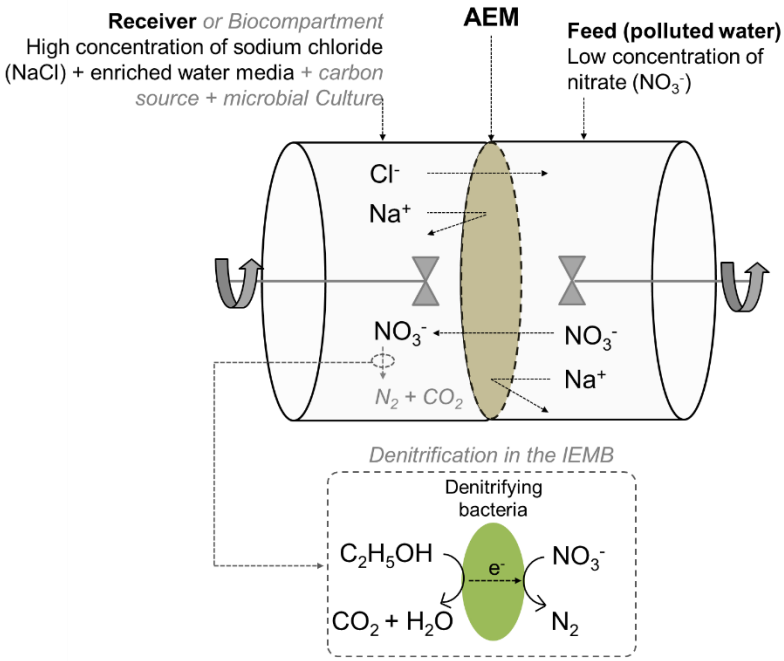

Figure 50. Schematic diagram of the test cell and representation of the main ionic transport in DD and IEMB experiments. Effective membrane area, 11.3 cm^2. Volume of each compartment, 175 mL. The modifications to operate as an IEMB are represented in grey colour and italic lettering. The receiver compartment under IEMB operation was referred to as biocompartment.

The experimental time was 96 h in the case of Pur-RE, Amb-RE and Lew-RE membranes, and 72 h in the case of AMH-PES (as nitrate was already completely removed from the feed after that period). The membranes were thoroughly rinsed with water before the chemical cleaning and after each step [207].

7.2.4.2. Operation as a Donnan dialyzer

The time course concentration of nitrate was measured in both compartments during the experiments as described in Section 7.2.4.4. The membrane performance in DD operation was evaluated in terms of nitrate removal yield from the feed (%), and nitrate recovery in the receiver solution (%), as detailed in Eq. (22) and (23), respectively [208].

$$Removal_{NO_3^-(t)} = \frac{C_{NO_3^-,feed\,(0)} - C_{NO_3^-,feed\,(t)}}{C_{NO_3^-,feed\,(0)}} \cdot 100\ \% \quad (22)$$

$$Recovery_{NO_3^-(t)} = \frac{C_{NO_3^-,receiv.(t)}}{C_{NO_3^-,feed\,(0)}} \cdot 100\ \% \quad (23)$$

where $C_{NO_3^-}$ is the concentration of nitrate.

The conductivity was checked in both compartments during the experiments.

7.2.4.3. Operation as an ion-exchange membrane bioreactor

Microbial culture

The activated sludge obtained from a laboratory bioreactor fed with real wastewater was used as inoculum. The inoculum was centrifuged for 30 min at 4000 rpm, under a temperature of 4ºC, for obtaining a pellet enriched in microorganisms and biomass. The pellet was resuspended in fresh nutrient enriched water media (composition detailed in Section 7.2.4.1.), 800 mg·L^{-1} of ethanol (i.e., the carbon source in the IEMB) and 80 mg·L^{-1} of nitrate (i.e., the electron acceptor under anoxic conditions, added as $NaNO_3$) were supplied to support the microbial activity and to ensure the acclimation of the bacteria to the experimental conditions. The culture was degasified with N_2 and CO_2 in order to preserve anaerobic conditions. Then, it was incubated at 37ºC for 5 days. The same procedure was repeated 3 times (centrifugation, resuspension in fresh enriched water media and addition of ethanol and nitrate). After that, the enriched microbial culture was placed in fresh enriched water media and stored at 4 ºC, being ready to be used as inoculum in the IEMB.

Ethanol permeation studies

For the operation as an IEMB, it is of primary importance to avoid the permeation of the carbon source (ethanol, in this case), from the receiver solution to the feed, in order to prevent cross contamination issues (i.e., secondary pollution) in the treated water. The diffusion coefficients of ethanol across the analysed membranes were measured in a two compartments cell. (i.e., two glass bottles of 250 mL each, sealed with a lid, under stirring at 400 rpm). Each membrane under study, with an effective area of 4.52 cm^2, was placed between the compartments. One of the compartments was filled with an aqueous ethanol solution (1000 $mg \cdot L^{-1}$ ethanol) and the other one was filled with MilliQ water. As long as ethanol was the only organic compound in the solutions, the Total Organic Carbon (TOC) concentration was analysed in both compartments during the experimental time course (15 days) and the concentration of ethanol was calculated. Then, the diffusion coefficients of ethanol through the membranes were calculated by the graphical representation of Fick's law (Eq. (24)) [54].

$$J_D = -D \cdot \frac{dC}{dl} \tag{24}$$

where J_D ($mol \cdot cm^{-2} \cdot s^{-1}$) is the flux of ethanol through the membrane, D ($cm^2 \cdot s^{-1}$) is the diffusion coefficient, dC ($mol \cdot cm^{-3}$) is the concentration gradient (the driving force), and dl (cm) is the membrane thickness. In order to estimate the diffusion coefficient D, the linear region of the experiments was considered, where the slope of the curve *C vs time* has constant value, and assuming $dC \approx \Delta C$ and $dl \approx l$.

Operation as a bioreactor

In the case of IEMB experiments, the receiver compartment (Fig. 50) was filled with fresh enriched water media and inoculated with 15 mL of enriched microbial culture (the experimental procedure for obtaining the microbial culture has been described in this section in "*Microbial culture*" subsection). Before inoculation, the microbial culture was stored at room

temperature for more than 48 h, for activation of the microbial metabolism. The anaerobic conditions in the receiver compartment were maintained during the experiment by continuously sparging nitrogen gas through the compartment headspace. The concentration of nitrate was measured in both compartments during the experimental time and nitrate removal yield was calculated using Eq. (22). In addition, the concentration of nitrite was measured in both compartments, to verify that nitrite traces were not accumulated, ensuring that the complete bio-reduction of nitrate to nitrogen was attained. Nitrite is more toxic than nitrate and its maximum allowed concentration is limited to 3 mg L^{-1} in drinking water [209]. Besides, the TOC in the feed (water) compartment was analysed to prove that the diffusion of ethanol from the biocompartment to the feed was avoided. The conductivity was checked in both compartments during the experiments.

7.2.4.4. Analytical methods

Nitrate and nitrite were analysed based on the colorimetric cadmium reduction method, according with the standard methods [124], using a Skalar SAN++ CFA analyser (Skalar Analytical B.V., The Netherlands). The TOC was measured using a TOC-V CSH total organic carbon analyser (Shimadzu Corp., Japan), then the corresponding concentration of ethanol was calculated by a conversion factor. The conductivity of the solutions was measured using a Sension +EC7 instruments (from Hach Company, United States).

7.2.5. 2D fluorescence spectroscopy

2D fluorescence spectroscopy has been recently proposed for in situ monitoring bioreactors and ion-exchange membrane processes [207,210,211]. In this work, 2D fluorescence spectroscopy was used to analyse alterations in the membrane surface caused by i) their use in the bioreactor experiments (as it is described in Section 7.2.4.3), ii) an accelerated organic fouling test (on pristine membranes) and iii) chemical cleaning (of pristine membranes and those used in IEMB).

The accelerated fouling test consisted of the passive immersion of the membranes in a 0.1 g L^{-1} aqueous Humic Acid (HA) solution for 1 h, at room temperature [212]. The cleaning treatment involved the passive immersion of the membranes in alkali and acid solutions, and consisted of the following steps, according to [207]:

1. Rinse with DI water
2. Passive immersion in 5000 mg·L^{-1} NaOH aqueous solution for 10 min, at room temperature.
3. Rinse with DI water
4. Passive immersion in a 20000 mg·L^{-1} citric acid aqueous solution for 30 min, at room temperature.
5. Rinse with DI water

A Varian Cary Eclipse fluorescence spectrophotometer, equipped with excitation and emission monochromators, and coupled to an optical fibre bundle probe was used. The optical fibre bundle is constituted by 294 optical fibres, each with a diameter of 200 μm and a length of 2 m. The Excitation-Emission Matrices (EEMs) of the membrane surface samples were obtained between 250 and 690 nm excitation and from 260 to 700 nm emission with 5 nm step and slits of 10 and 5 nm, respectively. EEMs of both, coated (top) and PET (bottom) surfaces of all membranes were acquired when pristine, after used in IEMB, after accelerated fouling test and after chemical cleaning of pristine and used in IEMB. All measurements were performed in triplicate.

Before performing a principal component analysis (PCA) of obtained EEMs, spectral data was standardized (by subtracting averages and dividing by standard deviations) for each pair of excitation emission intensity. OCTAVE GNU software was used to implement the computational routines in PCA (through PARAFAC algorithm [30]). PCA was performed by using the following two different data combinations: 1) only EEMs of the prepared membranes (Pur-RE, Amb-RE and Lew-RE, in a total of 91 spectra); 2) EEMs of the prepared membranes and commercial

membrane together (Pur-RE, Amb-RE, Lew-RE and AMH-PES in a total of 120 spectra). PARAFAC analysis of only modified membranes captured 81.76 % of the variance by the first two principal components (PCs), while PARAFAC analysis of all membranes (including commercial) captured 83.84 % variance by the first two PCs.

7.3. Results and discussion

7.3.1. Confocal micro-Raman spectroscopy

Confocal μ-Raman spectroscopy was used to understand better the polymeric composition/structure of the cross-section membrane Pur-RE (the best performing membrane under DD and IEMB operating conditions, as discussed below). Fig. 51a represents the examined locations (from a to j) along the membrane cross-section, and Fig. 51b shows the Raman spectra corresponding to these locations. The main characteristic Raman bands identifying the polymers in the membrane, as well as the Raman spectra of those polymers were characterised according to the literature [213], and are presented as Supplementary material in Table S 3 and Fig. S 13, respectively.

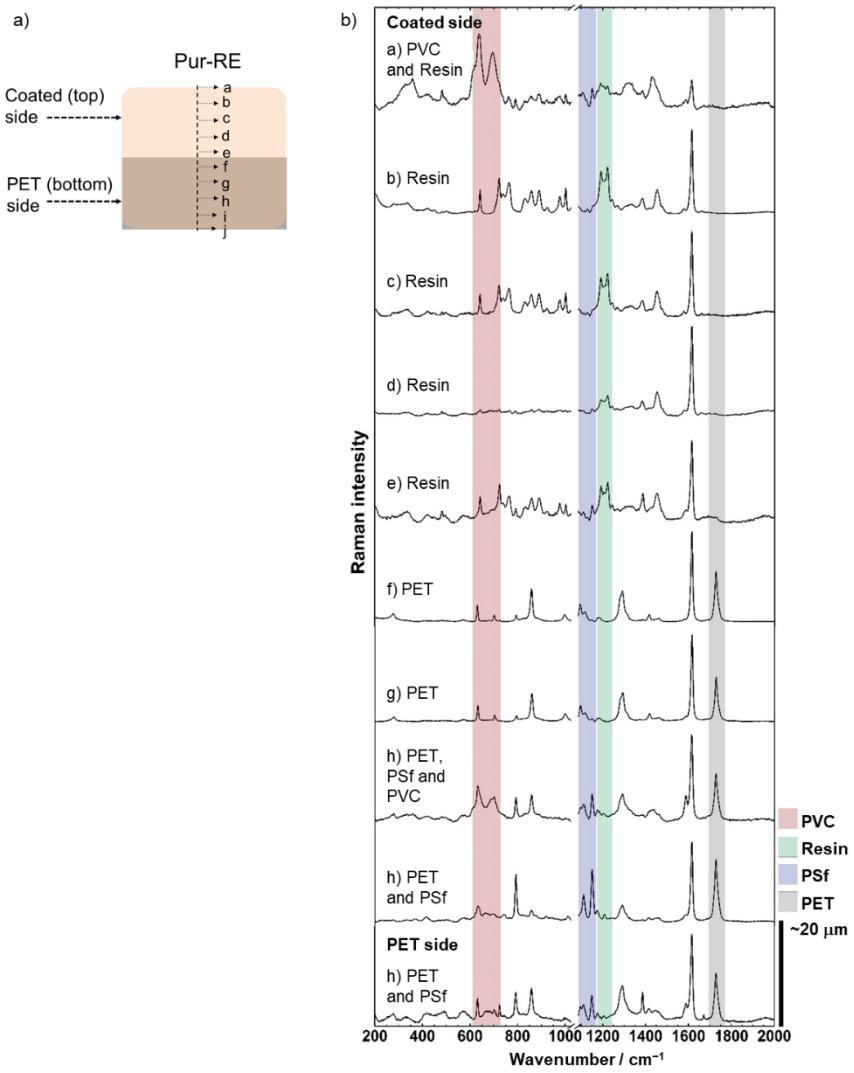

Figure 51. a) Schematic representation of the analysed points in the membrane section. b) μ-Raman spectra of the polymers in the membrane section, at the analysed points a to j. The main bands that allow for a clear identification of each polymer are highlighted.

At the outermost coated surface (top) of the membrane (point a), PVC is identified by its characteristic Raman bands at 638 and 695 cm^{-1} due to C-Cl stretching vibrations (highlighted with red in Fig. 51b). The PVC was used as polymer binder in the coating solution, thus its presence in point a demonstrated an effective formation of a film on the coated membrane

surface. At points a to e, the spectrum of the ion-exchange resin was found, particularly due to its characteristic Raman bands at 1190 and 1221 cm^{-1} attributed to ring C-H vibration modes (highlighted with green in Fig. 51b), which verifies the successful deposition of the ion-exchange resin in the coated (top) surface of the membrane and therefore, the presence of fixed charged functional groups. The lower intensity of the resin signal at the point a corresponds to an overshadowed effect by the PVC signal. Whereas at points f to j (i.e., the PET bottom part of the membrane), the ion-exchange resin spectrum is no longer present. At these points (f to j), the spectra corresponding to PET and PSF, in different combinations, can be distinguished by their characteristic Raman bands at 1727 cm^{-1} for PET C=O stretching vibration (highlighted with grey in Fig. 51b), and at 1150 and 1109 cm^{-1} for PSF C-O-C and SO_2 stretching vibrations, respectively (highlighted with blue in Fig. 51b). In the recycled membrane support, the PSF layer conforms the outermost top surface of the membrane covering the PET layer (see Fig.51b), whereas in Pur-RE, the signal corresponding to PSF was detected deeply inside the PET layer (points h to j). These results indicate that the employed organic solvent in the coating mixture (i.e., THF) has dissolved the PSF layer of the recycled membrane support, causing the percolation of dissolved PSF inside the PET layer. While the solvation of the PSF layer promotes the penetration of the polymer binder (i.e., PVC) into the recycled membrane support, as it is demonstrated by the presence of the PVC signal at point h. As a result, the adhesion of the coated layer to the recycled membrane support is strengthen, providing a high mechanical stability to the membrane [54]. In contrast, the penetration of the ion-exchange resin in the membrane support is probably limited by the size of the ion-exchange resin particles. Overall, the absence of charged functional groups in combination with the presence of non-conductive polymers in this region of the membrane (points h to j) contributes to the high electrical resistance, low IEC and low WC of the membrane (see Table 14) [56]. In conclusion, these results confirm successful upcycling of RO membranes into AEMs and the asymmetric distribution of the fixed charged functional

groups along the thickness of the PU-RE membrane. Besides, since the only difference between the prepared membranes was the type of ion-exchange resin used during the preparation, analogous results are expected for Amb-RE and Lew-RE.

7.3.2. Donnan dialysis (DD) and ion-exchange membrane bioreactor (IEMB) experiments

Time course concentration of nitrate in the feed and in the receiver compartments

Fig. 52 shows the time course concentration of nitrate in the feed and the receiver compartments and nitrate removal rates from the feed compartment during DD and IEMB experiments.

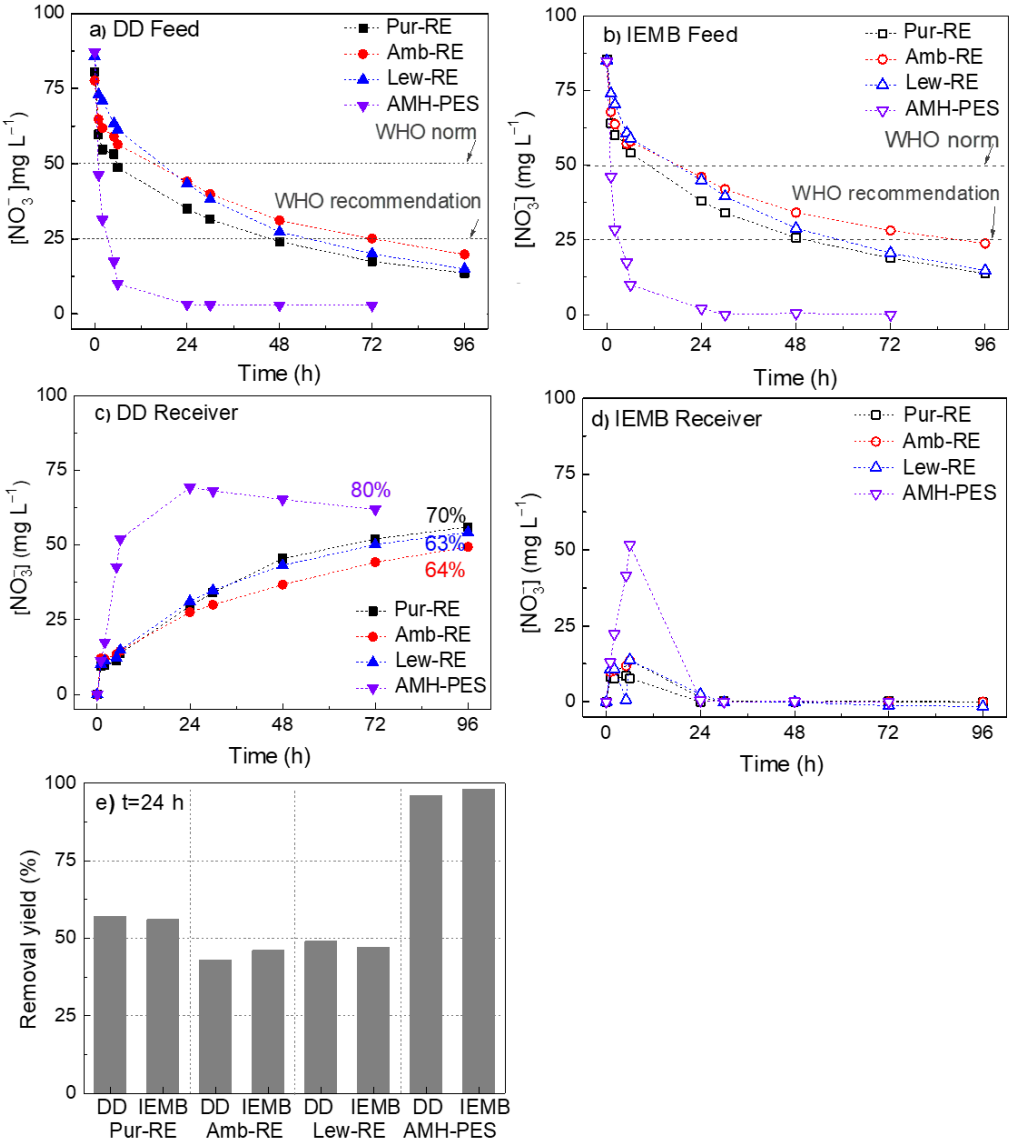

Figure 52. Time course concentration of nitrate ([NO_3^-]) in the feed compartment in a) DD experiments and b) IEMB experiments. Time course concentration of nitrate in the receiver compartment in c) DD experiments (the numbers in % indicate the recovery yield of nitrate at the end of the experiment) and d) IEMB experiments (where nitrate conversion to N_2 occurs). e) Nitrate removal yield (%) from the feed within 24 h operation as DD and IEMB. Membranes: Pur-RE, Amb-RE, Lew-RE, AMH-PES.

Fig. 52a and 52b show considerable differences in the performance of the membranes for reducing the concentration of the target ion to the maximum and the recommended levels (50 and 25 $mg \cdot L^{-1}$, respectively). Such differences are correlated to the membrane properties (reported in Table 1). Accordingly, the AMH-PES membrane clearly shows the best performance, achieving 96 % and 98 % removal within 24 h, under DD and IEMB operation conditions, respectively (Fig. 52e). This membrane has a relatively uniform distribution of the ion-exchange resin particles across the membrane section (reported before, in [54]), together with the highest IEC and WC (2.19 ± 0.09 $mmol \cdot g^{-1}$ and 50 ± 0 %, respectively), a high permselectivity (81 ± 1 %) and a relatively low electrical resistance (19 ± 3 $\Omega \cdot cm^2$), in comparison with the prepared membranes.

On contrast, the asymmetric distribution of the ion-exchange functional groups in the prepared membranes (confirmed by μ-Raman spectroscopy, section 7.3.1.), might reduce the counter-ion transport rate. Further, the relatively low ion-exchange capacity (IEC) of such membranes results in a lower number of fixed charged functional groups, meaning that a lower number of ion transport sites are available [214,215]. Besides, the low water content of the prepared membranes leads to a lower electrical conductivity [216]. As a result of the combination of the aforementioned properties, the prepared membranes have a high electrical resistance (see Table 14), as explained in detail in our previous works [54,56]. A high electrical resistance leads, under the same experimental conditions, to a slower effective transport of the ions (i.e., migration). Although, among the prepared membranes, Pur-RE shows the best performance, reaching a 57 % and 56 % removal within 24 h, under DD and IEMB operation conditions, respectively (Fig. 52e). These results might be related to the higher IEC and the lower electrical resistance of the Pur-RE membrane (0.75 $mmol \cdot g^{-1}$ and 56 $\Omega \cdot cm^2$, respectively), in comparison with the IEC and the electrical resistance of Amb-RE (0.62 $mmol \cdot g^{-1}$ and 129 $\Omega \cdot cm^2$, respectively) and Lew-RE membranes (0.39 $mmol \cdot g^{-1}$ and 120 $\Omega \cdot cm^2$, respectively) [217].

Fig. 52c shows the accumulation of nitrate in the receiver compartment during DD experiments. Among the prepared membranes Pur-RE membrane shows again the best performance for the recovery of nitrate under DD operation (recovery of 70 %), although the performance of AMH-PES is larger (recovery of 80 %). Differently, in Fig. 52d, corresponding to the IEMB operation, it can be observed that the integration of a bioreactor results in the successful elimination of nitrate from the receiver compartment by denitrifying bacteria in a single device and a single step. Moreover, the time course concentration analyses of nitrite (NO_2^-) showed that its accumulation was avoided in both compartments (results reported as Supplementary Material in Fig. S 14). The latter entails several advantages such as, avoiding the discharge of nitrite into the environment, while enabling a prolonged use of the receiver solution. Besides the concentration gradient of nitrate is effectively maintained during the process, which under a continuous operation would result in favoured nitrate transport in respect to that of other accompanying anions which are not bioreduced (not evident in the present case due to batch IEMB operating conditions and the use of a single anion (NO_3^-) in the feed) [218].

Co-ion leakage to the feed compartment

As membranes are not 100 % permselective, co-ion leakage from the receiver to the feed compartment is expected. The co-ion leakage reduces the electrochemical potential difference established across the membrane, decreasing the back-transport of the target counter-ion to the receiver compartment. Moreover, it increases the conductivity in the feed compartment. In this respect, the WHO establishes a maximum conductivity of 1 mS cm^{-1} for water intended for drinking purposes [209]. Fig. 53 shows the conductivity increase in the feed compartment after 72 h of experiment.

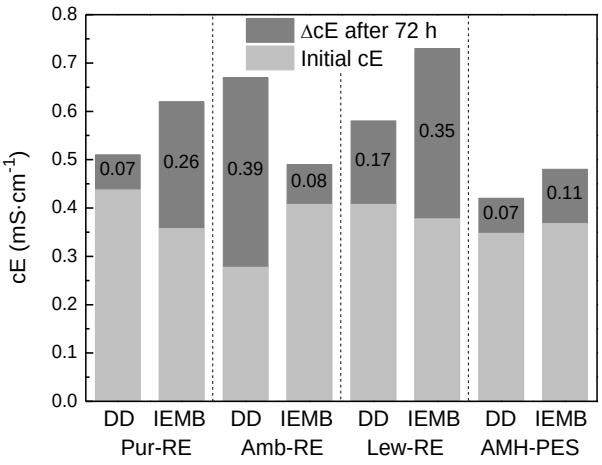

Figure 53. Increase of feed solution conductivity after 72 h of operation as a Donnan Dialyzer and as an IEMB.

As it can be observed in Fig. 53, that some co-ion leakage was occurred in all experiments, resulting in a slight conductivity increase of the feed solution (e.g., a 0.07 and a 0.26 $mS \cdot cm^{-1}$ increase using Pur-RE under DD and IEMB operating conditions, and a 0.07 and a 0.11 $mS \cdot cm^{-1}$ increase using AMH-PES under the same conditions). However, the final conductivity in the feed compartment was maintained in all the cases below 1 $mS \cdot cm^{-1}$. Even if the permselectivity of Pur-RE (65 %) is not as high as that of AMH-PES (81 %), these small increases in conductivity demonstrated that co-ion leakage is not a problem in this process [217]. Indeed, the Pur-RE membrane achieved a better performance than the Amb-RE membrane (with a permselectivity of 83 %), indicating that, in this case, other membrane properties may have a greater influence in the process performance, as it was discussed in the previous subsection.

Diffusion permeability of the carbon source

The migration of the carbon source from the receiver to the feed compartment during IEMB operation might generate secondary pollution problems in the treated water and lead to the undesired growth of bacteria.

Thus, for operation as a bioreactor, the membranes must assure a low permeability towards the employed carbon source, ethanol (selected as a non-charged electron donor) in this case. The TOC measurements performed during IEMB experiments showed that the migration of the carbon source and other metabolic by-products to the treated water was adequately avoided (i.e., TOC increase was not detected). To confirm this, additional tests on ethanol permeation were performed and the results are shown in Fig. 54.

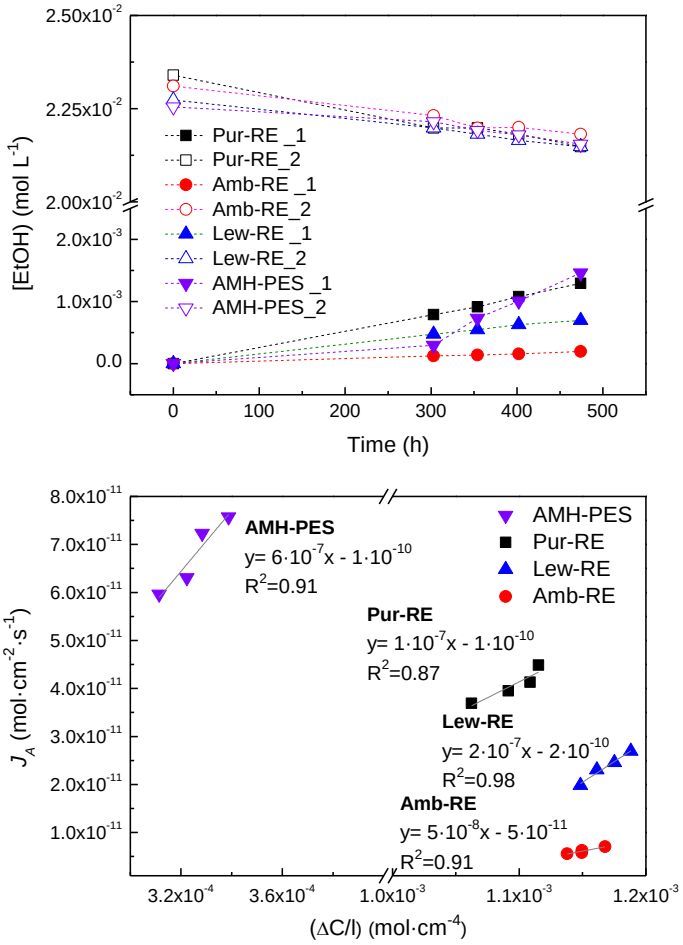

Figure 54. Studies on ethanol permeation across the membranes. a) Time course concentration change in the water compartment (1) and the ethanol compartment

(2), b) representation used for calculation of ethanol diffusion coefficients across the membranes and linear equations for each membrane.

From Fig. 54, the diffusion coefficients of ethanol through the membranes are determined as: $5 \cdot 10^{-8}$ $cm^2 \cdot s^{-1}$ Amb-RE < $1 \cdot 10^{-7}$ $cm^2 \cdot s^{-1}$ Pur-RE < $2 \cdot 10^{-7}$ $cm^2 \cdot s^{-1}$ Lew-RE < $6 \cdot 10^{-7}$ $cm^2 \cdot s^{-1}$ AMH-PES.

The advantageous lower diffusion coefficient of ethanol in Pur-RE, Amb-RE and Lew-RE in respect to AMH-PES could be a consequence of the lower water content of the prepared membranes [56,219].

Overall, this work investigated for the first time, the proof-of-concept validation of RO upcycled AEMs in DD and IEMB processes. Among the prepared membranes, Pur-RE shows the best performance in DD and IEMB operation as it combines the highest transmembrane flux of nitrate together with the best recovery yield in the receiver compartment (under DD operation), an adequately low co-ion leakage and an undetectable transport of the carbon source and microbial metabolic by-products to the treated water compartment (under IEMB operation). Still, the lower transmembrane ion flux of Pur-RE, in comparison with the reference commercial membrane could entail a limitation for its real application and, in this sense, future research should be dedicated to upgrade the performance of the membrane under DD and IEMB operating conditions. For that purpose, different strategies might be followed, either focused on improving membrane properties (e.g., by an activation treatment [55], using conductive nanomaterials as additives in the formulation [130,220], or increasing the selectivity towards the target counter ion [113]), or optimizing process parameters (e.g., increasing the relation between the membrane area per volume to be treated by using a plate and frame configuration [205], increasing the concentration of the stripping ion [221], or further avoiding co-ion leakage by choosing a divalent co-ion such as $CaCl_2$ [222].

7.3.3. 2D fluorescence spectroscopy

In this work, 2D fluorescence spectroscopy has been employed to gain a better understanding about the stability of the membranes against fouling and chemical cleaning. Such properties might be related to the lifetime of the membranes in a real application. In addition, understanding the fluorescence response of the membranes could help the implementation of an *in situ* monitorization of the bioreactors [211].

Due to the complexity of the EEMs obtained from the 2D fluorescence spectroscopic analysis, a Principal Components Analysis (PCA) was conducted to reduce the dimensionality of the data, while capturing the principal interrelations of the original data [223]. The PCA performed using all the data (i.e., Pur-RE, Amb-RE, Lew-RE and AMH-PES) is displayed as Supplementary Material in Fig. S 15. Due to significant differences among the PCs of the reference (AMH-PES) and the prepared membranes, another PCA was performed including only the spectral data of the prepared membranes (i.e., Pur-RE, Amb-RE, and Lew-RE, excluding AMH-PES), aiming at a more precise analysis of the relation between the PCs of the prepared membranes. Results corresponding to the PCA analysis of the coated side of prepared membranes are displayed in Fig. 55, while results corresponding to the PET side of the membranes are displayed as Supplementary Material in Fig. S 16.

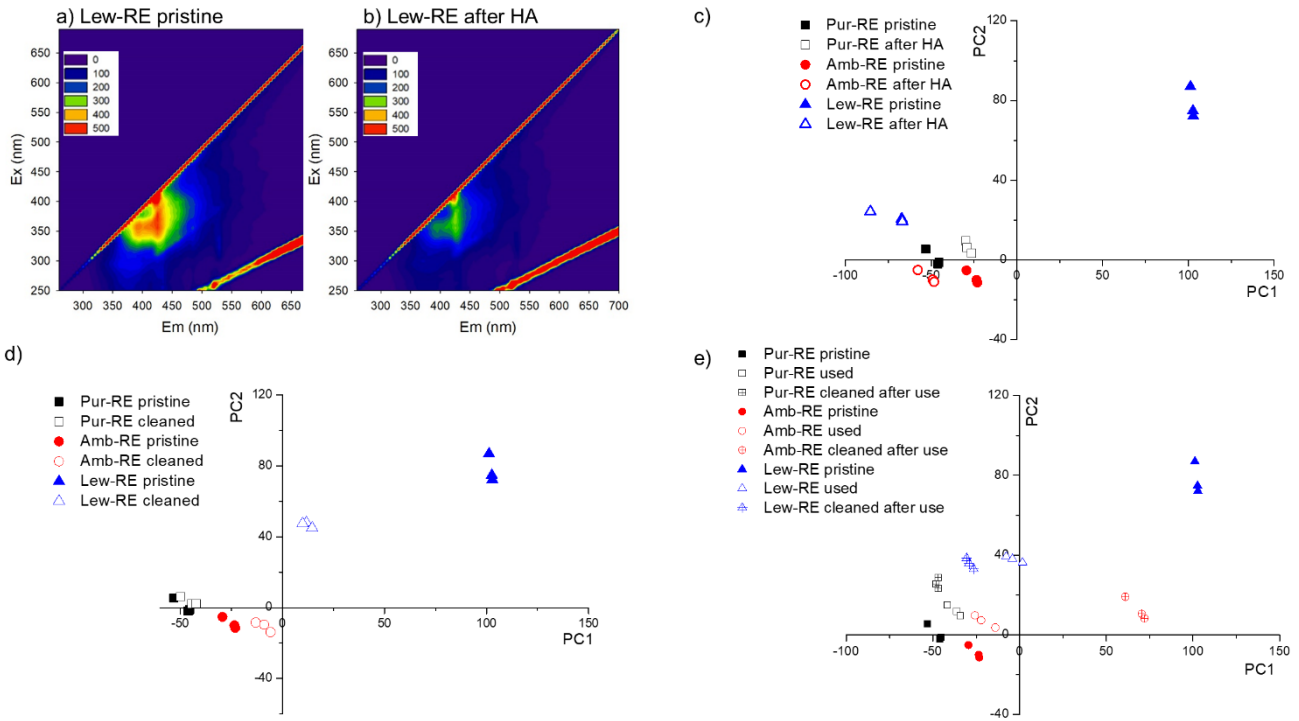

Figure 55. a) and b) Fluorescence spectra obtained from the coated (top) side of Lew-RE in pristine state (a) and after the accelerated fouling test (b); c) Scores for PC1 and PC2 obtained from the EEMs obtained from the coated (top) side of pristine membranes and membranes after the accelerated fouling test; d) Scores for PC1 and PC2 obtained from the EEMs obtained from the coated (top) side of pristine membranes and membranes after the chemical cleaning; e) Scores for PC1 and PC2 obtained from the EEMs of pristine membranes, used membranes (after the IEMB experiments), and cleaned membranes after their use in a first batch of experiments.

Figs. 55a and 55b show the EEMs of Lew-RE membrane before and after the accelerated fouling test. It can be observed that the pristine Lew-RE membrane displays a high fluorescence intensity at the wavelength (λ) region $\lambda_{excitation}$ = 320-420 nm / $\lambda_{emission}$ = 350-450 nm (Fig. 55a) while, after the accelerated fouling test, the excitation emission intensity is reduced (Fig. 55b). This reduction in the emission intensity might be attributed to the deposition of humic acids on the membrane surface, partially absorbing the light emitted by the membrane, and decreasing the emission intensity [207]. In respect to pristine membranes, it can be observed by the PCA that the PCs of the Lew-RE membrane differs from the PCs of Pur-RE and Amb-RE membranes, indicating differences between their EEMs. These results could be related to the different ion-exchange resins used in the preparation of the membranes, as they differ in the substituents at the ion-exchange sites (see Table 14), having different hydrophilic properties [56]. On contrast, the PET sides of the membranes were found to be rather similar to each other (Fig. S 16a, Supplementary Material), as the ion-exchange resin is barely present at the PET side (confirmed by μ-Ramn analyses).

In respect to the development of a fouling layer, the PCA analysis (Fig. 55c) shows a considerable distance between the PCs of the pristine and fouled Lew-RE membrane, indicating this membrane is the one that suffers higher alterations due to organic fouling.

Regarding the effect of the chemical cleaning on pristine membranes (Fig. 55d), it can be observed that the PC scores of the pristine and cleaned Lew-RE membrane are the most distant from each other, indicating that Lew-RE membrane seems to be significantly affected by the employed chemical cleaning. In contrast, the Pur-RE membrane shows a negligible alteration of its fluorescence spectra.

It can be observed in Fig 55e that, on the one hand, the fluorescence response of the Lew-RE membrane becomes significantly altered after its use in the IEMB. In contrast, Pur-RE and Amb-RE membranes show a small alteration after their use. It should be noticed that in these experiments the

biocompartment was faced to the PET surfaces of the membranes, thus the coated side should not be affected by biofouling. Therefore, the alteration shown by the Lew-RE membrane could be related to the adsorption of nitrate at the membrane surface, facilitated by the higher affinity of this membrane towards nitrate ions [56], as it was demonstrated before that nitrate can induce a quenching effect on the fluorescence spectra [224]. On the other hand, it can be observed in Fig 55e that the "pristine state" of the used membranes was not fully recovered after chemical cleaning. Indeed, the PCs are even more distant from the original (pristine state) after chemical cleaning. In the case of the Amb-RE membrane, the alteration induced by chemical cleaning on the used membrane seems to be more significant than in the case of the pristine membrane (results shown in Fig. 55d). Again, the Pur-RE membrane is the one that suffers a less significant alteration under the tested conditions. In contrast, the PET side of Lew-RE membrane shows the lowest alteration under these conditions (information detailed in Fig. S 16c, Supplementary Material).

In conclusion, it can be stated that the variations in the excitation emission spectra are well captured by the first two PCs in the performed PCA analysis. Concerning the resistance to alterations caused by organic fouling and the exposure to acid and alkali solutions, the Lew-RE membrane shows to be the least resistant, while the Pur-RE membrane appears to be the most stable one, under the tested conditions.

As a complementary study, an Attenuated total reflectance–Fourier transform infrared spectroscopy **(**ATR-FTIR) analysis of the membranes in pristine state and after the accelerated fouling test and the chemical cleaning of pristine membranes was conducted (see section 7.5.4 of the Supplementary Material). Interestingly, differences in the functional groups of the membranes (after the accelerated fouling test and the chemical cleaning) were not detected, indicating that the mentioned conditions were not harsh enough to induce chemical alterations perceived by this technique. Accordingly, it is worthy to remark that, through the

fluorescence response studies performed, it was possible to notice differences in the chemical composition of the membranes' surfaces, after the accelerated fouling test and the chemical cleaning, indicating therefore a high sensitivity of 2D fluorescence spectroscopy to detect subtle alterations at the membrane surfaces.

7.3.4. Preliminary membrane-associated costs and environmental implications

The aim of this section is to provide a preliminary estimation, for the first time, of the approximated material cost of Pur-RE membrane. In addition, the economic affordability of Pur-RE membrane and reference commercial IEM (AMH-PES) were compared, taking into consideration the differences in ion transport performances between the membranes. In light of the preliminary nature of this proof-of-concept study, CAPEX and OPEX considerations in relation to the industrial application of DD and IEMB systems are out of the scope of this work. The cost of recycling an end-of-life brackish water RO membrane into UF-like properties, including capital expenditure (CAPEX) and the operational expenditure costs (OPEX), has been estimated in a previous study [30], as 31.7 € per module. Considering an active membrane area of 37 m^2 per module, the cost of the recycled membrane support could approach 0.9 €·m^{-2}. Besides, the cost of the coating layer, regarding the current price in market of the employed reagents (displayed in Table S 4 as Supplementary Material) and excluding CAPEX and OPEX considerations, could approach approximately 2.4 €·m^{-2}. Under these considerations, the costs of the materials required to prepare the Pur-RE membrane could approach 3.3 €·m^{-2}. It is worth noting that this preliminary estimation does not consider the costs associated with module opening and repacking, which should be evaluated in future studies. For comparison, the selling price of AMH-PES Ralex ® membrane is between 70 and 100 €·m^{-2} [225]. Since transmembrane NO_3^- flux through Pur-RE membrane was lower than in the case of the reference commercial membrane, for the sake of a roughly preliminary comparison Table 15

shows the equivalent surface of Pur-RE membrane to reach the same removal rate of AMH-PES membrane. Two different scenarios have been considered, the first one calculating the equivalent membrane surface of Pur-RE considering the transmembrane ion flux to reach nitrate concentration below the maximum allowed (50 mg·L^{-1}), and a second one considering the transmembrane ion flux to reach a level below the recommended nitrate concentration (25 mg·L^{-1}). The transmembrane fluxes were calculated based on the data reported in section 7.3.2.

Table 15. Approximated cost of Pur-RE considering the differences between the target ion transmembrane flux ($J_{NO_3^-}$) in respect to the reference membrane (AMH-PES). $J_{NO_3^-\,(C_0-C_{50})}$, nitrate transmembrane flux from the initial conditions to reach a concentration below the maximum allowed level (50 mg·L^{-1}), $J_{NO_3^-\,(C_0-C_{25})}$, nitrate transmembrane flux from the initial conditions to reach a concentration below the maximum recommended level (25 mg·L^{-1}).

Transmembrane NO_3^- flux ($J_{NO_3^-}$)	**Pur-RE**	**AMH-PES**	**Pur-RE membrane surface (m²) equivalent to performance of 1 m² AMH-PES ***	**Pur-RE membrane cost (€) equivalent to performance of 1 m² AMH-PES ****
$J_{NO_3^-\,(C_0-C_{50})}$ (g·m^{-2}·h^{-1}) in DD	0.82	6.34	7.73	25.2
$J_{NO_3^-\,(C_0-C_{50})}$ (g·m^{-2}·h^{-1}) in the IEMB	0.18	2.70	14.81	48.3
$J_{NO_3^-\,(C_0-C_{50})}$ (g·m^{-2}·h^{-1}) in DD	0.81	6.00	7.39	24.1
$J_{NO_3^-\,(C_0-C_{50})}$ (g·m^{-2}·h^{-1}) in the IEMB	0.19	2.61	13.50	44.0

* Considering the data in section 3.2.1.

** Considering the estimated material cost for Pur-RE as 3.3 €·m^{-2}.

Certainly, a deeper economic assessment should be conducted (e.g., the cost of module opening and repacking should be evaluated, and CAPEX and OPEX should be considered), as well as an improvement in the production process (e.g., reducing the costs associated to the coating process, while improving the ion transport performance of the resulting

membranes), but, even in that case, it seems evident a significant economic benefit if this concept is brought to market. Besides, the European green policies for a sustainable transition (i.e., the European Green Deal [27] and the Circular Economy Action Plan [226]) advocate giving rise to taxation on landfill disposal, encouraging the extension of the service time of goods and products, and making recycling alternatives more attractive from an economic point of view.

From an environmental point of view, the recycling membrane concept presented in this study is an alternative to conventional ion-exchange membrane production. In this sense, in a previous study [30], savings of more than 175 kg CO_2 equivalent and 0.28 m^3 of freshwater (among other environmental indicators) were estimated trough the Life Cycle Assessment (LCA) of the recycling process of one end-of-life RO module into UF-like properties. Therefore, even if CO_2 equivalent emission, related to the coating process, is not yet accounted for, it is possible to envisage a positive environmental impact of the proposed recycling concept.

Overall, membrane recycling is a promising alternative to waste disposal by RO industry and it is a commitment to circular economy in membrane technology and the water sector. Furthermore, it has been demonstrated that passive mass transport processes such as DD and IEMB could be a promising technological niche for the application of such AEMs.

7.4. Conclusions

In the present work, the feasibility of using AEMs prepared from upcycled end-of-life RO membranes for the removal of nitrate from water using DD and IEMB systems is demonstrated. The main findings of the study are summarized as follows:

- μ Raman spectroscopy confirmed the successful deposition of the ion-exchange resin in the coated (top) surface of the membrane. Although, the analysis revealed an asymmetric distribution of the ion-exchange sites in the membrane cross-section, which might contribute to the relatively low

ion-exchange capacity and water content, and the relatively high electrical resistance of the membranes and, therefore, have a great influence on transport properties of the membrane.

- In respect to nitrate removal under DD and IEMB operation, the membrane incorporating Purolite® A600/9149 ion-exchange resin (Pur-RE membrane) achieved, among the prepared membranes, the best removal yields (57 % and 56 % of nitrate removal within 24 h under DD and IEMB operation, respectively), probably due to its higher ion-exchange capacity and lower electrical resistance, in comparison with the Amb-RE and the Lew-RE membranes. Furthermore, nitrate was biologically eliminated in the IEMB, favouring the reuse of the receiver solution, and avoiding the discharge of the pollutant into the environment.
- 2D fluorescence spectroscopy can effectively detect alterations in the excitation emission spectra of the membranes, caused by fouling and/or chemical cleaning. In this respect, the Pur-RE membrane was found to be the most stable membrane under the tested conditions.
- The relative low cost of the employed materials in the formulation of Pur-Re membrane anticipated an economic benefit of the presented membrane recycling concept.

Overall, this work shows the potential applicability of RO upcycled membranes as AEMs in electrochemical potential driven processes (DD and IEMB), for an efficient removal of nitrate from water at a minimum energy requirement. The developed membranes could be obtained at a lower cost than commercial ones and therefore facilitate the practical implementation of these passive transport processes. Lastly, membrane recycling represents a commitment for the transition to a circular economy.

7.5. Supplementary material

7.5.1. Confocal micro-Raman spectroscopy

Table S 3 shows the main Raman bands identifying the polymers in the membrane.

Table S 3 Main characteristic Raman bands (cm^{-1}), between 200-2000 cm^{-1}, for Polyvinyl chloride (PVC), the ion-exchange resin (Purolite® A600/9149), Polysulfone (PSF) and Polyester (PET), identified in the membrane Pur-RE [213].

PVC	Ion-exchange resin	PSF	PET	Vibrational assignments
638				ν(C-Cl)
695				ν(C-Cl)
	720			Ring δ(CH)
	764	792		Ring breathing
			858	Ring δ(CH)
		1109		ν(SO_2)
		1150		ν(C-O-C)
	1190			Ring ν(CH)
	1221			Ring ν(CH)
			1288	ν(C(=O)-O)
1428				δ(CH_2)
		1589		Ring ν(CC)
	1612	1609	1616	Ring ν(CC)
			1727	ν(C=O)

Fig. S 13 shows the μ-Raman spectra identifying different polymers present in the Pur-RE membrane.

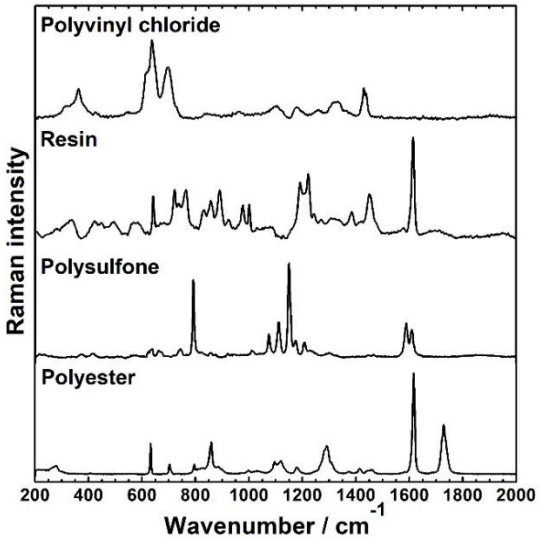

Figure S 13. μ-Raman spectra between 200-2000 cm^{-1} of polyvinyl chloride (PVC), the ion-exchange resin (Purolite ® A600/9149), polysulfone (PSF) and polyester (PET), identified in the membrane Pur-RE.

7.5.2. Ion-exchange membrane bioreactor (IEMB) experiments

Fig. S 14 shows the measured concentration of nitrite (NO_2^-) in the feed and in the receiver compartments during IEMB experiments.

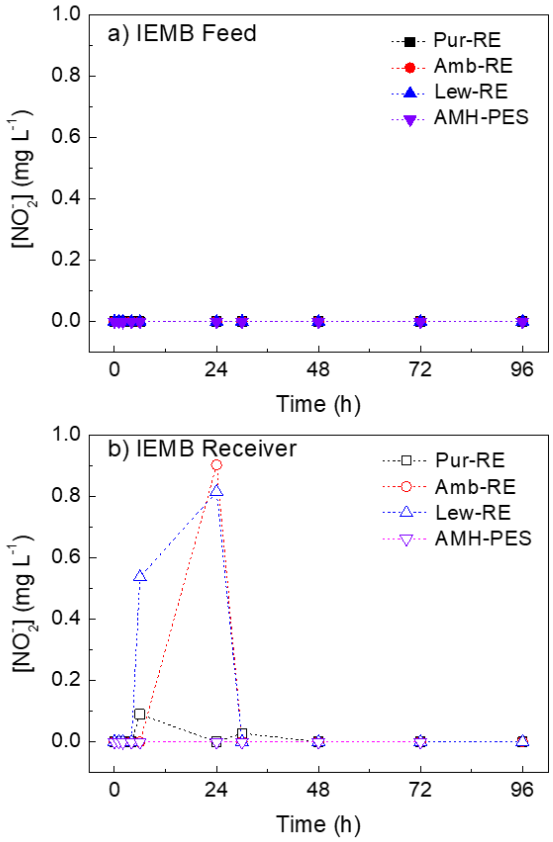

Figure S 14. Time course concentration of nitrite ([NO_2^-]) in IEMB experiments a) feed compartment, and b) receiver compartment. Membranes: Pur-RE, Amb-RE, Lew-RE, AMH-PES.

It can be observed that nitrite was not detected at any time in the feed compartment. In the receiver compartment, appearance of the intermediate nitrite trace accumulation was detected (at concentrations below 1 mg·L^{-1}), which was completely eliminated as the experiment progressed.

7.5.3. 2D fluorescence spectroscopy.

PCA including Pur-RE, Amb-RE and Lew-RE and AMH-PES

Fig. S 15 shows the correlation between the first two Principal Components (PCs) obtained from the PCA analysis performed including all the tested membranes (Pur-RE, Amb-RE, Lew-RE and AMH-PES).

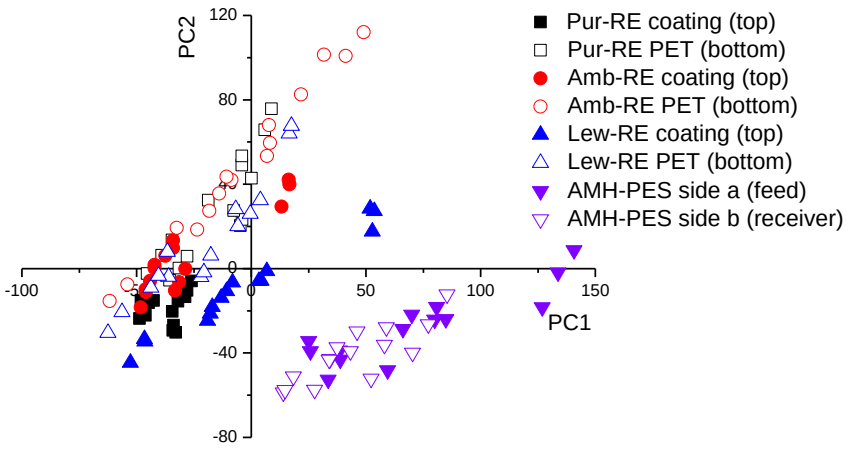

Figure S 15. Scores for PC1 and PC2 obtained from the PCA of all EEMs of the tested membranes. Side a and side b in AMH-PES refers to the membrane surfaces in contact with the feed and the receiver compartments, respectively.

With these PCs, two different data clusters can be well differenced, one corresponding to the prepared membranes (Pur-RE, Amb-RE and Lew-RE), and another one corresponding to the commercial membrane (AMH-PES). Even if those clusters are well divided by the PCs, they are not completely unrelated as the data in both clusters follows a similar direction [210]. Interestingly, differences between the coating layer and the PET bottom surface of the prepared membranes can be distinguished, as a reflect of the asymmetric membrane structure, confirmed by confocal μ-Raman spectroscopy.

Differences between Pur-RE, Amb-RE and Lew-RE membranes at the PET surface.

Figure S 16 shows the correlation between the first two first PCs of the EEMs obtained at PET surface of the prepared membranes in pristine state, after the fouling test, after the chemical cleaning treatment and after their use in the bioreactor and a posterior cleaning.

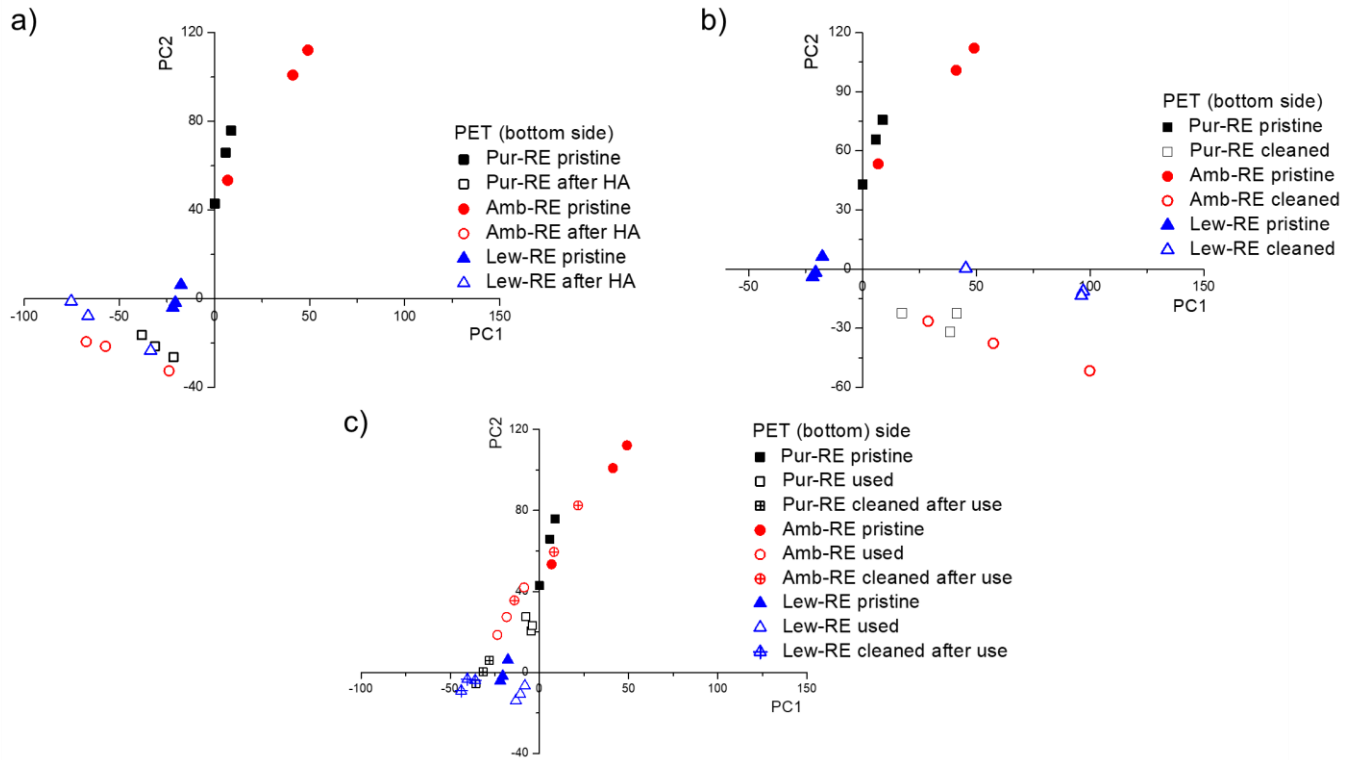

Figure S 16. Scores for PC1 and PC2 obtained from the EEMs of the PET surface in pristine membranes, and a) membranes after the accelerated fouling test, b) membranes after the chemical cleaning and c) membranes. After their use in the bioreactor (i.e., after the IEMB experiments) and posterior cleaning.

As expected, PCA analyses found similarities between the PET (bottom) surfaces in pristine membranes (i.e., PC scores aligned in the same direction), due to the fact that the ion exchange resin (different in each membrane) is not present at this side of the membrane (confirmed μ-Raman spectroscopy).

Regarding the alterations of the fluorescence spectra caused by the fouling treatment (Fig S 16a), it can be stated that HA fouling affects in a greater extent the PET surface of the membranes in comparison with the coating layer, which could be attributed to the lower hydrophilicity of the PET fabric [227].

In addition, in Fig S 16b it can be observed that the cleaning treatment affected in a similar way to all the tested membranes, causing significant alterations on the EEMs of the PET surfaces, in respect to the pristine state.

Lastly, in Fig. S 16c, it can be observed that, as expected, the use of the membranes in the bioreactor affected to the fluorescence response of the PET (bottom) surfaces of the membranes (in contact with the biocompartment during the experiments). In contrast to the results at the coated (top) surface of the membrane, the PET (bottom) surface of Lew-RE membrane shows the lowest alteration of the fluorescence response. In this case, the hydrophobic properties of Lewatit ® Sybron Ionac ® SR-7 ion-exchange resin could lead to the penetration of HA-like compounds into the PET side of the membranes and their transport to the coated (top) side. Causing a greater alteration at the coated (top) side than at the PET (bottom) side of the membrane.

7.5.4. Attenuated total reflectance–Fourier transform infrared spectroscopy (ATR-FTIR)

Fourier transform infrared (FTIR) measurements were carried out using a spectrometer (Perkin-Elmer, Waltham, MA, USA) coupled with an attenuated total reflection (ATR) device. Sixteen scans were averaged from 4000 to 650 cm^{-1} and with a resolution of 4 cm^{-1}. The effect of the accelerated

fouling test and the cleaning treatment on the functional groups of pristine membranes was studied. For that purpose, Pur-RE, Amb-RE, Lew-RE and AMH-PES membranes in pristine state and after the mentioned treatments were analysed. The membranes were dried in an oven at 50 ºC prior to the analysis.

Fig. S 17 shows the ATR-FTIR spectra of the analysed membranes in pristine state, after the accelerated fouling test, and after chemical cleaning of pristine membranes.

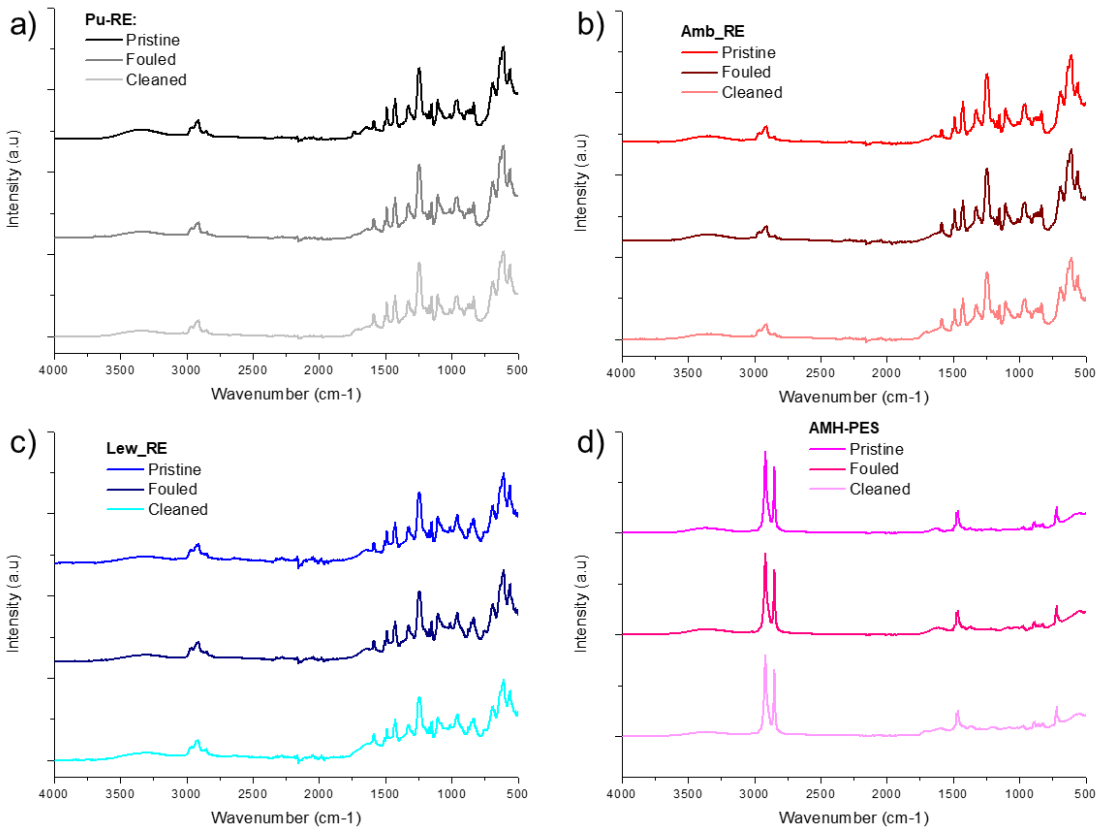

Figure S 17. ATR-FTIR spectra of studied membranes in pristine state, after the accelerated fouling test and after the chemical cleaning treatment cleaning, a) Pur-RE, b) Amb-RE, c) Lew-RE, d) AMH-PES.

It can be observed in Fig. S 17 (a to d) that the ATR-FTIR spectra of the membranes after the accelerated fouling test and the chemical cleaning remain unchanged in respect to the pristine state. These results indicate that these treatments did not induce significant chemical alterations in the functional groups of the membranes. In contrast, the fluorescence responses of the membranes were significantly altered, as it was stated by 2D fluorescence spectroscopy analysis (Sections 7.3.3 and 7.5.3).

7.5.5. Estimation of the material cost of the coating layer

Table S 4. Calculation of the price of consumable materials for the preparation of 1 m^2 of AEM using the methodology described in Sections 3.2.3 and 3.2.4 of the Chapter 3 [54]

Consumable materials		€ per unit	Amount per m^{-2} AEM	Price per m^2 AEM (€ m^{-2})	Reference
Organic solvent	Tetrahydrofuran (THF)	5.36 – 5.43 €·L^{-1} [a]	0.40 L	2.16	[228]
Polymer binder	Polyvinylchloride (PVC) powder	0.70 – 0.72 €·kg^{-1} [b]	0.0198 kg	0.01	[229]
Anion-Exchange Resin	Purolite ® A600/9149	6.74 €·kg^{-1} [c]	0.0361 kg [d]	0.24	Purolite[9®]

[a] 36500-3700 yuan per metric ton (data referred to 2021), considering a density of 0.889 kg·m^{-3} (at 25ºC).

[b] 835-850 U.S. dollar per metric ton (data referred to 2020-2022).

[c] 168.75 € per 25 kg (data referred to 2021).

[d] Considering a weight loss of 45 % of the product during drying stage before membrane preparation.

8

Chapter 8. General conclusions and future research.

RO desalination is forecasted to maintain a constant growth in the near future. As long as fouling remains an inevitable drawback in membrane technology, membrane replacement will keep generating an increasing amount of discarded EoL RO modules. This situation reinforces the urgent need to research on the development of membrane reuse and recycling technologies. The compendium of studies addressed in the present doctoral thesis reveals fundamental notions for the **indirect recycling of EoL RO membranes as AEMs.** These membranes have been widely characterized to get a better understanding of their properties, with the aim to elucidate the effect of such properties in membrane performance. Moreover, different applications have been studied in order to identify **potential applications** for such membranes. The main conclusions from this doctoral thesis can be summarized as follows.

8.1. General conclusions

The employed methodology for the preparation of AEMs from EoL RO (*Chapter 3*) resulted in a **strong adhesion of the coated layer to the recycled membrane support**, facilitating the mechanical durability of the membranes. Moreover, the membranes acquired a high **mechanical stability**, provided by the recycled pressure filtration membrane. The appropriated combination of the coating layer thickness and the solvent evaporation time resulted in a **high permselectivity**. Nevertheless, the combination of the coated layer with the recycled membrane support contributed to a **high electric resistance** of the membranes. Which **increased the energy consumption** associated to their use in brackish water desalination by ED.

To complement the presented indirect membrane recycling approach, s**upplementary studies** were devoted to the consideration of **recycling alternatives for other plastic components** of the EoL RO module. In *Chapter 3,* the **recycling of PP feed spacers** as turbulence promoters, end caps and electrode rinse compartments in the ED stack was undertaken. In

such a way, an ED cell with an **84 % of recycled plastic** (54 % of the total weight of the cell, including the metallic components) was assembled. Besides, in *Appendix A*, **different recycled supporting materials** from the EoL RO module were tested for the preparation of the AEMs.

With the aim to reduce the electrical resistance of the prepared membranes, an **acid/alkali activation treatment** was developed (*Chapter 4*). This treatment significantly **decreased the energy consumption** and **upgraded the performance** of the membranes in brackish water desalination by ED. The proposed activation treatment was a **simple, economic, and efficient strategy** to rise the electrical conductivity of the membranes. Therefore, it **could help to the implementation** of the developed AEMs (from EoL RO) in electrodialytic processes.

As long as brackish water desalination is the most representative electrodialytic application of IEMs, the feasibility of using the prepared membranes in such application was first investigated (*Chapters 3 and 4*). Whereas other applications in a closer agreement with the circular economy principles, such as the recovery of valuable compounds from waste streams (i.e., nitrate recovery from fertilizer industry wastewater), are likely to be more suitable for the developed AEMs. Indeed, the development of monovalent and/or ion **selective AEMs could open a broader number of applications** for such membranes. Consequently, *Chapters 5 and 6* were dedicated to the development of different alternatives to boost the **selectivity towards monovalent or specific ions**.

In *Chapter 5*, a two steps **surface modification** strategy was developed by which a considerable increase in the **monovalent selective and antifouling properties** of the membranes was acquired. In that respect, **catechol-based biochemistry** showed a potential relevance due to an inherent capacity to self-assemble on diverse materials under aqueous media. Besides, the resulting coating facilitated the **anchorage of** additional **functional materials**, such as charged functional groups, to provide an enhanced repulsion of multivalent ions and organic foulants. In this

Chapter the surface modification of commercial AEMs was attempted, whereas the developed modification strategy could be probably applied to the RO upcycled AEMs, if required.

In *Chapter 6*, the selectivity towards nitrate of the RO upcycled AEMs was enhanced by the adjustment of the **type of the ion-exchange resin** used during membrane preparation. As a consequence, the **versatility of the developed membrane preparation methodology** was demonstrated. In this case, the selectivity was probably related to enhanced **hydrophobic interactions** between the ions in the solution and the functional groups in the membranes. In this way, the membrane incorporating an ion-exchange resin with propyl chains as substituents at the quaternary amine, demonstrated a preferential transport of less solvated ions (i.e., nitrate), along with a limited transport of highly hydrated ions (i.e., sulphates). Furthermore, the use of the recycled pressure filtration membrane as support further boosted the rejection of divalent ions, probably as a result of an **enhanced sieving effect**.

Lastly, in *Chapter 7*, **passive mass transport processes such as DD and related processes (i.e., the IEMB)** were presented as a **feasible technological niche** for the developed AEMs. In such a way, the removal of ionic micropollutants (i.e., nitrate) was attained at a **minimum energy requirement**. DD and IEMB systems have been widely studied at lab scale, although their application at an industrial scale is mainly limited by the high cost of commercially available IEMs. In that respect, the developed AEMs (from EoL RO) may represent an **economic advantage** in those passive transport processes.

Overall, the present thesis has contributed to conception of **new experimental knowledge on the indirect recycling of EoL RO membranes as AEM.** Membrane recycling approach **meets the objectives of the EC towards a circular and sustainable economic growth**, by increasing the lifespan of existing products, thus reducing pressure on raw materials and waste generation. Therefore, it is a commitment to the transformation of the

European strategic policies, as a part of the 2008/98/CE directive on waste, the European Green Deal, and the Circular Economy Action Plan.

Still some questions remain unsolved, and suggestions for addressing them in future research are provided as follows.

8.2. Future research lines

Future studies should assess a revision of membrane composition, in order to **approach eco design principles**. On the one hand, the replacement of the organic solvent (THF) by a **green solvent** (i.e., methyl lactate, 2-methyltetrahydrofuran) is highly encouraged. Besides, the shift to **other membrane manufacturing processes** (i.e., press moulding or 3D printing) would allow the complete elimination of the solvent from the membrane formulation. On the other hand, **bio-based polymers** fabricated from renewable sources (i.e., polylactic acid and polyhydroxyalkanoates) **or petroleum-based biodegradable polymers** (i.e., polycaprolactone, polybutylene succinate), would entail a greener alternative to PVC. Whereas the modification of membrane composition involves a complete revision of membrane preparation methodology. On the whole, the sustainability of the developed membranes should be analysed under the perspective of the **Life Cycle Assessment**.

In addition, a deeper understanding about the **influence of the membrane support** properties (i.e., porosity, hydrophilicity) in the resulting membranes would be required. Further, the **chemical mechanisms** taking place at the functional groups of the membrane during the activation treatment should be studied.

Considering the advantages of passive mass transport processes in terms of energy requirements, the **scaling up of DD and IEMB concepts** could be attempt. For that purpose, a **plate and frame module configuration** operated under continuous flow could be employed. The influence of a **multicomponent feed** (i.e., natural polluted water) in the performance of the process should be evaluated. In that respect, the use of

membranes with **monovalent or ion selective properties** could entail an interesting asset. In order to expand the implementations of such systems, the **removal of different ionic micropollutants** could be undertaken (i.e., fluoride, perchlorate, bromate, arsenate). Owing to the simplicity of installation and overall low operating cost, the implementation of DD and IEMB systems for **household water treatment** at remote areas (not connected to a safe water supply system) is envisaged. Such an approach could help meeting the objectives of sustainable development (clean water and sanitation), while implementing the membrane recycling concept presented in this thesis.

References

[1] UNU-INWEH, UN-ESCAP, Water Security & the Global Water Agenda. The UN-Water analytical brief, 2013. https://doi.org/10.1017/CBO9781107415324.004.

[2] UNESCO, The United Nations World Water Development Report 2020: Water and climate change, 2020.

[3] J. Schewe, J. Heinke, D. Gerten, I. Haddeland, N.W. Arnell, D.B. Clark, R. Dankers, S. Eisner, B.M. Fekete, F.J. Colón-González, S.N. Gosling, H. Kim, X. Liu, Y. Masaki, F.T. Portmann, Y. Satoh, T. Stacke, Q. Tang, Y. Wada, D. Wisser, T. Albrecht, K. Frieler, F. Piontek, L. Warszawski, P. Kabat, Multimodel assessment of water scarcity under climate change, Proc. Natl. Acad. Sci. U. S. A. 111 (2014) 3245–3250. https://doi.org/10.1073/pnas.1222460110.

[4] M.M. Mekonnen, A.Y. Hoekstra, Four billion people facing severe water scarcity, Sci. Adv. (2016) 1–7. https://doi.org/10.1126/sciadv.1500323.

[5] M. Abu-zeid, I.A. Shiklomanov, Water Resources as a Challenge of the twenty-first century, World Meteorological Organization, 2004.

[6] International Water Association, Desalination – Past, Present and Future, (2016). https://iwa-network.org/desalination-past-present-future/ (accessed May 5, 2021).

[7] E. Jones, M. Qadir, M.T.H. van Vliet, V. Smakhtin, S. mu Kang, The state of desalination and brine production: A global outlook, Sci. Total Environ. 657 (2019) 1343–1356. https://doi.org/10.1016/j.scitotenv.2018.12.076.

[8] N. Voutchkov, Energy use for membrane seawater desalination – current status and trends, Desalination. 431 (2018) 2–14. https://doi.org/10.1016/j.desal.2017.10.033.

[9] B. Van der Bruggen, Membrane Technology, 2017. https://doi.org/10.1002/0471238961.1305130202011105.a01.pub3.

[10] S. Atkinson, RO membranes and components market is growing at 10.5% CAGR, Membr. Technol. 2015 (2015) 4. https://doi.org/10.1016/s0958-2118(15)30092-6.

[11] Y. Ibrahim, R.A. Ismail, A. Ogungbenro, T. Pankratz, F. Banat, H.A. Arafat, The sociopolitical factors impacting the adoption and proliferation of desalination: A critical review, Desalination. 498 (2021) 114798. https://doi.org/10.1016/j.desal.2020.114798.

[12] Adroit Market Research, Water Desalination Market to grow at a CAGR of 9.5% to hit $32 billion by 2025, (2020). https://bit.ly/3wPdELo (accessed November 15, 2021).

[13] B. Mayor, Growth patterns in mature desalination technologies and analogies with the energy field, Desalination. 457 (2019) 75–84. https://doi.org/10.1016/j.desal.2019.01.029.

[14] S.F. Anis, R. Hashaikeh, N. Hilal, Reverse osmosis pretreatment technologies and future trends: A comprehensive review, Desalination. 452 (2019) 159–195. https://doi.org/10.1016/j.desal.2018.11.006.

[15] J. Landaburu-Aguirre, R. García-Pacheco, S. Molina, L. Rodríguez-Sáez, J. Rabadán, E. García-Calvo, Fouling prevention, preparing for re-use and membrane recycling. Towards circular economy in RO desalination, Desalination. 393 (2016) 16–30. https://doi.org/10.1016/j.desal.2016.04.002.

[16] A. Criscuoli, A. Figoli, Pressure-driven and thermally-driven membrane operations for the treatment of arsenic-contaminated waters: A comparison, J. Hazard. Mater. (2018) 1–9. https://doi.org/10.1016/j.jhazmat.2018.07.047.

[17] D. Rana, T. Matsuura, M. Kassim, A. Ismail, Reverse Osmosis Membrane, in: Handb. Membr. Sep. Chem. Pharm. Food, Biotechnol. Appl., 2015: pp. 35–52. https://doi.org/10.1201/b18319-5.

[18] B. Van Der Bruggen, C. Vandecasteele, T. Van Gestel, W. Doyenb, R. Leysenb, Review of Pressure-Driven Membrane Processes, Environ. Prog. 22 (2003) 46–56. https://doi.org/https://doi.org/10.1002/ep.670220116.

[19] S.P. Nunes, K.-V. Peinemann, Membrane technology in the chemical industry, Second, Re, WILEY-VCH, 2006.

[20] R.W. Baker, Membrane Technology and Applications, Second edi, WILEY-VCH, 2004. https://doi.org/10.1016/S0376-7388(00)83139-7.

[21] S. Molina Martínez, Preparación de membranas porosas a partir de poliamidas aromáticas hidrofílicas. Estudios de aplicación en operaciones de ultrafiltración y pervaporación., University Complutense of Madrid, 2013.

[22] W. Lawler, Z. Bradford-Hartke, M.J. Cran, M. Duke, G. Leslie, B.P. Ladewig, P. Le-Clech, Towards new opportunities for reuse, recycling and disposal of used reverse osmosis membranes, Desalination. 299 (2012) 103–112. https://doi.org/10.1016/j.desal.2012.05.030.

[23] S. Jiang, Y. Li, B.P. Ladewig, A review of reverse osmosis membrane fouling and control strategies, Sci. Total Environ. 595 (2017) 567–583. https://doi.org/10.1016/j.scitotenv.2017.03.235.

[24] L.F. Greenlee, D.F. Lawler, B.D. Freeman, B. Marrot, P. Moulin, Reverse

osmosis desalination: Water sources, technology, and today's challenges, Water Res. 43 (2009) 2317–2348. https://doi.org/10.1016/j.watres.2009.03.010.

[25] J. Senán-Salinas, A. Blanco, R. García-Pacheco, J. Landaburu-Aguirre, E. García-Calvo, Prospective Life Cycle Assessment and economic analysis of direct recycling of end-of-life reverse osmosis membranes based on Geographic Information Systems, J. Clean. Prod. 282 (2021). https://doi.org/10.1016/j.jclepro.2020.124400.

[26] European Comission, Directive 2008/98/EC of the European Parliament and of the Council of 19 November 2008 on Waste and repealing certain Directives, Off. J. Eur. Union. L 312 (2008) 3–30.

[27] C. Fetting, The European Green Deal, Brussels, 2019.

[28] European Comission, A new Circular Economy Action Plan For a cleaner and more competitive Europe, 2020. https://doi.org/10.7312/columbia/9780231167352.003.0015.

[29] R. García-Pacheco, W. Lawler, J. Landaburu-Aguirre, E. Gacría-Calvo, P. Le-Clech, End-of-Life Membranes: Challenges and Opportunities, in: Compr. Membr. Sci. Eng., 2017: pp. 1–19. https://doi.org/10.1016/B978-0-08-093250-7.00018-9.

[30] J. Senán-Salinas, R. García-Pacheco, J. Landaburu-Aguirre, E. García-Calvo, Recycling of end-of-life reverse osmosis membranes: Comparative LCA and cost-effectiveness analysis at pilot scale, Resour. Conserv. Recycl. 150 (2019) 104423. https://doi.org/10.1016/j.resconrec.2019.104423.

[31] European Comission, Directive 2009/125/EC of the European Parliament and of the council of 21 October 2009 establishing a framework for the setting of ecodesign requirements for energy-related products., Off. J. Eur. Union. 285 (2009) 10–34. https://doi.org/10.1016/j.cirp.2012.03.121.

[32] X. Dong, D. Lu, T.A.L. Harris, I.C. Escobar, Polymers and solvents used in membrane fabrication: A review focusing on sustainable membrane development, Membranes. 11 (2021). https://doi.org/10.3390/membranes11050309.

[33] F. Galiano, K. Briceño, T. Marino, A. Molino, K.V. Christensen, A. Figoli, Advances in biopolymer-based membrane preparation and applications, J. Memb. Sci. 564 (2018) 562–586. https://doi.org/10.1016/j.memsci.2018.07.059.

[34] M. Asadollahi, D. Bastani, S.A. Musavi, Enhancement of surface properties and performance of reverse osmosis membranes after

surface modification: A review, Desalination. 420 (2017) 330–383. https://doi.org/https://doi.org/10.1016/j.desal.2017.05.027.

[35] S. Kasemset, A. Lee, D.J. Miller, B.D. Freeman, M.M. Sharma, Effect of polydopamine deposition conditions on fouling resistance, physical properties, and permeation properties of reverse osmosis membranes in oil/water separation, J. Memb. Sci. 425–426 (2013) 208–216. https://doi.org/10.1016/j.memsci.2012.08.049.

[36] H. Choi, Y. Jung, S. Han, T. Tak, Y. Kwon, Surface modification of SWRO membranes using hydroxyl poly (oxyethylene) methacrylate and zwitterionic carboxylated polyethyleneimine, J. Memb. Sci. 486 (2015) 97–105. https://doi.org/10.1016/j.memsci.2015.03.040.

[37] R. Yang, J. Xu, G. Ozaydin-ince, S.Y. Wong, K.K. Gleason, Surface-tethered zwitterionic ultrathin antifouling coatings on Reverse Osmosis membranes by initiated chemical vapor deposition, Chem. Mater. 23 (2011) 1263–1272. https://doi.org/10.1021/cm1031392.

[38] C. Dong, Z. Wang, J. Wu, Y. Wang, J. Wang, S. Wang, A green strategy to immobilize silver nanoparticles onto reverse osmosis membrane for enhanced anti-biofouling property, Desalian. 401 (2017) 32–41. https://doi.org/10.1016/j.desal.2016.06.034.

[39] A.K. Ghosh, E.M. V Hoek, Impacts of support membrane structure and chemistry on polyamide-polysulfone interfacial composite membranes, J. Memb. Sci. 336 (2009) 140–148.

[40] I. Juhn, A.R. Greenberg, V.P. Khare, Synthesis and characterization of interfacially polymerized polyamide thin films, Desalination. 191 (2006) 279–290. https://doi.org/10.1016/j.desal.2006.03.004.

[41] Y. Jin, Z. Su, Effects of polymerization conditions on hydrophilic groups in aromatic polyamide thin films, J. Memb. Sci. 330 (2009) 175–179. https://doi.org/10.1016/j.memsci.2008.12.055.

[42] A.F. Corral, U. Yenal, R. Strickle, D. Yan, E. Holler, C. Hill, W.P. Ela, R.G. Arnold, Comparison of slow sand filtration and microfiltration as pretreatments for inland desalination via reverse osmosis, Desalination. 334 (2014) 1–9. https://doi.org/10.1016/j.desal.2013.11.034.

[43] A. Matin, T. Laoui, W. Falath, M. Farooque, Fouling control in reverse osmosis for water desalination & reuse: Current practices & emerging environment-friendly technologies, Sci. Total Environ. 765 (2021) 142721. https://doi.org/10.1016/j.scitotenv.2020.142721.

[44] R. García-Pacheco, J. Landaburu-Aguirre, P. Terrero-Rodríguez, E. Campos, F. Molina-Serrano, J. Rabadán, D. Zarzo, E. García-Calvo, Validation of recycled membranes for treating brackish water at pilot

scale, Desalination. 433 (2018) 199–208. https://doi.org/10.1016/j.desal.2017.12.034.

[45] K. Yanagi, Chota, Mori, Advanced reverse osmosis process with sponge ball cleaning for the reclamation of municipal sewage, Desalination. 32 (1980) 391–398. https://doi.org/10.1016/S0011-9164(00)86039-7.

[46] S.S. Madaenl, T. Mohamamdi, M. Kazemi, Chemical cleaning of reverse osmosis membranes, Desalination. 134 (2001) 77–82. https://doi.org/10.1016/S0011-9164(01)00117-5.

[47] D. Feng, J.S.J. Van Deventer, C. Aldrich, Ultrasonic defouling of reverse osmosis membranes used to treat wastewater effluents, 50 (2006) 318–323. https://doi.org/10.1016/j.seppur.2005.12.005.

[48] W. Jiang, X. Xu, L. Lin, H. Wang, R. Shaw, D. Lucero, A pilot study of an electromagnetic field for control of reverse osmosis membrane fouling and scaling during brackish groundwater desalination, Water. 11 (2019) 1015. https://doi.org/10.3390/w11051015.

[49] W. Lawler, J. Alvarez-gaitan, G. Leslie, P. Le-clech, Comparative life cycle assessment of end-of-life options for reverse osmosis membranes, Desalination. 357 (2015) 45–54. https://doi.org/10.1016/j.desal.2014.10.013.

[50] S. Muñoz, R. Frank, I. Pilar, C. Pérez, F. Xavier Simón, Life + Remembrane : end-of-Life recovery of reverse osmosis membranes, FuturEnviro. (2014) 25–29.

[51] J. Morón-López, L. Nieto-Reyes, S. Aguado, R. El-Shehawy, S. Molina, Recycling of end-of-life reverse osmosis membranes for membrane biofilms reactors (MBfRs). Effect of chlorination on the membrane surface and gas permeability., Chemosphere. 231 (2019) 103–112. https://doi.org/10.1016/j.chemosphere.2019.05.108.

[52] J. Morón-López, L. Nieto-Reyes, S. Molina, M.Á. Lezcano, Exploring microcystin-degrading bacteria thriving on recycled membranes during a cyanobacterial bloom, Sci. Total Environ. 736 (2020). https://doi.org/10.1016/j.scitotenv.2020.139672.

[53] L. Rodríguez-Sáez, J. Landaburu-Aguirre, S. Molina, M.C. García-Payo, E. García-Calvo, Study of surface modification of recycled ultrafiltration membranes using statistical design of experiments, Surfaces and Interfaces. 23 (2021). https://doi.org/10.1016/j.surfin.2021.100978.

[54] A. Lejarazu-Larrañaga, S. Molina, J.M. Ortiz, R. Navarro, E. García-Calvo, Circular economy in membrane technology: Using end-of-life reverse osmosis modules for preparation of recycled anion exchange membranes and validation in electrodialysis, J. Memb. Sci. 593 (2020)

117423. https://doi.org/10.1016/j.memsci.2019.117423.

[55] A. Lejarazu-Larrañaga, S. Molina, J.M. Ortiz, G. Riccardelli, E. García-Calvo, Influence of acid/base activation treatment in the performance of recycled electromembrane for fresh water production by electrodialysis, Chemosphere. 248 (2020) 126027. https://doi.org/10.1016/j.chemosphere.2020.126027.

[56] A. Lejarazu-Larrañaga, J.M. Ortiz, S. Molina, Y. Zhao, E. García-Calvo, Nitrate-selective anion exchange membranes prepared using discarded reverse osmosis membranes as support, Membranes. 10 (2020) 377. https://doi.org/10.3390/membranes10120377.

[57] J. Contreras-mart, C. Garc, Electrospun nanostructured membrane engineering using reverse osmosis recycled modules: membrane distillation application, Nanomaterials. 11 (2021) 1601. https://doi.org/10.3390/nano11061601.

[58] J. Contreras-Martínez, C. García-Payo, P. Arribas, L. Rodríguez-Sáez, A. Lejarazu-Larrañaga, E. García-Calvo, M. Khayet, Recycled reverse osmosis membranes for forward osmosis technology, Desalination. 519 (2022) 115312. https://doi.org/10.1016/j.desal.2021.115312.

[59] LIFE+ RELEACH (LIFE13 ENV/ES/000970), (2013). https://releach.eu/ (accessed June 1, 2021).

[60] M.O. Awaleh, M.M. Ahmed, Y.D. Soubaneh, F.B. Hoch, S.M. Bouh, E.S. Dirieh, Wastewater reclamation using discarded reverse osmosis membranes for reuse in irrigation in Djibouti, an arid country, Water Sci. Technol. 67 (2013) 1362–1369. https://doi.org/10.2166/wst.2013.011.

[61] J.J. Rodríguez, V. Jiménez, O. Trujillo, J. Veza, Reuse of reverse osmosis membranes in advanced wastewater treatment, Desalination. 150 (2002) 219–225. https://doi.org/10.1016/S0011-9164(02)00977-3.

[62] J.M. Veza, J.J. Rodriguez-Gonzalez, Second use for old reverse osmosis membranes: wastewater treatment, Desalination. 157 (2003) 65–72. https://doi.org/10.1016/S0011-9164(03)00384-9.

[63] R. García-Pacheco, J. Landaburu-Aguirre, S. Molina, L. Rodríguez-Sáez, S.B. Teli, E. García-Calvo, Transformation of end-of-life RO membranes into NF and UF membranes: Evaluation of membrane performance, J. Memb. Sci. 495 (2015) 305–315. https://doi.org/10.1016/j.memsci.2015.08.025.

[64] M. Pontié, Old RO membranes: solutions for reuse, Desalin. Water Treat. 53 (2015) 1492–1498. https://doi.org/10.1080/19443994.2014.943060.

[65] W. Lawler, A. Antony, M. Cran, M. Duke, G. Leslie, P. Le-Clech, Production and characterisation of UF membranes by chemical conversion of used RO membranes, J. Memb. Sci. 447 (2016) 203–211.

[66] J. Morón-López, L. Nieto-Reyes, J. Senán-Salinas, S. Molina, R. El-Shehawy, Recycled desalination membranes as a support material for biofilm development: A new approach for microcystin removal during water treatment, Sci. Total Environ. 647 (2019) 785–793. https://doi.org/10.1016/j.scitotenv.2018.07.435.

[67] E. Campos Pozuelo, P. Terrero Rodríguez, D. Zarzo Martínez, F.J. Molina Serrano, M. Calzada Garzón, R. García Pacheco, S. Molina Martínez, L. Rodríguez Sáez, F.J. Rabadán, J. Landaburu Aguirre, A. Ortiz de Lejarazu Larrañaga, E. García Calvo, Spanish Patent PCT/EP2016/30931. Transformation of spiral wound polyamide membranes after its industrial lifespan., n.d., 2016.

[68] S. Molina, R. García-Pacheco, L. Rodríguez-Sáez, E. García-Calvo, E. Campos, D. Zarzo, J. González, J. De Abajo, Transformation of end-of-life RO membranes into recycled NF and UF membranes, surface characterization (15WC-51551), in: Proc IDAWC15, San Diego, 30 August-4 Sept. 2015, n.d.

[69] S. Molina, J. Landaburu-Aguirre, L. Rodríguez-Sáez, R. García-Pacheco, J.G. de la Campa, E. García-Calvo, Effect of sodium hypochlorite exposure on polysulfone recycled UF membranes and their surface characterization, Polym. Degrad. Stab. 150 (2018) 46–56. https://doi.org/10.1016/j.polymdegradstab.2018.02.012.

[70] R. García-Pacheco, Q. Li, J. Comas, R.A. Taylor, P. Le-Clech, Novel housing designs for nanofiltration and ultrafiltration gravity-driven recycled membrane-based systems, Sci. Total Environ. 767 (2020) 144181. https://doi.org/10.1016/j.scitotenv.2020.144181.

[71] A. Lejarazu-larrañaga, J.M. Ortiz, S. Molina, S. Pawlowski, Nitrate Removal by Donnan Dialysis and Anion-Exchange Membrane Bioreactor Using Upcycled End-of Life Reverse Osmosis Membranes, Membranes. 12 (2022) 101. https://doi.org/doi.org/10.3390/membranes12020101.

[72] M. Pontié, S. Awad, M. Tazerout, O. Chaouachi, B. Chaouachi, Recycling and energy recovery solutions of end-of-life reverse osmosis (RO) membrane materials: A sustainable approach, Desalination. 423 (2017) 30–40.

[73] A. Antelava, S. Damilos, S. Hafeez, G. Manos, S.M. Al-Salem, B.K. Sharma, K. Kohli, A. Constantinou, Plastic Solid Waste (PSW) in the

context of Life Cycle Assessment (LCA) and sustainable management, Environ. Manage. 64 (2019) 230–244. https://doi.org/10.1007/s00267-019-01178-3.

[74] European Comission Joint Research Centre, Supporting environmentally sound decisions for waste management. Technical guide to Life Cycle Thinking (LCT) and Life Cycle Assessment (LCA) for waste experts and LCA practitioners, 2011. https://doi.org/10.2788/52632.

[75] A.K. Panda, R.K. Singh, D.K. Mishra, Thermolysis of waste plastics to liquid fuel. A suitable method for plastic waste management and manufacture of value added products-A world prospective, Renew. Sustain. Energy Rev. 14 (2010) 233–248. https://doi.org/10.1016/j.rser.2009.07.005.

[76] P.T. Benavides, P. Sun, J. Han, J.B. Dunn, M. Wang, Life-cycle analysis of fuels from post-use non-recycled plastics, Fuel. 203 (2017) 11–22. https://doi.org/10.1016/j.fuel.2017.04.070.

[77] M. El-Fadel, A.N. Findikakis, J.O. Leckie, Environmental impacts of solid waste landfilling, J. Environ. Manage. 50 (1997) 1–25. https://doi.org/10.1006/jema.1995.0131.

[78] Z. Yang, F. Lü, H. Zhang, W. Wang, L. Shao, J. Ye, P. He, Is incineration the terminator of plastics and microplastics?, J. Hazard. Mater. 401 (2021) 123429. https://doi.org/10.1016/j.jhazmat.2020.123429.

[79] J. Krook, N. Svensson, M. Eklund, Landfill mining: A critical review of two decades of research, Waste Manag. 32 (2012) 513–520. https://doi.org/10.1016/j.wasman.2011.10.015.

[80] H. Strathmann, Ion exchange membrane separation processes, Elsevier B.V, 2004.

[81] T. Lim, S. Kim, Non-precious hydrogen evolution reaction catalysts: Stepping forward to practical polymer electrolyte membrane-based zero-gap water electrolyzers, Chem. Eng. J. (2021) 133681. https://doi.org/10.1016/j.cej.2021.133681.

[82] I. Vincent, D. Bessarabov, Low cost hydrogen production by anion exchange membrane electrolysis: A review, Renew. Sustain. Energy Rev. 81 (2018) 1690–1704. https://doi.org/10.1016/j.rser.2017.05.258.

[83] G. Merle, M. Wessling, K. Nijmeijer, Anion exchange membranes for alkaline fuel cells: A review, J. Memb. Sci. 377 (2011) 1–35. https://doi.org/10.1016/j.memsci.2011.04.043.

[84] A. Clemente, R. Costa-Castelló, Redox flow batteries: A literature

review oriented to automatic control, Energies. 13 (2020) 1–31. https://doi.org/10.3390/en13174514.

[85] H. Strathmann, Electrodialysis, a mature technology with a multitude of new applications, Desalination. 264 (2010) 268–288. https://doi.org/10.1016/j.desal.2010.04.069.

[86] B.E. Logan, Exoelectrogenic bacteria that power microbial fuel cells, Nat. Rev. Microbiol. 7 (2009) 375–381. https://doi.org/10.1038/nrmicro2113.

[87] Z. Borjas, A. Esteve-Núñez, J.M. Ortiz, Strategies for merging microbial fuel cell technologies in water desalination processes: Start-up protocol and desalination efficiency assessment, J. Power Sources. 356 (2017) 519–528. https://doi.org/10.1016/j.jpowsour.2017.02.052.

[88] R. Abu-Rjal, V. Chinaryan, M.Z. Bazant, I. Rubinstein, B. Zaltzman, Effect of concentration polarization on permselectivity, Phys. Rev. E - Stat. Nonlinear, Soft Matter Phys. 89 (2014) 1–10. https://doi.org/10.1103/PhysRevE.89.012302.

[89] X. Nebavskaya, V. Sarapulova, D. Butylskii, C. Larchet, N. Pimenskaya, Electrochemical properties of homogeneous and heterogeneous anion exchange membranes coated with cation exchange polyelectrolyte, Membranes. 9 (2019). https://doi.org/10.3390/membranes9010013.

[90] E. Güler, R. Elizen, D.A. Vermaas, M. Saakes, K. Nijmeijer, Performance-determining membrane properties in reverse electrodialysis, J. Memb. Sci. 446 (2013) 266–276. https://doi.org/10.1016/j.memsci.2013.06.045.

[91] Y. Zhao, K. Tang, H. Liu, B. Van Der Bruggen, A. Sotto, J. Shen, C. Gao, An anion exchange membrane modified by alternate electro- deposition layers with enhanced monovalent selectivity, J. Memb. Sci. 520 (2016) 262–271. https://doi.org/10.1016/j.memsci.2016.07.026.

[92] Y. Zhao, J. Zhu, J. Li, Z. Zhao, S.I. Charchalac Ochoa, J. Shen, C. Gao, B. Van der Bruggen, Robust multilayer graphene-organic frameworks for selective separation of monovalent anions, ACS Appl. Mater. Interfaces. 10 (2018) 18426–18433. https://doi.org/10.1021/acsami.8b03839.

[93] Y. Zhao, W. Shi, B. Van der Bruggen, C. Gao, J. Shen, Tunable nanoscale interlayer of graphene with symmetrical polyelectrolyte multilayer architecture for lithium extraction, Adv. Mater. Interfaces. 1701449 (2018) 1–5. https://doi.org/10.1002/admi.201701449.

[94] G. Saracco, M.C. Zanetti, M. Onofrio, Novel application of monovalent-ion-permselective membranes to the recovery treatment of an industrial wastewater by electrodialysis, Ind. Eng. Chem. Res. 32 (1993) 657–662.

https://doi.org/10.1021/ie00016a012.

[95] S. Chen, C. Li, H.-D. Hsu, P.-C. Lee, Y.-M. Chang, C.-H. Yang, Concentration and purification of chromate from electroplating wastewater by two-stage electrodialysis processes, J. Hazard. Mater. 161 (2009) 1075–1080. https://doi.org/10.1016/j.jhazmat.2008.04.106.

[96] Y. Zhang, B. Van der Bruggen, L. Pinoy, B. Meesschaert, Separation of nutrient ions and organic compounds from salts in RO concentrates by standard and monovalent selective ion-exchange membranes used in electrodialysis, J. Memb. Sci. 332 (2009) 104–112. https://doi.org/10.1016/j.memsci.2009.01.030.

[97] Y. Zhang, S. Paepen, L. Pinoy, B. Meesschaert, B. Van der Bruggen, Selectrodialysis: Fractionation of divalent ions from monovalent ions in a novel electrodialysis stack, Sep. Purif. Technol. 88 (2012) 191–201. https://doi.org/10.1016/j.seppur.2011.12.017.

[98] N. Arahman, S. Mulyati, M. Rahmah, R. Takagi, The removal of fluoride from water based on applied current and membrane types in electrodialyis, J. Fluor. Chem. 191 (2016) 97–102. https://doi.org/10.1016/j.jfluchem.2016.10.002.

[99] A. Elmidaoui, F. Elhannouni, M.A.M. Sahli, L. Chay, H. Elabbassi, Pollution of nitrate in Moroccan ground water: removal by electrodialysis, Desalination. 136 (2001) 325–332.

[100] Y. Onoue, Y. Mizutani, R. Yamame, Selectivity of cation exchange membranes for NaCl-MgCl2 systems, J. Electrochem. Soc. Japan. 27 (1959) 482.

[101] T. Luo, S. Abdu, M. Wessling, Selectivity of ion exchange membranes: A review, J. Memb. Sci. 555 (2018) 429–454. https://doi.org/10.1016/j.memsci.2018.03.051.

[102] F. Kotoka, I. Merino-Garcia, S. Velizarov, Surface Modifications of Anion Exchange Membranes for an Improved Reverse Electrodialysis Process Performance: A Review, Membranes. 10 (2020) 160. https://doi.org/10.3390/membranes10080160.

[103] T. Sata, Studies on ion exchange membranes with permselectivity for specific ions in electrodialysis, J. Memb. Sci. 93 (1994) 117–135. https://doi.org/10.1016/0376-7388(94)80001-4.

[104] C. Li, G. Wang, D. Yu, F. Sheng, M.A. Shehzad, T. He, T. Xu, X. Ren, M. Cao, B. Wu, L. Ge, Cross-linked anion exchange membranes with hydrophobic side-chains for anion separation, J. Memb. Sci. 581 (2019) 150–157. https://doi.org/10.1016/j.memsci.2019.03.059.

[105] J. Pan, J. Ding, Y. Zheng, C. Gao, B. Van Der Bruggen, One-pot approach to prepare internally cross-linked monovalent selective anion exchange membranes, J. Memb. Sci. 553 (2018) 43–53. https://doi.org/10.1016/j.memsci.2018.02.035.

[106] J.L. Stair, J.J. Harris, M.L. Bruening, Enhancement of the ion-transport selectivity of layered polyelectrolyte membranes through cross-linking and hybridization, Chem. Mater. 13 (2001) 2641–2648. https://doi.org/10.1021/cm010166e.

[107] A. Lejarazu-Larrañaga, Y. Zhao, S. Molina, E. García-Calvo, B. Van der Bruggen, Alternating current enhanced deposition of a monovalent selective coating for anion exchange membranes with antifouling properties, Sep. Purif. Technol. 229 (2019) 115807. https://doi.org/10.1016/j.seppur.2019.115807.

[108] Z. Zheng, P. Xiao, H. Ruan, J. Liao, C. Gao, B. Van der Bruggen, J. Shen, Mussel-inspired surface functionalization of AEM for simultaneously improved monovalent anion selectivity and antibacterial property, Membranes. 9 (2019) 36. https://doi.org/10.3390/membranes9030036.

[109] H. Liu, H. Ruan, Y. Zhao, J. Pan, A. Sotto, C. Gao, B. van der Bruggen, J. Shen, A facile avenue to modify polyelectrolyte multilayers on anion exchange membranes to enhance monovalent selectivity and durability simultaneously, J. Memb. Sci. 543 (2017) 310–318. https://doi.org/10.1016/j.memsci.2017.08.072.

[110] Y. Zhang, R. Liu, Q. Lang, M. Tan, Y. Zhang, Composite anion exchange membrane made by layer-by-layer method for selective ion separation and water migration control, Sep. Purif. Technol. 192 (2018) 278–286. https://doi.org/10.1016/j.seppur.2017.10.022.

[111] S. Yang, Y. Liu, J. Liao, H. Liu, Y. Jiang, B. Van Der Bruggen, J. Shen, C. Gao, Codeposition modification of cation exchange membranes with dopamine and crown ether to achieve high K+ electrodialysis selectivity, ACS Appl. Mater. Interfaces. 11 (2019) 17730–17741. https://doi.org/10.1021/acsami.8b21031.

[112] T. Sata, T. Yamaguchi, K. Matsusaki, Effect of hydrophobicity of ion exchange groups of anion exchange membranes on permselectivity between two anions, J. Phys. Chem. 99 (1995) 12875–12882. https://doi.org/10.1021/j100034a028.

[113] T. Mubita, S. Porada, P. Aerts, A. Van Der Wal, Heterogeneous anion exchange membranes with nitrate selectivity and low electrical resistance, J. Memb. Sci. (2020) 118000. https://doi.org/10.1016/j.memsci.2020.118000.

[114] T. Sata, Studies on anion exchange membranes having permselectivity for specific anions in electrodialysis - effect of hydrophilicity of anion exchange membranes on permselectivity of anions, J. Memb. Sci. 167 (2000) 1–31. https://doi.org/10.1016/S0376-7388(99)00277-X.

[115] K. Bouzek, S. Moravcová, J. Schauer, L. Brožová, Z. Pientka, Heterogeneous ion-selective membranes: The influence of the inert matrix polymer on the membrane properties, J. Appl. Electrochem. 40 (2010) 1005–1018. https://doi.org/10.1007/s10800-009-9974-3.

[116] V.I. Zabolotskii, S.A. Loza, M. V. Sharafan, Physicochemical properties of profiled heterogeneous ion-exchange membranes, Russ. J. Electrochem. 41 (2005) 1053–1060. https://doi.org/10.1007/s11175-005-0180-2.

[117] P. V. Vyas, P. Ray, S.K. Adhikary, B.G. Shah, R. Rangarajan, Studies of the effect of variation of blend ratio on permselectivity and heterogeneity of ion-exchange membranes, J. Colloid Interface Sci. 257 (2003) 127–134. https://doi.org/10.1016/S0021-9797(02)00025-5.

[118] C. Klaysom, S.H. Moon, B.P. Ladewig, G.Q.M. Lu, L. Wang, Preparation of porous ion-exchange membranes (IEMs) and their characterizations, J. Memb. Sci. 371 (2011) 37–44. https://doi.org/10.1016/j.memsci.2011.01.008.

[119] L. Zarybnicka, E. Stranska, Preparation of cation exchange filament for 3D membrane print, Rapid Prototyp. J. 26 (2020) 1435–1445. https://doi.org/10.1108/RPJ-03-2019-0082.

[120] J. Seo, D.I. Kushner, M.A. Hickner, 3D printing of micropatterned anion exchange membranes, ACS Appl. Mater. Interfaces. 8 (2016) 16656–16663. https://doi.org/10.1021/acsami.6b03455.

[121] R. García-Pacheco, E. García-Calvo, J. Landaburu-Aguirre, Nanofiltration and ultrafiltration membranes from end-of-life reverse osmosis membranes: A study of recycling, University of Alcalá de Henares, 2017.

[122] Y. Tanaka, Ion exchange membranes, fundamentals and applications, First edit, Elsevier, The Netherlands, 2007.

[123] F. Karas, J. Hnát, M. Paidar, J. Schauer, K. Bouzek, Determination of the ion-exchange capacity of anion-selective membranes, Int. J. Hydrogen Energy. 39 (2014) 5054–5062. https://doi.org/10.1016/j.ijhydene.2014.01.074.

[124] American Public Health Association, American Water Works Association, Water Environment Federation, APHA Method 4500-NO3: Standard methods for the examination of water and wastewater, 18th

ed., Washington DC, USA, 1992.

[125] D.R. Lide, Handbook of Chemistry and Physics, 84th ed., 1995.

[126] C. Klaysom, R. Marschall, L. Wang, B.P. Ladewig, G.Q.M. Lu, Synthesis of composite ion-exchange membranes and their electrochemical properties for desalination applications, J. Mater. Chem. 20 (2010) 4669–4674. https://doi.org/10.1039/b925357b.

[127] European Comission, Council Directive 98/83/EC of 3 November 1998 on the quality of water intended for human consumption, Off. J. Eur. Communities. 330 (1998) 32–54. https://doi.org/10.1017/cbo9780511610851.055.

[128] S.M. Hosseini, S.S. Madaeni, A.R. Khodabakhshi, Preparation and characterization of ABS/HIPS heterogeneous cation exchange membranes with various blend ratios of polymer binder, J. Memb. Sci. 351 (2010) 178–188. https://doi.org/10.1016/j.memsci.2010.01.045.

[129] S.M. Hosseini, S. Rafiei, A.R. Hamidi, A.R. Moghadassi, S.S. Madaeni, Preparation and electrochemical characterization of mixed matrix heterogeneous cation exchange membranes filled with zeolite nanoparticles: Ionic transport property in desalination, Desalination. 351 (2014) 138–144. https://doi.org/10.1016/j.desal.2014.07.036.

[130] S.M. Hosseini, F. Jeddi, M. Nemati, S.S. Madaeni, A.R. Moghadassi, Electrodialysis heterogeneous anion exchange membrane modified by PANI/MWCNT composite nanoparticles: Preparation, characterization and ionic transport property in desalination, Desalination. 341 (2014) 107–114. https://doi.org/10.1016/j.desal.2014.03.001.

[131] P. V. Vyas, B.G. Shah, G.S. Trivedi, P. Ray, S.K. Adhikary, R. Rangarajan, Characterization of heterogeneous anion-exchange membrane, J. Memb. Sci. 187 (2001) 39–46. https://doi.org/10.1016/S0376-7388(00)00613-X.

[132] R. Zhang, S. Yu, W. Shi, J. Zhu, B. Van Der Bruggen, Support Membrane Pore Blockage (SMPB): an important phenomenon during the fabrication of thin film composite membranes via interfacial polymerization, Sep. Purif. Technol. 215 (2019) 670–680. https://doi.org/10.1016/j.seppur.2019.01.045.

[133] Y. Zhang, L. Zou, B.P. Ladewig, D. Mulcahy, Synthesis and characterisation of superhydrophilic conductive heterogeneous PANI/PVDF anion-exchange membranes, Desalination. 362 (2015) 59–67. https://doi.org/10.1016/j.desal.2015.02.004.

[134] L. Brožová, J. Křivčík, D. Neděla, V. Kysela, J. Žitka, The influence of activation of heterogeneous ion-exchange membranes on their

electrochemical properties, Desalin. Water Treat. 56 (2015) 3228–3232. https://doi.org/10.1080/19443994.2014.980975.

[135] S.M. Hosseini, S.S. Madaeni, A.R. Khodabakhshi, Preparation and characterization of heterogeneous cation exchange membranes based on S-poly vinyl chloride and polycarbonate, Sep. Sci. Technol. 46 (2011) 794–808. https://doi.org/10.1080/01496395.2010.534122.

[136] M. Ulbricht, Advanced functional polymer membranes, Polymer (Guildf). 47 (2006) 2217–2262. https://doi.org/10.1016/j.polymer.2006.01.084.

[137] R. Navarro, M. Pérez-Perrino, M. Gómez-Tardajos, H. Reinecke, Phthalate plasticizers covalently bound to PVC : plasticization with suppressed migration, Macromolecules. 43 (2010) 2377–2381. https://doi.org/10.1021/ma902740t.

[138] M. Herrero, R. Navarro, N. García, C. Mijangos, H. Reinecke, Surface selectivities in wet chemically modified PVC films. Influence of reaction conditions, Langmuir. 21 (2005) 4425–4430. https://doi.org/10.1021/la047172k.

[139] M. Porozhnyy, P. Huguet, M. Cretin, E. Safronova, V. Nikonenko, Mathematical modeling of transport properties of proton-exchange membranes containing immobilized nanoparticles, Int. J. Hydrogen Energy. 41 (2016) 15605–15614. https://doi.org/10.1016/j.ijhydene.2016.06.057.

[140] T. Rottiers, K. Ghyselbrecht, B. Meesschaert, B. Van Der Bruggen, L. Pinoy, Influence of the type of anion membrane on solvent fl ux and back diffusion in electrodialysis of concentrated NaCl solutions, Chem. Eng. Sci. 113 (2014) 95–100. https://doi.org/10.1016/j.ces.2014.04.008.

[141] N. Kononenko, V. Nikonenko, D. Grande, C. Larchet, L. Dammak, M. Fomenko, Y. Volfkovich, Porous structure of ion exchange membranes investigated by various techniques, Adv. Colloid Interface Sci. 246 (2017) 196–216. https://doi.org/10.1016/j.cis.2017.05.007.

[142] J. Hnát, M. Paidar, J. Schauer, J. Žitka, K. Bouzek, Polymer anion-selective membranes for electrolytic splitting of water. Part II: Enhancement of ionic conductivity and performance under conditions of alkaline water electrolysis, J. Appl. Electrochem. 42 (2012) 545–554. https://doi.org/10.1007/s10800-012-0432-2.

[143] S.K. Patel, C.L. Ritt, A. Deshmukh, Z. Wang, M. Qin, R. Epsztein, M. Elimelech, The relative insignificance of advanced materials in enhancing the energy efficiency of desalination technologies, Energy Environ. Sci. (2020). https://doi.org/10.1039/d0ee00341g.

[144] D.A. Cowan, J.H. Brown, Effect of Turbulence on Limiting Current in Electrodialysis Cells, Ind. Eng. Chem. 51 (1959) 1445–1448. https://doi.org/10.1021/ie50600a026.

[145] D. Seader, E.J. Henley, Separation process principles, 3rd ed., 2006.

[146] N. Van Linden, H. Spanjers, J.B. van Lier, Application of dynamic current density for increased concentration factors and reduced energy consumption for concentrating ammonium by electrodialysis, Water Res. 163 (2019) 114856. https://doi.org/10.1016/j.watres.2019.114856.

[147] W. Garcia-Vasquez, L. Dammak, C. Larchet, V. Nikonenko, D. Grande, Effects of acid-base cleaning procedure on structure and properties of anion-exchange membranes used in electrodialysis, J. Memb. Sci. 507 (2016) 12–23. https://doi.org/10.1016/j.memsci.2016.02.006.

[148] T. Sata, M. Tsujimoto, T. Yamaguchi, K. Matsusaki, Change of anion exchange membranes in an aqueous sodium hydroxide solution at high temperature, J. Memb. Sci. 112 (1996) 161–170. https://doi.org/10.1016/0376-7388(95)00292-8.

[149] R. Guo, B. Wang, Y. Jia, M. Wang, Development of acid block anion exchange membrane by structure design and its possible application in waste acid recovery, Sep. PurificationTechnology. 186 (2017) 188–196. https://doi.org/10.1016/j.seppur.2017.06.006.

[150] M. Liu, D. Wu, S. Yu, C. Gao, Influence of the polyacyl chloride structure on the reverse osmosis performance, surface properties and chlorine stability of the thin-film composite polyamide membranes, J. Memb. Sci. 326 (2009) 205–214. https://doi.org/10.1016/j.memsci.2008.10.004.

[151] J. Křivčík, D. Neděla, J. Hadrava, L. Brožová, Increasing selectivity of a heterogeneous ion-exchange membrane, Desalin. Water Treat. 56 (2015) 3160–3166. https://doi.org/10.1080/19443994.2014.980970.

[152] H. Lee, S.M. Dellatore, W.M. Miller, P.B. Messersmith, Mussel-inspired surface chemistry for multifunctional coatings, Science (80-.). 318 (2007) 426–430. https://doi.org/10.1126/science.1147241.

[153] H.C. Yang, J. Luo, Y. Lv, P. Shen, Z.K. Xu, Surface engineering of polymer membranes via mussel-inspired chemistry, J. Memb. Sci. 483 (2015) 42–59. https://doi.org/10.1016/j.memsci.2015.02.027.

[154] M. Weinhold, S. Soubatch, R. Temirov, M. Rohlfing, B. Jastorff, F.S. Tautz, C. Doose, Structure and bonding of the multifunctional amino acid L-DOPA on Au(110), J. Phys. Chem. B. 110 (2006) 23756–23769. https://doi.org/10.1021/jp064956t.

[155] R.A. Zangmeister, T.A. Morris, M.J. Tarlov, Characterization of polydopamine thin films deposited at short times by autoxidation of dopamine, Langmuir. 29 (2013) 8619–8628. https://doi.org/10.1021/la400587j.

[156] D.R. Dreyer, D.J. Miller, B.D. Freeman, D.R. Paul, C.W. Bielawski, Elucidating the structure of poly(dopamine), Langmuir. 28 (2012) 6428–6435. https://doi.org/10.1021/la204831b.

[157] Q. Ye, F. Zhou, W. Liu, Bioinspired catecholic chemistry for surface modification, Chem. Soc. Rev. 40 (2011) 4244–4258. https://doi.org/10.1039/c1cs15026j.

[158] Y. Zhao, Y. Li, S. Yuan, J. Zhu, S. Houtmeyers, J. Li, R. Dewil, G. Congjie, B. Van der Bruggen, Chemically assembled anion exchange membrane surface for monovalent anion selectivity and fouling reduction, J. Mater. Chem. A. 7 (2019) 6348–6356. https://doi.org/10.1039/C8TA11868J.

[159] C. Zhang, Y. Ou, W. Lei, L. Wan, J. Ji, Z. Xu, CuSO4 /H2O2-Induced rapid deposition of polydopamine coatings with high uniformity and enhanced stability, Angew. Chemie - Int. Ed. 55 (2016) 3054–3057. https://doi.org/10.1002/anie.201510724.

[160] X. Du, L. Li, A. Behboodi-Sadabad, Farid Welle, J. Li, S. Heissler, H. Zhang, N. Plumeré, P.A. Levkin, Bio-inspired strategy for controlled dopamine polymerization in basic solutions, Polym. Chem. 8 (2017) 2145–2151. https://doi.org/10.1039/C7PY00051K.

[161] B.D. McCloskey, H.B. Park, H. Ju, B.W. Rowe, D.J. Miller, B.D. Freeman, A bioinspired fouling-resistant surface modification for water purification membranes, J. Memb. Sci. 413–414 (2012) 82–90. https://doi.org/10.1016/j.memsci.2012.04.021.

[162] B.D. McCloskey, H.B. Park, H. Ju, B.W. Rowe, D.J. Miller, B.J. Chun, K. Kin, B.D. Freeman, Influence of polydopamine deposition conditions on pure water flux and foulant adhesion resistance of reverse osmosis, ultrafiltration and microfiltration membranes, Polymer (Guildf). 51 (2010) 3472–3485. https://doi.org/10.1016/j.polymer.2010.05.008.

[163] B.H. Lee, J. Rho, P.B. Messersmith, Facile conjugation of biomolecules onto surfaces via mussel adhesive protein inspired coatings, Adv. Mater. 21 (2009) 431–434. https://doi.org/10.1002/adma.200801222.

[164] A. He, C. Zhang, Y. Lv, Q.Z. Zhong, X. Yang, Z.K. Xu, Mussel-inspired coatings directed and accelerated by an electric field, Macromol. Rapid Commun. 37 (2016) 1460–1465. https://doi.org/10.1002/marc.201600271.

[165] A. Chávez-Valdez, A.R. Boccaccini, Innovations in electrophoretic deposition: alternating current and pulsed direct current methods,

Electrochim. Acta. 65 (2012) 70–89. https://doi.org/10.1016/j.electacta.2012.01.015.

[166] Y. Zhao, H. Liu, K. Tang, Y. Jin, J. Pan, B. Van der Bruggen, J. Shen, C. Gao, Mimicking the cell membrane: bio-inspired simultaneous functions with monovalent anion selectivity and antifouling properties of anion exchange membrane, Sci. Rep. 6 (2016) 1–13. https://doi.org/10.1038/srep37285.

[167] Y. Zhao, C. Gao, B. Van der Bruggen, Technology-driven layer-by-layer assembly of a membrane for selective separation of monovalent anions and antifouling, Nanoscale. 11 (2019) 2264–2274. https://doi.org/10.1039/c8nr09086f.

[168] B. Van der Bruggen, A. Koninckx, C. Vandecasteele, Separation of monovalent and divalent ions from aqueous solution by electrodialysis and nanofiltration, Water Res. 38 (2004) 1347–1353. https://doi.org/10.1016/j.watres.2003.11.008.

[169] Y. Zhao, K. Tang, Q. Liu, B. Van der Bruggen, A. Sotto Díaz, J. Pan, C. Gao, J. Shen, Recovery of chemically degraded polyethyleneimine by a re-modification method: prolong the lifetime of cation exchange membranes, RSC Adv. 6 (2016) 16548–16554. https://doi.org/10.1039/C5RA27916J.

[170] Y. Zhao, J. Zhu, J. Ding, B. Van der Bruggen, J. Shen, C. Gao, Electric-pulse layer-by-layer assembled of anion exchange membrane with enhanced monovalent selectivity, J. Memb. Sci. 548 (2018) 81–90. https://doi.org/10.1016/j.memsci.2017.11.007.

[171] H. Niu, Y. Zhang, Y. Liu, B. LUO, N. Xin, W. Shi, MOFs-derived Co9S8 embedded graphene/hollow carbon spheres film with macroporous frameworks for hybrid supercapacitor with superior volumetric energy density, J. Mater. Chem. A. 7 (2019) 8503-8509. https://doi.org/10.1039/C8TA11983J.

[172] Y. Liu, H. Niu, W. Gu, X. Cai, B. Mao, D. Li, W. Shi, In-situ construction of hierarchical CdS/MoS2 microboxes for enhanced visible-light photocatalytic H2 production, Chem. Eng. J. 339 (2018) 117–124. https://doi.org/10.1016/j.cej.2018.01.124.

[173] M. Vaselbehagh, H. Karkhanechi, S. Mulyati, R. Takagi, H. Matsuyama, Improved antifouling of anion-exchange membrane by polydopamine coating in electrodialysis process, Desalination. 332 (2014) 126–133. https://doi.org/10.1016/j.desal.2013.10.031.

[174] K. Boussu, A. Volodin, J. Snauwaert, C. Van Haesendonck, C. Vandecasteele, Roughness and hydrophobicity studies of nanofiltration

membranes using different modes of AFM, J. Colloid Interface Sci. 286 (2005) 632–638. https://doi.org/10.1016/j.jcis.2005.01.095.

[175] E. Güler, W. Van Baak, M. Saakes, K. Nijmeijer, Monovalent-ion-selective membranes for reverse electrodialysis, J. Memb. Sci. 455 (2014) 254–270. https://doi.org/10.1016/j.memsci.2013.12.054.

[176] Y. Liu, X. Cai, B. Luo, M. Yan, J. Jiang, W. Shi, MnO2 decorated on carbon sphere intercalated graphene film for high-performance supercapacitor electrodes, Carbon N. Y. 107 (2016) 426–432. https://doi.org/10.1016/j.carbon.2016.06.025.

[177] Y. Zhao, K. Tang, H. Ruan, L. Xue, B. Van der Bruggen, C. Gao, J. Shen, Sulfonated reduced graphene oxide modification layers to improve monovalent anions selectivity and controllable resistance of anion exchange membrane, J. Memb. Sci. 536 (2017) 167–175. https://doi.org/10.1016/j.memsci.2017.05.002.

[178] H.S. J.J. Krol, M. Wessling, Concentration polarization with monopolar ion exchange membranes: current-voltage curves and water dissociation, J. Memb. Sci. 162 (1999) 145–154. https://doi.org/10.1016/S0376-7388(99)00133-7.

[179] Y. Tanaka, Ion Exchange Membranes: fundamental and aplications, 2nd editio, Elsevier, 2015. https://doi.org/10.1016/B978-0-444-63319-4.00002-X.

[180] S. Mikhaylin, L. Bazinet, Fouling on ion-exchange membranes: classification, characterization and strategies of prevention and control, Adv. Colloid Interface Sci. 229 (2016) 34–56. https://doi.org/10.1016/j.cis.2015.12.006.

[181] S. Mulyati, R. Takagi, A. Fujii, Y. Ohmukai, H. Matsuyama, Simultaneous improvement of the monovalent anion selectivity and antifouling properties of an anion exchange membrane in an electrodialysis process, using polyelectrolyte multilayer deposition, J. Memb. Sci. 431 (2013) 113–120. https://doi.org/10.1016/j.memsci.2012.12.022.

[182] H. Ruan, Z. Zheng, J. Pan, C. Gao, B. Van der Bruggen, J. Shen, Mussel-inspired sulfonated polydopamine coating on anion exchange membrane for improving permselectivity and anti-fouling property, J. Memb. Sci. 550 (2018) 427–435. https://doi.org/10.1016/j.memsci.2018.01.005.

[183] Bijay-Singh, E. Craswell, Fertilizers and nitrate pollution of surface and ground water: An increasingly pervasive global problem, SN Appl. Sci. 3 (2021) 1–24. https://doi.org/10.1007/s42452-021-04521-8.

[184] M.H. Ward, R.R. Jones, J.D. Brender, T.M. de Kok, P.J. Weyer, B.T. Nolan, C.M. Villanueva, S.G. van Breda, Drinking water nitrate and human health: An updated review, Int. J. Environ. Res. Public Health. 15 (2018) 1–31. https://doi.org/10.3390/ijerph15071557.

[185] A.M. Fan, V.E. Steinberg, Health implications of nitrate and nitrite in drinking water: An update on methemoglobinemia occurrence and reproductive and developmental toxicity, Regul. Toxicol. Pharmacol. 23 (1996) 35–43. https://doi.org/10.1006/rtph.1996.0006.

[186] S.K.M. Huno, E.R. Rene, E.D. Van Hullebusch, A.P. Annachhatre, Nitrate removal from groundwater: A review of natural and engineered processes, J. Water Supply Res. Technol. - Aqua. 67 (2018) 885–902. https://doi.org/10.2166/aqua.2018.194.

[187] J.M. Ortiz, E. Exposito, F. Gallud, V. García-García, V. Montiel, A. Aldaz, Desalination of underground brackish waters using an electrodialysis system powered directly by photovoltaic energy, Sol. Energy Mater. Sol. Cells. 92 (2008) 1677–1688. https://doi.org/10.1016/j.solmat.2008.07.020.

[188] T. Sata, Ion Exchange Membranes: Preparation, Characterization, Modification and Application, Royal Society of Chemistry, 2004. https://doi.org/10.1039/9781847551177.

[189] S.M. Hosseini, A. Gholami, S.S. Madaeni, A.R. Moghadassi, A.R. Hamidi, Fabrication of (polyvinyl chloride/cellulose acetate) electrodialysis heterogeneous cation exchange membrane: Characterization and performance in desalination process, Desalination. 306 (2012) 51–59. https://doi.org/10.1016/j.desal.2012.07.028.

[190] A. Awasthi, D. Datta, Application of Amberlite XAD-7HP resin impregnated with Aliquat 336 for the removal of Reactive Blue - 13 dye: Batch and fixed-bed column studies, J. Environ. Chem. Eng. 7 (2019) 103502. https://doi.org/10.1016/j.jece.2019.103502.

[191] E.R. Nightingale, Phenomenological theory of ion solvation. Effective radii of hydrated ions, J. Phys. Chem. 63 (1959) 1381–1387. https://doi.org/10.1021/j150579a011.

[192] D.W. Smith, Ionic hydration enthalpies, J. Chem. Educ. 54 (1977) 540–542. https://doi.org/10.1021/ed054p540.

[193] Y. Jin, Y. Zhao, H. Liu, A. Sotto, C. Gao, J. Shen, A durable and antifouling monovalent selective anion exchange membrane modified by polydopamine and sulfonated reduced graphene oxide, Sep. Purif. Technol. 207 (2018) 116–123.

https://doi.org/10.1016/j.seppur.2018.06.053.

[194] J. Kamcev, D.R. Paul, B.D. Freeman, Effect of fixed charge group concentration on equilibrium ion sorption in ion exchange membranes, J. Mater. Chem. A. 5 (2017) 4638–4650. https://doi.org/10.1039/c6ta07954g.

[195] G. Saracco, M.C. Zanetti, Ion transport through monovalent-anion-permselective membranes, Ind. Eng. Chem. Res. (1994) 96–101. https://doi.org/10.1021/ie00025a013.

[196] G. Saracco, Transport properties of monovalent-ion-permselective membranes, Chem. Eng. Sci. 52 (1997) 3019–3031. https://doi.org/10.1016/S0009-2509(97)00107-3.

[197] L. Gurreri, A. Tamburini, A. Cipollina, G. Micale, Electrodialysis applications in wastewater treatment for environmental protection and resources recovery: A systematic review on progress and perspectives, Membranes. 10 (2020) 1–93. https://doi.org/10.3390/membranes10070146.

[198] B. Zhao, H. Zhao, J. Ni, Arsenate removal by Donnan dialysis: Effects of the accompanying components, Sep. Purif. Technol. 72 (2010) 250–255. https://doi.org/10.1016/j.seppur.2010.02.013.

[199] M. Pessoa-Lopes, J.G. Crespo, S. Velizarov, Arsenate removal from sulphate-containing water streams by an ion-exchange membrane process, Sep. Purif. Technol. 166 (2016) 125–134. https://doi.org/10.1016/j.seppur.2016.04.032.

[200] M. Pessoa Lopes, C.F. Galinha, J.G. Crespo, S. Velizarov, Optimisation of arsenate removal from water by an integrated ion-exchange membrane process coupled with Fe co-precipitation, Sep. Purif. Technol. 246 (2020) 116894. https://doi.org/10.1016/j.seppur.2020.116894.

[201] J.G. Crespo, S. Velizarov, M.A. Reis, Membrane bioreactors for the removal of anionic micropollutants from drinking water, Curr. Opin. Biotechnol. 15 (2004) 463–468. https://doi.org/10.1016/j.copbio.2004.07.001.

[202] A.D. Fonseca, J.G. Crespo, J.S. Almeida, M.A. Reis, Drinking water denitrification using a novel ion-exchange membrane bioreactor, Environ. Sci. Technol. 34 (2000) 1557–1562. https://doi.org/10.1021/es9910762.

[203] C.T. Matos, R. Fortunato, S. Velizarov, M.A.M. Reis, G.Ã. Crespo, Removal of mono-valent oxyanions from water in an ion exchange membrane bioreactor: Influence of membrane permselectivity, Water

Res. 42 (2008) 1785–1795. https://doi.org/10.1016/j.watres.2007.11.006.

[204] Mega Group Companies, Product data sheet. Ralex® membrane AMHPES, (n.d.). https://www.mega.cz/files/datasheet/MEGA-RALEX-AMH-PES-en.pdf (accessed June 3, 2021).

[205] A.R. Ricardo, S. Velizarov, J.G. Crespo, M.A.M. Reis, Validation of the ion-exchange membrane bioreactor concept in a plate-and-frame module configuration, Process Biochem. 47 (2012) 1832–1838. https://doi.org/10.1016/j.procbio.2012.06.019.

[206] C.T. Matos, S. Velizarov, J.G. Crespo, M.A.M. Reis, Simultaneous removal of perchlorate and nitrate from drinking water using the ion exchange membrane bioreactor concept, Water Res. 40 (2006) 231–240. https://doi.org/10.1016/j.watres.2005.10.022.

[207] S. Pawlowski, C.F. Galinha, J.G. Crespo, S. Velizarov, 2D fluorescence spectroscopy for monitoring ion-exchange membrane based technologies - Reverse electrodialysis (RED), Water Res. 88 (2016) 184–198. https://doi.org/10.1016/j.watres.2015.10.010.

[208] S. Velizarov, Transport of arsenate through anion-exchange membranes in Donnan dialysis, J. Memb. Sci. 425–426 (2013) 243–250. https://doi.org/10.1016/j.memsci.2012.09.012.

[209] World Health Organization, Guidelines for drinking-water quality, Fourth Edi, World Health Organization, 2017.

[210] C.F. Galinha, G. Carvalho, C.A.M. Portugal, G. Guglielmi, R. Oliveira, J.G. Crespo, M.A.M. Reis, Real-time monitoring of membrane bioreactors with 2D-fluorescence data and statistically based models, Water Sci. Technol. 63 (2011) 1381–1388. https://doi.org/10.2166/wst.2011.195.

[211] S. Pawlowski, C.F. Galinha, J.G. Crespo, S. Velizarov, Prediction of reverse electrodialysis performance by inclusion of 2D fluorescence spectroscopy data into multivariate statistical models, Sep. Purif. Technol. 150 (2015) 159–169. https://doi.org/10.1016/j.seppur.2015.06.032.

[212] D. Golubenko, A. Yaroslavtsev, Development of surface-sulfonated graft anion-exchange membranes with monovalent ion selectivity and antifouling properties for electromembrane processes, J. Memb. Sci. 612 (2020) 118408. https://doi.org/10.1016/j.memsci.2020.118408.

[213] D.O. Hummel, Atlas of Plastics Additives. Analysis by Spectrometric Methods, Springer-Verlag, Berlin, 2002.

[214] N.P. Berezina, N.A. Kononenko, O.A. Dyomina, N.P. Gnusin,

Characterization of ion-exchange membrane materials: Properties vs structure, Adv. Colloid Interface Sci. 139 (2008) 3–28. https://doi.org/10.1016/j.cis.2008.01.002.

[215] K. Pyrzynska, Preconcentration and recovery of metal ions by Donnan dialysis, Microchim. Acta. 153 (2006) 117–126. https://doi.org/10.1007/s00604-005-0434-4.

[216] I.A. Stenina, A.B. Yaroslavtsev, Ionic mobility in ion-exchange membranes, Membranes. 11 (2021). https://doi.org/10.3390/membranes11030198.

[217] S. Velizarov, J.G. Crespo, M.A. Reis, Ion exchange membrane bioreactor for selective removal of nitrate from drinking water: Control of ion fluxes and process performance, Biotechnol. Prog. 18 (2002) 296–302. https://doi.org/10.1021/bp010160u.

[218] S. Velizarov, C.M. Rodrigues, M.A. Reis, J.G. Crespo, Mechanism of charged pollutants removal in an ion exchange membrane bioreactor: Drinking water denitrification, Biotechnol. Bioeng. 71 (2000) 245–254. https://doi.org/DOI: 10.1002/1097-0290(2000)71:4<245::aid-bit1014>3.0.co;2-f.

[219] P.A. Yurova, Y.A. Karavanova, Y.G. Gorbunova, A.B. Yaroslavtsev, Transport properties of asymmetric ion-exchange membranes based on MC-40, MF-4SC, and polyaniline, Pet. Chem. 54 (2014) 551–555. https://doi.org/10.1134/S0965544114070147.

[220] S.M. Hosseini, M. Nemati, F. Jeddi, E. Salehi, A.R. Khodabakhshi, S.S. Madaeni, Fabrication of mixed matrix heterogeneous cation exchange membrane modified by titanium dioxide nanoparticles: Mono/bivalent ionic transport property in desalination, Desalination. 359 (2015) 167–175. https://doi.org/10.1016/j.desal.2014.12.043.

[221] A. Breytus, D. Hasson, R. Semiat, H. Shemer, Ion exchange membrane adsorption in Donnan dialysis, Sep. Purif. Technol. 226 (2019) 252–258. https://doi.org/10.1016/j.seppur.2019.05.084.

[222] B. Zhao, H. Zhao, S. Dockko, J. Ni, Arsenate removal from simulated groundwater with a Donnan dialyzer, J. Hazard. Mater. 215–216 (2012) 159–165. https://doi.org/10.1016/j.jhazmat.2012.02.048.

[223] R. Bro, PARAFAC. Tutorial and applications, Chemom. Intell. Lab. Syst. 38 (1997) 149–171. https://doi.org/10.1016/S0169-7439(97)00032-4.

[224] C.F. Galinha, G. Carvalho, C.A.M. Portugal, G. Guglielmi, M.A.M. Reis, J.G. Crespo, Two-dimensional fluorescence as a fingerprinting tool for monitoring wastewater treatment systems, J. Chem. Technol. Biotechnol. 86 (2011) 985–992. https://doi.org/10.1002/jctb.2613.

[225] S. Melnikov, S. Loza, M. Sharafan, V. Zabolotskiy, Electrodialysis treatment of secondary steam condensate obtained during production of ammonium nitrate. Technical and economic analysis, Sep. Purif. Technol. 157 (2016) 179–191. https://doi.org/10.1016/j.seppur.2015.11.025.

[226] European Commission, Circular economy action plan. For a cleaner and more competitive Europe, Eur. Comm. (2020) 28. https://doi.org/10.2779/05068.

[227] M. Zaman, H. Liu, H. Xiao, F. Chibante, Y. Ni, Hydrophilic modification of polyester fabric by applying nanocrystalline cellulose containing surface finish, Carbohydr. Polym. 91 (2013) 560–567. https://doi.org/10.1016/j.carbpol.2012.08.070.

[228] Tetrahydrofuran Market Price & Analysis, (2021). https://www.echemi.com/productsInformation/pd20150901266-tetrahydrofuran.html (accessed September 7, 2021).

[229] Statista, Price of polyvinyl chloride worldwide from 2017 to 2020 with estimated figures for 2021 to 2022, (2021). https://www.statista.com/statistics/1171131/price-polyvinyl-chloride-forecast-globally/#statisticContainer (accessed September 6, 2021).

[230] E.M.V. Hoek, J. Allred, T. Knoell, B.H. Jeong, Modeling the effects of fouling on full-scale reverse osmosis processes, J. Memb. Sci. 314 (2008) 33–49. https://doi.org/10.1016/j.memsci.2008.01.025.

[231] J. Schauer, J. Hnát, L. Brožová, J. Žitka, K. Bouzek, Heterogeneous anion-selective membranes: Influence of a water-soluble component in the membrane on the morphology and ionic conductivity, J. Memb. Sci. 401–402 (2012) 83–88. https://doi.org/10.1016/j.memsci.2012.01.038.

[232] S.M. Hosseini, E. Jashni, M. Habibi, M. Nemati, B. Van der Bruggen, Evaluating the ion transport characteristics of novel graphene oxide nanoplates entrapped mixed matrix cation exchange membranes in water deionization, J. Memb. Sci. 541 (2017) 641–652. https://doi.org/10.1016/j.memsci.2017.07.022.

[233] L. Brožová, J. Křivčík, D. Neděla, V. Kysela, J. Žitka, The influence of activation of heterogeneous ion- exchange membranes on their electrochemical properties, Desalin. Water Treat. 56:12 (2015) 3228–3232. https://doi.org/10.1080/19443994.2014.980975.

A

Appendix A. Testing different recycled supports for the preparation of Anion-Exchange Membranes

.

This Appendix has been published as:

A. Lejarazu-Larrañaga, S. Molina, J. M. Ortiz, E. García-Calvo, Preparación de membranas de intercambio iónico sobre soportes reciclados de membranas desechadas, VIII Jornadas de Jóvenes Investigadores de la UAH (pp. 207-215), Universidad de Alcalá, Ed.: Alcalá de Henares, Spain, 2021; ISBN 978-84-18254-50-5.

A.1. Introduction

Complementarily to the Chapter 3, the adequation of other types of supporting materials extracted from the EoL RO membrane, for their use in the preparation of AEMs was studied. On the one hand, the polypropylene (PP) woven permeate spacer was tested, and on the other hand, the EoL RO membranes were tested after 3 different pretreatments: (1) the physical removal of the fouling, the PA and PSF layers, (2) the chemical elimination of the fouling and partial removal of the PA layer (i.e., recycled NF-like membranes), and (3) the chemical complete removal of the fouling and the PA layer (i.e., recycled UF-like membranes).

A.2. Material and methods

A.2.1. Chemical reagents

NaClO, 14 %, THF, NaCl, and Na_2SO_4 were purchased from Scharlab, S.L., Spain. Commercial bulk polymerized PVC (Mw 112,000 $g \cdot mol^{-1}$) was supplied by ATOCHEM, S.A., Spain. Amberlite® IRA-402, strongly basic anion-exchanger (Cl^- form, total exchange capacity ≥ 1.0 mol/L) was supplied by Merck, KGaA, Germany. MilliQ water was employed throughout the experiments.

A.2.2. Membranes

An EoL PA-TFC RO membrane module (TM 720-400, from Toray Industries, Inc., Japan) has been used for the preparation of the membranes. This module was discarded by a brackish water desalination plant after overcoming its lifespan. Differently from the membranes prepared in the Chapter 3, in this case the module was not subjected to a recycling treatment in the passive pilot plant and thus, the extracted membrane coupons conserved the fouling and the dense polyamide layer.

The performance of the prepared membranes was compared with commercial heterogeneous anion-exchange AMH-PES membrane from Ralex® (Mega a.s., Czech Republic).

A.2.3. Membrane autopsy and sample extraction

The EoL RO module was first opened by membrane autopsy and membrane coupons, permeate spacers, and feed spacers were extracted.

A.2.4. Pre-treating the recycled supports

Before using these elements for the preparation of the membranes, a pretreatment is needed. The pretreatment will eliminate the fouling and a part of the dense polyamide layer of the RO membrane. The EoL RO membranes usually present a fouled surface. The fouling can be inorganic (salt precipitation), organic (humic acids, proteins…), or biofouling (biofilm forming bacteria) [230]. These membranes have a polyester (PET) layer used as mechanical support, a polysulfone (PSF) porous layer and the dense polyamide (PA) layer where the fouling is deposited [69].

In the case of the PET permeate spacer, a simple cleaning with water and a disinfection with a low exposure to NaClO (~500 ppm·h). are conducted. In respect to the EoL RO membrane samples, three different options were tested: i) the physical elimination of the fouling, the PA and the PSF layers together, obtaining the PET layer of the membrane, ii) the chemical elimination of the fouling and partial removal of the PA layer by short exposure doses of NaClO (5,500 ppm·h), obtaining membranes with NF-like properties (in terms of salt rejection and hydraulic permeability) and iii) the chemical complete elimination of the fouling and the PA layer by long exposure doses of NaClO (>300,000 ppm·h), obtaining membranes with UF-like properties (in terms of salt rejection and hydraulic permeability) [63].

A.2.5. Preparation of Anion-Exchange Membranes

For the preparation of the AEMs, the procedure described in the Section 3.2.4. (Chapter 3) was used (i.e., casting the polymeric mixture containing an anion-exchange resin on the recycled support). In this case, an 800 μm casting thickness was applied and the solvent was evaporated

for 60 min before the phase inversion in the water bath (i.e., the preparation conditions that were selected in our previous work (Chapter 3 [54])).

A.2.6. Characterization of Anion-Exchange Membranes

In this work, the thickness and the electrochemical properties were evaluated. The procedures described in Sections 3.2.5.2 and 3.2.5.3 (Chapter 3), respectively were used.

A.3. Results and discussion

Table A1 shows the thickness, electrical resistance and permselectivity of the different recycled supports before casting the polymeric mixture.

Table A 1. Thickness, electrical resistance and permselectivity of the recycled supports (before casting the polymeric mixture).

Recycled support	Thickness (μm)	Electrical resistance ($\Omega \cdot cm^2$)	Permselectivity (%)
PET permeate spacer	245 ± 2	0 ± 0	0 ± 0
PET mechanical support of RO membrane	79 ± 2	7 ± 0	0 ± 0
NF-like membrane	123 ± 1	10 ± 2	11 ± 3
UF-like membrane	126 ± 1	17± 2	0 ± 0

In the case of the PP feed spacer, despite its thickness, the mix of the electrolyte solutions was not avoided due the open mesh of this support, dropping its electrical resistance to 0 $\Omega \cdot cm^2$. On the other hand, the electrical resistance of the PET support is lower than in the cases of NF and UF-like membranes. This fact could be attributes to the higher porosity of the PET support, promoting a better electrical conductivity [231]. None of the tested support present permselectivity to neither anions nor cations apart from the NF-like membrane which present a slight capacity for the

rejection of the anions, which could be attributed to the PA remaining in the membrane.

Table A2 shows the thickness the electrical resistance and the permselectivity of the AEMs prepared using the different recycled supports.

Table A 2. Thickness, electrical resistance and permselectivity of the membrane prepared using the different recycled supports (after casting the polymeric mixture).

Recycled support	Thickness (μm)	Electrical resistance ($\Omega \cdot cm^2$)	Permselectivity (%)
PP permeate spacer	305 ± 5	- [a]	- [a]
PET mechanical support of RO membrane	140 ± 7	114 ± 7	60 ± 5
NF-like membrane	184 ± 9	- [b]	- [b]
UF-like membrane	176 ± 4	77 ± 3	87 ± 1

[a] The coated layer does not prevent the mixture of the electrolyte solutions.

[b] The coated layer is peeled off from the support.

On the one hand, it has been noticed that the volume of the polymeric mixture applied on the PP feed spacer is not enough for the formation of a defect-free film, as result, the solutions in the test cell are mixed. Thus, this support is not convenient for the preparation of AEM under the tested conditions. On the other hand, the AEM prepared using the PET support from the RO membrane did not reach an adequate permselectivity (in comparison with the commercial AMH-PES, which permselectivity was measured as 84 ± 3 % in our previous work [54]). Interestingly, the coated layer on the NF-like membrane is easily peeled off, which could be attributed to the PA remaining on the membrane surface. The PA is not dissolved by the organic solvent present in the polymeric mixture (THF),

which could reduce the adhesion of the coating to the membrane support. Lastly, the AEM prepared using the UF-like membrane as support have an adequate permselectivity (87 %) combined with a high electrical resistance (77 $\Omega \cdot cm^2$) [54]. The higher electrical resistance of the membrane could be reflected on a higher energy consumption in an electro-separation process. Several techniques have been found in the literature to enable a reduction of the electrical resistance of the membranes, for instance, the addition of conductive nanoparticles such as graphene oxide [232], or subjecting the membranes to an activation treatment to promote the complete dissociation of the functional groups in the membrane [233]. In this line, the development of an activation treatment suitable for this type of AEM was further explored in Chapter 4.

A.4. Conclusions

From this work, it can be concluded that among the recycled supports tested in this work, the membrane with UF-like properties is the most suitable one for the preparation of AEMs. Using recycled UF-like membranes as mechanical support, AEMs with an adequate permselectivity were obtained. Nevertheless, for a practical application of these membranes, the reduction of the electrical resistance of the should be addressed (see Chapter 4). Another possibility to enable their use, avoiding at the same time, a high energy consumption, could be their application in diffusive transport processes such as Donnan Dialysis and Ion-Exchange Membrane Bioreactor (see Chapter 7), where the driving force is the concentration gradient across the membrane and thus, it is not required the application of an external electric potential for generation the transport of the ions.

B

Appendix B. Communications in conferences, internationalization, and recognized awards

The research conducted during this Thesis has resulted in the following communications in conferences, international research stays and recognized awards.

A. Communications in conferences

Oral communications

A. Lejarazu-Larrañaga, S. Molina, J. M. Ortiz, R. Navarro, E. García-Calvo, Preparation of Anion-Exchange Membranes using recycled membranes as support for water treatment: Towards the circular economy approach. **Webinar organized by the European Membrane Society (EMS)**. Online. March 3, 2021.

A. Lejarazu-Larrañaga, S. Molina, J. M. Ortiz, E. García-Calvo, Preparación de membranas de Intercambio Iónico sobre soportes reciclados de membranas desechadas. **VIII Jornadas de Jóvenes Investigadores de la Universidad de Alcalá**. Online. December 9-11, 2020.

A. Lejarazu-Larrañaga, S. Molina, J. M. Ortiz, E. García-Calvo, Nitrate selective anion-exchange membranes prepared by using discarded Reverse Osmosis membranes as support. **MELPRO 2020**, International conference focused on membrane and electromembrane processes. Online. November 8-11, 2020.

A. Lejarazu-Larrañaga, S. Molina, J. M. Ortiz, E. García-Calvo, "Membranas de intercambio iónico sobre soportes reciclados en procesos de electro-separación para tratamiento de agua". **V Workshop of the Network of Excellence E3TECH,** Environmental and Energy Applications of the Electrochemical Technology. Online. November 28-31,2020.

A. Lejarazu-Larrañaga, S. Molina, J. M. Ortiz, R. Navarro, E. García-Calvo, Preparation of ion-exchange membranes by using end-of-life reverse osmosis membranes and application in electrodialysis. International Congress of Chemical Engineering (**ANQUE-ICCE 3**). 19-21 June 2019. Santander (Spain).

Posters

A. Lejarazu-Larrañaga, S. Molina, J. M. Ortiz, G. Riccardelli, E. García-Calvo, Increasing the performance in electrodialysis of Ion-Exchange Membranes prepared using discarded Reverse Osmosis membranes as support. **ICOM 2020**, International Congress on Membranes & Membrane Processes. Online. 7-11 December.

A. Lejarazu-Larrañaga, S. Molina, J. M. Ortiz, E. García-Calvo, Nitrate selective Anion-Exchange Membranes prepared by using discarded Reverse Osmosis membranes as support. **ICOM 2020**, International Congress on Membranes & Membrane Processes. Online. 7-11 December.

A. Lejarazu-Larrañaga, S. Molina, J. M. Ortiz, G. Riccardelli, E. García-Calvo, Increasing the performance of Anion-Exchange Membranes prepared from discarded Reverse Osmosis membranes. **MELPRO 2020**, International conference focused on membrane and electromembrane processes. Online. November 8-11, 2020.

A. Lejarazu-Larrañaga, S. Molina, J. M. Ortiz, G. Riccardelli, E. García-Calvo, "Mejorando la eficiencia en electrodiálisis de membranas de intercambio aniónico preparadas sobre membranas recicladas". **V Workshop of the Network of Excellence E3TECH,** Environmental and Energy Applications of the Electrochemical Technology. Online. November 28-31, 2020.

A. Lejarazu-Larrañaga, S. Molina, J. M. Ortiz, R. Navarro, J. Landaburu-Aguirre, E. García-Calvo, Preparation of heterogeneous anion-exchange membranes from recycled membranes. **Euromembrane**. 9-13 July 2018. Valencia (Spain).

R. García-Pacheco, A. Lejarazu-Larrañaga, J. Landaburu-Aguirre, S. Molina, T. Ransome, E. García-Calvo, Usage of ppm·h concept for membrane aging. Polyamide tolerance to free chlorine. **Euromembrane**. 9-13 July 2018. Valencia (Spain).

B. International research stays

Dates	24/09/2018-23/12/2018
Host supervisor	Prof. Bart Van der Bruggen
Department	Process Engineering for Sustainable Systems (PROCESS). Department of Chemical Engineering (CIT).
Institution	**Katholieke Universiteit of Leuven (KU Leuven)**
City, Country	Leuven, Belgium
Publication	A. Lejarazu-Larrañaga, Y. Zhao, S. Molina, E. García-Calvo, B. Van der Bruggen, Alternating current enhanced deposition of a monovalent selective coating for anion-exchange membranes with antifouling properties, Sep. Purif. Technol. 229 (2019) 115807.

Dates	14/09/2020 -14/12/2020
Host supervisors	Prof. Joao G. Crespo and Prof. Svetlozar Velizarov
Department	LAQV-REQUIMTE, Department of Chemistry, NOVA School of Science and Technology, FCT NOVA
Institution	**Universidade NOVA de Lisboa (UNL)**
City, Country	Caparica, Lisbon, Portugal
Publication	A. Lejarazu-Larrañaga, J. M. Ortiz, S. Molina, S. Pawlowski, C. F. Galinha, V. Otero, E. García-Calvo, S. Velizarov, J. G. Crespo, Nitrate removal by Donnan Dialysis and Ion-Exchange Membrane Bioreactor using upcycled end-of-life Reverse Osmosis membranes as Anion-Exchange Membranes, Membranes 12 (2022) 101.

C. Awards

2020 European Membrane Society **BEST PAPER AWARD** for the paper *"Circular economy in membrane technology: Using end-of-life reverse osmosis modules for preparation of recycled anion-exchange membranes and validation in electrodialysis"* published in the Journal of Membrane Science 593, 117423.

BEST ORAL COMMMUNICATION AWARD for the communication "*Preparation of ion-exchange membranes by using end-of-life reverse osmosis membranes and application in electrodialysis"* in the First International Young Researchers Symposium on Applications of Electrochemical Technology celebrated as part of the International Congress of Chemical Engineering (**ANQUE-ICCE 3**). 19-21 June 2019. Santander (Spain).

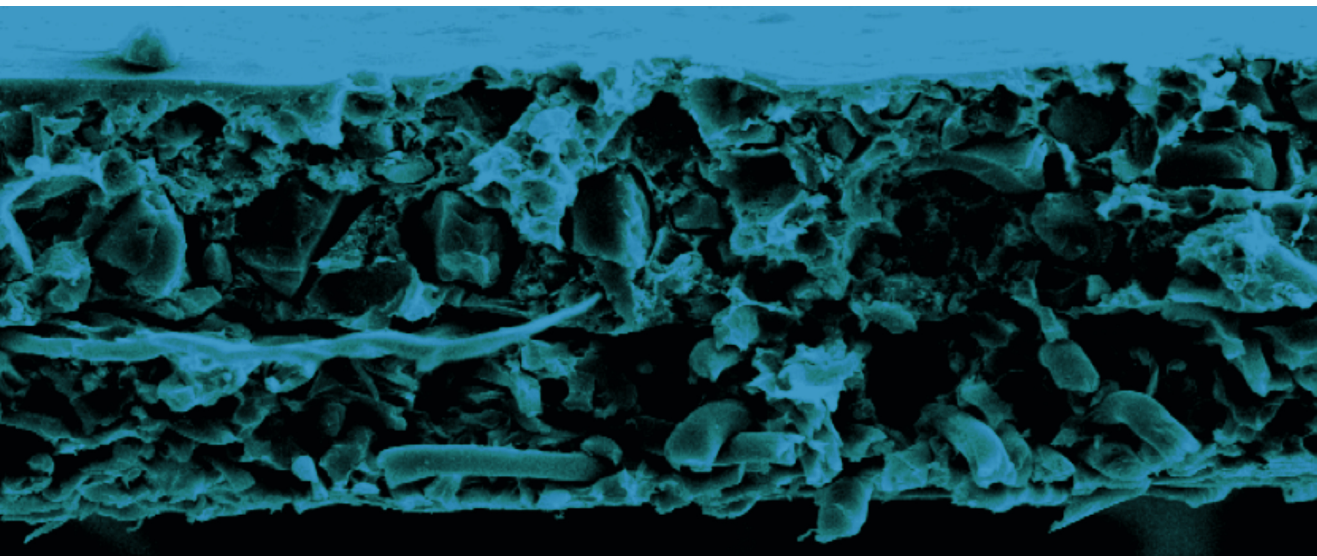

The increasing number of end-of-life reverse osmosis membrane modules yearly dumped in landfills comprises an important environmental concern. In this context, the development of innovative membrane reuse and recycling alternatives can help reducing the waste generation and fostering the transition towards a circular economy in the water sector. In the present doctoral thesis, the indirect recycling of end-of-life reverse osmosis membranes as anion-exchange membranes has been addressed. The technical feasibility of the developed membranes has been validated under different processes for water treatment, including, brackish water desalination by electrodialysis, selective counter-ion separation, and nitrate transport by Donnan dialysis and simultaneous removal in an ion-exchange membrane bioreactor.